PHYSICOCHEMICAL, THERMOANALYTICAL, ELECTROCHEMICAL AND ANTITUMOUR STUDIES OF TRANSITION METAL COMPLEXES OF SCHIFF BASES DERIVED FROM HETEROCYCLIC CARBONYL COMPOUNDS

Thesis
submitted to
University of Calicut
in partial fulfillment of the requirements
for the award of the Degree of

Doctor of Philosophy in Chemistry

By

NIMMY KURIAKOSE

Under the guidance of

Dr. JOBY THOMAS K.

RESEARCH AND POSTGRADUATE DEPARTMENT OF CHEMISTRY
ST. THOMAS' COLLEGE (AUTONOMOUS)
(UNIVERSITY OF CALICUT)
THRISSUR, KERALA - 680001

October 2015

RESEARCH AND POSTGRADUATE DEPARTMENT OF CHEMISTRY
ST. THOMAS' COLLEGE (Autonomous)
THRISSUR, KERALA-680001
(Nationally reaccredited at 'A' level by NAAC & affiliated to University of Calicut)

Dr. Joby Thomas K., M.Sc., M.Phil., MBA, Ph.D
Associate Professor & Head

30.10.2015

CERTIFICATE

This is to certify that the thesis entitled ***"Physicochemical, Thermoanalytical, Electrochemical and Antitumour Studies of Transition Metal Complexes of Schiff Bases Derived From Heterocyclic Carbonyl Compounds"*** *is an authentic record of research work carried out by* ***Ms. Nimmy Kuriakose*** *under my supervision in partial fulfillment of the requirements for the degree of Doctor of Philosophy in Chemistry of University of Calicut and further that no part thereof has been presented before for any other degree.*

Dr. Joby Thomas. K
(Supervising Teacher)

DECLARATION

I hereby declare that the thesis entitled, ***"Physicochemical, Thermoanalytical, Electrochemical and Antitumour Studies of Transition Metal Complexes of Schiff Bases Derived From Heterocyclic Carbonyl Compounds"****, submitted to the University of Calicut in partial fulfillment of the requirements for the award of the Degree of Doctor of Philosophy in Chemistry is a bonafide research work done by me under the supervision and guidance of Dr. Joby Thomas. K., Associate Professor and Head, Research and Post graduate Department of Chemistry, St. Thomas' College (Autonomous), Thrissur.*

I further declare that this thesis has not previously formed the basis of any degree, diploma or any other similar title.

30.10.2015 ***Nimmy Kuriakose***

ACKNOWLEDGEMENTS

"Feeling gratitude and not expressing it, is like wrapping a present and not giving it."

It is hard to find words to express my gratitude to all who helped me in submitting this thesis in a perfect manner. I am eternally grateful to God almighty for all the blessings showered upon me during this work. I would also like to acknowledge my Guide and my Mentor Dr. Joby Thomas K, who made me capable of realizing my goal. His guidance and support has been amazing and I whole heartedly thank everything he had done for me. He is a teacher whose support, wisdom and warmth will continue to inspire me.

Let me thank my family members for supporting and encouraging me in all dimensions in making my dream a reality, especially my husband Mr. Shaju, my children Franklin and Milin, appachan, amma, my sisters and in-laws.

The support rendered by the St. Thomas College Team - Dr. P.O. Jenson, Principal, all the faculty members of Chemistry Department, especially former Heads of this Department Dr. Babu Joseph and Dr. Joy Anto, Dr. Paulson Mathew, Dr. Sunil Jose. T. and former Lab Assistant Sri. M. P. Varghese has been really high. They served as a light house in my journey towards the completion of this voyage.

I would like to express my deep gratitude for the support and help rendered by my research colleagues Dr. Aby Paul., Dr. Vinod P. Raphael, Dr. Shaju. K. S., Sr. Mareena, Ms. Reeja, Mrs. Sini, Ms. Vidya, Ms. Raghi, Ms. Binsi, Mr. Aji, Mrs. Drishya and Mr. Dinoop.

The motivation rendered by Dr. Francy Kakkassery of the Zoology Dept. of St. Thomas College was really amazing. The help given by Amala Cancer Research Centre, Thrissur was really appreciable. Dr. Ramdas Kuttan was the catalyst for the successful completion of the antitumour studies. The advice given by Dr. Abraham Joseph, his student Mr. Sam John of Chemistry Dept. of Calicut University and Dr. Stanly Jacob of C-MET, Athani, helped me a lot in doing the Corrosion studies.

A memorable support in the completion of this work came from the Bursar of St. Thomas College, Thrissur, Rev. Fr. Martin Kolambrath. Right from arranging the infrastructure and in providing a well equipped laboratory were the real turning point in my work which saved a lot of time and money. I really value the blessings of the former faculty member of Chemistry Department of Calicut University, Prof. Dr. Geetha Parmeswaran, the one who motivated me to do my research in the field of Schiff bases.

I hereby acknowledge the help rendered by the STIC-CUSAT, NIIST Trivandrum, Mr. Anoop Thomas of IISER Trivandrum in analyzing the compounds, which were really worthwhile to mention. I also thank the staff of CHMK Library and the Chemistry Dept. Library of Calicut University for helping me frame a smooth bibliography. My heartfelt thanks go to Dr. Vinod V. M., Assistant Librarian of CHMK Library who helped me to obtain the Plagiarism check certificate.

Last but not the least, I sincerely thank the hard work of Mr. M. I. Pauly of educare, Thrissur, who did the DTP work for this project.

Nimmy Kuriakose

To
My Family

PREFACE

Schiff bases are a class of compounds which have profound use as ligands as well as in the form of complexes. The versatile use of Schiff bases is due to its ability to coordinate to the metal ions via the azomethine nitrogen. Schiff bases are useful chelators because of their ease of preparation and structural varieties. Multidentate Schiff base ligands and their coordination with metals attract much attention because of their biological relevance. Heterocyclic Schiff bases have wide application in therapeutic fields either as potential drug or diagnostic probes and also in analytical tools. The presence of hetero atoms in such ligands gives them excellent characteristics like corrosion inhibition property. During the present course of study five monovalent Schiff base ligands and their transition metal complexes were prepared and characterized. Antitumour studies of the copper complexes of all these Schiff bases were conducted. Investigations of the corrosion inhibition capacity of the newly synthesized Schiff bases have been carried out in different acid media. Thermoanalytical studies of some of the complexes were also conducted. For convenience and better understanding, the entire work has been presented in this thesis as four parts.

In the first part of the thesis, five novel heterocyclic Schiff bases namely 3-(1H-indol-3-yl)-2-[(E)-(thiophen-2-ylmethylidene)amino]propanoic acid (I3YT2YMAPA), (E)-3-[thiophen-2-ylmethyleneamino]benzoic acid (T2YMABA), (E)-4-(5-[(2-carbamo thioylhydrazono)methyl]thiophen-2-yl)benzoic acid (CTHMT2YBA), (E)-4-(5-[(2-phenylhydrazono)methyl]thiophen-2-yl)benzoic acid (PHMT2YBA) and (E)-4-(5-[(2-carbamothioylhydrazono)methyl]furan-2-yl)benzoic acid (CTHMF2YBA) were synthesized and characterized by different techniques like CHNS analysis and spectral

studies such as FTIR, NMR, mass and UV-visible. The chelating abilities of these Schiff bases were investigated by synthesizing a number of transition metal complexes. Elemental analysis shows that majority of the metal complexes obey 1:1 stoichiometry between the metal and ligand. Out of the five studied Schiff bases, majority of them acted as monovalent bidentate ligands in metal complexes, coordinating through azomethine nitrogen and carboxylate oxygen. Then these complexes were also subjected to characterization studies by elemental analysis, magnetic moment measurements, conductance measurements, IR, UV-visible and ^{1}Hnmr spectral analysis.

This part is divided into seven chapters. The first chapter includes details of literature survey and the scope of present investigation. Various physicochemical methods employed for the elucidation of the structures of the Schiff bases and their metal chelates are discussed in chapter 2. Details of synthesis and characterization of Schiff bases, 3-(1H-indol-3-yl)-2-[(E)-(thiophen-2-ylmethylidene)amino]propanoic acid (I3YT2YMAPA), (E)-3-[thiophen -2-ylmethyleneamino]benzoic acid (T2YMABA), (E)-4-(5-[(2-carbamothioylhydrazono) methyl]thiophen-2-yl)benzoic acid (CTHMT2YBA), (E)-4-(5-[(2-phenylhydrazono) methyl]thiophen-2-yl)benzoic acid (PHMT2YBA) and (E)-4-(5-[(2-carbamothioyl hydrazono)methyl]furan-2-yl)benzoic acid (CTHMF2YBA) and their transition metal complexes are presented in the chapters 3, 4, 5, 6 and 7 respectively. This part ends with a brief summary and references.

Thermogravimetric studies of Cr(III) and Ni(II) complexes of novel Schiff base ligands such as I3YT2YMAPA, T2YMABA, CTHMT2YBA, PHMT2YBA and CTHMF2YBA are given in Part II. The regions of thermal stability and the temperature of decomposition of each of these complexes were found out. Also the temperatures of

maximum rate of decomposition were assigned from the thermograms. Kinetic studies were done based on these thermogravimetric data by employing mechanistic and non mechanistic equations. Kinetic parameters like Arrhenius frequency factor, energy of activation and entropy of activation of all the decomposition stages were calculated. The mechanism of decomposition reaction in each stage and hence the order of decomposition reactions also were determined. The thermal stabilities of the chelates were compared with the aid of energy of activation, initial/final decomposition temperature, inflection temperature and peak temperature from the TG and DTA data. In order to ascertain the order of the decomposition reactions, nine mechanistic equations and an integral equation formulated by Coats and Redfern, which is a non mechanistic equation, were employed. Comparing the correlation between the kinetic parameters obtained from these mechanistic equations and the Coats-Redfern method, reaction mechanisms and orders of different decomposition stages were ascertained.

First chapter of this part involves an introduction on different thermoanalytical methods like TGA and DTA. The relevance of various methods for the determination of kinetic parameters of solid-state reactions using thermogravimetric data, especially the Coats-Redfern method is discussed here. The scope of present studies is also mentioned. Details of the instruments used are given in chapter 2. The thermal decomposition data and the evaluation of kinetic parameters of Cr(III) complexes of the Schiff bases, T2YMABA, PHMT2YBA, CTHMT2YBA and CTHMF2YBA are discussed obviously and reported in chapter 3. Whereas in chapter 4, the thermal behaviour and kinetic studies of Ni(II) complexes of T2YMABA, PHMT2YBA, CTHMT2YBA, CTHMF2YBA and

I3YT2YMAPA are explained. All the results are briefly summarized at the end of this part followed by references.

Part III deals with the detailed investigations of the corrosion inhibition capacity of the newly synthesized Schiff bases on mild steel in hydrochloric acid and sulphuric acid media. The corrosion inhibition studies were carried out with conventional gravimetric method and electrochemical methods such as electrochemical impedance spectroscopy (EIS) and potentiodynamic polarization studies. In the polarization analysis, Tafel extrapolation method and Linear polarization method were performed separately. Both Nyquist plot and Bode plot analysis were utilized to get much density on the inhibitory action of the novel Schiff bases by EIS method. Adsorption isotherms were plotted from the results of gravimetric weight loss studies in order to predict the mechanism of corrosion inhibition by the Schiff bases. Thermodynamic parameters like free energy of adsorption and adsorption equilibrium constant were also determined for confirming the nature of adsorption. Weight loss method was followed to compare the inhibition efficiencies of Schiff bases and their respective parent amines in acid medium. Corrosion studies clearly established that all the studied Schiff bases were excellent corrosion inhibitors on mild steel in hydrochloric acid medium. Generally the corrosion inhibition efficiency was poor in H_2SO_4 medium than in HCl medium. Surface morphological analysis was also conducted to establish the mechanism of corrosion inhibition of these inhibitors.

This part is comprised of three chapters, whereas the third chapter consists of two subsections. Chapter 1 details the different aspects of corrosion and corrosion inhibitors. A report of thorough literature survey on corrosion inhibition studies and the scope of the

present study are also included in this chapter. The details of different corrosion monitoring techniques are discussed in chapter 2. Results and discussion of corrosion inhibition investigations of the newly synthesized Schiff bases in different acid media have been reported well in chapter 3. This chapter is divided into two sections; In section I corrosion inhibition studies of Schiff base inhibitors on mild steel in 1.0 M HCl is given and in Section II, the studies in 0.5M H_2SO_4 medium are detailed. A brief summary of the corrosion studies along with the references are followed thereafter.

The details of antitumour studies are explained well in Part IV of this thesis. The antitumour activity of copper(II) complexes of ten different potential Schiff base ligands such as 3-(1H-indol-3-yl)-2-[(E)-(thiophen-2-ylmethylidene)amino]propanoic acid (I3YT2YMAPA), (E)-3-[thiophen-2-ylmethyleneamino]benzoic acid (T2YMABA), (E)-4-(5-[(2-carbamothioylhydrazono)methyl]thiophen-2-yl)benzoic acid (CTHMT2YBA), (E)-4-(5-[(2-phenylhydrazono)methyl]thiophen-2-yl)benzoic acid (PHMT2YBA) and (E)-4-(5-[(2-carbamothioylhydrazono)methyl]furan-2-yl)benzoic acid (CTHMF2YBA), 2-(1-[pyridin-3-yl]ethylidene)hydrazinecarbothioamide (P3YEHCTA), 3-(1-[2-phenyl hydrazono]ethyl)pyridine (PHEP), 3-[anthracen-9(10H)-ylideneamino]propanoic acid (A9Y3APA), 2-[anthracen-9(10H)-ylideneamino]-3-(1H–imidazole–4-yl)propanoic acid (A9Y3IMPA) and 2-[anthracen-9(10H)-ylideneamino]-3-phenylpropanoic acid (A9Y3PPA) were examined on Dalton's lymphoma ascites tumour cells. Firstly, Cu(II) complexes of these Schiff bases were prepared and screened for their *in vitro* cytotoxic activity. The trypan blue exclusion method was adopted and the results revealed that all the complexes have excellent cytotoxic activity against the tumour cell suspension. Three complexes which showed the highest activity during *in vitro* cytotoxic analysis were

chosen for the *in vivo* studies on Swiss albino mice. Ascites tumour reduction analysis explored the increased capacity of the copper compounds on chelation. Also the activities of these compounds were compared with that of the standard drug cyclophosphamide.

Chapter 1 of this part includes an elaborate introduction on different types of tumour and the details of earlier antitumour investigations. Objectives and scope of the investigation are also given in this chapter. Chapter 2 includes different strategies adopted for studying the inhibitory effect of copper complexes of various Schiff bases. Results and discussion of the antitumour studies of various Schiff base complexes are portrayed in chapter 3. This part terminates with the summary and bibliography.

Publications in journals and presentations in seminars

Nimmy Kuriakose “Physicochemical, thermoanalytical, electrochemical and antitumour studies of transition metal complexes of schiff bases derived from heterocyclic carbonyl compounds” Thesis. Department of Chemistry, St. Thomas College, University of Calicut, 2015

List of Publications

1) **Nimmy Kuriakose**, Joby Thomas K*, Vinod P Raphael, Shaju K S," (E)-3-[thiophen-2-ylmethyleneamino]benzoic Acid: Structural and Corrosion Inhibition Studies" *Chemical Science Reviews and Letters*, , 5(17), (2016) 14-20.
2) **Nimmy Kuriakose**, Joby Thomas K*, Vinod P Raphael, Shaju K S," analysis of structure and corrosion inhibition properties of (e)-4-(5-[(2-phenylhydrazono) methyl]thiophen-2-yl)benzoic acid", *Int. J. Chem. Sci & Res.* , v6 i1(2016) 07 – 17.
3) **Nimmy Kuriakose,** Joby Thomas K, Vinod P. Raphael, Shaju K. S., "Mild steel corrosion inhibition capacity of Schiff base derived from Thiophene-2-carbaldehyde: gravimetric and electrochemical investigation", *Chemical Science Reviews and Letters*, 3(12) (2014) 1060-1067.
4) **Nimmy Kuriakose,** Joby Thomas Kakkassery, Vinod P. Raphael, Shaju K. Shanmughan, "Electrochemical Impedance Spectroscopy and potentiodynamic polarization analysis on anticorrosive activity of Thiophene-2-carbaldehyde derivative in acid medium", *Indian J. Mater. Sci.,* 2014(2014), Article ID 124065, 6 pages.
5) Shaju K.Shanmughan, Joby Thomas K, Vinod P. Raphael, **Nimmy Kuriakose,** "Electrochemical and AFM studies on adsorption behavior of a polynuclear Schiff base at carbon steel in HCl medium", *Current Chemistry Letters*, 4 (2015) 67-76.
6) Vinod P Raphael, Joby Thomas K*, K.S. Shaju and **Nimmy Kuriakose, "**Chelating Competency and electrochemical Response of a Heterocyclic

Phenylhydrazone and its Copper Chelate", *Oriental J. Chemistry,* Vol. 30, No. (4) (2014) 2099-2104.

7) Shaju K.S, Joby Thomas K, Vinod P. Raphael, **Nimmy Kuriakose,** "Spectral and cyclic voltametric studies on Cu(II)-Schiff base complex derived from anthracene-9(10 H)-one", *IOSR J. Appl. Chem.*, 7(10) I (2014) 64-68.

8) Joby Thomas K, Vinod P. Raphael, **Nimmy Kuriakose**, K.S.Shaju, "Spectroscopic and corrosion inhibition investigations on Schiff bases derived from aromatic aminosulphonic acids", *ISST J. Appl. Chem.,* 3(2) (2012) 1-4.

Conference Papers

1) **Nimmy Kuriakose**, Joby Thomas K., Tinu Pius P., Jisha V., "Aminosulphonic acid derivatives: Potential corrosion inhibitors", Proceedings of International Conference on Advances in Material Science (ICAMS 2013) p.136, held at Sree Sankara College, kalady, Kerala, October 23-24, 2013.
2) Shaju K S, Joby Thomas K, Vinod P Raphael, **Nimmy Kuriakose**, "Corrosion inhibition on carbon steel by Schiff base derived from 2-Amino -3 Phenyl Propanoic acid and it's synergistic effect with iodide", Proceedings of International Conference on Advances in Material Science (ICAMS 2013) p.136, held at Sree Sankara College, kalady, Kerala, October 23-24, 2013.
3) Vinod. P. Raphael, Joby Thomas K, Shaju K. S, **Nimmy Kuriakose**, "Corrosion Inhibition Investigations of 3-Acetylpyridine Thiosemicarbazone on Carbon Steel in Hydrochloric Acid Medium", Proceedings of International Corrosion Prevention Symposium (CORSYM-2013), held at Chennai, February 28 – March 02, 2013.
4) K. P. Mary, K. Joby Thomas, **Nimmy Kuriakose**, Vinod Raphael, "Structural and antimicrobial investigations on transition metal complexes of arylazo derivatives of acetyl acetone glycine and dimedone glycine", Proceedings of 22nd Swadesi Science Congress held at Central Plantation Crops Research Institute, Kasaragod, November 6-8, 2012.

Papers communicated / to be communicated

1) Quantum Mechanical and Electrochemical Investigations on Corrosion Inhibition Properties of novel heterocyclic Schiff bases - communicated to Current Chemistry Letters.
2) Cytotoxic and antitumour studies of copper(II) complex of 3-[thiophen-2-ylmethyleneamino]benzoic acid – to be communicated.
3) Spectroscopic and corrosion inhibition investigations on Schiff bases derived from phenyl hydrazone derivative – to be communicated.
4) Electrochemical studies on mild steel corrosion inhibition by a heterocyclic Schiff base derived from thiosemicarbazide – to be communicated.
5) Corrosion inhibition and antitumour studies of Schiff bases derived from Thiophene-2-carbaldehyde– to be communicated.

Abbreviations used

MS	Mild Steel
M	Central metal ion in the complex
L	Ligand moiety in a complex
Ac	Acetate part in the complex
BM	Bohr Magneton
DMSO	Dimethyl sulphoxide
AIPA	2-amino-3-(3-indolyl)propionic acid
3ABA	3-aminobenzoic acid
PH	Phenylhydrazine
TCH	Thiocarbamoyl hydrazide
FT2YBA	4-(5-formylthiophen-2yl)benzoic acid
FF2YBA	4-(5-formylfuran-2yl)benzoic acid
I3YT2YMAPA	3-(1H-indol-3-yl)-2-[(thiophen-2-ylmethylidene)amino]propanoic acid
T2YMABA	3-[thiophen-2-ylmethyleneamino]benzoic acid
PHMT2YBA	4-(5-[(2-phenylhydrazono)methy]thiophen-2-yl)benzoic acid
CTHMT2YBA	4-(5-[(2-carbamothioylhydrazono)methyl]thiophen-2-yl)benzoic acid
CTHMF2YBA	4-(5-[(2-carbamothioylhydrazono)methyl]furan-2-yl)benzoic acid
EIS	Electrochemical Impedence Spectroscopy
DLA	Dalton's lymphoma ascites

LIST OF CONTENTS

LIST OF TABLES

LIST OF FIGURES

Part I
Synthesis and Characterization

Chapter 1

Nimmy Kuriakose “Physicochemical, thermoanalytical, electrochemical and antitumour studies of transition metal complexes of schiff bases derived from heterocyclic carbonyl compounds” Thesis. Department of Chemistry, St. Thomas College, University of Calicut, 2015

CHAPTER I

INTRODUCTION AND REVIEW

Coordination chemistry has always been a challenging and fascinating field to inorganic chemists. Metal complexes derived from carbonyl and amino compounds have found multidimensional applications apart from being instrumental in the tremendous development of coordination chemistry. The real impetus towards the progress in coordination chemistry of these potential chelating species was probably provided by the remarkable biological activity observed for some of these derivatives. These findings have led recently to an increased interest in the chemistry of transition metal chelates of Schiff bases and related ligands. There is wide scope for extensive studies regarding the coordination compounds of transition metals with Schiff bases derived from heterocyclic carbonyl compounds.

Schiff bases

Schiff bases are common ligands in coordination chemistry. They are a class of compounds which have profound use as ligands as well as in the form of complexes. These are named after Hugo Joseph Schiff who is one of the founders of modern chemistry. Schiff bases have an influencing role in the development of coordination chemistry. A Schiff base is a compound with a functional group that contains a carbon-nitrogen double bond with the nitrogen atom connected to an aryl or alkyl group[1]. They have the general formula $R^1R^2C=NR^3$, where R is an organic side chain. A Schiff base is synonymous with azomethine and is also called as imines.

Schiff bases can be synthesized from aliphatic/aromatic amines and carbonyl compounds (aldehydes or ketones) by nucleophilic addition forming an

unstable hemiaminal, followed by acid or base catalyzed dehydration to generate an imine. The dehydration of the carbinolamine is the rate-determining step of Schiff base formation. If the amine is protonated, it becomes non-nucleophilic and the equilibrium is shifted to the left and the hemiaminal formation cannot occur. Therefore, many Schiff base synthesis are best carried out at mildly acidic pH. The imine nitrogen is basic and exhibits pi-acceptor properties. Schiff base ligands are typically derived from primary amines and carbonyl compounds[2].

$$\underset{\text{Primary amine}}{R\text{-}NH_2} + \underset{\text{Aldehyde / Ketone}}{>C=O} \rightarrow \underset{\text{Schiff Base}}{>C=N\text{-}R} + H_2O$$

Schiff bases are used as precursors of countless organic processes, for the production of intermediates or products. It can be summarised into four different types of organic reactions in which Schiff bases are widely used: (1) addition of organometallic reagents or hydride to C=N bond (2) hetero Diels-Alder reaction to furnish six membered nitrogen containing heterocyclic compounds (3) skeletons for the building-up scaffolds; for eg, the famous salen scaffold which is used as 'privileged ligand' for the formation of the corresponding chiral salen metal complexes (4) Staudinger reaction with ketene to furnish biologically important β-lactam ring. The figure given below represents one of the common Schiff base ligand, Salen and its complex.

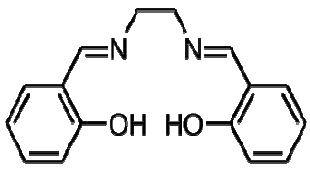

(a)

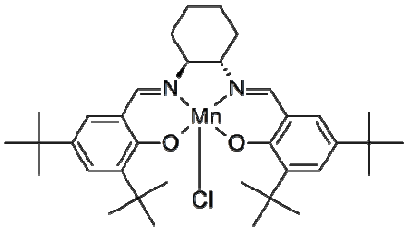

(b)

(a) Salen : a common tetradentate ligand and (b) Jacobsen's catalyst : derived from chiral salen ligand.

Schiff bases are useful chelators because of their ease of preparation and structural varieties[3-6]. Its variable denticities and subtle steric and electronic control on their framework make these molecules excellent ligands. Recently a great deal of interest have developed in the synthesis and characterization of transition metal complexes containing Schiff bases as ligands due to their applications as catalysts for many asymmetric reactions. In 1968 Ryoji Noyori developed a copper-Schiff base complex for the metal-carbenoid cyclopropanation of styrene and was awarded a share of the Nobel Prize in Chemistry in the year 2001.

Schiff bases are important intermediates in bio-processes like transamination reaction (from amino-acid to ketoacid and vice versa). It is interesting to study the use of Schiff bases which have wide application in pharmaceutical or biological fields and also in analytical tools. Some Schiff bases including radioactive nuclide complexes show anticancer, antibacterial, antifungal and antiviral agents[7-11]. Moreover, Schiff bases are present in various natural, semi-synthetic, and synthetic compounds and have been demonstrated to be essential because of their biological activities[12, 13].

Another outstanding application of Schiff bases is their use as an effective corrosion inhibitor, which is based on their ability to get adsorbed spontaneously to form a monolayer on the surface to be protected. A large number of different Schiff base ligands have been used as cation carriers in potentiometric sensors as they have shown excellent selectivity, sensitivity and stability for specific metal ions[14-19].

A number of Schiff base chelating agents, used for the detection of metal ions, can also be applied for their quantitative determination. Photometric methods are there which are based on the colour formation resulting from the reaction between Schiff base

and the metal ion. Tantaru et. al.[20] have prepared Salen-type Schiff base, 1-ethyl-salicylidene-bis-ethylene diamine by condensing ethyl-o-hydroxyphenyl ketone with ethylene diamine. These Schiff's bases possess very good capacity of complexation with Mn(II) ions, resulting brown complexes. The Schiff base forms a brown complex with Mn(II) cation, with maximum absorbance at 460 nm. The complex showed a maximum stability at pH 6.0. Spectrophotometric determination of Mn(II) using this Schiff base as reagent were successfully applied to pharmaceutical products containing Mn(II) cation. A Schiff base namely bis-(3-methoxysalicylaldehyde)-1,6-diaminohexane was used by Mashhadizadeh et. al.[21] for the extraction of copper . Holzbecher[22] proposed that Schiff bases prepared from salicyladehyde and aniline can be used for titration of acids with bases and the compound O-[N-(O-hydroxyphenyl)formimidoyl]phenol can be used for the quantitative determination of aluminium. Further, the use of Schiff bases as sensors and solid phase extraction sorbents are increasing in analytical chemistry techniques.

Now a days many Schiff bases are utilized as synthons in the preparation of a number of industrial and biologically active compounds like formazans, 4-thiazolidinines and benzoxazines.The fact that the Schiff base derivatives employed in various processes are environmental-friendly, encourage the researchers for designing of novel heterocyclic and aryl Schiff bases.

Transition metal complexes of Schiff bases – a review

The versatile use of Schiff bases as ligands is due to its ability to coordinate to the metal ions via the azomethine nitrogen. Literature survey reveals that Schiff bases and their complexes are extensively studied and used in many fields. Multidentate Schiff base ligands and their coordination with metals attract much attention because of their

biological relevance. The geometry, oxidation state and redox characteristics of these complexes make them an interesting and challenging class of compounds for the researchers.

A large number of copper complexes have remarkable biological catalytic properties and are used in dyes and polymers, as plant growth regulators and in pharmaceutical fields. N. Raman et. al.[23] prepared complexes of Cu(II), Ni(II), Co(II), and Zn(II) metals with Schiff base derived from benzil-2,4-dinitrophenylhydrazone and aniline. ^{1}H NMR, ^{13}C NMR, IR, UV-Vis, EPR and CV studies were carried out to propose the structure of these complexes. Mixed ligands complexes of Cr(III), Co(III), Ni(II) and Cu(II) were synthesized by R. K. Upadhyay et. al.[24] with 2-imino-3–(2-hydroxylphenyl)-1-thiazolidin-4-one and they were characterized by elemental analysis, infrared and UV-Visible spectroscopy. The Cu(II) complex had square planar geometry and the others, Cr(III), Co(III) and Ni(II) complexes exhibited octahedral geometry.

Zahid H. Chohan et. al.[25] reported that substituted pyridine Schiff base complexes of copper(II), zinc(II), nickel(II) and cobalt(II) were synthesized and characterized by physical, analytical and spectral data. The ligands were deprotonated on complexation with Co(II), Ni(II) and Zn(II) and showed tridentate nature. The complexes had the general formula $[M(L)_2]$ with octahedral geometry. The antibacterial activity of the Schiff bases and their complexes were analysed on bacterial strains such as *E. coli*, *P. aeruginosa and S. aureus*. It was also reported that on chelation, the Schiff bases become more antibacterial as compared to uncomplexed Schiff bases.

Emad Yousif and co-workers[26] succeeded in synthesizing five new complexes of 2N-salicylidene-5-(*p*-nitro phenyl)-1,3,4-thiadiazole. The VO(II), Co(II), Rh(III), Pd(II)

and Au(III) complexes were monomeric and four-coordinated. Micro elemental analysis, mass spectroscopy, FTIR spectroscopy, UV–Vis spectroscopy, ^{1}H and ^{13}C NMR, conductivity and magnetic susceptibility measurements were conducted to ascertain the structure. VO(II) and Co(II) complexes existed as square pyramidal and tetrahedral respectively while all others had square planar geometry. The *in vitro* antibacterial activity studies established the enhanced activity of the complexes than the ligands.

A novel multidentate and macrocyclic Schiff base (10,21-bis-iminomethyl-3,6,14,17-tricyclo[1,1,3,17]tetracosa-1(23),2,6,8,10,12(24),13,17,19,21-decaene-23,24-disodium) and its copper(II), Zinc(II), Manganese(II) and Cobalt(II) complexes were obtained by Riyadh M. Ahmed et. al.[27] in 2013. The ligand consisting of two submacrocyclic units, formed tetranuclear macrocyclic-based complexes by the condensation reaction between sodium 2,4,6-triformyl phenolate and ethylenediamine in 2: 3 mole ratio. Physicochemical and spectroscopic studies suggested that Mn(II), Co(II) and Zn(II) complexes had tetrahedral structure and square planar geometry for Ni(II) and Cu(II) complexes. Antibacterial studies on gram positive and gram negative bacteria proved the inhibitive action of the complexes which was more prominent than the ligand.

Copper(II), nickel(II), zinc(II) and Cobalt(II) complexes were prepared in situ by Aurora Reiss and team mates[28] by the condensation of salicylaldehyde with cefotaxime in the presence of divalent metal salts. The complexes having the general formula $ML_2(H_2O)_2$ were of non-electrolyte type as evident from the molar conductance measurements. Tetragonal geometry was proposed for the Cu(II) complex and octahedral geometry for all others. The authors reported that programs based on quantum molecular studies and chemical modeling were employed to formulate the structure of the ligand

and the complexes. They conducted antibacterial studies on *E. coli*, *P. aeruginosa, K. pneumoniae, B. subtilis* and *S. aureus* and concluded that all the complexes have excellent activity against the bacterial stain.

A bidentate Schiff base ligand was obtained from 2-hydroxy-3-formylquinoline and substituted p-iodoaniline by M. Mustapha et. al.[29] in 2011. They succeeded in synthesizing Cu(II), Ni(II) and Zn(II) complexes of square planar geometry. Another Schiff base was derived from 4-aminoantipyrine, 3-hydroxy-4-nitrobenzaldehyde and o-phenylenediamine by N. Raman[30] and he was able to prepare a series of complexes with cobalt(II), manganese(II), copper(II), zinc(II) and mercury(II) ions. Usual characterization techniques like IR, UV–Vis, ^{1}H NMR, ESR, mass spectra, magnetic susceptibility, molar conductance etc. were performed on the newly synthesized compounds to decide the structures of complexes as ML type. The VO(IV) complex was assigned square–pyramidal geometry and all others square–planar geometry. Cyclic voltammetry was applied to analyse the redox behaviour of copper and vanadyl complexes. In this case also the antibacterial activity was checked and proved that on chelation the inhibitory activity is enhanced. It is reported that only Ni, Co and Cu complexes could cleave the DNA through redox chemistry.

Muna. A. Hadi[31] was able to synthesize a nitrogen and oxygen donor Schiff base by reacting 2-amino benzoic acid and 4-(N,N-dimethyl amino) benzaldehyde which was a monobasic bidentate ligand. This ligand formed chelates with Cu(II), Zn(II) and Cd(II) ions in 1:2 metal-ligand stoichiometry. Conductivity measurements of the complexes gave results which were consistent with those expected.

Recently manganese and cobalt complexes of unsymmetrical Schiff bases were synthesized and characterized by Fatima T. Esmadi[32]. The ligand was the product of reaction between o-phenylenediamine derivatives and 1-hydroxy-2-acetonaphthone and then followed by reaction with the salicyaldehyde, 2-pyridinecarboxaldehyde, 2-hydroxynaphthaldehyde and 2-quinolinecarboxaldehyde. The unsymmetrical tetradentate ligands were then converted into monocentric complexes and characterized by IR and UV-visible spectroscopy, elemental analysis, magnetic susceptibility and electrical conductivity studies. Gram-positive and gram-negative pathogens were taken for the evaluation of the antibacterial activity of the complexes. The manganese complexes showed significant activity against *S. aureus.* Some manganese and cobalt complexes exhibited genotoxic activity in cultured human blood lymphocytes with 8-hydroxy-2-deoxy guanosine (8-OHdG) assay in the concentration range 0.1–10µg/mL. The exhibition of mutagenicity by some complexes leaves a scope for further research.

Condensation of dehydroacetic acid, 3-nitrobenzaldehyde and 6-methyl- 1,3,5-triazine-2,4-diamine (L) in alcohol medium gave a Schiff base and neutral tetradentate zinc(II), chromium(III), cobalt(II), Ferric(III) and copper(II) complexes were obtained by V. L. Borde et. al.[33] ^{1}H NMR, UV- visible, X-ray diffraction, microanalytical data, molar conductance, magnetic susceptibility and thermogravimetric analysis were also conducted. Antibacterial studies on *S. aureus, E. coli* and *B. subtilis* (gram positive)*, K. pneumonae* (gram negative) were conducted which gave good results.

Synthesis of a ligand from 2-hydroxy-5-methylacetophenone and glycine and its complexation with UO_2(VI), manganese(II), cobalt(II), iron(II), nickel(II), cadmium(II), zinc(II) and copper(II) ions were reported by V.B. Badwaik et. al.[34] They were

characterized by IR, ESR and electronic spectra, magnetic susceptibility measurements, electrical conductance, and thermogravimetric analysis. The complexes were found to be semiconducting in solid state DC electrical conductivity measurements in the range 313–398 K. The ligand was a monobasic bidentate (OO) donor in Zn complex whereas a dibasic tridentate (ONO) donor in other complexes. Antibacterial activities against many gram positive and gram negative bacterial strains were studied both for ligand and complexes.

A uni-negative tridentate ligand was invented by Suraj B. Ade[35] et. al. from 2-amino-4-chlorobenzoic acid and isatin. Chloride salts of Ti(IV), Zr(IV) and Cd(II) were used to convert into complexes in alcoholic medium. Characterization methods and spectral studies suggested six and four coordinated geometry for those complexes and the presence of coordinated water molecule. Tertiary nitrogen, ketonic carbonyl and carboxylic group were the donor sites in the ligand.

Achut S. Munde[36] studied the Schiff base formed from dehydroacetic acid, 4-methyl-o-phenylenediamine and salicylaldehyde and its complexes. The ligand acted as a dibasic tetradentate with ONNO donor atoms towards Cu(II), Ni(II), Co(II), Mn(II) and Fe(III) ions with 1:1 metal ligand stoichiometry. The physico-chemical studies suggested octahedral geometry for the Co(II), Mn(II) and Fe(III) complexes and square planar geometry for Ni(II) and Cu(II) complexes. TGA and DTA studies of the complexes were conducted and Horowitz–Metzger and Coats–Redfern methods were employed to determine the kinetic parameters. The powder X-ray diffraction data suggested a monoclinic crystal system for the Co(II), Mn(II) and Fe(III) complexes. Anti-fungicidal

activity against *A. niger* and *T. viride* and antibacterial activity against *S. aureus* and *E. coli* were analysed using the ligand and their metal complexes.

Badma Priya et. al.[37] reported that a Schiff base, from L-tryptophan and ′2–hydroxyacetophenone and its zinc(II), copper(II), cobalt(II), cadmium(II) and nickel(II) complexes were synthesized. The ternary ligand and complexes were characterized by spectroscopic methods. The complexes were found to have potential antimicrobial activity against *K. pneumonia, S. enterica* and *E. coli* and antifungal activity against *R. nigricans, A. flavus* and *P. notatum*.

A bidentate ligand and its complexes with Cu(II), Ni(II), Co(II) and Zn(II) ions were isolated by Sudhir S. Sawant[38] from 4-methyl-7-hydroxy-8-formylcoumarin and N-methylaminopropylenediamine. The bidentate ligand, upon complexation gave octahedral geometry. Here, the ligand and complexes were exhibiting antibacterial and antifungal activity; particularly the complexes were superior.

Complexes of Schiff bases derived from thiophene-2-carbaldehyde - a review

Literature survey reveals that a number of Schiff bases were derived from heterocyclic carbonyl compounds. The presence of hetero atoms in such ligands gives them excellent characteristics. Many researchers have reported the synthesis and characterization of Schiff bases derived from thiophene-2-carbaldehyde. A few of them are mentioned here.

Gehad Geindy Mohamed et. al.[39] synthesized a Schiff base ligand from 2-thiophenecarboxaldehyde and 2-aminothiophenol and characterized it. They reported that the ligand was tridentate on coordination to the metal ions like Co(II), Ni(II) and Cu(II) with SNS donor sites of azomethine–N, thiophene-S and thiol-S. These complexes were

assigned octahedral and tetrahedral geometries based on the magnetic and solid reflectance spectral data. On thermal decomposition these hydrated chelates lost water of hydration initially and followed by decomposition of the anions and ligand molecules. Coats-Redfern method was employed to calculate the thermodynamic parameters like ΔH, E, ΔS and ΔG from the thermogravimetric curves. The antibacterial activities of these complexes were screened on fungi and bacterial species like *P. aeruginosa, E. coli* and *S. Pyogones*. Here also, the complexes were proved to be potential inhibitors than the ligands.

Thiophene-2-carbaldehyde was condensed with 2-aminothiophenol and propane-1,2-diamine to prepare Schiff bases by Mohammad Nasir Uddin[40] and coworkers. Cadmium(II), zinc(II), nickel(II) and copper(II) complexes were prepared and characterized by elemental analysis, magnetic and spectroscopic measurements. The coordination of the ligand through nitrogen of the azomethine (-HC=N-) group and the sulfur atom of the thiophene ring was established by IR and NMR spectra. Magnetic susceptibility and conductance measurements suggested octahedral geometry and non-electrolytic nature of the complexes. *In vitro* antibacterial screening against four human pathogenic bacteria showed that some of metal chelates had high antibacterial activity and the ligands showed only moderate activity.

Microwave irradiation method was adopted for the condensation of 2-amino-1,3,4-thiadiazole with thiophene-2-carbaldehyde, furfuraldehyde and pyrrole-2-carboxaldehyde to prepare Schiff base ligands by K. P. Srivastava et. al.[41]. The process was carried out using acid catalyst in a water suspension medium and excellent yield is reported. The ligands were tridentate with two nitrogen and one oxygen atom as donor

atoms. Then copper(II), nickel(II), zinc(II) and cabalt(II) complexes were synthesized and spectrometrically and analytically studied. The antibacterial activity against four gram negative and two gram positive bacterial strains were evaluated by agar-well diffusion method and the conclusion was that upon complexation the inhibitory action was considerably increased for all compounds.

Schiff base derived from furan-2-carbaldehyde and 2-aminobenzoic acid and its complexes with Fe(III), Co(II), Ni(II), Cu(II) and Zn(II) were reported by M. M. Omar et. al[42]. Characterizations of these compounds were based on different spectroscopic, magnetic, electrical and elemental analysis. Thermal behaviour of these chelates was studied and the thermodynamic parameters were calculated using Coats-Redfern method. The ligand and its metal complexes showed biological activity against some bacterial species.

Scope of present investigation

A thorough literature survey on Schiff base compounds reveals that much systematic investigation has already been done on metal complexes of Schiff bases derived from heterocyclic carbonyl compounds. The presence of hetero atom in such Schiff bases gave them special characteristics[43-45]. It will be worthwhile to study the characteristics of Schiff bases derived from thiophene-2-carbaldehyde, furan-2-carbaldehyde and their derivatives. The synthesis, characterization and investigations on the applications of some novel Schiff bases are the prime focus of present work.

Different Schiff base ligands can be prepared from thiophene-2-carbaldehyde and furan -2-carbaldehyde with different amino compounds. Also the aryl derivatives of these heterocyclic carbonyl compounds can be converted into Schiff bases. The chelating

ability of these ligands will be evaluated by complexation with transition metal ions. Physicochemical methods such as spectroscopic, electrical, magnetic and elemental analysis can be utilized for the proper formulation of the structures of Schiff bases and their metal complexes. The thermogravimetric analysis will be useful to evaluate the thermal stabilities and the decomposition patterns of these complexes. The inhibition ability of these Schiff bases against mild steel corrosion in different acid media can be investigated by conventional weight loss method, electrochemical methods like electrochemical impedance spectroscopy (EIS) and potentiodynamic polarization studies. Also it is proposed to evaluate the antitumour activities of the copper(II) complexes of these Schiff base ligands.

Part I
Synthesis and Characterization

Chapter 2

Nimmy Kuriakose “Physicochemical, thermoanalytical, electrochemical and antitumour studies of transition metal complexes of schiff bases derived from heterocyclic carbonyl compounds” Thesis. Department of Chemistry, St. Thomas College, University of Calicut, 2015

CHAPTER 2

MATERIALS AND METHODS

In this chapter a brief description of the reagents and general procedures used for the preparation and characterization of the Schiff base ligands and complexes are described.

Materials

Analar grade samples of thiophene-2-carbaldehyde, furan-2-carbaldehyde, 3-aminobenzoic acid, phenyl hydrazine and thiocarbamoylhydrazide were purchased from Fluka for the preparation of ligands. Metal acetates from Qualigens (AR samples) were used for synthesis of the metal complexes. The medium employed for the synthesis of the compounds was pure ethanol. Solvent DMSO obtained from E Merck was used for the UV-Visible spectral studies and electrolytic conductance measurements. The general procedures for the preparation of the ligands and complexes with different metals are given in the following chapters.

Analytical methods

CHNS analysis

Estimation of carbon, hydrogen, nitrogen and sulphur in the ligands and their metal complexes were performed by microanalysis using Elementar make Vario EL III model CHN analyzer.

Spectral studies

Spectral tools like UV-Visible, infrared, ^{1}Hnmr, ^{13}Cnmr, and GCMS were used to elucidate the structure and geometry of the complexes.

***Infrared spectra*:** The infrared spectra of all the ligands and metal complexes were recorded using KBr disc technique on a Shimadzu model FT-IR Spectrometer (Model IR affinity-1). The measurements were carried out in the range 4000-400$cm^{-1.}$ The spectra help to distinguish and ascertain different groups present in the ligands and complexes since each group is characterized by definite frequency. Moreover the coordination of the ligands with the metal ion can be established with corresponding spectra.

***Electronic spectra*:** The UV-Visible spectra of the Schiff base ligands and complexes were recorded on a Shimadzu UV-Visible-1800 spectrophotometer. DMSO was used as solvent. The main perspective of electronic spectra also is structure identification.

***Mass spectra*:** Gas chromatography was conducted prior to the mass spectral studies on the Schiff bases so that purities of the compounds were confirmed. Mass spectra were recorded using QP 2010 model Shimadzu GCMS at a source temperature of 300^0C.

***NMR spectra*:** ^{1}Hnmr and ^{13}Cnmr spectral studies of ligands and complexes were performed in dmso-d_6 solvent using the instrument BRUKER AVANCE III HD**.**

Estimation of metals

Preliminary estimation of metal content in the complexes was done by pyrolytic method. About 0.2 g of the metal complex was taken in a previously weighed silica crucible and heated strongly for 2 hours using an electric bunsen. The complexes were decomposed into their respective metal oxide. It was cooled and the metal oxide left behind was weighed. From this, the percentage of metal was estimated for each complex.

Then further estimations were conducted as follows. A known amount of the metal complex was digested with a mixture of concentrated nitric and perchloric acid for one hour, during which the metal complexes were decomposed. The process was repeated for

three times by adding definite volume of nitric acid- perchloric acid mixture. The mixture was cooled and extracted with concentrated HCl. Then quantitatively transferred this solution into a volumetric flask. Estimations of different metals were conducted by taking definite volume of the solution and the percentage of the metal was found out.

Chromium was estimated by photometric method using diphenyl carbazide as the the colouring agent. Complexometric titration was employed for the estimation of nickel, cobalt and zinc using EDTA as the complexing agent. Murexide, eriochrome black-T and xylenol orange were used as indicators for nickel, cobalt and zinc respectively. Copper was estimated by iodometric titration using sodium thiosulphate as the titrant and starch as the indicator. Nickel content was also estimated by gravimetric method, using dimethylglyoxime as the precipitating agent.

Physicochemical measurements

Physicochemical techniques such as molar conductance and magnetic susceptibility measurements were conducted to elucidate the structure and geometry of the complexes. Thermogravimetric studies were also carried out.

Molar conductance measurements

ELICO Conductivity meter was employed for determination of molar conductance of the complexes. Cell constant was maintained as 1 in all measurements. 10^{-3}M concentration of solution in DMSO solvent at 30±2°C was used for measurements. This parameter gave an idea about the electrolytic nature of the compounds.

Magnetic susceptibility measurements

Gouy method was adopted for measuring the magnetic susceptibilities of the complexes at room temperature. The apparatus was from Sherwood, UK (Mark 1) and

$Hg[Co(NCS)_4]$ was used as the calibrant. The effective magnetic moments were calculated using the equation, μ_{eff} =2.84 ΨM, where ΨM is the molar susceptibility corrected for diamagnetism and T is the absolute temperature. Pascal constants were used for diamagnetic corrections due to magnetic contribution by various atoms and structural units. The theoretical magnetic moment values were calculated using the formula, μ_{eff} = g S(S+1) where g is the gyromagnetic ratio and S the total spin quantum number.

Thermogravimetric analysis

Thermogravimetric analysis (TGA) and differential thermal analysis (DTA) of the complexes were recorded on a Perkin Elmer 7 series thermal analyzer in air or oxygen atmosphere at a heating rate of $10°Cm^{-1}$. The mass loss data from the thermograms can be evaluated to assign the decomposition of particular group from the compound and also the thermal stability of the complexes.

Part I
Synthesis and Characterization

Chapter 3

Nimmy Kuriakose “Physicochemical, thermoanalytical, electrochemical and antitumour studies of transition metal complexes of schiff bases derived from heterocyclic carbonyl compounds” Thesis. Department of Chemistry, St. Thomas College, University of Calicut, 2015

CHAPTER 3

STUDIES ON SCHIFF BASE, 3-(1H-INDOL-3-YL)-2-[(E)-(THIOPHEN-2-YL METHYLIDENE)AMINO]PROPANOIC ACID AND ITS TRANSITION METAL COMPLEXES

The Schiff base, 3-(1H-indol-3-yl)-2-[(E)-(thiophen-2-ylmethylidene)amino] propanoic acid (I3YT2YMAPA) was synthesized and characterized by IR, UV-visible, NMR and mass spectroscopic techniques. Elemental analysis was also carried out. Transition metal complexes of this ligand were prepared with Cr(III), Ni(II), Cu(II) and Zn(II) ions. All the complexes were characterized by NMR, IR and UV-visible spectroscopic methods, magnetic moment measurements, elemental analysis and molar conductance measurements. The synthesis and characterization of the ligand and complexes are detailed in this chapter.

Synthesis of ligand

Equimolar mixture of thiophene-2-carbaldehyde and (s)-2-amino-3-(3-indolyl) propanoic acid were taken in ethanol medium and was refluxed for 3 hours on a water bath. The volume of the reaction mixture was reduced by evaporation and cooled. Then the mixture was poured into ice cold water to obtain pale yellow coloured solid. The heterocyclic Schiff base, 3-(1H-indol-3-yl)-2-[(E)-(thiophen-2-ylmethylidene)amino] propanoic acid was obtained with 78% yield and the melting point noted was 264^0C. The elemental analysis data of the ligand is given in Table 1.2.

Characterization of ligand

All the ligands were amorphous solids and stable to light and air. They were characterized by various techniques and the details are given below.

IR spectral studies

Characteristic stretching frequencies of various bonds in I3YT2YMAPA were obtained from the IR spectrum. The data is given in Table 1.3. A sharp peak observed at 3400cm^{-1}, corresponds to stretching vibration of the N-H group in the indole ring. Another band of fairly strong intensity at 3039cm^{-1} was due to the aromatic C-H bond stretching vibration. The C-H bond involving sp^3 hybridized carbon gave characteristic bands at 2927cm^{-1} and 2854cm^{-1}. The asymmetric stretching vibrations of the caboxylate group appeared as a band of medium intensity at 1664cm^{-1}. A sharp peak was obtained at 1591cm^{-1} which was characteristic of the azomethine group. A band at 1014cm^{-1} corresponds to $\upsilon_{C\text{-}O}$. In plane and out of plane deformations were shown at 1014cm^{-1} and 746cm^{-1} respectively.

NMR spectral studies

The ^{1}Hnmr spectrum of the Schiff base is given in Figure 1.1. Thirteen non equivalent hydrogen atoms which were in different electronic environments gave characteristic peaks in the nmr spectrum. The assignments of the signals are given in Table 1.1. The carboxylic proton in the molecule gave a distinct singlet at 10.83δ. A peak at 3.37δ can be assigned to the azomethine proton. The NH proton in the tryptophan part appeared as a broad signal at 3.24δ. The presence of a sharp singlet at 2.43δ can be assigned to the CH proton in the five membered ring of the tryptophan part. A peak obtained at 2.89δ can be assigned to CH_2 group adjacent to the indole ring. The aromatic protons gave characteristic peaks at 6.8-7.5δ.

The proton decoupled ^{13}Cnmr spectrum of the Schiff base is represented in Figure 1.2. Sixteen carbon atoms in different electronic environments gave their own

characteristic peaks in the spectrum. The signal of the carboxylic acid carbon appeared at 169.78ppm. The azomethine carbon showed a peak at 136.32ppm. The aromatic carbons in the thiophene and tryptophan rings appeared at 109.73-136.32ppm region. Methylene and azomethine carbon atoms exhibited their peaks at 27.19 and 54.78ppm respectively. The signal assignments are given in Table 1.1.

Table 1.1 ^{1}Hnmr and ^{13}Cnmr spectral data of I3YT2YMAPA

^{1}Hnmr			^{13}Cnmr		
	δ value	Assignment/ Labelled No.	δ value	Assignment/ Labelled No.	
	2.89	1(CH_2)	27.19	1(CH_2)	
	2.43	2	54.78	2	
	3.37	3(CH=N)	136.32	3(CH=N)	
	3.24	4(NH)	123.96	4	
	7.13	5	109.73	5	
	7.27	6	109.73	6	
	6.91	7	118.23	7	
	6.99	8	111.28	8	
	7.49	9	111.28	9	
	7.27	10	118.23	10	
	6.90	11	136.32	11	
	7.49	12	127.26	12	
	10.83	13(COOH)	118.34	13	
			120.86	14	
			118.34	15	
			169.78	16(COOH)	

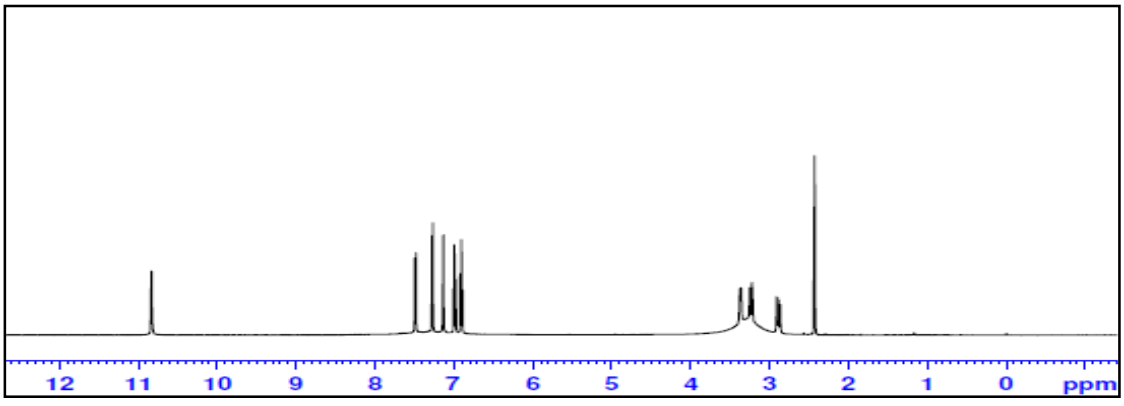

Fig.1.1 ^{1}Hnmr spectrum of I3YT2YMAPA

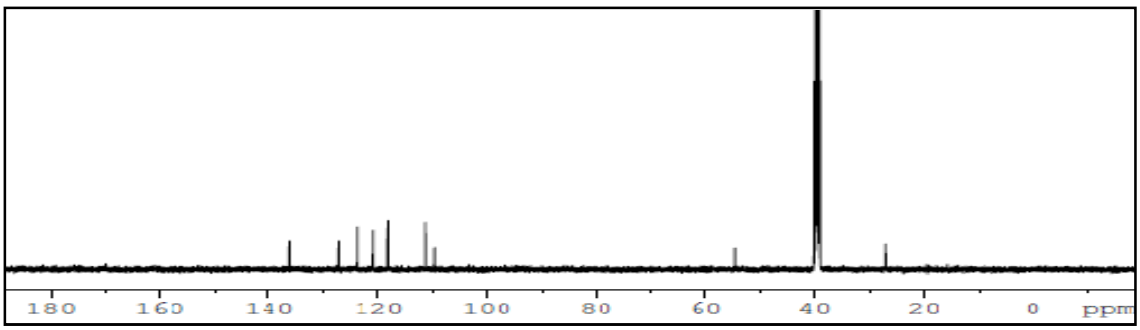

Fig.1.2 ^{13}Cnmr spectrum of I3YT2YMAPA

Mass spectral studies

The molecular ion peak appeared at m/z 298 as a very weak signal and isotopic peaks were found to be absent. The base peak was shown at m/z 130 due to $[C_9H_8N]^+$ ion. The loss of OH moiety gave a signal at m/z 281. A medium intensity peak at m/z 204 corresponds to the fragment $[C_{11}H_{12}N_2O_2]^+$. The $[C_8H_7N]^+$ fragment showed a signal at m/z 117. The appearance of peaks at m/z 103 and 77 were due to the fragments $[C_8H_7]^+$ and $[C_6H_5]^+$ respectively. The mass spectrum is represented in Figure 1.3.

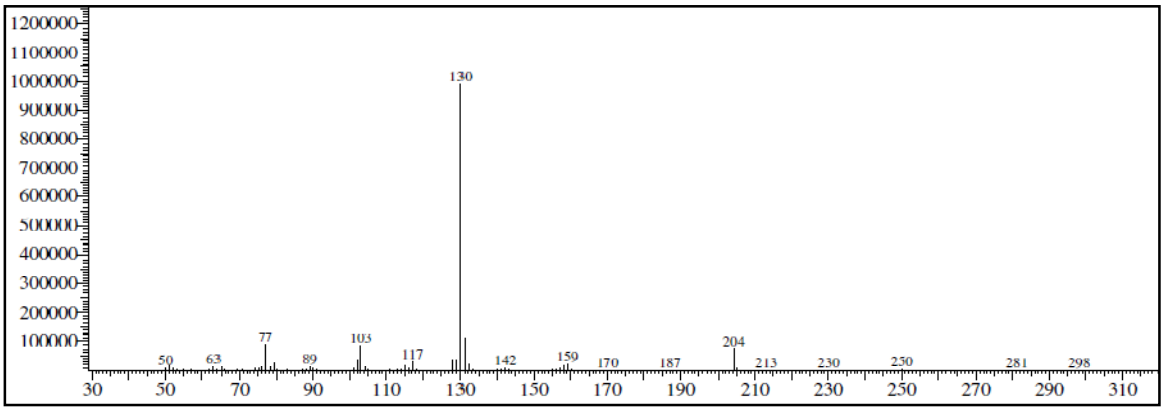

Fig.1.3 Mass spectrum of I3YT2YMAPA

Electronic spectral studies

Two peaks were obtained in the UV-visible spectrum of the Schiff base. They were exhibited at 35335cm^{-1} and 32679cm^{-1} which can be assigned to $\pi \rightarrow \pi^*$ and $n \rightarrow \pi^*$ transitions respectively.

All the above characterization results lead to the assignment of structure of the Schiff base, 3-(1H-indol-3-yl)-2-[(E)-(thiophen-2-ylmethylidene)amino]propanoic acid (I3YT2YMAPA) as shown in Figure 1.4.

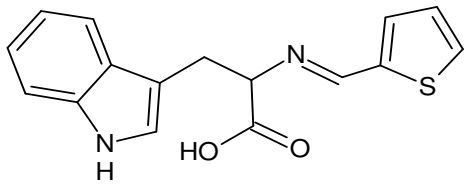

Fig.1.4 Structure of I3YT2YMAPA

Synthesis of complexes

Cr(III), Ni(II), Cu(II) and Zn(II) complexes of the Schiff base, 3-(1H-indol-3-yl)-2-[(E)-(thiophen-2-ylmethylidene)amino]propanoic acid (I3YT2YMAPA) were synthesized as follows.

Acetate salts of chromium, nickel, copper and zinc were used for the synthesis. 2mM solution of the Schiff base, I3YT2YMAPA in 15ml ethanol was refluxed on a water bath. When the solution was boiled, 2mM hot ethanolic solution of the metal salt was added and again refluxed for 2 hours. Then reduced the volume, cooled and poured the contents into ice cold water. The precipitated complex was filtered, washed and dried over an. $CaCl_2$. Melting points of the complexes were noted. The melting points of all the complexes were higher than that of the ligand.

Characterization of complexes

All the complexes were amorphous solids and stable to light and air. They are characterized by various techniques like elemental analysis, magnetic moment

measurements, molar conductance studies, spectral studies and thermogravimetric analysis. The details are given below.

Elemental analysis

Elemental analysis provides the key to structural determination of the complexes. The metal percentage of copper complex was determined by volumetric method iodometrically while that of chromium and nickel complexes were done by colorimetric and gravimetric methods respectively. The theoretical and calculated values were found to be in good agreement in the case of all complexes. 1:1 stoichiometry was found to exist between the metal and ligand in all the chelates. The CHNS data of the complexes are given in Table 1.2 which also establishes the 1:1 ratio between metal and ligand.

Magnetic moment studies

Magnetic moment measurements helped in ascertaining the geometries of the complexes. The Cr(III) and Ni(II) chelates were found to have magnetic moment 3.61BM and 2.99BM respectively and octahedral geometry was assigned for both complexes. In the case of copper complex μ_{eff} was 1.61BM and hence square planar geometry was fixed for it[46]. Diamagnetic character was found for Zn(II) complex, which is quite justifiable with its d^{10} configuration and hence tetrahedral geometry was assigned[47].

Molar conductance studies

The electrolytic behaviour of metal chelates was investigated by molar conductance studies. The measurements were done in DMSO medium and all chelates showed molar conductance in the range 5-7$\Omega^{-1}cm^2mol^{-1}$. So non-electrolytic behaviour was assigned for all the chelates. It can also be confirmed that counter ions were absent outside the coordination sphere. The data is represented in Table 1.2.

IR spectral studies

The IR spectral data of the ligand and metal chelates are displayed in Table 1.3. The shifting in vibrational frequencies of the complexes on comparison with that of the ligand can be clearly understood from the data provided. The vibrational frequency of the azomethine group was found to be lowered in the case of all complexes which confirmed the coordination of the group towards the metal ion[48-50]. Appearance of new bands around 3330cm^{-1} for all the complexes ensured the presence of coordinated water molecules. Antisymmetric and symmetric stretching vibrations of the COO group gave characteristic peaks in the spectrum of all the chelates. The shift in frequency of these bands to lower region establishes the coordination through the carboxylate oxygen to the central metal ion. Moreover the appearance of new bands for M-O and M-N bonds, unequivocally confirm the ON donor sites of the Schiff base.

NMR spectral studies

The NMR spectra of the complexes were complicated when compared to that of the ligand. All the peaks showed downward shift in the spectra which ensured the binding of the ligand with the metal ion through coordination sites. The disappearance of COOH peak in the spectra of chelates confirms the metal-oxygen bond through carboxylate group, after deprotonation.

Electronic spectral studies

The complexes exhibited additional bands for d-d transitions and charge transfer processes, other than the intra ligand electronic transitions (ILT). Upon complex formation all the ILT bands were shifted to longer wavelength region. Cr(III) complex showed three d-d transitions at 26463cm^{-1}, 31354cm^{-1} and 37325cm^{-1} which were due to

$^4A_2(F) \rightarrow {}^4T_2$, $^4A_2(F) \rightarrow {}^4T_2(F)$ and $^4A_2 \rightarrow {}^4T_1(P)$ transitions respectively in the octahedral field. The Ni(II) complex exhibited two bands at 31328cm^{-1} and 33671cm^{-1} which corresponds to $^3A_2 \rightarrow {}^3T_2$ and $^3A_2 \rightarrow {}^3T_1(F)$ electronic transitions. These transitions confirmed the octahedral geometry for the chelate[51]. For the Cu(II) complex, two bands at 29158cm^{-1} and 39217cm^{-1} can be assigned to the transitions $^2B_1 \rightarrow {}^2A_1$ and $^2B_1 \rightarrow {}^2B_2$ respectively and hence suggested square planar geometry. Appearance of an intense peak at 26732cm^{-1} in the electronic spectrum of Zn(II) complex was due to ligand to metal CT band.

Thermogravimetric studies

Thermogravimetric analysis of the Ni(II) complex of I3YT2YMAPA exhibited three stage decomposition pattern. The first stage comprised of two substages. In the first substage (60-120^{0}C) the coordinated water molecule was lost from the chelate molecule. The remaining two water molecules and the acetate group were lost in the next substage (120-305^{0}C). The second stage represented the loss of tryptophan moiety from the ligand. Finally rest of the ligand was undergone decomposition so as to yield the oxide (NiO) and represented the third stage. The overall mass loss according to the TG curve is 84.20%. The theoretical mass loss for the conversion of the complex into metal oxide is 84.08%. The results are well documented in part IV.

All the above discussions clearly established that the structures of metal chelates of I3YT2YMAPA are as represented in Figure 1.5.

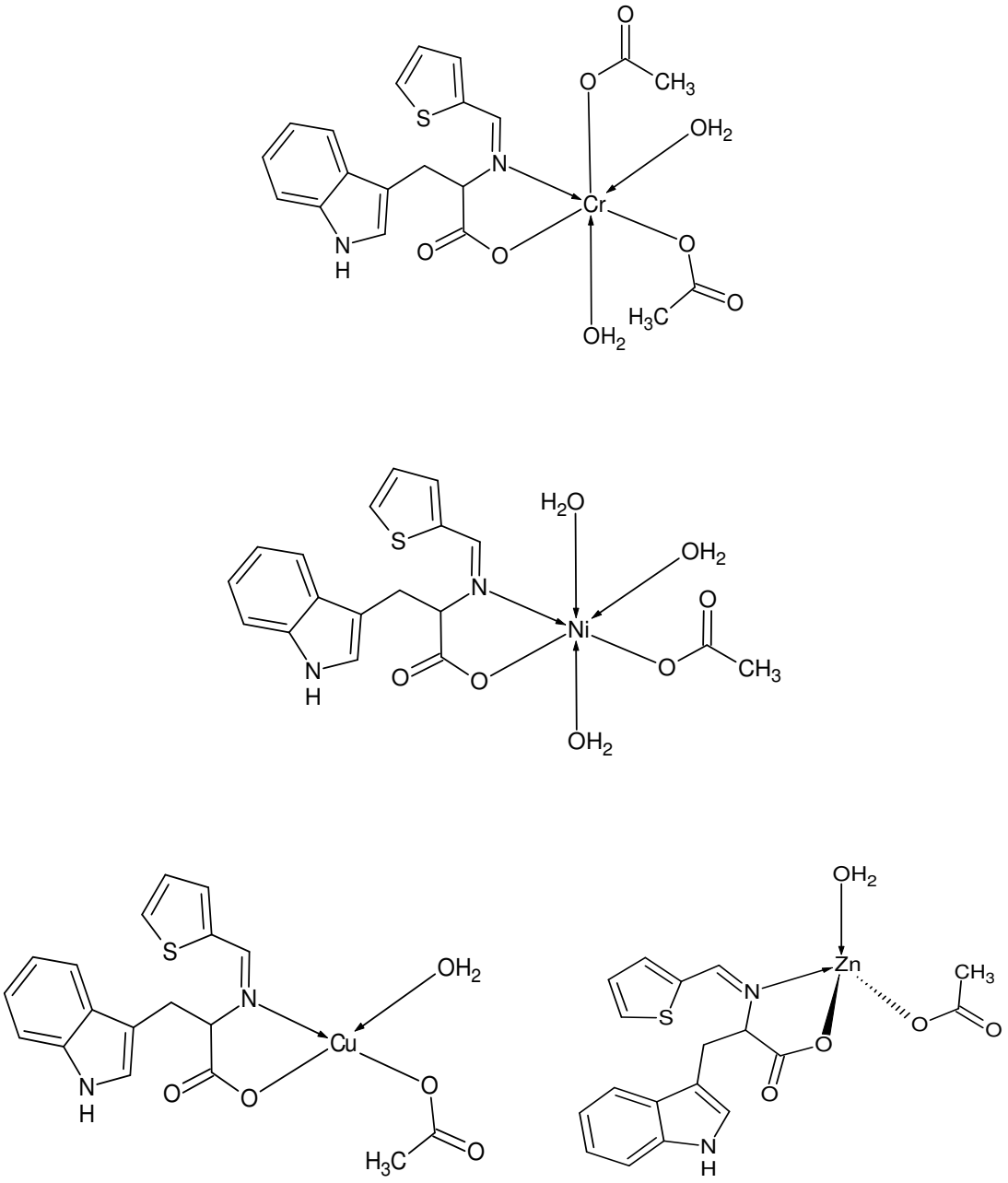

Fig.1.5 Structures of metal complexes of I3YT2YMAPA

Table 1.2 Microanalytical, magnetic and conductance data of the ligand I3YT2YMAPA and its transition metal complexes

Complex	Colour	Yield (%)	Mol. Wt.	M.P (^{0}C)	Metal % Found (Calculated)	C % Found (Calculated)	H % Found (Calculated)	N % Found (Calculated)	S % Found (Calculated)	μ_{eff} (BM)	Molar Conductance ($\Omega^{-1}cm^2mol^{-1}$)	Geometry
I3YT2YMAPA (LH)	Palle yellow	78	298	264	-	63.98 (64.43)	4.67 (4.70)	9.84 (9.40)	10.68 (10.74)	-	-	-
$[CrLAc_2(H_2O)_2]$	Pale brown	68	503	>300	10.26 (10.34)	46.88 (47.71)	4.31 (4.77)	6.21 (5.57)	5.86 (6.36)	3.61	6	Octahedral
$[NiLAc(H_2O)_3]$	Pale Green	73	469	>300	13.25 (12.52)	45.97 (46.08)	4.71 (5.33)	5.74 (5.97)	6.04 (6.83)	2.99	5	Octahedral
$[CuLAc(H_2O)]$	Blue	80	438	262	14.98 (14.52)	50.34 (49.37)	4.53 (4.11)	6.98 (6.39)	8.57 (7.31)	1.61	6	Square planar
$[ZnLAc(H_2O)]$	Off white	66	440	>300	14.80 (14.88)	48.46 (49.16)	5.11 (5.00)	6.27 (6.37)	7.10 (7.28)	D	7	Tetrahedral

Ac: Acetate, D: Diamagnetic

Table 1.3 Characteristic infrared absorption frequencies of I3YT2YMAPA and its transition metal complexes

Complex	υ_{N-H}	υ_{H2O}	$\upsilon_{C-H\ (Ar)}$	$\upsilon_{C-H\ (SP^3\ C)}$	$\upsilon_{COO\ (asym)}$	$\upsilon_{C=N}$	$\upsilon_{COO\ (sym)}$	υ_{C-O}	In plane bending	Out of plane bending	υ_{M-O}	υ_{M-N}
I3YT2YMAPA (LH)	3400	-	3039	2927, 2854	1664	1591	-	1129	1014	746	-	-
$[CrLAc_2(H_2O)_2]$	3402	3305	3138	2929	1631	1583	1541	1242	1004	758	640	510
$[NiLAc(H_2O)_3]$	3404	3332	3057	2922, 2852	1630	1583	1456	1233	1045	744	628	503
$[CuLAc(H_2O)]$	3388	3334	3095	2906	1625	1571	1473	1105	1006	738	601	508
$[ZnLAc(H_2O)]$	3402	3331	3120	2954, 2389	1618	1595	1454	1089	1043	740	598	491

Part I
Synthesis and Characterization

Chapter 4

Nimmy Kuriakose “Physicochemical, thermoanalytical, electrochemical and antitumour studies of transition metal complexes of schiff bases derived from heterocyclic carbonyl compounds” Thesis. Department of Chemistry, St. Thomas College, University of Calicut, 2015

CHAPTER 4

STUDIES ON SCHIFF BASE, 3-[THIOPHEN-2-YLMETHYLENEAMINO] BENZOIC ACID AND ITS TRANSITION METAL COMPLEXES

A novel Schiff base (E)-3-[thiophen-2-ylmethyleneamino]benzoic acid was synthesized and characterized by elemental analysis and various spectroscopic techniques. The chelating efficacy of the ligand was explored by synthesizing transition metal complexes with metal ions of chromium, nickel, copper, zinc and cadmium. The details of synthesis and characterization of both the ligand and complexes are detailed in this chapter.

Synthesis of ligand

The Schiff base (E)-3-[thiophen-2-ylmethyleneamino]benzoic acid (T2YMABA) was synthesized by mixing equimolar mixture of ethanolic solutions of thiophene-2-carbaldehyde and 3-aminobenzoic acid. The mixture was refluxed for 3 hours on a boiling water bath. Then volume of the reaction mixture was reduced by evaporation and allowed to cool. Finally the mixture was poured into ice cold water to get pale yellow coloured ligand. It was filtered and dried. The yield of the product was 82% and the melting point recorded was 136^0C. The elemental analysis data of the ligand is given in Table 1.5.

Characterization of ligand

The ligand was characterized by different spectroscopic tools like infrared, NMR, mass and electronic spectroscopy**.**

IR spectral studies

The IR spectrum of the compound showed a scalloped band at 3000cm^{-1} corresponding to vibration of the OH group, which was overlapped with aromatic C-H stretching vibration. The vibrational frequency band of sp^2 hybridized C-H bond showed the corresponding band at 3062cm^{-1}. The asymmetric stretching vibrations of carboxylic group gave a characteristic band at 1689cm^{-1}. The azomethine moiety (C=N) was identified by the peak at 1579cm^{-1}. υ_{C-O} was observed at 1292cm^{-1}. The in-plane deformation was shown at 1197cm^{-1} and out of plane deformations were at 914cm^{-1} and 717cm^{-1}. The data is given in Table 1.6.

NMR spectral studies

The proton NMR spectrum of the Schiff base T2YMABA is given in Figure 1.6. A singlet at 12.93δ can be assigned to the proton of the COOH group. The proton attached to the azomethine carbon gave a singlet at 3.25δ which was broadened due to presence of nearby nitrogen. The aromatic protons of both thiophene ring and benzene ring appeared in 7.17δ–7.77δ region. These seven peaks showed multiplicity according to ortho, meta and para coupling. The assignments of signals are given in table 1.4.

In the ^{13}Cnmr spectrum twelve peaks were obtained corresponding to twelve chemically different carbons. The carboxylic carbon gave a sharp peak at 167ppm. The azomethine carbon appeared at 154ppm. There were ten aromatic carbons present in thiophene ring and benzene ring together. Correspondingly ten different peaks were obtained in the region 121–150ppm region. The spectrum is given in Figure 1.7.

Table 1.4 [1]Hnmr and [13]Cnmr spectral data of T2YMABA

[1]Hnmr			[13]Cnmr		
	δ value	Assignment/ Labelled No.	δ value	Assignment/ Labelled No.	
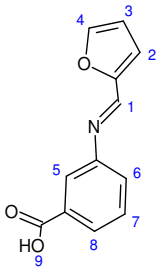	3.25(br,s)	1(CH=N)	154.99	1(CH=N)	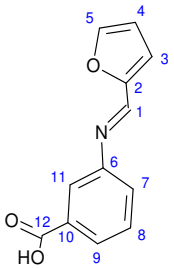
	7.67	2	128.29	2	
	7.44	3	126.70	3	
	7.17	4	121.34	4	
	8.79	5	125.77	5	
	7.73	6	142.19	6	
	7.70	7	132.01	7	
	7.77	8	129.54	8	
	12.93(s)	9	131.57	9	
			150.94	10	
			134.19	11	
			167.03	12(COOH)	

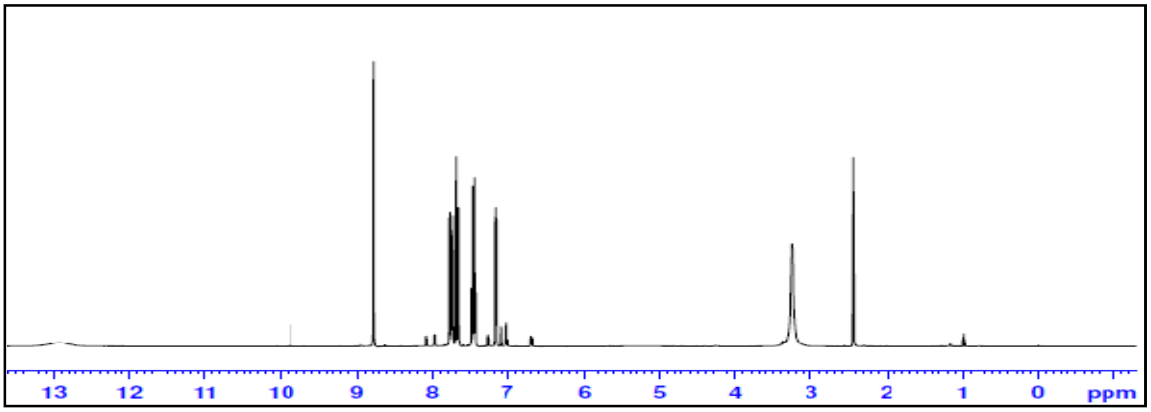

Fig.1.6 [1]Hnmr spectrum of T2YMABA

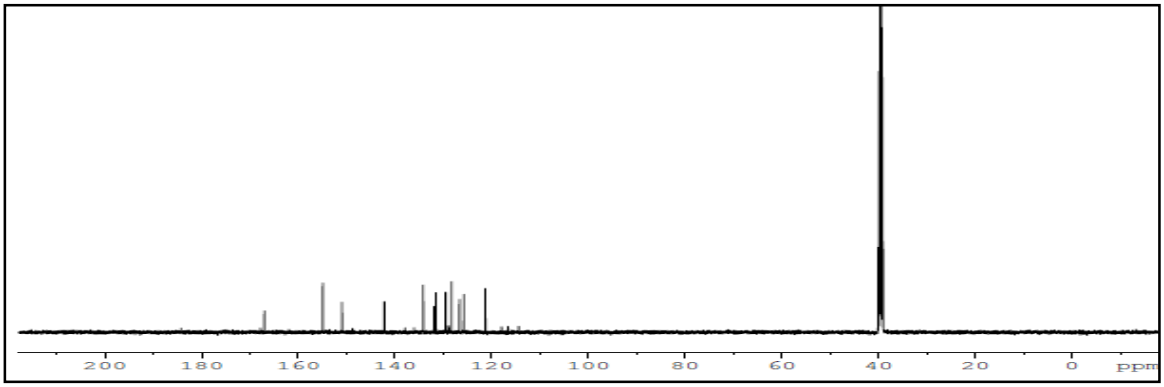

Fig.1.7 [13]Cnmr spectrum of T2YMABA

Mass spectral studies

The mass spectrum is represented in Figure 1.8. The presence of only one peak in the gas chromatogram showed the purity of the compound. The molecular ion peak was obtained at m/z 231 which was the base peak. This indicated the stability of the compound. A peak obtained at m/z 232 represents [M+1] peak. The [M]:[M+1] ratio observed in the EIMS was 100:13.5 which establishes the presence of twelve carbon atoms in the molecule. The [M+2] peak at m/z 233 was due to presence of sulphur. The fragment $[C_{12}H_8NO_2S]^+$ was indicated by peak at m/z 230. Loss of a COOH from the molecule resulted with a peak at m/z 186 which corresponds to $[C_{11}H_8NS]^+$. Peaks at m/z 121 and 84 were due to the fragments $[C_7H_5O_2]^+$ and $[C_4H_4S]^+$ respectively.

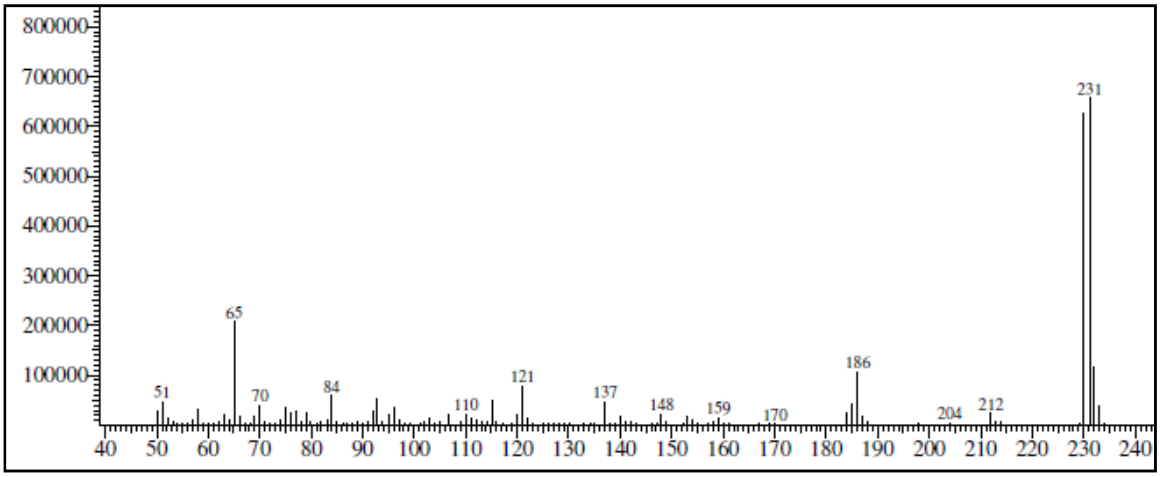

Fig.1.8 Mass spectrum of T2YMABA

Electronic spectral studies

The appearance of two peaks at 39062cm^{-1} and 32154cm^{-1} in the electronic spectrum of the Schiff base T2YMABA can be attributed to $\pi\rightarrow\pi^*$ and $n\rightarrow\pi^*$ electronic transitions in the molecule.

On the basis of all the above discussions the structure of the Schiff base T2YMABA can be represented as in Figure1.9.

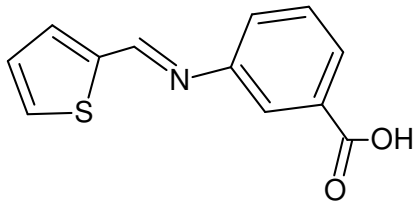

Fig.1.9 Structure of T2YMABA

Synthesis of complexes

Cr(III), Ni(II), Cu(II), Zn(II) and Cd(II) complexes of the Schiff base 3-[thiophen-2-ylmethyleneamino]benzoic acid were synthesized as per the procedure detailed hereafter. The Schiff base (E)-3-[thiophen-2-ylmethyleneamino]benzoic acid and the metal salt were taken in 1:1 ratio in ethanolic medium. The mixture was refluxed for two hours on a water bath. Finally the volume of the solution was reduced by evaporation and then cooled. The precipitated complexes were filtered and washed with ethanol-water mixture. The complexes were first dried on a water bath and then kept over an.$CaCl_2$. Melting points of all the complexes were noted. All the chelates were obtained in good yield.

Characterization of complexes

The metallic chelates of T2YMABA were characterized by elemental and spectral studies. IR and ^{1}Hnmr spectral studies were helpful in determining the denticity of the ligand. All the complexes were found to be stable to air and light. The following explanations give the structural evaluation of the metal complexes.

Elemental analysis

Analysis of the elements in the complexes gave identification regarding the stoichiometry of the complexes. The elemental analysis data are given in Table 1.5. There is good correlation between the observed and calculated values. The percentages of

elements obtained indicated the correct molecular formula of the complexes. All the complexes were found to have 1:1 stoichiometry between the metal and ligand T2YMABA.

Magnetic moment measurements

The effective magnetic moment values of the chelates are given in the Table 1.5. Measurements of magnetic susceptibility values provided a strong support for the determination of exact geometry of the complexes. The chromium(III) complex with a d^3 system, had magnetic moment 3.41BM which is slightly less than the expected value. This may be due to the antiferromagnetic interaction between the metal ions and hence an octahedral dimeric structure with two bridged acetate groups was assigned for this complex[52-54]. In the case of nickel(II) complex also octahedral geometry was assigned since the magnetic behavior was shown with 2.69BM value. The existence of cupric ion state in the copper complex of T2YMABA was ascertained by the appearance of μ_{eff} value 1.72BM, which is quite expected for d^9 configuration. Therefore square planar geometry was fixed for Cu(II) chelate. Tetrahedral geometry was assigned for both the zinc(II) and cadmium(II) complexes. These chelates were found to be diamagnetic in their magnetic moment measurement studies and this result was very much expected since Zn(II) and Cd(II) ions were having no unpaired electrons[55-57].

Molar conductance studies

Molar conductance measurements were conducted in DMSO solvent. All the transition metal complexes of T2YMABA exhibited molar conductance values in the range 3-10$\Omega^{-1}cm^2mol^{-1}$ suggesting that all the compounds were non-electrolytic in nature. The data is represented in Table1.5.

IR spectral studies

The IR spectral data of all the complexes are given in Table1.6. The coordination of the ligand through the azomethine group was confirmed by the downward shift of the peak in the spectra of all the complexes. The appearance of new bands around 3400cm^{-1} which was absent in the spectrum of the ligand, confirmed the presence of coordinated water molecules in all the chelates. The asymmetric stretching vibrations of the carboxylate group showed considerable shift in frequencies for all the complexes which clearly indicated the coordination of the group to the metal ion. The difference between the asymmetric and symmetric stretching vibrations ($\Delta\upsilon$) was found to be greater than 150cm^{-1} which confirmed the monodentate nature of the carboxylate group[58]. The appearance of new bands corresponding to υ_{M-N} and υ_{M-O} transitions strongly confirmed the complexations in all chelates.

^{1}Hnmr spectral studies

The ^{1}Hnmr spectra of complexes provided supporting evidences in assigning the binding sites of the ligand. The down field shift of the peaks, compared with the spectra of the ligand, indicated the complexation. The disappearance of carboxylic proton peak in the ^{1}Hnmr spectra of the complexes confirmed the coordination of the deprotonated carboxylic group of the ligand to the central metal atom. The shift in the azomethine proton peak to low field region indicated the involvement of C=N group in coordination.

Electronic spectral studies

Intra ligand electronic transitions and d-d transitions were shown as peaks in the optical absorption spectrum of all the complexes. In the case of Cr(III) complex two additional bands at 38910cm^{-1} and 30441cm^{-1} were obtained which corresponds to and

$^4A_2 \rightarrow {}^4T_1(P)$ and $^4A_2(F) \rightarrow {}^4T_2(F)$ transitions. $^3A_2 \rightarrow {}^3T_2$ and $^3A_2 \rightarrow {}^3T_1(F)$ electronic transitions in the nickel(II) complex in an octahedral environment gave characteristic peaks at 31104cm^{-1} and 38462cm^{-1} respectively. In copper(II) complex $^2B_1 \rightarrow {}^2A_1$ and $^2B_1 \rightarrow {}^2B_2$ transitions were shown as peaks at 30581cm^{-1} and 37665cm^{-1} respectively and complex was assigned square planar geometry. Only two intra ligand transition bands were exhibited in Zn(II) complex at 30912cm^{-1} and 38536cm^{-1} and charge transfer transitions were found to be absent in the electronic spectrum. Cd(II) complex exhibited a LMCT band at 38911cm^{-1}.

Thermogravimetric studies

TGA and DTA studies of Cr(III) complex of T2YMABA gave a four stage decomposition pattern. The loss of two coordinated water molecules from the sample moiety was observed in the temperature range of 60-140^{0}C. The loss of two acetate groups and two CO_2 molecules occurred in two substages of the second stage, i.e., IIa and IIb respectively. Rest of both the ligands and two bridged acetate groups were removed in the third and fourth stages respectively. The overall mass loss according to the TG curve was 81.53% and the theoretical mass loss was 81.82%.

The decomposition pattern of Ni(II) complex of T2YMABA comprised of two stages. In the first stage all the three coordinated water molecules from the complex were lost in the temperature range 117-243^{0}C. The loss of ligand and acetate group was observed in the second stage at 429^{0}C. The overall mass loss according to the TG curve and the theoretical mass loss for the conversion of the complex into corresponding oxide were 81.15% and 81.34% respectively. These data were to be in agreement with the result obtained during pyrolytic studies.

All the characterization methods detailed above led to assignment of structures of the complexes of T2YMABA as given in Figure 1.10.

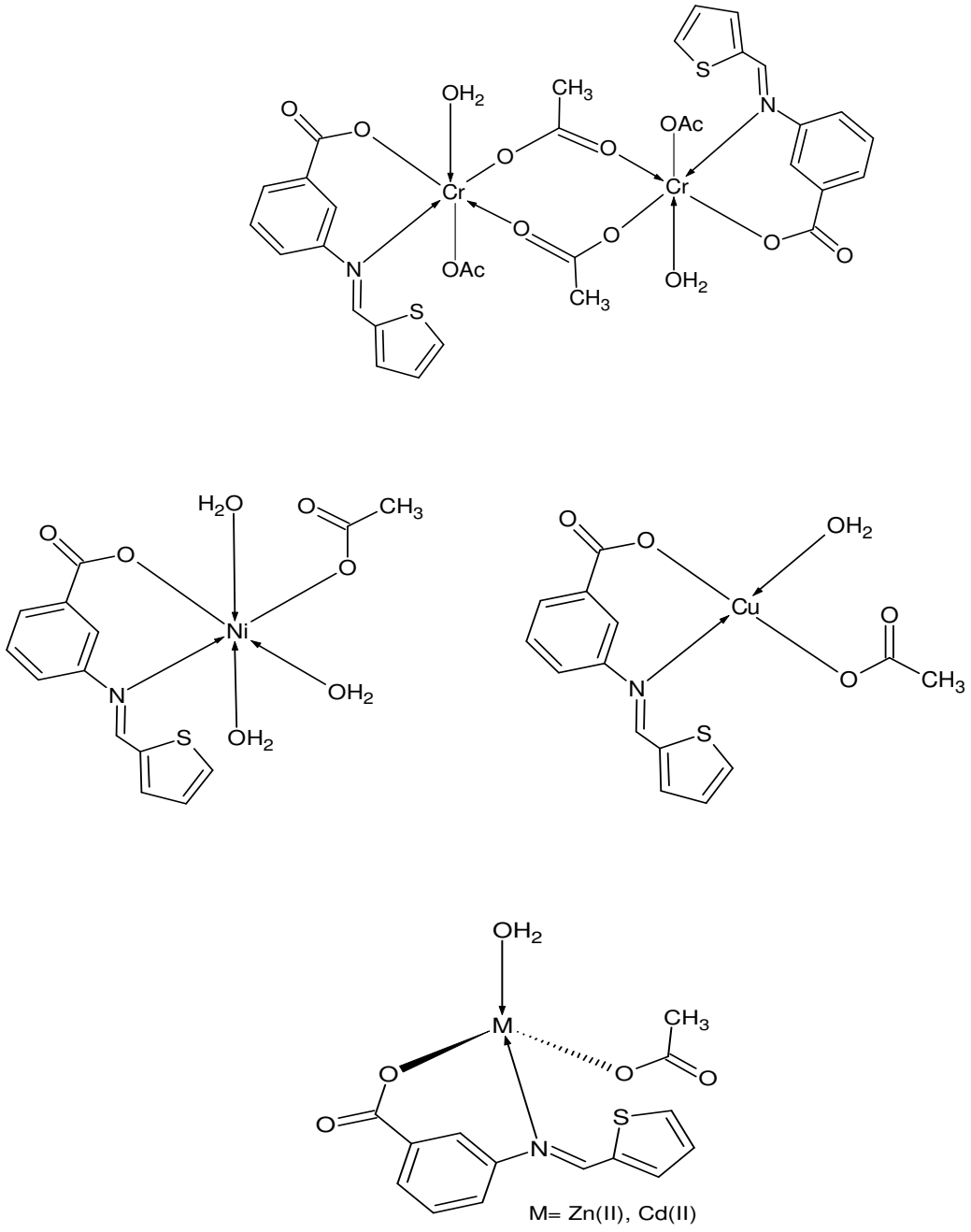

Fig.1.10 Structures of metal complexes of T2YMABA

Table 1.5 Microanalytical, magnetic and conductance data of the ligand T2YMABA and its transition metal complexes

Complex	Colour	Yield (%)	Mol. Wt.	M.P (^{0}C)	Metal % Found (Calculated)	C % Found (Calculated)	H % Found (Calculated)	N % Found (Calculated)	S % Found (Calculated)	μ_{eff} (BM)	Molar Conductance ($\Omega^{-1}cm^2mol^{-1}$)	Geometry
T2YMABA(LH)	Pale yellow	70	231	136	-	63.84 (62.34)	3.81 (3.90)	7.04 (6.06)	14.11 (13.85)	-	-	-
$[CrLAc_2(H_2O)]_2$	Pale green	76	418	>300	13.86 (12.44)	46.75 (45.93)	3.76 (3.83)	2.48 (3.55)	6.48 (7.66)	3.41	5	Octahedral
$[NiLAc(H_2O)_3]$	Pale Green	81	402	>300	15.28 (14.61)	42.60 (41.82)	4.30 (4.23)	4.20 (3.49)	8.65 (7.97)	2.69	8	Octahedral
$[CuLAc(H_2O)]$	Blue	81	371	>300	17.13 (17.16)	45.16 (45.33)	3.01 (3.51)	4.34 (3.78)	8.75 (8.63)	1.72	7	Square planar
$[ZnLAc(H_2O)]$	Grey	64	372	>300	18.50 (17.56)	46.45 (45.11)	3.92 (3.49)	4.04 (3.76)	8.68 (8.59)	D	10	Tetrahedral
$[CdLAc(H_2O)]$	Pale brown	70	419	>300	25.89 (26.73)	41.17 (40.10)	3.09 (3.10)	4.28 (3.34)	8.18 (7.64)	D	3	Tetrahedral

Ac: Acetate, D: Diamagnetic

Table 1.6 Characteristic infrared absorption frequencies of T2YMABA and its transition metal complexes

Complex	υ_{O-H}	υ_{H2O}	$\upsilon_{C-H(SP^2)}$	$\upsilon_{COO(asym)}$	$\upsilon_{C=N}$	$\upsilon_{COO(sym)}$	$\upsilon_{C-Hbend}$	υ_{C-O}	In plane bending.	Out of plane bending	υ_{M-O}	υ_{M-N}
T2YMABA(LH)	~3000 (Scalloped band)	-	3062	1689	1579	-	1415	1292	1197	914, 717	-	-
$[CrLAc_2(H_2O)]_2$	-	3373	3103	1616	1560	1541	1456, 1406	1202	1042	903, 767	576	518
$[NiLAc(H_2O)_3]$	-	3387	3064	1606	1552	1527	1452, 1398	1244	1014	925, 771	582	504
$[CuLAc(H_2O)]$	-	3423	3136	1629	1568	1525	1456, 1404	1151	1074	896, 759,677	564	459
$[ZnLAc(H_2O)]$	-	3452	3099	1627	1571	1498	1404, 1390	1165	1078	925, 759,680	538	439
$[CdLAc(H_2O)]$	-	3354	3057	1681	1579	1543	1448, 1388	1240	988	916, 777,678	557	513

Part I
Synthesis and Characterization

Chapter 5

Nimmy Kuriakose “Physicochemical, thermoanalytical, electrochemical and antitumour studies of transition metal complexes of schiff bases derived from heterocyclic carbonyl compounds” Thesis. Department of Chemistry, St. Thomas College, University of Calicut, 2015

CHAPTER 5

STUDIES ON SCHIFF BASE, 4-(5-[(2-CARBAMOTHIOYLHYDRAZONO) METHYL]THIOPHEN-2-YL)BENZOIC ACID AND ITS TRANSITION METAL COMPLEXES

Synthesis and characterization of the Schiff base (E)-4-(5-[(2-carbamothioyl hydrazono)methyl]thiophen-2-yl)benzoic acid is explained in detail in this chapter. The chelating efficiency of this ligand was tested with metal ions Cr(III), Co(II), Ni(II), Cu(II) and Zn(II). These complexes were also subjected to characterization studies like elemental analysis, magnetic moment measurements and spectroscopic techniques like IR, UV-Visible and NMR spectroscopy.

The Schiff base was prepared by a two step process, first step being Meervin arylation of the thiophene-2-carbaldehyde, followed by condensation reaction with the amino compound.

Thiophene-2-carbaldehyde was arylated by the standard method for Meerwin arylation[56]. A solution of p-aminobenzoic acid (75mM) in 100ml of water was prepared along with the addition of 40ml conc. HCl. This solution was cooled in an ice bath to lower the temperature of 0-5^{0}C range. To this, a solution of 91mM solution of sodium nitrite in 35ml of water was added slowly and stirred well. In order to complete the diazotization reaction, the mixture was kept for 20 minutes. Then added 75mM solution of thiophene-2-carbaldehyde in 50ml acetone to the above solution followed by $CuCl_2.2H_2O$ solution (23mM in 25ml water) with stirring. Kept this reaction mixture for two days with occasional shaking. A yellow coloured precipitate formed was filtered, washed with plenty of warm water and dried. The melting point of this arylated

derivative, 4-(5-formylthiophen-2yl)benzoic acid (FT2YBA) was 281^{0}C. The scheme of Meerwin arylation is given in Figure 1.11.

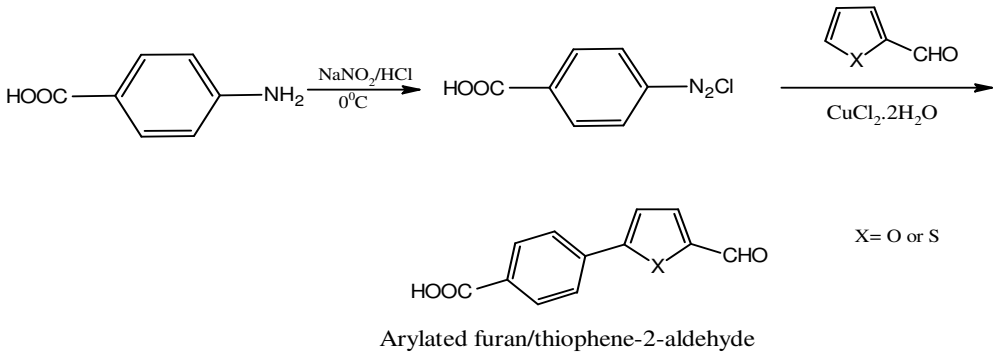

Fig.1.11 Synthetic strategy of arylated derivative (Meerwin arylation)

Synthesis of ligand

3mM of 4-(5-formylthiophen-2-yl)benzoic acid was dissolved in hot ethanol and refluxed on a water bath. To this, hot thiocarbamoyl hydrazide solution (3mM) prepared in ethanol-water mixture was added slowly. Continued the refluxing for further 3 hours. The volume of the reaction mixture was reduced by evaporation and cooled. Then the contents were added to ice cold water with constant stirring. The precipitated ligand, (E)-4-(5-[(2-carbamothioyl hydrazono)methyl]thiophen-2-yl)benzoic acid (CTHMT2YBA) was filtered, washed with ethanol-water mixture and dried. The melting point of CTHMT2YBA was 288^{0}C.

Characterization of ligand

The Schiff base CTHMT2YBA was characterized as per the following methods.

Elemental analysis

The elemental analysis data of the Schiff base is given in Table 1.8. The experimentally obtained values were in good agreement with the calculated values. The

measured percentage of nitrogen content in the Schiff base prepared was 13.84% while the theoretically expected value was 13.70%.

IR spectral studies

The infrared spectral data of CTHMT2YBA is represented in Table 1.9. The characteristic vibrational frequencies of primary amino group were shown as distinct peaks at 3490cm^{-1} and 3369cm^{-1}. The carboxylate symmetric and asymmetric vibrations were assigned at 1577$cm^{-1}$and 1695cm^{-1} respectively. Medium intense band found at 1608cm^{-1} can be attributed to the stretching vibrations of azomethine group (CH=N). The in-plane deformation was shown at 1006cm^{-1} and out of plane deformations were at 814cm^{-1} and 777cm^{-1}.

NMR spectral studies

The proton NMR spectrum of Schiff base CTHMT2YBA exhibited nine distinct proton signals. The assignments of peaks are given in Table 1.7. A broad singlet observed at 3.25δ was due to the NH_2 protons. Another broad singlet at 8.16δ was assigned to NH proton of the thiosemicarbazide part. The azomethine proton gave a peak at 8.27δ. Four aromatic protons both in the thiophene ring and benzene ring appeared as doublets in the region 7.50δ-7.96δ. The appearance of a weak signal at 12.92δ due to the SH proton confirmed the existence of tautomerism. The carboxylic proton exhibited its signal at 11.47δ.

^{13}Cnmr spectrum is shown in Figure 1.13. The presence of eleven chemically different carbon atoms was confirmed by this spectrum. The thionyl carbon exhibited its signal at 166.80ppm. The azomethine carbon was identified at 125.35ppm. Carbon atoms of the thiophene ring appeared at 139.41ppm, 134.21ppm and 131.11ppm. The aromatic carbons of the benzene ring exhibited four signals in the range 128ppm-143ppm. The

presence of carbonyl group in the compound araising from the carboxylate group was established by a characteristic signal at 177.66ppm. The assignments of signals to different carbon are expressed in Table 1.7.

Table 1.7 [1]Hnmr and [13]Cnmr spectral data of CTHMT2YBA

[1]Hnmr			[13]Cnmr		
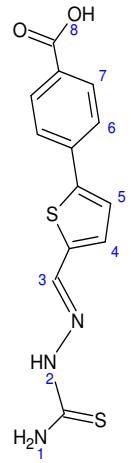	δ value	Assignment/ Labelled No.	δ value	Assignment/ Labelled	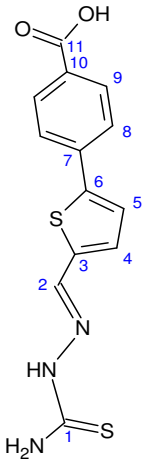
	3.25(br,s,2H)	1(NH_2)	166.80	1	
	8.16(br,s,1H)	2(NH)	125.35	2	
	8.27(1H)	3(CH=N)	139.41	3	
	7.91(d,1H)	4	134.21	4	
	7.50(d,1H)	5	131.11	5	
	7.74(d,2H)	6	125.95	6	
	7.96(d,2H)	7	128.72	7	
	11.47(s,1H)	8(COOH)	137.33	8	
	12.92(br,s,1H)	9(SH)	139.41	9	
			143.80	10	
			177.66	11	

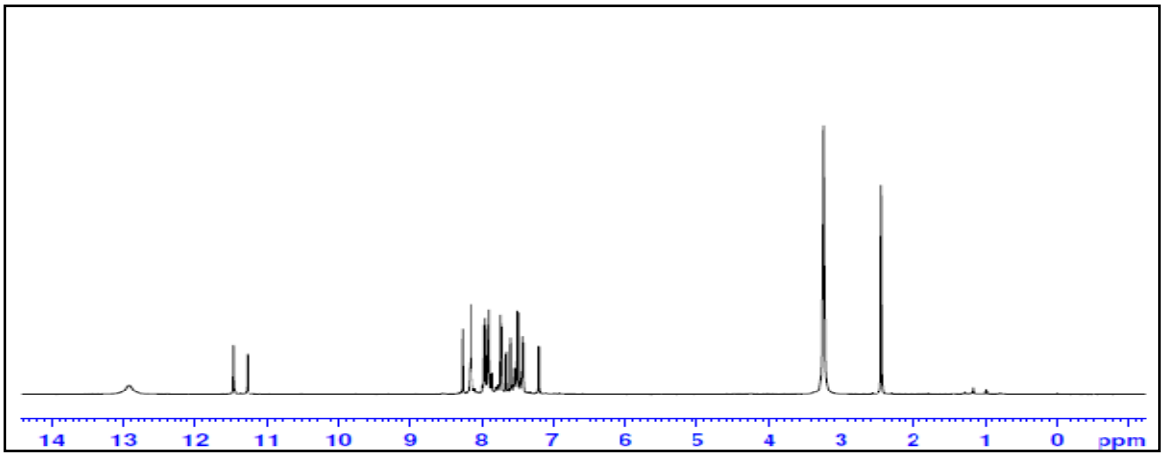

Fig.1.12 [1]Hnmr spectrum of CTHMT2YBA

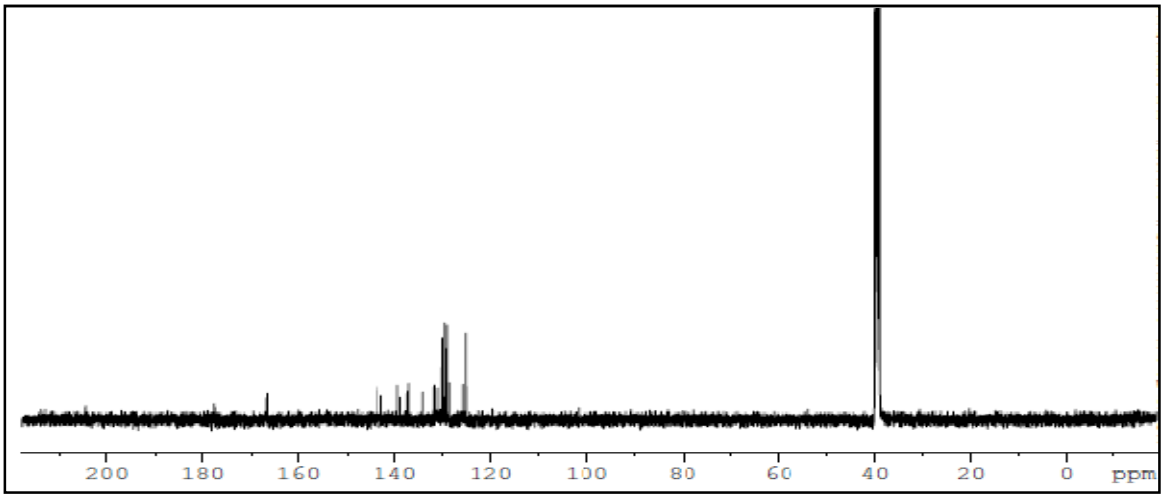

Fig.1.13 ^{13}Cnmr spectrum of CTHMT2YBA

Mass spectral studies

In the mass spectrum of CTHMT2YBA, the molecular ion peak at m/z 305 was very much weak with relative abundance less than 5. The loss of OH moiety from the Schiff base resulted in a peak at m/z 288. The formation of fragments at m/z 256 and m/z 242 were due to the fragments $[C_{13}H_8N_2O_2S]^+$ and $[C_{13}H_{10}N_2OS]^+$ respectively. Further fragmentation resulted in the daughter ion $[C_{12}H_8N_2S]^+$ which had m/z value 212. A peak observed at m/z 204 can be attributed to the fragment $[C_{11}H_8O_2S]^+$. The base peak was obtained at m/z 139 by $[C_6H_7N_2S]^+$ fragment. Two peaks at m/z 96 and m/z 75 were due to $[C_5H_4S]^+$ and $[NH_2\text{-}CS\text{-}NH]^+$ species respectively. The spectrum is given in Figure 1.14.

Electronic spectral studies

The two important peaks were exhibited by the Schiff base CTHMT2YBA in the UV-visible spectrum at 26281cm^{-1} and 39063cm^{-1}, which were assignable to n→π* and π→π* electronic transitions. From the discussion, the structure of the Schiff base can be represented as in Figure 1.15.

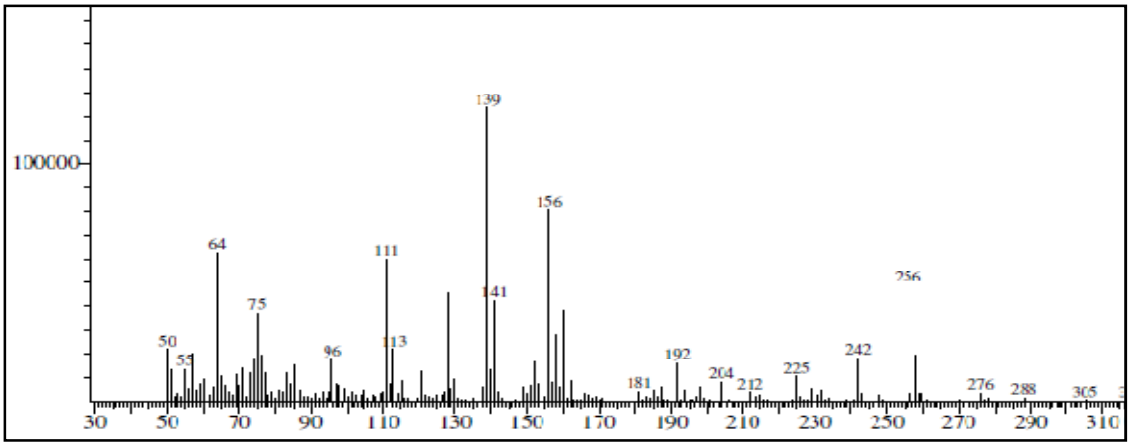

Fig.1.14 Mass spectrum of CTHMT2YBA

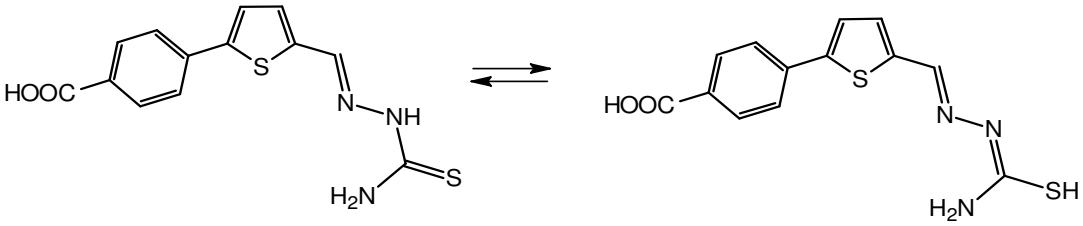

Fig.1.15 Tautomeric forms of CTHMT2YBA

Synthesis of complexes

Transition metal complexes of the Schiff base CTHMT2YBA were synthesized with Cr(III), Co(II), Ni(II), Cu(II) and Zn(II) ions. 2mM solution of the Schiff base CTHMT2YBA was heated to boiling on a waterbath and added hot ethanolic solution of the metal salt (2mM) slowly. The pH was adjusted by adding sodium acetate to the mixture. Then it was refluxed continuously for 4 hours. Finally the volume was reduced by boiling and cooled. Then the contents were poured into crushed ice and shaken well. The precipitated complex was filtered, washed with etanol-water mixture and dried. Melting points of all the complexes were noted. The yield, colour and other characteristics of the complexes are given in Table 1.8.

Characterization of complexes

Analytical tools adopted for the characterization of complexes include magnetic moment measurements, elemental analysis, conductance measurements and spectral studies like electronic and infrared spectroscopy. These analyses are described in detail here.

Elemental analysis

Estimation of elements in the complexes gave a definite idea about the exact molecular formula of the complexes. The CHNS analysis data is provided in Table 1.8. The observed values were very close to the theoretical values. It was found that Cr(III), Cu(II) and Zn(II) complexes were of 1:1 stoichiometry whereas Co(II) and Ni(II) complexes possess 1:2 stoichiometry between the metal and ligand.

Magnetic moment studies

Measurement of magnetic moment data helped to identify the geometry of the complexes. The results are given in Table 1.8. Chromium(III), cobalt(II) and nickel(II) complexes were assigned octahedral geometry since they exhibited magnetic moment values 3.54BM, 3.75BM and 2.82BM respectively. The copper chelate showed 1.75BM and a square planar geometry was found to be suitable for it. For the zinc complex diamagnetic nature was observed and this result matched with the fact that Zn(II) ion has d^{10} configuration. Tetrahedral geometry was therefore suggested for it.

Molar conductance studies

For all the complexes, the molar conductance data was measured in DMSO medium. The values obtained were in the range 10-16$\Omega^{-1}cm^2mol^{-1}$and hence it was concluded that in all the complexes counter ions were not present outside the coordination sphere. Therefore non-electrolytic behaviour was assigned for them.

IR spectral studies

In the IR spectra of the complexes, the downward shift of the vibrational frequencies of the azomethine bond, compared to that in the ligand CTHMT2YBA, strongly confirmed the coordination of imine nitrogen to metal in all complexes. Additional bands in the region 3200-3300cm^{-1} were attributed to the coordinated water molecules in all the chelates. Again the new M-S and M-N bonds showed their presence in the complex as characteristic peaks in the low field region. On comparing the symmetric and asymmetric stretching vibrations of the carboxylate group in ligand and the complexes, it can be concluded that the COOH group is not participating in coordination with the metal ion. The IR spectral data is given in Table 1.9.

NMR spectral studies

The non-involvement of carboxylate group in coordination is well elucidated by the ^{1}Hnmr spectral studies of the complexes. In the proton magnetic resonance spectrum of all the chelates, there was a characteristic peak at 11.5δ as found in the pmr spectrum of the ligand. At the same time the signal obtained at 12.92δ in the case of Schiff base spectrum, was disappeared in the spectra of chelates, which clearly indicates the coordination of sulphur atom in the thiocarbamoyl hydrazide part of the ligand to the central metal ion.

Electronic spectral studies

Intra ligand electronic transitions and d-d transitions were obtained from the electronic spectra of the complexes. The shifting of these bands to longer wavelength region was a clear indication of complexation. There were three bands in the electronic spectrum of Cr(III) chelate at 26809, 38986 and 40404cm^{-1}, which were characteristic of

$^4A_2(F) \rightarrow {}^4T_2$, $^4A_2(F) \rightarrow {}^4T_2(F)$ and $^4A_2 \rightarrow {}^4T_1(P)$ electronic transitions of an octahedral field. $^3A_2 \rightarrow {}^3T_2$ and $^3A_2 \rightarrow {}^3T_1(F)$ electronic transitions in Ni(II) complex gave two absorption bands at 30303 and 40160cm^{-1}respectively and octahedral geometry was assigned for the complex. In the Cu(II) complex, for which a square planar geometry was assigned, $^2B_1 \rightarrow {}^2A_1$ and $^2B_1 \rightarrow {}^2B_2$ transitions were shown at 27285 and 35026cm^{-1} respectively . The absorption bands observed at 26882cm^{-1} for Zn(II) complex was due to the L→M charge transfer transition.

Thermogravimetric studies

The Cr(III) and Ni(II) complexes of CTHMT2YBA were found to be stable upto 60^0C. The decomposition of Cr(III) complex followed a definite three stage pattern. In the first stage (60-150^0C) two coordinated water molecules were lost. Two acetate groups and two CO_2 molecules are removed in the second stage. The third stage was due to the loss of rest of both the ligands and two bridged acetates. The decomposition of Ni(II) complex also resulted with a definite three stage pattern. The first was assigned to the loss of two water molecules. The second stage consisted of three substages. In the first substage two COOH groups were lost. Then two NH_2 groups and two phenyl groups were removed in the second and third substages respectively. The third stage corresponded to the loss of rest of both the ligands. The percentage mass losses according to the TG curves and the theoretical values were in good agreement for both the complexes. The mass loss from the pyrolysis was also found out. The results are explained in Part IV.

Based on the above explanations, the structures of the complexes of the Schiff base can be represented as in Figure 1.16. In all the chelates the Schiff base, CTHMT2YBA acts as monovalent bidentate ligand.

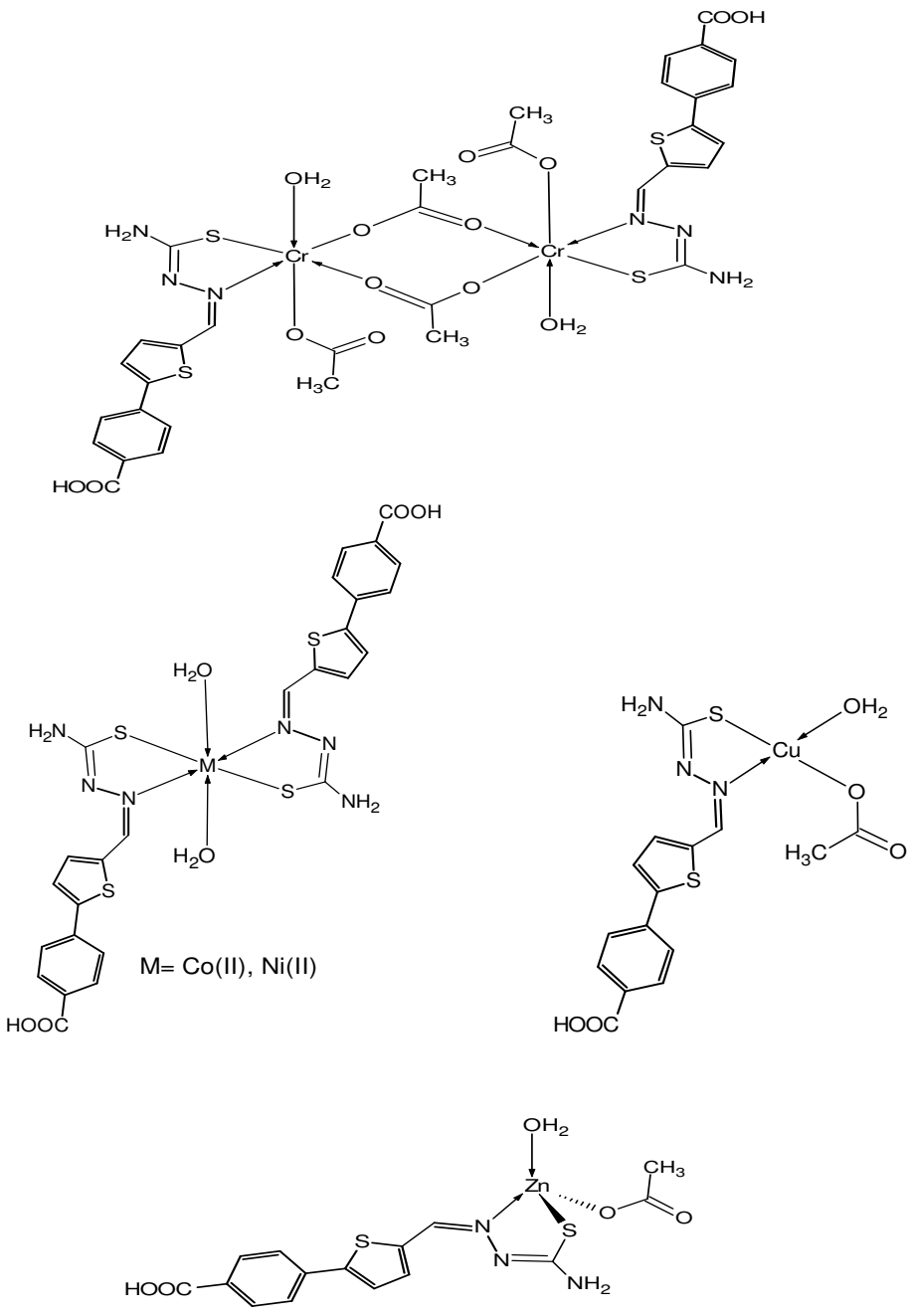

Fig.1.16 Structure of metal complexes of CTHMT2YBA

Table 1.8 Microanalytical, magnetic and conductance data of the ligand CTHMT2YBA and its transition metal complexes

Complex	Colour	Yield (%)	Mol. Wt.	M.P (^{0}C)	Metal% Found (Calculated)	C % Found (Calculated)	H % Found (Calculated)	N % Found (Calculated)	S % Found (Calculated)	μ_{eff} (BM)	Molar Conductance ($\Omega^{-1}cm^2mol^{-1}$)	Geometry
CTHMT2YBA (LH)	Pale brown	72	305	288	-	52.98 (51.15)	4.16 (3.60)	13.84 (13.70)	20.48 (20.98)	-	-	-
$[CrLAc_2(H_2O)]_2$	Pale brown	68	492	>300	11.35 (10.57)	41.01 (41.46)	4.12 (3.66)	7.85 (8.54)	12.33 (13.01)	3.54	16	Octahedral
$[CoL_2(H_2O)_2]$	Black	60	703	>300	7.86 (8.38)	43.86 (44.39)	4.10 (3.41)	12.45 (11.95)	19.03 (18.21)	3.75	12	Octahedral
$[NiL_2(H_2O)_2]$	Pale Green	70	703	>300	9.18 (8.35)	43.58 (44.40)	4.21 (3.42)	12.66 (11.95)	19.16 (18.23)	2.82	10	Octahedral
$[CuLAc(H_2O)]$	Gray	78	445	>300	13.86 (14.29)	39.32 (40.49)	4.17 (3.37)	10.03 (9.45)	15.14 (14.40)	1.75	15	Square planar
$[ZnLAc(H_2O)]$	Off white	66	446	>300	15.51 (14.65)	41.08 (40.32)	4.23 (3.36)	8.65 (9.41)	13.89 (14.33)	D	12	Tetrahedral

Ac: Acetate, D: Diamagnetic

Table 1.9 Characteristic infrared absorption frequencies of CTHMT2YBA and its transition metal complexes

Complex	υ_{N-H}	υ_{H2O}	$\upsilon_{C-H(Ar)}$	υ_{COO} (asym)	$\upsilon_{C=N}$	υ_{COO} (sym)	υ_{C-O}	In plane bending	Out of plane bending	υ_{M-N}	υ_{M-S}
CTHMT2YBA (LH)	3490, 3369	-	3174	1695	1608	1577	1284	1006	814, 777	-	-
$[CrLAc_2(H_2O)]_2$	3423, 3361	3321	3197	1689	1598	1544	1276	1097	808, 777	567	530
$[CoL_2(H_2O)_2]$	3421, 3400	3284	3170	1689	1602	1570	1246	1007	810, 777	556	489
$[NiL_2(H_2O)_2]$	3415, 3398	3296	3184	1685	1604	1570	1251	1076	827, 779	592	511
$[CuLAc(H_2O)]$	3421, 3360	3277	3159	1687	1598	1544	1286	1012	823, 773	596	492
$[ZnLAc(H_2O)]$	3415, 3392	3282	3170	1689	1598	1552	1278	1051	837, 781	551	501

Part I
Synthesis and Characterization

Chapter 6

Nimmy Kuriakose “Physicochemical, thermoanalytical, electrochemical and antitumour studies of transition metal complexes of schiff bases derived from heterocyclic carbonyl compounds” Thesis. Department of Chemistry, St. Thomas College, University of Calicut, 2015

CHAPTER 6

STUDIES ON SCHIFF BASE, 4-(5-[(2-PHENYLHYDRAZONO)METHYL] THIOPHEN-2-YL)BENZOIC ACID AND ITS TRANSITION METAL COMPLEXES

This chapter deals with the synthesis and characterization of a novel Schiff base, (E)-4-(5-[(2-phenylhydrazono)methyl]thiophen-2-yl)benzoic acid (PHMT2YBA). The chelating efficiency of this ligand was investigated by complexation with Cr(III), Co(II), Ni(II), Cu(II) and Zinc(II) ions. These complexes were also subjected to characterization studies like elemental analysis, magnetic moment measurements, conductance studies and spectroscopic analysis like IR, UV-Visible and NMR spectroscopy.

The Schiff base was prepared by a two step process, first step being Meervin arylation of the thiophene-2-carbaldehyde, followed by condensation reaction with phenylhydrazine. The arylation process was explained in detail in the previous chapter.

Synthesis of ligand

4-(5-formylthiophen-2-yl)benzoic acid solution was prepared by dissolving 2mM in hot ethanol and it was refluxed on a water bath. To this, hot solution of phenylhydrazine in ethanol-water mixture was added slowly. Continued the refluxing for 2 hours. The reaction mixture was reduced in volume by evaporation and then cooled. Then the contents were added to ice cold water and stirred well. The precipitated ligand was filtered, washed with ethanol-water mixture and dried. The melting point of the Schiff base (E)-4-(5-[(2-phenylhydrazono)methyl]thiophen-2-yl)benzoic acid (PHMT2YBA) was found to be 292 ^{0}C.

Characterization of ligand

The ligand 4-(5-[(2-phenylhydrazono)methyl]thiophen-2-yl)benzoic acid was subjected to characterization studies in order to determine the structure. Elemental analysis and spectral studies were carried out and the details are as follows.

Elemental analysis

The elemental analysis data of the Schiff base PHMT2YBA is given in Table 1.11. The experimentally obtained percentages of elements like carbon, hydrogen, nitrogen and sulphur were in good agreement with the calculated values.

IR spectral studies

In the IR spectrum, the characteristic vibrational frequencies of N-H bond were shown at 3308cm^{-1}. The aromatic C-H bond was observed at 3054cm^{-1}. The symmetric and asymmetric vibrations of the carboxylate group were assigned at 1514$cm^{-1}$and 1685cm^{-1} respectively. The azomethine group was identified by a peak at 1618cm^{-1}. A strong band appeared at 1257cm^{-1} can be attributed to C-O stretching vibrations. The in-plane deformation was shown at 1109cm^{-1} and out of plane deformations were at 750cm^{-1} and 696cm^{-1}. The IR spectral data is given in Table 1.12.

NMR spectral studies

In the proton NMR spectra, ten nonequivalent protons were identified. A broad singlet at 8.01δ was assigned to the NH proton. A double doublet appeared at 7.88δ was due to the aromatic proton which is adjacent to nitrogen in the phenyl hydrazine ring. The protons on next carbon atoms of the ring gave a doublet signal at 7.15δ and a medium signal 6.69δ respectively. Proton on the azomethine carbon gave a singlet peak at 10.4δ. The aromatic protons of the thiophene ring were identified at 6.95δ and 7.49δ, whereas

protons on the benzene ring were at 7.53δ and 7.98δ. The carboxylic acid proton gave a broad singlet peak at 12.93δ. The spectrum is shown in Figure 1.17.

The proton decoupled ^{13}Cnmr spectrum of PHMT2YBA gave characteristic peaks for 14 chemically different carbon atoms. The carboxylic acid and azomethine carbons were assigned with signals at 166.28ppm and 131.42ppm respectively. All the carbon atoms of aromatic rings in the molecule gave characteristic peaks in the range 112ppm-145ppm. The assignments of signals are given in Table 1.10 and the spectrum is given in Figure 1.18.

Table 1.10 ^{1}Hnmr and ^{13}Cnmr spectral data of PHMT2YBA

^{1}Hnmr			^{13}Cnmr		
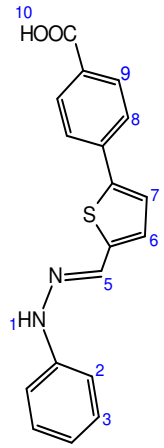	δ value	Assignment/ Labelled No.	δ value	Assignment/ Labelled No.	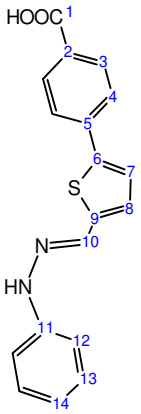
	8.01(br,s)	1(NH)	166.28	1	
	7.88(dd)	2	144.74	2	
	7.15(dd)	3	130.15	3	
	6.69(m)	4	125.75	4	
	10.40(s)	5(CH=N)	127.80	5	
	7.49(d)	6	131.12	6	
	6.95(d)	7	128.97	7	
	7.53(d)	8	129.15	8	
	7.98(d)	9	131.12	9	
	12.93(br,s)	10(COOH)	131.42	10	
			141.95	11	
			129.68	12	
			112.02	13	
			119.07	14	

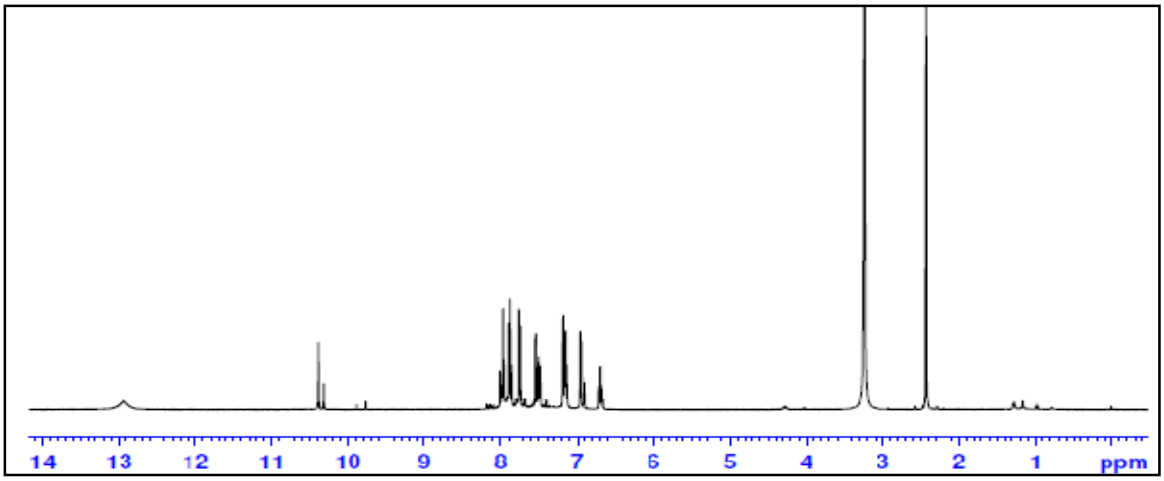

Fig.1.17[1]Hnmr spectrum of PHMT2YBA

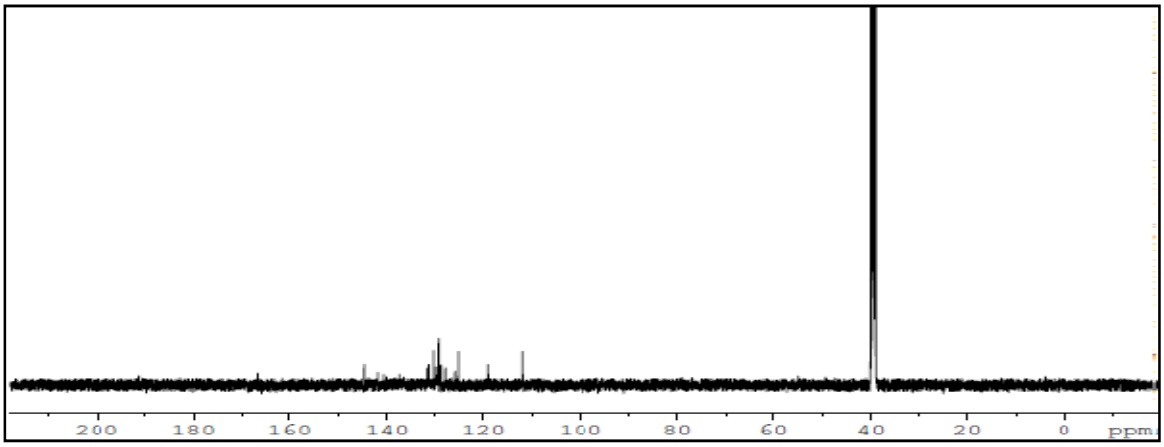

Fig.1.18 [13]Cnmr spectrum of PHMT2YBA

Mass spectral studies

The molecular ion peak at m/z 322 was the base peak itself for PHMT2YBA**.** Appearance of peak at m/z 323 can be assigned to the $[M+1]^+$species. The $[M]^+$:$[M+1]^+$ ratio (100:20.0) suggest that 18 carbon atoms were present in the molecule. Loss of an oxygen atom gave a peak at m/z 306. The peaks at m/z 159 and 187 were due to the fragments $[C_{10}H_6S]^+$ and $[C_{11}H_7OS]^+$ respectively. $[C_7H_6N_2]^+$ and $[C_6H_5N]^+$ fragments from phenyl hydrazone part gave peaks at m/z 118 and 91 respectively. The mass spectrum is given in Figure 1.19.

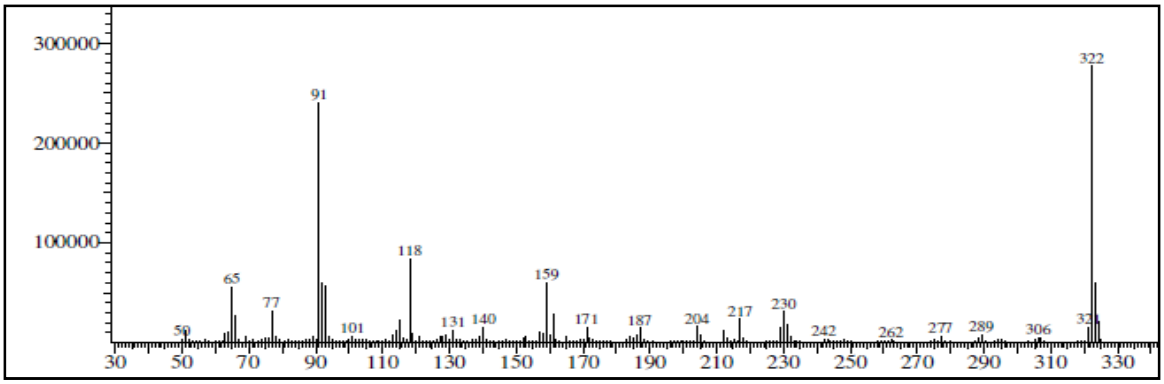

Fig.1.19 Mass spectrum of PHMT2YBA

Electronic spectral studies

The Schiff base PHMT2YBA exhibited two important peaks in the UV-visible spectrum at 33113cm^{-1} and 38986cm^{-1}, which can be assigned to n→π* and π→π* electronic transitions. From the discussion, the structure of the Schiff base can be represented as in Figure 1.20.

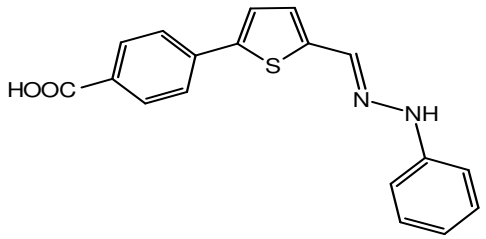

Fig.1.20 Structure of PHMT2YBA

Synthesis of complexes

Transition metal complexes of the Schiff base PHMT2YBA were synthesized with Cr(III), Co(II), Ni(II), Cu(II) and Zn(II) ions. 2mM solution of the Schiff base PHMT2YBA was heated to boiling on a waterbath. To that added hot ethanolic solution of the metal salt (2mM) slowly. The mixture was refluxed continuously for 3 hours. Finally the volume was reduced by boiling and cooled. The precipitated complex was filtered, washed several times with etanol-water mixture and dried. Melting points of all

the complexes were found to be greater than 300^0C. All the complexes were coloured and obtained in good yield. The copper complex was obtained with maximum yield compared to other complexes. The yield and colours of the complexes are given in Table 1.11.

Characterization of complexes

Different analytical techniques adopted for the characterization of complexes include magnetic moment measurements, elemental analysis, conductance measurements, electronic and infrared spectral studies. These analyses are described in detail here.

Elemental analysis

Estimation of different elements in the complexes gave a definite idea about the exact molecular formula of the complexes. The CHNS analysis data is provided in Table 1.11. The experimentally obtained values were found to be very close to the theoretical values. It was found that Cr(III), Cu(II) and Zn(II) complexes were of 1:1 stoichiometry whereas in Co(II) and Ni(II) complexes 1:2 stoichiometry was followed between the metal ion and the ligand.

Magnetic moment studies

The geometry of the complexes can be identified by the measurement of magnetic moments. Chromium(III) complex was assigned octahedral geometry whereas cobalt(II) and nickel(II) complexes were found to be in distorted octahedral geometry since they exhibited magnetic moment values 3.81BM, 4.01BM and 3.15BM respectively[57-60]. The copper(II) chelate exhibited 1.63BM and a square planar geometry was fixed for it. For the zinc(II) complex diamagnetic nature was observed since there was d^{10} configuration and tetrahedral geometry was ascertained for this complex.

Molar conductance studies

The electrical conductivity of the complexes were analysed in the solvent dimethyl sulphoxide. The molar conductance values obtained were in the range 5-16Ω^{-1} cm^2mol^{-1}, suggesting that all the complexes were non-electrolytic in nature and counter ions were not present in them. Table1.11 includes the conductance data of the complexes.

IR spectral studies

The assignments of IR spectral peaks are given in the Table 1.12. The presence of new vibrational bands around 3400cm^{-1} signified the presence of coordinated water molecule in each complex. The vibrational frequencies of C=N were found to be decreased suggesting the participation of this group in the complexation process. Appearance of new M-O and M-N bonds strongly support the coordination of the oxygen and nitrogen atom to the metal ion. Since there is not much shift in the symmetric and asymmetric stretching vibrations of the carboxylate group in the spectra of complexes, compared with that of the ligand, it can be concluded that the carboxylate group is not involved in coordination with the metal ions in all the complexes.

^{1}Hnmr spectral studies

In the proton magnetic resonance spectra of the complexes, the characteristic peak of the carboxylate group was not found to be shifted, compared with that of the ligand. The appearance of peak at 12.9δ supported the fact that carboxylate group was not coordinated to the central metal ion in the complexes. The downward shift of the azomethine proton peak in the spectra of the complexes confirmed the involvement of azomethine group in the coordination.

Electronic spectral studies

Both the K band and R band undergone bathochromic shift in the electronic spectra of the complexes, compared to that of the ligand, which established the coordination of the Schiff base with the metal ion.

The appearance of three bands in the electronic spectrum of Cr(III) complex at 24213cm^{-1}, 33333cm^{-1} and 38834cm^{-1} were due to $^4A_2(F)\rightarrow{}^4T_2$, $^4A_2(F)\rightarrow{}^4T_2(F)$ and $^4A_2\rightarrow{}^4T_1(P)$ electronic transitions in an octahedral field. The three electronic transitions $^4T_1(F)\rightarrow{}^4T_2$, $^4T_1(F)\rightarrow{}^4A_2$ and $^4T_1(F)\rightarrow{}^4T_1(P)$ for Co(II) which was a d^7 system, were exhibited at 24540cm^{-1}, 33956cm^{-1} and 38911cm^{-1} respectively. $^3A_2\rightarrow{}^3T_2$, $^3A_2\rightarrow{}^3T_1(F)$ and $^3A_2\rightarrow{}^3T_1(P)$ electronic transitions in Ni(II) complex gave three absorption bands at 24301cm^{-1}, 32949cm^{-1} and 38911cm^{-1}respectively and octahedral geometry was assigned for the complex. In the Cu(II) complex, for which square planar geometry was assigned, $^2B_1\rightarrow{}^2A_1$ and $^2B_1\rightarrow{}^2B_2$ transitions were expressed at 33727cm^{-1} and 39063cm^{-1} respectively . An intense peak at 38986cm^{-1} in the electronic spectrum of Zn(II) chelate was assigned to ligand to metal charge transfer transition.

Thermogravimetric studies

The thermogram of the Cr(III) complex showed three stages of decomposition. Two coordinated water molecules and one acetate group were lost in the first and second stages respectively. In the third stage, the ligand and two acetate groups are removed from the complex molecule at 700^0C. Ni(II) complex underwent a two stage decomposition pattern. Loss of two water molecules and two carboxyphenyl moieties were observed at 70-342^0C in the initial stage. Two acetate groups and the rest of both the ligands were lost in the second stage.

Based on the above explanations, the structures of the complexes of the Schiff base PHMT2YBA can be represented as in Figure 1.21. Also it is confirmed that in all the complexes, the Schiff base behaves as a monodentate species.

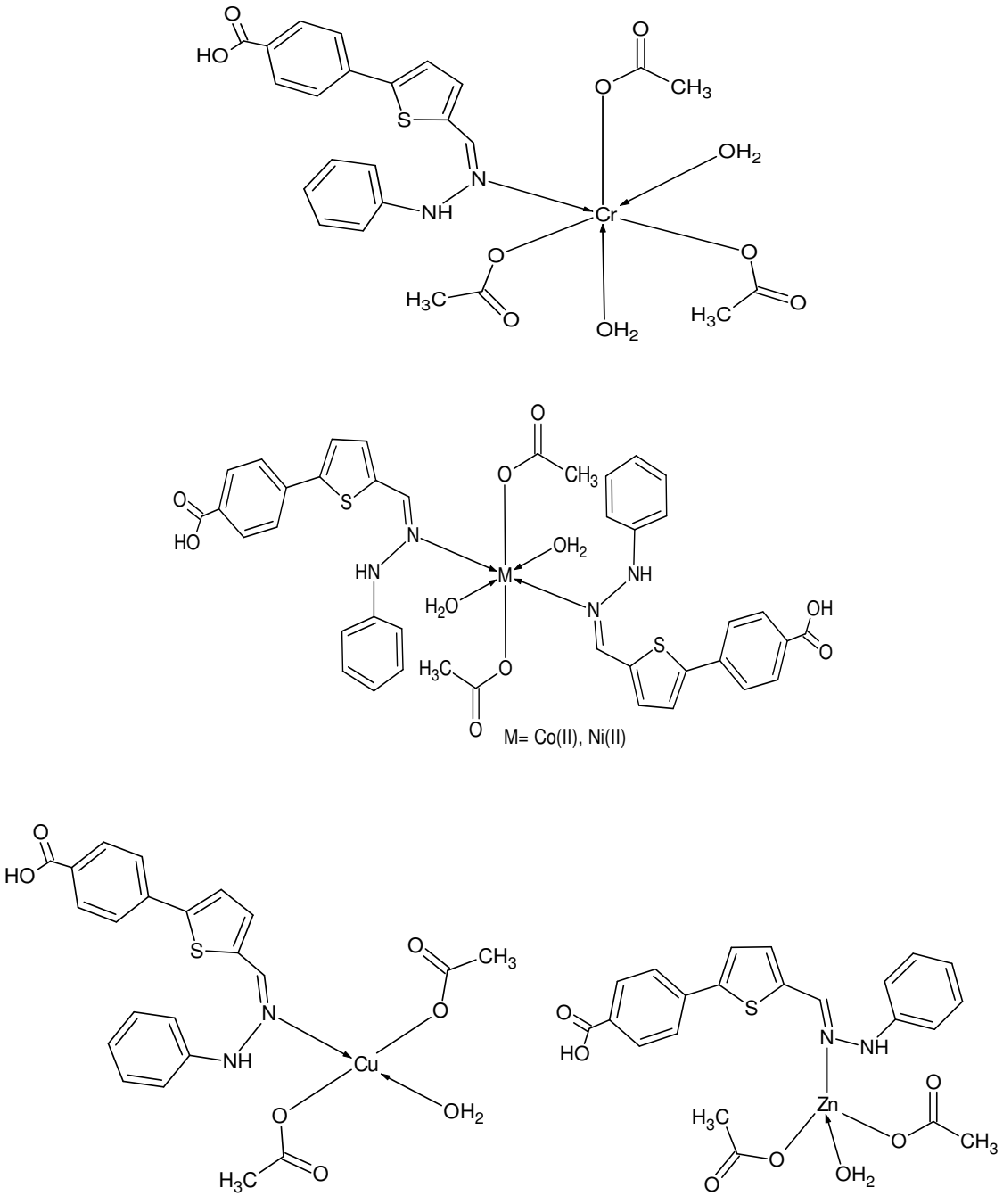

Fig.1.21 Structures of metal complexes of PHMT2YBA

Table 1.11 Microanalytical, magnetic and conductance data of the ligand PHMT2YBA and its transition metal complexes

Complex	Colour	Yield (%)	Mol. Wt.	M.P (^{0}C)	Metal% Found (Calculated)	C % Found (Calculated)	H % Found (Calculated)	N % Found (Calculated)	S % Found (Calculated)	μ_{eff} (BM)	Molar Conductance ($\Omega^{-1}cm^2mol^{-1}$)	Geometry
PHMT2YBA (LH)	Pale brown	68	322	292	-	66.98 (67.08)	4.06 (4.35)	9.58 (8.70)	8.99 (9.94)	-	-	-
$[CrLAc_3(H_2O)_2]$	Pale brown	66	587	>300	7.35 (8.86)	48.51 (49.06)	5.12 (4.60)	5.38 (4.77)	6.73 (5.54)	3.81	8	Octahedral
$[CoL_2Ac_2(H_2O)_2]$	Black	60	857	>300	6.02 (6.88)	55.5 (56.01)	3.62 (4.43)	5.74 (6.53)	6.98 (7.47)	4.01	12	Octahedral (distorted)
$[NiL_2Ac_2(H_2O)_2]$	Pale Green	68	857	>300	6.01 (6.85)	55.86 (56.03)	4.98 (4.44)	5.99 (6.54)	8.02 (7.47)	3.15	6	Octahedral (distorted)
$[CuLAc_2(H_2O)]$	Brown	72	522	>300	12.86 (12.18)	49.59 (50.62)	4.13 (4.60)	6.04 (5.37)	7.01 (6.14)	1.63	7	Square planar
$[ZnLAc_2(H_2O)]$	Off white	64	523	>300	12.25 (12.49)	50.89 (50.44)	4.33 (4.56)	4.86 (5.35)	5.68 (6.11)	D	10	Tetrahedral

Ac: Acetate, D: Diamagnetic

Table 1.12 Characteristic infrared absorption frequencies of PHMT2YBA and its transition metal complexes

Complex	υ_{N-H}	υ_{H2O}	$\upsilon_{C-H(Ar)}$	$\upsilon_{COO(asym)}$	$\upsilon_{C=N}$	$\upsilon_{COO(sym)}$	υ_{C-O}	In plane bending	Out of plane bending	υ_{M-N}
PHMT2YBA (LH)	3308	-	3054	1685	1618	1514	1257	1109	750, 696	-
$[CrLAc_3(H_2O)_2]$	3305	3373	3070	1687	1604	1544	1259	1120	775, 690	565
$[CoL_2Ac_2(H_2O)_2]$	3305	3414	3064	1689	1598	1566	1257	1103	750, 692	547
$[NiL_2Ac_2(H_2O)_2]$	3304	3381	3037	1691	1597	1498	1255	1109	752, 694	551
$[CuLAc_2(H_2O)]$	3315	3400	3066	1656	1593	1544	1259	1102	775	536
$[ZnLAc_2(H_2O)]$	3305	3404	3062	1687	1600	1517	1259	1111	781, 748,694	508

Part I
Synthesis and Characterization

Chapter 7

Nimmy Kuriakose “Physicochemical, thermoanalytical, electrochemical and antitumour studies of transition metal complexes of schiff bases derived from heterocyclic carbonyl compounds” Thesis. Department of Chemistry, St. Thomas College, University of Calicut, 2015

CHAPTER 7

STUDIES ON SCHIFF BASE, 4-(5-[(2-CARBAMOTHIOYLHYDRAZONO) METHYL]FURAN-2-YL)BENZOIC ACID AND ITS TRANSITION METAL COMPLEXES

A novel heterocyclic Schiff base, (E)-4-(5-[(2-carbamothioylhydrazono)methyl] furan-2-yl)benzoic acid (CTHMF2YBA) was synthesized and characterized. The chelating efficiency of this ligand was investigated with metal ions Cr(III), Co(II), Ni(II), Cu(II) and Zn(II). The synthetic methods and characterization techniques like elemental analysis, magnetic moment measurements and spectroscopic studies like IR, ^{1}H nmr and ^{13}C nmr electronic spectroscopy are detailed in this chapter.

Synthesis of ligand

The Schiff base was synthesized by a two step process. In first step furan-2-carbaldehyde was arylated by Meervin arylation process, followed by condensation reaction with the amino compound, thiocarbamoyl hydrazide.

4-(5-formylfuran-2-yl)benzoic acid solution was prepared by dissolving 2mM in hot ethanol and it was heated to boiling on a water bath. To this, hot solution of thiocarbamoyl hydrazide in ethanol-water mixture was added slowly. This mixture was refluxed continuously for 3 hours. The reaction mixture was reduced in volume by evaporation and then cooled. Then the contents were added to ice cold water and stirred well. The precipitated ligand was filtered, washed with ethanol-water mixture and dried. The melting point of the Schiff base CTHMF2YBA was found to be $278^{0}C$.

Characterization of ligand

Elemental analysis

The elemental analysis data of the Schiff base CTHMF2YBA is given in Table 1.14.

The experimentally obtained percentages of elements like carbon, hydrogen, nitrogen and sulphur were in good agreement with the calculated values.

IR spectral studies

The IR spectral assignments are given in Table 1.15. The NH_2 group gave its characteristic vibrational frequencies at 3377cm^{-1} and 3259cm^{-1}. The aromatic C-H bond vibration was observed at 3165cm^{-1}. The S-H bond of the ligand gave one peak at 2540cm^{-1}. The symmetric and asymmetric vibrations of carboxylate group were found at 1553$cm^{-1}$and 1689cm^{-1} respectively. The azomethine group was identified by a peak at 1614cm^{-1}. υ_{C-O} was observed at 1286cm^{-1}. The in-plane deformation was shown at 1103cm^{-1} and out of plane deformations were observed at 921cm^{-1}, 798cm^{-1} and 771cm^{-1}.

NMR spectral studies

According to the proton NMR spectrum of CTHMF2YBA nine distinct protons were there in the Schiff base molecule. The assignments of peaks are given in Table 1.13. A broad singlet observed at 3.25δ was due to the NH_2 protons. Another broad singlet at 8.23δ was assigned to NH proton of the thiosemicarbazide part. The azomethine proton gave a peak at 7.74δ which was a broad singlet. Aromatic protons in the thiophene ring appeared as doublets at 7.21δ and 7.05δ and those in the benzene ring appeared as two proton doublets at 7.88δ and 7.92δ. The carboxylic proton exhibited its signal at 11.47δ. Possibility of tautomerism in the molecule was confirmed by the appearance of a broad singlet peak at 12.9δ due to the SH proton.

^{13}Cnmr spectrum is shown in Figure 1.23. Eventhough the molecule contains 13 carbon atoms, the presence of eleven chemically different carbon atoms was confirmed by this spectrum. The thiosemicrbazone carbon exhibited its signal at 166.84ppm. The

azomethine carbon was identified at 123.82ppm. Carbon atoms of the thiophene ring appeared at 149.98ppm, 131.62ppm and 110.45ppm. The aromatic carbons of the benzene ring exhibited four signals in the range 129ppm-153ppm. The peak at 177.81ppm was due to carboxylate carbon. The assignment of signals to different carbon is expressed in Table 1.13.

Table 1.13 ^{1}Hnmr and ^{13}Cnmr spectral data of CTHMF2YBA

^{1}Hnmr			^{13}Cnmr		
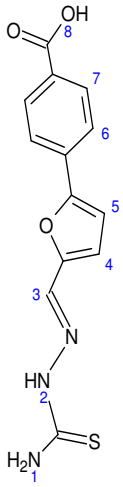	δ value	Assignment/ Labelled No.	δ value	Assignment/ Labelled No.	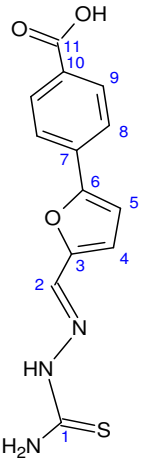
	3.25(br,s,2H)	1(NH_2)	166.84	1	
	8.23(br,s,1H)	2(NH)	123.82	2	
	7.74(br,s,1H)	3(CH=N)	149.98	3	
	7.21(d,1H)	4	131.62	4	
	7.05(d,1H)	5	110.45	5	
	7.88(d,2H)	6	133.20	6	
	7.92(d,2H)	7	115.26	7	
	11.47(s,1H)	8(COOH)	129.77	8	
	12.9(br,s,1H)	9(SH)	129.94	9	
			153.37	10	
			177.81	11	

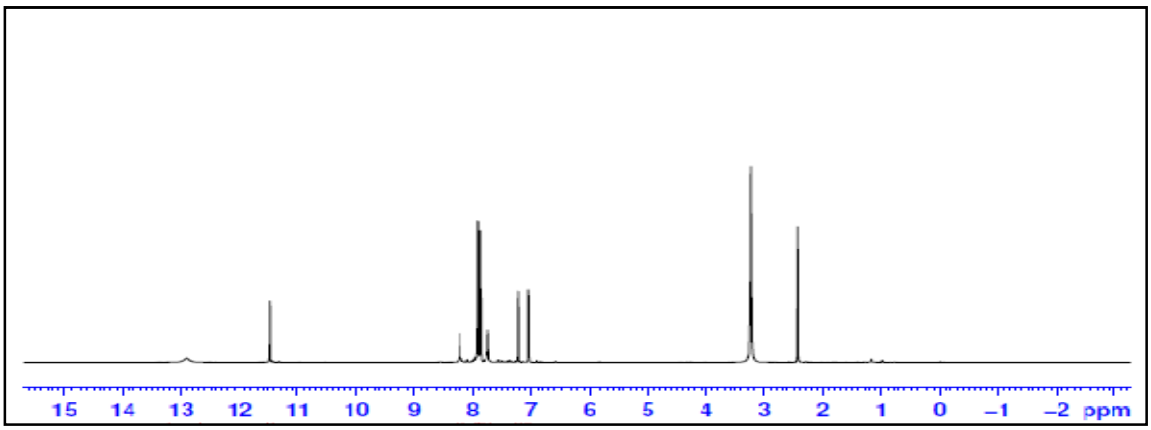

Fig.1.22 ^{1}Hnmr spectrum of CTHMF2YBA

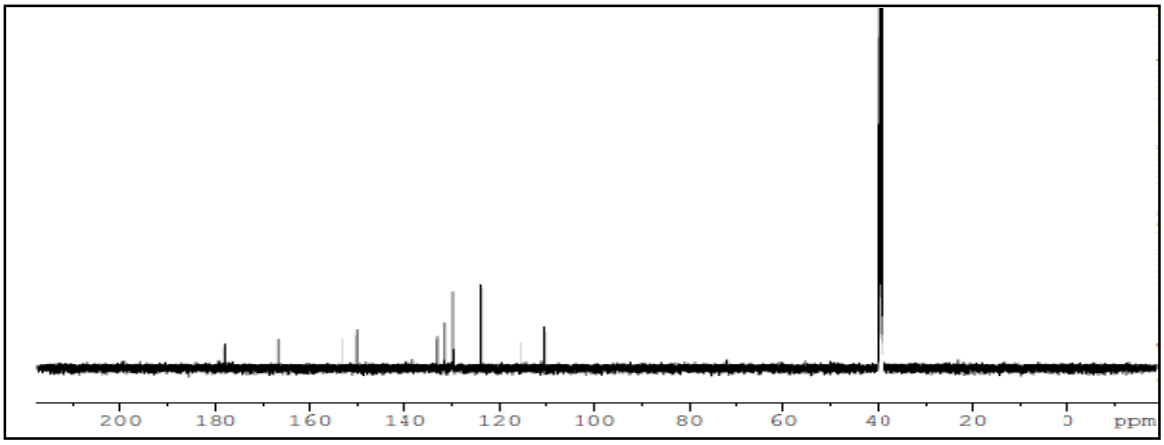

Fig.1.23 ^{13}Cnmr spectrum of CTHMF2YBA

Mass spectral studies

The appearance of only one peak in the gas chromatogram indicated the purity of the synthesized compound. In the mass spectrum of CTHMF2YBA, the molecular ion peak was observed at m/z 289. Appearance of peak at m/z 290 can be assigned to the $[M+1]^+$species. The $[M]^+$:$[M+1]^+$ ratio (100:16.5) suggested that 13 carbon atoms were present in the molecule. $[M+2]^+$ peak at m/z 292 was also present with $[M]^+$:$[M+2]^+$ ratio 100:5. The loss of OH moiety resulted in a peak at m/z 272 which was the base peak. The formation of fragments at m/z 230 and m/z 213 were due to the fragments $[C_{12}H_{10}N_2O_3]^+$ and $[C_{12}H_7NO_3]^+$ respectively. Further fragmentation resulted in species $[C_{12}H_8O_3]^+$, $[C_{12}H_6NO_2]^+$, $[C_{11}H_8O_3]^+$ and $[C_{10}H_7O_2]^+$ which gave their peaks at m/z values at 200, 196, 188 and 159 respectively. The fragment $[C_3H_7N_3O_2S]^+$ was shown at m/z 149 and $[C_3H_5N_3OS]^+$ at m/z 131. Two important peaks at m/z 76 and m/z 59 were due to $[CH_4N_2S]^+$ and $[HS\text{-}C{\equiv}N]^+$ species respectively. Figure 1.24 gives the mass spectrum of the CTHMF2YBA molecule.

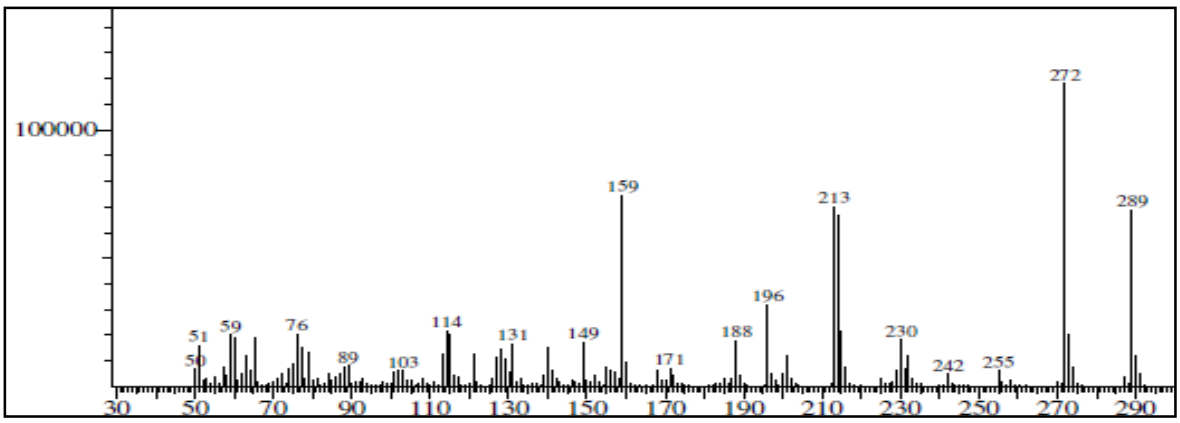

Fig.1.24 Mass spectrum of CTHMF2YBA

Electronic spectral studies

The Schiff base CTHMF2YBA exhibited two peaks in the UV-visible spectrum at 26595cm^{-1} and 33557cm^{-1}, which can be assigned to n→π* and π→π* electronic transitions. Based on the analytical data observed, the following structure is assigned for the Schiff base (Figure 1.25), which can exist in thioketo-thioenol tautomeric forms.

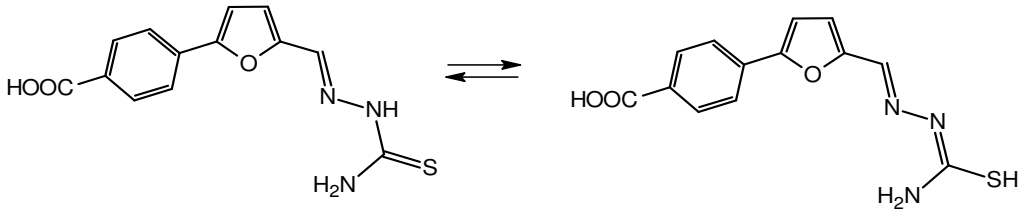

Fig.1.25 Tautomeric forms of CTHMF2YBA

Synthesis of complexes

Transition metal complexes of the Schiff base CTHMF2YBA were synthesized with Cr(III), Co(II), Ni(II), Cu(II) and Zn(II) ions. 2mM solution of the Schiff base CTHMF2YBA was heated to boiling on a waterbath. To that added hot ethanolic solution of the metal salt (2mM) slowly. The mixture was refluxed continuously for 3 hours. Finally the volume was reduced by boiling and cooled. Then the contents were poured into crushed ice and shaken well. The precipitated complex was filtered, washed with

etanol-water mixture and dried. Melting points of the complexes were noted. All the complexes were found to have higher melting points than the ligand. The yield and colours of the complexes are given in Table 1.14.

Characterization of complexes

All the complexes were found to be light and air stable. Generally they were soluble in aprotic polar solvents like DMSO and DMF. But solubility was very poor in common organic solvents like ethanol, diethyl ether, benzene, chloroform etc. All the complexes were subjected to different characterization techniques like magnetic moment measurements, elemental analysis, conductance measurements and spectral studies like IR and electronic spectra. The descriptions of these analyses are followed.

Elemental analysis

Estimation of elements in the complexes gave a definite idea about the exact molecular formula of the complexes. The CHNS analysis data is provided in Table 1.14. A good correlation was found between the observed values and calculated values. It was found that Cr(III), Cu(II) and Zn(II) complexes were of 1:1 stoichiometry whereas in Co(II) and Ni(II) complexes 1:2 stoichiometry was followed between the metal ion and the ligand.

Magnetic moment studies

Measurement of magnetic moment values gave an idea about the geometry of the complexes. Chromium and cobalt complexes were found to have octahedral geometry since they exhibited magnetic moment values 3.01BM and 3.31BM respectively. The nickel complex had a magnetic moment value of 2.56BM which indicated that it is of high spin octahedral geometry. The copper complex showed 1.97BM and a square planar

geometry was assigned for it. For the zinc complex diamagnetic nature was observed and tetrahedral geometry was fixed for it.

Molar conductance studies

For all the CTHMF2YBA complexes, the molar conductance data was measured in DMSO medium. Solutions of 10^{-3}M concentration were used for the measurements. The values obtained were in the range 6-14$\Omega^{-1}cm^2mol^{-1}$ suggesting that in all the complexes counter ions were not present outside the coordination sphere and thus all were non-electrolytic in nature.

IR spectral studies

Table 1.15 shows the assignments of IR spectral peaks of the complexes. The presence of new vibrational bands around 3250cm^{-1} showed the presence of coordinated water molecule in each complex. The υ_{S-H} was absent in the spectra of all the complexes which was observable in the ligand spectrum. The involvement of the sulphur atom of the thiocarbamoyl hydrazide part in coordination was thus confirmed. The decrease in vibrational frequency of C=N group gave a clear indication of participation of azomethine nitrogen in the complexation process. Further confirmation regarding the coordination sites in the ligand was established from the appearance of additional bands in the lower frequency regions such as ~ 670-680cm^{-1}(M-N) and ~ 500-550cm^{-1} (M-S). The absence of shifts in the symmetric and asymmetric stretching vibrations of the carboxylate group in the spectra of complexes suggested that COOH group is not coordinated to the metal ion in all the complexes.

Electronic spectral studies

In all metal chelates the intra ligand electronic transitions were shifted to longer

wavelength region suggesting the occurrence of complexation. In the electronic spectra of Cr(III) chelate absorption peaks at 26595cm^{-1}, 33898cm^{-1} and 39215cm^{-1} were due to $^4A_2(F)\rightarrow{}^4T_2$, $^4A_2(F)\rightarrow{}^4T_2(F)$ and $^4A_2\rightarrow{}^4T_1(P)$ electronic transitions in an octahedral field. For the Co(II) complex three electronic transitions $^4T_1(F)\rightarrow{}^4T_2$, $^4T_1(F)\rightarrow{}^4A_2$ and $^4T_1(F)\rightarrow{}^4T_1(P)$ were exhibited at 26560cm^{-1}, 33670cm^{-1} and 39062cm^{-1} respectively. $^3A_2\rightarrow{}^3T_2$ and $^3A_2\rightarrow{}^3T_1(F)$ electronic transitions in Ni(II) complex gave peaks at 26490cm^{-1} and 39062cm^{-1} respectively and octahedral geometry was assigned for the complex. In the Cu(II) complex, for which a square planar geometry was assigned, $^2B_1\rightarrow{}^2A_1$ and $^2B_1\rightarrow{}^2B_2$ transitions were expressed at 26525cm^{-1} and 39138cm^{-1} respectively. An intense peak at 39138cm^{-1} in the electronic spectrum of Zn(II) chelate was assigned to ligand to metal charge transfer transition.

Thermogravimetric studies

Cr(III) complex of the ligand CTHMF2YBA had a four stage decomposition pattern in the TGA analysis. Loss of two water molecules was observed in the temperature interval 62-137^{0}C. Then in the second stage two amino groups, two CO_2 molecules and two acetate groups were lost. Two bridged acetate groups were removed and in the third stage of decomposition. Lastly, rest of both the ligands were lost with the peak temperature 451^{0}C. But for the Ni(II) complex a three stage decomposition pattern was observed. Loss of two water molecules was assigned in the first stage. Two COOH groups, two NH_2 molecules and two phenyl rings were lost at around 235^{0}C, 259^{0}C and 319^{0}C respectively in second stage. In the third stage the rest of both the ligands were lost. The mass loss according to the thermogravimetric curves and the theoretical values were found to be in good agreement for both the complexes.

Based on the above explanations, the structures of the complexes of the Schiff base CTHMF2YBA can be represented as in Figure 1.26.

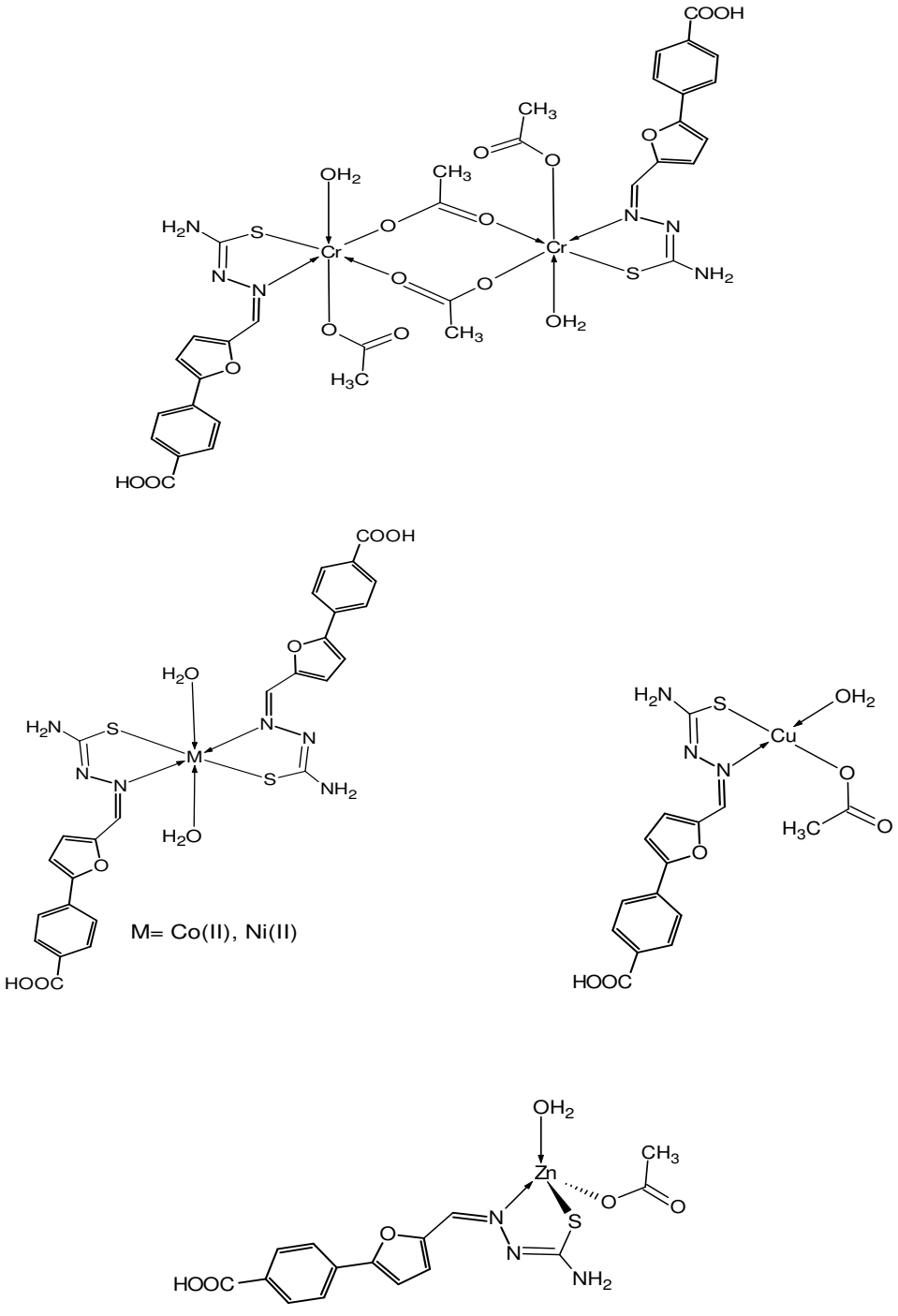

Fig.1.26 Structures of metal complexes of CTHMF2YBA

Table 1.14 Microanalytical, magnetic and conductance data of the ligand CTHMF2YBA and its transition metal complexes

Complex	Colour	Yield (%)	Mol. Wt.	M.P (^{0}C)	Metal% Found (Calculated)	C % Found (Calculated)	H % Found (Calculated)	N % Found (Calculated)	S % Found (Calculated)	μ_{eff} (BM)	Molar Conductance ($\Omega^{-1}cm^2mol^{-1}$)	Geometry
CTHMF2YBA(LH)	Pale brown	66	289	278	-	53.02 (53.98)	4.02 (3.81)	13.94 (14.53)	10.87 (11.07)	-	-	-
$[CrLAc_2(H_2O)]_2$	Pale brown	74	476	>300	11.22 (10.92)	41.69 (42.86)	4.12 (3.58)	12.00 (12.52)	8.66 (9.54)	3.01	6	Octahedral
$[CoL_2(H_2O)_2]$	Gray	62	671	>300	8.04 (8.79)	45.65 (46.50)	3.64 (3.58)	11.88 (12.52)	9.96 (9.54)	3.31	10	Octahedral
$[NiL_2(H_2O)_2]$	Pale Green	68	671	>300	9.69 (8.76)	47.35 (46.52)	4.34 (3.58)	12.14 (12.52)	8.62 (9.54)	2.56	14	Octahedral
$[CuLAc(H_2O)]$	Brown	76	429	>300	14.36 (14.83)	42.68 (42.00)	4.23 (3.50)	8.65 (9.80)	7.91 (7.47)	1.97	7	Square planar
$[ZnLAc(H_2O)]$	Off white	70	430	>300	14.38 (15.19)	40.88 (41.82)	4.43 (3.49)	9.14 (9.76)	6.84 (7.44)	D	12	Tetrahedral

Ac: Acetate, D: Diamagnetic

Table 1.15 Characteristic infrared absorption frequencies of CTHMF2YBA and its transition metal complexes

Complex	υ_{N-H}	υ_{H2O}	$\upsilon_{C-H(Ar)}$	$\upsilon_{COO(asym)}$	$\upsilon_{C=N}$	$\upsilon_{COO(sym)}$	υ_{C-O}	In plane bending	Out of plane bending	υ_{M-N}	υ_{M-S}
CTHMF2YBA (LH)	3377, 3259	-	3165	1689	1614	1553	1286	1103	921, 798, 771	-	-
$[CrLAc_2(H_2O)]_2$	3419, 3398	3263	3157	1680	1604	1544	1282	1105	795,760	670	515
$[CoL_2(H_2O)_2]$	3419, 3403	3277	3157	1685	1606	1546	1282	1101	792,769	671	520
$[NiL_2(H_2O)_2]$	3408, 3383	3319	3155	1678	1604	1510	1278	1058	799,771	677	503
$[CuLAc(H_2O)]$	3421, 3408	3292	3163	1687	1606	1546	1276	1111	790,773	672	549
$[ZnLAc(H_2O)]$	3392, 3403	3263	3155	1680	1602	1544	1282	1122	930, 802,783	671	533

SUMMARY

Five novel heterocyclic Schiff bases namely 3-(1H-indol-3-yl)-2-[(E)-(thiophen-2-ylmethylidene)amino]propanoic acid (I3YT2YMAPA), (E)-3-[thiophen-2-ylmethylene amino]benzoic acid (T2YMABA), (E)-4-(5-[(2-carbamothioylhydrazono)methyl] thiophen-2-yl)benzoic acid (CTHMT2YBA), (E)-4-(5-[(2-phenylhydrazono)methyl] thiophen-2-yl)benzoic acid (PHMT2YBA) and (E)-4-(5-[(2-carbamothioylhydrazono) methyl]furan-2-yl)benzoic acid (CTHMF2YBA) were synthesized and characterized by different techniques like CHNS analysis and spectral studies such as FTIR, NMR, mass and UV-visible. The chelating abilities of these Schiff bases were investigated by synthesizing a number of transition metal complexes. Then these complexes were also subjected to characterization studies by elemental analysis, magnetic moment measurements, conductance measurements, IR, UV-visible and ^{1}Hnmr spectral analysis. All the results are detailed in this part. The thermogravimetric studies of Cr(III) and Ni(II) complexes of all the ligands were also conducted.

The Schiff base 3-(1H-indol-3-yl)-2-[(E)-(thiophen-2-ylmethylidene)amino] propanoic acid (I3YT2YMAPA) was synthesized from thiophene-2-carbaldehyde and the amino acid (s)-2-amino-3-(3-indolyl)propanoic acid. Transition metal complexes of this ligand were prepared with Cr(III), Ni(II), Cu(II) and Zn(II) ions. 1:1 stoichiometry was found to exist between the metal and ligand in all the complexes. The Cr(III) and Ni(II) chelates were found to have octahedral geometry. In the case of copper complex a square planar geometry was fixed. Diamagnetic character was found for Zn(II) complex in the magnetic studies and tetrahedral geometry was assigned for it. The ligand acted as a monovalent bidentate ligand in all the complexes. The azomethine group and the

caboxylate group were coordinated to the metal ion, which was verified by FTIR spectral analysis. The TGA and DTA analysis of the Ni(II) complex exhibited a three stage decomposition pattern.

The chelating efficacy of the ligand T2YMABA was explored by synthesizing transition metal complexes with metal ions of chromium, nickel, copper, zinc and cadmium. All the complexes were found to have 1:1 stoichiometry between the metal and ligand T2YMABA. The ligand was monovalent and bidentate in nature coordinating through azomethine group nitrogen and carboxylate group oxygen atoms. The Cr(III) complex was found to exist in dimeric form. For chromium(III) and nickel(II) complexes octahedral geometry were assigned according to their magnetic behavior. Copper(II) chelate was exhibiting square planar geometry. Tetrahedral geometry was assigned for both the zinc(II) and cadmium(II) complexes. Molar conductance data suggested that all the compounds were non-electrolytic in nature. The Cr(II) complex and Ni(II) complex exhibited four stage and two stage decomposition pattern respectively in TGA and DTA studies.

The Schiff base CTHMT2YBA was prepared by a two step process, first step being Meervin arylation of the thiophene-2-carbaldehyde, followed by condensation reaction with thiocarbamoyl hydrazide. Transition metal complexes of CTHMT2YBA were synthesized with Cr(III), Co(II), Ni(II), Cu(II) and Zn(II) ions and characterized by different techniques. It was concluded that Cr(III), Cu(II) and Zn(II) complexes were of 1:1 stoichiometry whereas in Co(II) and Ni(II) complexes 1:2 stoichiometry was followed. The Cr(III) complex was found to exist in a dimeric form. The Schiff base CTHMT2YBA exhibited tautomerism which was verified by NMR and IR spectral

studies. This Schiff base acted as a monovalent bidentate ligand during complexation. The thermogravimetric analysis of Cr(II) and Ni(II) complexes exhibited well defined three stage decomposition patterns .

Transition metal complexes of the Schiff base PHMT2YBA were synthesized with Cr(III), Co(II), Ni(II), Cu(II) and Zn(II) ions and characterized. It was found that Cr(III), Cu(II) and Zn(II) complexes were of 1:1 stoichiometry whereas Co(II) and Ni(II) complexes followed 1:2 stoichiometry. The denticity of the ligand was found to be one. Chromium(III) complex was assigned octahedral geometry whereas cobalt(II) and nickel(II) complexes were given distorted octahedral geometry. For copper(II) and zinc(II) complexes square planar and tetrahedral geometries were assigned respectively. The Cr(III) and Ni(II) complexes showed three and two decomposition stages respectively in their TGA/ DTA analysis.

Cr(III), Co(II), Ni(II), Cu(II) and Zn(II) complexes of the Schiff base CTHMF2YBA were synthesized and characterized. It was found that Cr(III), Cu(II) and Zn(II) complexes were of 1:1 stoichiometry whereas in Co(II) and Ni(II) complexes 1:2 stoichiometry was followed. The ligand exhibited thioketo-thioenol tautomerism as revealed by the NMR and IR studies. Chromium, cobalt and nickel complexes were found to have octahedral geometry and copper complex showed square planar geometry. For the zinc complex diamagnetic nature was observed and tetrahedral geometry was assigned for it. The thermogravimetric curves of Cr(III) and Ni(II) complexes were recorded and it was found that chromium complex had four and nickel complex had three decomposition stages.

In short, five potential novel heterocyclic Schiff base ligands derived from thiophene-2-carbaldehyde and furan-2-carbaldehyde with different amino compounds and their twenty four transition metal chelates were synthesized and characterized using most modern analytical tools and explained in detail in this part.

.

REFERENCES

1. A.G. Quiruga, C. N. Raninger, *Coord. Chem. Rev*., 248 (2004) 119.
2. D. X. West, A. E. Liberta, S. B. Padhye, R. C. Chikate, P. B. Sonawane, A.S. Kumbhar, R. G. Yerande, *Coord. Chem. Rev*., 123 (1993).
3. T. Wang, Guoz, *Curr. Med. Chem*., 13 (2006) 525.
4. A. C. F. Coires, *Anticancer Agents in Med. Chem*., 7 (2007) 484.
5. T. S. Lobana, R. Shama, G. Bawa, S. Khanna, *Coord. Chem. Rev*., 253 (2009) 977.
6. S. B. Desai, P. B. Desai, K. R. Desai, *Heterocycl. Commun*., 7 (2001) 83.
7. P. Przybylski, A. Huczynski, K. Pyta, B. Brzezinski, F. Bartl, *Curr. Org. Chem*., 13(9) (2009) 124.
8. A. A. Abdel Aziz, A. N. M. Salem, M. A. Sayed, M. M. Aboaly, *J. Mol. Struct*., 1010 (2012) 130.
9. D. Sinha, A.K. Tiwari, S. Singh, G. Shukla, P. Mishra, H. Chandra, A. K. Mishra, *Eur. J. Med. Chem*., 43 (2008) 160.
10. A. O. De Souza, F. C. S. Galetti, C. L. Silva, B. Bicalho, M. M. Parma, S. F. Fonseca, A. J. Marsaioli, A.C.L.B Trindade, R. P. Freitas-Gi, F.S. BezerraS, *Quim. Nova*, 30 (2007) 1563.
11. P. Rathelo, P. Vanell, M. Gasquet, F. Delmas, M. P. Crozet, P. Timon-David, J. Maldonado., *Eur. J. Med. Chem.*, 30 (1995) 503.
12. G. Bringmann, M. Dreyer, J. H. Faber, P. W. Dalsgaard, D. Staerk, J. W. Jaroszewsk, *J. Nat. Prod*., 67 (2004) 743.
13. Z. Guo, R. Xing, S. Liu, Z. Zhong, X. Ji, L. Wang, *Carbohydr. Res*., (2007) 342.
14. M.B. Gholivand, F. Ahmadi, E. Rafiee, *Electroanalysis*, 18 (2006) 1620.

15. M.R. Ganjali, S.Shirvani-Arani, P. Norouzi, M. Rezapour, M.Salavati-Niasari, *Mikrochim. Acta*, 146 (2004) 35.
16. W. Wroblewski, Z. Brzozka, D. M. Rudkevich, D. N. Reinhoudt, *Sens. Actuators* B, 37 (1996) 151.
17. W. Wroblewski, K. Wojciechowski, A. Dybko, Z. Brzozka, R. J. M. Egberink, B. H. M. Snellink-Ruel, D.N. Reinhoudt, *Sens. Actuators* , 68 (20003) 13.
18. M.R. Ganjali, F. Mizani, M. Salavati-Niasari, *Anal. Chim. Acta*, 481 (2003) 85.
19. M. Shamsipur, S. Ershad, N. Samadi, A.R. Esmaeilbeig, R. Kia, A. Abdolmaleki, *Electroanalysis*, 17 (2005) 1828.
20. G. Tantaru, V. Dorneanu, M. Stan., *J. Pharm. Biomed. Anal*., 27 (2002) 827.
21. M. Mashhadizadeh, M. Pesteh, Mahzad Talakesh, I. Sheikhshoaie, M. Ardakani, M. Karimi, *Spectrochimica Acta,* Part B, 63 (2008) 885.
22. Z. Holzbecher, *Chem. Listy*, 52 (1958) 425.
23. N. Raman, S. Ravichandran, C. Thangarajaj*, Chem. Sci.*, 116(4) (2004) 215.
24. A. Hadush, R.K. Upadhyay, T. Kebede, *Oriental J. Chem.*, 29(3) (2008).
25. Z. H. Chohan, A. Munawar, C. T. Supuran, *Met. Based Drugs*, 8(3) (2001) 137.
26. E. Yousif, A. Majeed, K. Al-Sammarrae, N. Salih, J. Salimon, B. Abdullah, *Arabian J. Chem.*, doi:10.1016/j.arabjc.2013.06.006 (2013).
27. R. M. Ahmed, E. I. Yousif, H. A. Hasan, M. J. Al-Jeboori, *Sci. World J.*, Article ID 289805 (2013).
28. A. Reiss, M. Carmen Chifiriuc, E. Amzoiu, C. Ionuţ Spînu, *Bioinorg. Chem. Appl.*, Article ID 926287, 2014 (2014).

29. M. Mustapha, B. R. Thorat, Sudhir Sawant, R. G. Atram , Ramesh Yamgar, *J. Chem. Pharm. Res.,* 3(4) (2011) 5.

30. N. Raman, J. Dhaveethu Raja, A. Sakthivel, *J. Chem. Sci*., 119(4) (2007) 303.

31. M.. A. Hadi, *J. Kerbala Univ.*, 7 (4) (2009) 52.

32. F. T. Esmadi, O. F. Khabour, K. Abbas, A. Elah Mohammad, R. T. Obeidat, D. Mfady, *Drug and Chem. Toxi.* (doi:10.3109/01480545.2015.1017882) (2015).

33. V. L. Borde, S. G. Shankarwar, C. D. Thakur, A. G. Shankarwar, *Pelagia Res. Lib. Adv. Appl. Sci. Res.,* 5(6) (2014) 229.

34. V.B. Badwaik, R.D. Deshmukh, A.S. Aswar, *J. Coord. Chem.,* 62 (12) (2009) 2037.

35. S. B. Ade, M. N. Deshpande, J. H. Deshmukh, *Rasayan J. Chem.*, 5 (1) (2012) 10.

36. A. S. Munde, A. N. Jagdale, S. M. Jadhav , T. K. Chondhekar*, J. Serb. Chem. Soc*., 75 (3) (2010) 349.

37. B. Priya D, S. Lakshmi, *Int. J. Chem. Tech. Res.,* 6 (1) (2014) 87.

38. S. S. Sawant, V. Pawar , S. Janrao , R. S. Yamgar, Y. Nivid, *Int. J. Res. Pharm. Chem.*, 3 (3) (2013).

39. G. G. Mohamed, M. Mohamed Omar, A. M. Hindy, *Turk. J. Chem*., 30 (2006) 361.

40. M. N. Uddin, D. A. M. Chowdhury, M. M. Rony, M. Ershad Halim, *Modern Chemistry*, 2(2) (2014) 6.

41. K. P. Srivastava, A. Kumar, R. Singh, *J. Chem. Pharm. Res*., 2(6) (2010) 68.

42. M. M. Omar, G. G. Mohamed, A. M. M. Hindy, *J. Therm. Anal. Cal.*, 86(2) (2006) 315.

43. A. Paul, K. J. Thomas, V. P. Raphael, K. S. Shaju, *Oriental J. Chem*., 28(3) (2012) 1501.

44. V. P. Raphael, K. J. Thomas, K. S. Shaju, A. Paul, *ISRN Corrosion*, (2013) doi: 10.1155/2013/390823.

45. A. Paul, J. Thomas K., V. P. Raphael, K. S. Shaju, *IOSR J. Appl. Chem*., 1(6) (2012) 17.

46. N. H. Al-Shaalan, *Molecules*, 16 (2011) 8629.

47. G. G. Mohammed, M. M. Omar, A. M. Hindy, *Turk. J. Chem*., 30 (2006) 361.

48. A. A. R. Despaigne, J.G. Da Silva, A. C. M. Do Carmo, O. E. Piro, E. E. Castellano, H. Beraldo, *J. Mol. Struct*., 920 (2009) 97.

49. A. A. Soliman, W. Linert, *Thermochim. Acta*, 333 (1999) 67.

50. G. L. Parrilha, R. P. Vieira, A. P. Rebolledo, I. C. Mendes, L. M. Lima, E. J. Barreiro, O. E. Piro, E. E. Castellano, H. Beraldo, *Polyhedron,* 30 (2011) 1891.

51. R. Prasad, P. P. Thankachan, M. T. Thomas, R. Pathak, *J. Ind. Chem. Soc.*, 78 (2001) 28.

52. M. F. Alias, M. O. Hamza, T. A. Kareem, *J. Al-Nahrain Univ.,* 14 (2) (2011) 10.

53. Soleimani, Esmaiel, *J. Therm. Anal. Calori.*, 111 (1) (2013) 129.

54. V. Ciornea, S. Shova, Gh. Novitchi, D. Ganzhu, O. N. Kazheva, A. Gulea, Yu. A. Simonov, *Russ. J. Coord. Chem.,* 35 (11) (2009) 817.

55. L. G. Wang, *Acta Cryst*., 63 (2007) 479.

56. T. H. Al-Noor, A. T. Al-Jeboori, R. L. Sadaw, *Chem. Proc. Engg. Res*., 13 (2013) 112.

57. S. Paulo, *J. Braz. Chem. Soc*., 19 (3) (2008) 845.

58. Z. F. Davood, M.W. Ibrahim, *Natl. J. Chem.*, 30 (2008) 330.

59. L. Racane, V. T. Kulenovic, D. W. Boykin, G. Karminski-Zamola, *Molecules*, 8 (2003) 342.

60. A. Bury, A. E. Underhill, D. R. Kemp, N. J. O'Shea, J. P. Smith, P. S Gomm, F. Hallway, *Inorg. Chim. Acta*, 138 (1987) 85.

61. N. Mondal, D. K. Dey, S. Mitra, K. M. A. Malik, *Polyhedron*, 19 (2000) 2707.

Part II
Thermoanalytical studies

Chapter 1

Nimmy Kuriakose “Physicochemical, thermoanalytical, electrochemical and antitumour studies of transition metal complexes of schiff bases derived from heterocyclic carbonyl compounds” Thesis. Department of Chemistry, St. Thomas College, University of Calicut, 2015

CHAPTER 1

INTRODUCTION AND REVIEW

In thermoanalytical methods the thermal behavior of the substance is recorded as a function of temperature and/or time and the recorded curves are considered as thermal spectra, usually called thermograms. Thermal methods of chemical analysis are thermogravimetric analysis (TGA), derivative thermogravimetry (DTG), differential thermal analysis (DTA), differential scanning calorimetry (DSC), thermomechanical analysis (TMA), dynamic mechanical analysis (DMA) etc[1]. The increasing awareness in the area of thermoanalytical methods is evidenced by the increasing number of research papers published every year incorporating the thermal behavior of wide variety of materials.

TGA and DTA are valuable techniques because their applications do not usually impose any restriction on the systems being studied. With the development of sophisticated, rugged and sensitive automatic recording thermobalances, there is an increasing tendency to use TGA as the first stage in a multi-instrument approach for the analysis of materials[2-4].

Thermogravimetric analysis (TGA)

The technique of thermogravimetric analysis involves the weighing of the substance under investigation while it is being heated at a predetermined and preferably linear rate. There are three types of thermogravimetry (i) static or isothermal gravimetry (ii) quasistatic TGA and (iii) dynamic thermogravimetry. In isothermal gravimetry, the sample weight is recorded as a function of time at a constant temperature. In the second

method the sample is heated to constant weight at each step in a series of increasing temperatures. In dynamic thermogravimetry, the sample is heated at a uniform rate and this method is suitable for the determination of approximate quantitative thermal behavior of the system.

As in thermogravimetry, the derivative thermogravimetric analysis (DTG) involves the measurement of rate of change of weight of the specimen as it is being heated at a uniform slow rate. DTG curves involve a number of peaks and the area covered by these peaks is proportional to the total change in weight of the sample. Thermogravimetric measurements are affected by factors such as atmosphere near the sample, heat of the reaction, heating rate and sample characteristics. TG and DTG studies are widely used in qualitative and quantitative analysis and thermal stability studies.

Kinetic studies using thermogravimetric measurements

The kinetic parameters of solid-state reactions which involve weight loss or gain can be investigated using thermogravimetric data[5–8]. Freeman and Carroll[9] have proved many of the advantages of this method over the conventional isothermal method. The use of one single sample for investigation is one of the highlighted advantages of this method. However, the influence of procedural details such as, pre-history of sample, crucible geometry, heating rate and particle size, on the parameters has yet to be fully explored. It is also important that accurate temperature measurement should be ensured both for precision and also to detect any departure from a linear heating rate due to endo or exothermic reactions. The usage of small samples can effectively eliminate such deviations.

TG and DTA methods are employed for the study of kinetics of a chemical reaction and to determine basic kinetic constants such as the rate constant, activation energy, order of reaction and frequency factor. In these methods a change in some physical property like weight, enthalpy or volume as a function of temperature is measured continuously and automatically.

There are two approaches for kinetic studies: isothermal method and dynamic method. Isothermal method involves the determination of degree of transformation at constant temperature as a function of time and the dynamic method involves the determination of degree of transformation as a function of time during a linear increase of temperature. Kinetic studies by TGA are based on Arrhenius equation,

$$K = A \exp\left(-\frac{E_a}{RT}\right)$$

where K= rate constant, A= Arrhenius factor, R= universal gas constant, E_a= energy of activation and T= temperature in Kelvin scale.

Non-isothermal methods have been used extensively for the determination of kinetic parameters. Many authors have employed different computational methods among which the Freeman Carroll, Flynn-Wall-Ozawa, Coats Redfern, Horowitz Metzger, Doyle modified by Zsako and Satava-Skvarfi methods are well known and have been tested by several researchers[10,11].

Non isothermal methods are more faster than the isothermal processes, since the latter requires long running time. Therefore multiple experiments are to be conducted in order to derive kinetic parameters by isothermal methods, but even with a single step it is possible to calculate the kinetic parameters by non-isothermal process[12].

Method of Coats and Redfern

Coats and Redfern[13] developed a method for the calculation of activation energy from non-isothermal TG data at a constant heating rate. This is an integral method[14-17] that evaluates various orders of reaction and compares the linearity in each case to determine the correct order. For a first-order reaction process, Coats and Redfern provided an approximation[18]. This rate equation considers the functional conversion relation, which depends on relation mechanism type.

In this method, the temperature integral is determined using the Rainville function[19] and the Coats-Redfern equation is derived as

$$\ln\left[\frac{g(\alpha)}{T^2}\right] = \ln\left[\frac{AR}{\phi E}\left(1-\frac{2RT}{E}\right)\right] - \frac{E}{RT} \quad (1)$$

where $g(\alpha) = 1-(1-\alpha)^{(1-n)} / (1-n)$, α is the fractional decomposition and n is the order of the reaction. The term $\ln\left[\frac{AR}{\phi E}\left(1-\frac{2RT}{E}\right)\right]$ will be a constant for the usual value of E and temperature range in which the reaction generally occurs, since the term 2RT/E is very much smaller than 1. Therefore $\ln[g(\alpha)/T^2]$ is plotted against 1/T for all possible mechanisms and the best straight line determined the operating mechanism. The slope and the intercept of the linear plot can be employed to calculate E and A. The entropy of activation, ΔS can be evaluated from the pre-exponential factor A, using the equation

$$A=\frac{kT_s}{h}\exp\left[\frac{\Delta S}{R}\right] \quad (2)$$

where k is the Boltzmann constant, T_s is the peak temperature from DTA/DTG, h is the Plancks constant and R is the universal gas constant. A trial and error method is suggested for determining the form of $g(\alpha)$ and the value of n.

Decomposition reaction mechanism

Mathematical treatment of decomposition reaction mechanism can be performed by non- isothermal kinetic methods. These methods are based on the principle that a non-isothermal reaction will be proceded isothermally in an infinitesimal time interval, as Sestak et. al.[20] and Satava[21] had described it. An Arrhenius type equation is suitable to express the rate of such decomposition reaction as follows,

$$\frac{d\alpha}{dt} = A\, exp\left(-\frac{E}{RT}\right) f(\alpha) \tag{3}$$

where A is the pre-exponential factor, t is the time and $f(\alpha)$ is characteristic of the mechanism of the reaction.

For a linear heating rate, $\phi = \frac{dT}{dt}$ and substituting in the above equation

$$\frac{d\alpha}{f(\alpha)} = \int_0^T \frac{A}{\phi}\, e^{-E/RT}\, dT \tag{4}$$

On integration of the left hand side of the equation,

$$\int_0^\alpha \frac{d\alpha}{f(\alpha)} = g(\alpha) = \int_0^T \frac{A}{\phi}\, e^{-E/RT} dT \tag{5}$$

where g (α) is the integrated form of $f(\alpha)$. It is possible to propose a series of forms of $f(\alpha)$ and from the one, which is the best representation of the experimental data, the mechanism of decomposition reaction is suggested. The kinetic parameters can be obtained from the nine probable reaction mechanisms proposed by Satava, which are listed in Table 2.1. Coats-Redfern method in the general form (equation 6) is chosen, since it is one of the best solutions[22,23] recommended and then the various g(α) values are substituted.

$$\ln \frac{g(\alpha)}{T^2} = \ln \left[\frac{AR}{\phi E} - \frac{E}{RT} \right] \tag{6}$$

By the method of least squares the linear plots were drawn from the nine forms of $\ln[g(\alpha)/T^2]$ versus 1/T. The kinetic parameters like E, A, ΔS and the corresponding correlation coefficient r for the linear plots were calculated.

Differential thermal analysis (DTA)

In differential thermal analysis a sample and a reference material are heated or cooled in close proximity at same linear heating rate in a furnace and the temperature difference (ΔT) between the sample and the reference material are continuously recorded as a function of temperature. α- Alumina is often used as the reference material which behaves satisfactorily up to 2000^0C[24]. By the use of this technique, the qualitative identification of a compound is possible by determining the temperature at which endothermic or exothermic reaction takes place as the substance is linearly heated. The endothermal and exothermal bands appearing in the thermogram give information regarding the enthalpy changes. A usual DTA endotherm consists of depressions indicating the energy gains in the specimen under investigation. Instrumental factors such as furnace atmosphere, geometry and material of sample holder, heating rate and response of the recording devices affect the DTA analysis. The characteristics of the sample like particle size, amount, heat capacity, packing density and thermal conductivity also play important role in determining the shape of the curve.

Many research papers are there which have reported the use of thermoanalytical methods for the study of decomposition reaction of Schiff base complexes[26-41].

Table 2.1 Nine mechanistic equations by Satava

No.	Function	Equation	Rate Controlling Process
I	D_1	$\alpha^2 = kt$	One dimensional Diffusion
II	D_2	$(1-\alpha)\ln(1-\alpha) + \alpha = kt$	Two dimensional diffusion; Cylindrical symmetry
III	D_3	$[1-(1-\alpha)^{1/3}]^2 = kt$	Three dimensional diffusion Spherical symmetry; Jander equation
IV	D_4	$(1- 2/3\alpha) - (1-\alpha)^{2/3} = kt$	Three dimensional diffusion, Spherical symmetry; Ginstling-Brounshtein equation
V	F_1	$-\ln(1-\alpha) = kt$	Random nucleation; One nucleus at each particle; Mampel equation
VI	A_2	$-\ln(1-\alpha)^{1/2} = kt$	Random nucleation; Avrami equation I
VII	A_3	$-\ln(1-\alpha)^{1/3} = kt$	Random nucleation; Avrami equation II
VIII	R_2	$1-(1-\alpha)^{1/2} = kt$	Phase boundary reaction; Cylindrical symmetry
IX	R_3	$1-(1-\alpha)^{1/3} = kt$	Phase boundary reaction; Spherical symmetry

Scope of present investigation

The thermogravimetric and differential thermogravimetric studies of Cr(III) and Ni(II) complexes of 3-(1H-indol-3-yl)-2-[(E)-(thiophen-2-ylmethylidene)amino] propanoic acid (I3YT2YMAPA), (E)-3-[thiophen-2-ylmethyleneamino]benzoic acid (T2YMABA), (E)-4-(5-[(2-carbamothioylhydrazono)methyl]thiophen-2-yl)benzoic acid (CTHMT2YBA), (E)-4-(5-[(2-phenylhydrazono)methyl]thiophen-2-yl)benzoic acid (PHMT2YBA) and (E)-4-(5-[(2-carbamothioylhydrazono)methyl]furan-2-yl)benzoic acid (CTHMF2YBA) are presented in this part. The regions of thermal stability and the temperature of inception and decomposition are noted from the data. Also the temperatures of maximum rate of decomposition of each complex were assigned from the thermograms. The comparison of TG and DTA results makes it possible to explain the thermal stability and different stages of decomposition of complexes. The intermediate products are confirmed by chemical analysis and infrared spectral techniques.

The Coats-Redfern method which is an integral method was employed for the mathematical analysis of the non-isothermal TG curves and the activation parameters have been evaluated for all these complexes. The mechanism of decomposition has been established from the thermogravimetric data using the nine mechanistic equations in comparison with the Coats-Redfern method.

Part II
Thermoanalytical studies

Chapter 2

Nimmy Kuriakose “Physicochemical, thermoanalytical, electrochemical and antitumour studies of transition metal complexes of schiff bases derived from heterocyclic carbonyl compounds” Thesis. Department of Chemistry, St. Thomas College, University of Calicut, 2015

CHAPTER 2

MATERIALS, METHODS AND INSTRUMENTS

Reagents

Analar grade chemicals supplied by E. Merck were used for the synthetic strategies of the compounds. Commercial solvents were distilled by adopting the standard methods. Detailed discussions regarding the reagents are given in Part I.

Preparation of ligands and complexes

The Schiff base ligands, 3-(1H-indol-3-yl)-2-[(E)-(thiophen-2-ylmethylidene) amino]propanoic acid (I3YT2YMAPA), (E)-3-[thiophen-2-ylmethyleneamino]benzoic acid (T2YMABA), (E)-4-(5-[(2-carbamothioylhydrazono)methyl]thiophen-2-yl)benzoic acid (CTHMT2YBA), (E)-4-(5-[(2-phenylhydrazono)methyl]thiophen-2-yl)benzoic acid (PHMT2YBA) and (E)-4-(5-[(2-carbamothioylhydrazono)methyl]furan-2-yl)benzoic acid (CTHMF2YBA) were synthesized by the condensation reaction between the corresponding carbonyl compound and the amino compound in ethanolic medium. The Cr(III) and Ni(II) complexes of these ligands were prepared by refluxing with the corresponding metal acetates. The preparative aspects of these ligands and complexes are explained in Part I.

Instruments

The instruments used for the present thermoanalytical studies are Perkin Elmer STA 6000/Diamond TG/DTA thermal analyser system with PT-PT/Rh (Type R) thermocouples and Bruker AXS D8 advance diffractometer.

Thermogravimetric analyses of the coordination complexes were carried out with air as the initial purge gas, at a heating rate of 10^0C/min employing about 3-7mg of each complex.

Part II
Thermoanalytical studies

Chapter 3

Nimmy Kuriakose “Physicochemical, thermoanalytical, electrochemical and antitumour studies of transition metal complexes of schiff bases derived from heterocyclic carbonyl compounds” Thesis. Department of Chemistry, St. Thomas College, University of Calicut, 2015

CHAPTER 3

THERMAL DECOMPOSITION KINETICS OF Cr(III) COMPLEXES OF T2YMABA, PHMT2YBA, CTHMT2YBA AND CTHMF2YBA

Cr(III) complexes of four novel potential Schiff bases, (E)-3-[thiophen-2-ylmethyleneamino]benzoic acid (T2YMABA), (E)-4-(5-[(2-phenylhydrazono)methyl] thiophen-2-yl)benzoic acid (PHMT2YBA), (E)-4-(5-[(2-carbamothioylhydrazono) methyl]thiophen-2-yl)benzoic acid (CTHMT2YBA) and (E)-4-(5-[(2-carbamothioyl hydrazono)methyl]furan-2-yl)benzoic acid (CTHMF2YBA) were synthesized and characterized by different analytical techniques. The details are well explained in Part 1. The thermal behavior of these Cr(III) complexes were studied using thermogravimetry and differential thermal analysis. Using Coats-Redfern method and nine mechanistic equations, the thermodynamic and kinetic parameters like activation energy, change in entropy and Arrhenius frequency factor were calculated. Non-isothermal methods were employed for the evaluation of reaction mechanism using the nine mechanistic equations given by Sestak and Berggren and Satava. The thermal behaviors of all these complexes are described in detail here.

Figures 2.1 to 2.4 represent the structures and instrumental TGA/DTA curves of Cr(III) complexes with four different ligands. The thermal decomposition data of these compounds are given in Tables 2.2 and 2.3.

Thermogravimetric curves of $[CrL^1Ac_2(H_2O)]_2$ (where L^1=T2YMABA) gave a four stage decomposition pattern, in which the second stage comprises of two substages. The first stage of the curve represents the loss of two water molecules from the sample moiety in the temperature range of 60-140^{0}C. This confirmed the presence of coordinated

water molecules in the complex[45]. The loss of two non-bridged acetate groups and two CO_2 molecules from the ligands are exhibited in second stage, i.e. IIa and IIb respectively. The third stage represents the loss of the rest of both the ligands and the removal of two bridged acetate groups is depicted in the fourth stage of decomposition. The overall mass loss according to the TG curve is 81.53% and the theoretical mass loss for the conversion of the complex into Cr_2O_3 is 81.82%. The mass loss according to the pyrolytic data was also found to be in agreement with these results (81.10%).

The complex $[CrL^2Ac_3(H_2O)_2]$ (where L^2=PHMT2YBA) has three stages of decomposition reaction. The first one is due to the removal of two coordinated water molecules from the complex[46-48]. The second stage decomposition corresponds to the loss of one acetate group at around 290^0C and the in the last stage, the ligand and two acetate groups are removed from the complex molecule at 700^0C. The overall mass loss according to the TG curve is 87.37% and the theoretical mass loss for the conversion of the complex into metal oxide is 87.05%. The mass loss according to the pyrolytic data was found to be 86.54%.

The decomposition of Cr(III) complex of CTHMT2YBA, $[CrL^3Ac_2(H_2O)]_2$ also resulted with a definite three stage pattern. The first stage (60-150^0C) is assigned to the loss of two water molecules. Two non-bridged acetate groups and two CO_2 molecules from the ligand are removed in the second stage. The third stage of decomposition corresponds to the loss of rest of both the ligands and two bridged acetates. The percentage mass loss according to the TG curve is 84.82% which is in good agreement with the theoretical value (84.35%). The mass loss from the pyrolysis is found to be 83.94%.

Cr(III) complex of the ligand CTHMF2YBA, $[CrL^4Ac_2(H_2O)]_2$ underwent a four stage decomposition pattern. Loss of two water molecules are observed in the temperature interval 62-137^{0}C in the initial stage. The second stage consists of three substages in the temperature range 137-288^{0}C. Two amino groups, two CO_2 molecules and two acetate groups are lost subsequently in each of these substages. Then in the third stage, two bridged acetate groups are removed and in fourth stage, the rest of both the ligands are lost. Overall mass loss of 83.70% is observed from the thermogravimetric curves. The theoretical and pyrolytic mass loss percentages are 84.03% and 82.95% respectively, which also confirms the probable assignments suggested for the decomposition stages.

Kinetics of decomposition

The mechanism of decomposition reaction of a chelate can be assigned by selecting the appropriate mechanistic equation which has a high degree of correlation coefficient[49-51]. The corresponding function g(α) is chosen from which the kinetic parameters E, A and ΔS were calculated which are in good agreement with those obtained by the integral method.

From the kinetic parameters derived, it is assigned that the first stage decomposition, the first substage of second decomposition step and the third decomposition stage of the chelate $[CrL^1Ac_2(H_2O)]_2$ follows first order kinetics. Since the parameters E, A and ΔS values obtained from the Coats-Redfern method with n=1 are in close agreement with those obtained from the Mampel equation, it can be inferred that the rate controlling process of the reaction is random nucleation with the formation of one nucleus in each particle and is independent of thermal techniques used. For the substage

IIb and fourth stage of decomposition of Cr(III) complex, R_3 mechanism with order of the reaction 2/3 can be assigned which is evident from the comparison of kinetic parameters from mechanistic and non mechanistic Coats-Redfern equation. The R_3 mechanism is based on phase boundary reaction, spherical symmetry and gives the maximum correlation for these decomposition stages.

For the Cr(III) complex of (E)-4-(5-[(2-phenylhydrazono)methyl]thiophen-2-yl) benzoic acid (PHMT2YBA) and (E)-4-(5-[(2-carbamothioylhydrazono)methyl]thiophen-2-yl)benzoic acid (CTHMT2YBA), all the different stages of decomposition process are assigned first order kinetics since the kinetic parameters calculated from the Coats-Redfern equation with n=1 are in good agreement with those obtained for the F_1 mechanism based on Mampel equation. This indicates that the rate controlling process is random nucleation.

In the case of first stage decomposition of the Cr(III) complex of (E)-4-(5-((2-carbamothioylhydrazono)methyl)furan-2-yl)benzoic acid (CTHMF2YBA), the kinetic parameters derived using the non mechanistic equation with n=1/3 are in good agreement with those values obtained from the equation VIII of mechanistic equations. It is therefore concluded that the decomposition process where two coordinated water molecules are removed from the complex, follows R_2 mechanism based on phase boundary reaction with cylindrical symmetry. For all other stages of decomposition, first order kinetics is assigned. The rate controlling process is random nucleation which follows F_1 mechanism based on Mampel equation.

The kinetic parameters such as energy of activation E, pre-exponential factor A and entropy of activation ΔS calculated for the various stages of decomposition of the

complexes using mechanistic and non mechanistic kinetic equations are summarized in Tables 2.4 to 2.8. The mechanisms of decomposition of various stages as well as the order of decomposition of all the various stages of the complexes are given in Tables 2.9 to 2.11. It can be noted that the larger the activation energy for the decomposition, greater the thermal stability of the compound. The relative thermal stabilities of these chelates can be given as $[CrL^3Ac_2(H_2O)]_2$<$[CrL^4Ac_2(H_2O)]_2$<$[CrL^1Ac_2(H_2O)]_2$< $[CrL^2Ac_3(H_2O)_2]$. From the thermal studies it is quite evident that the monomeric structure is more stable to heat than the dimeric structure.

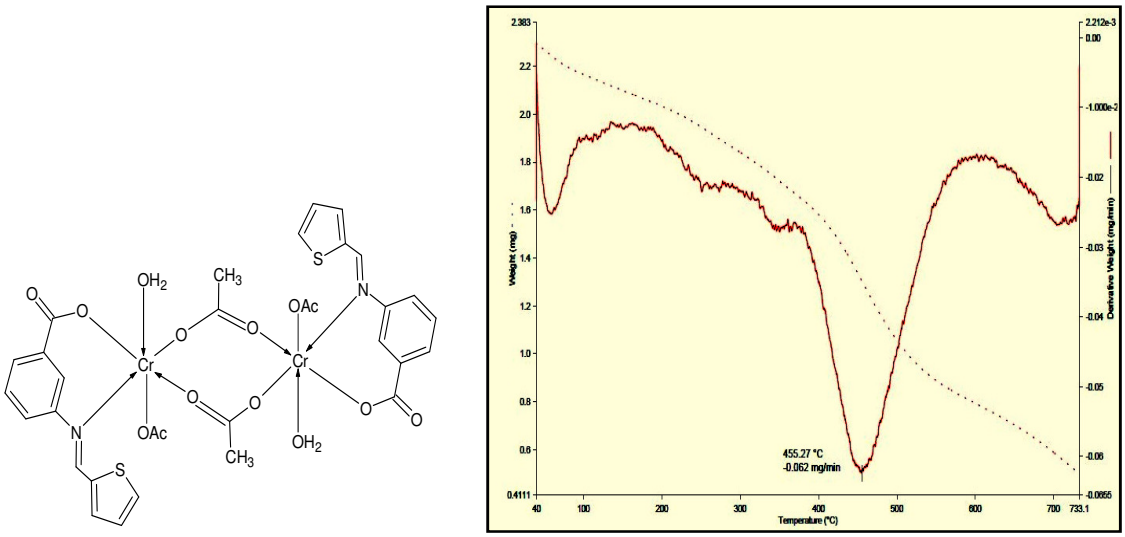

Fig. 2.1 Structure, TGA and DTA curves of $[CrL^1Ac_2(H_2O)]_2$

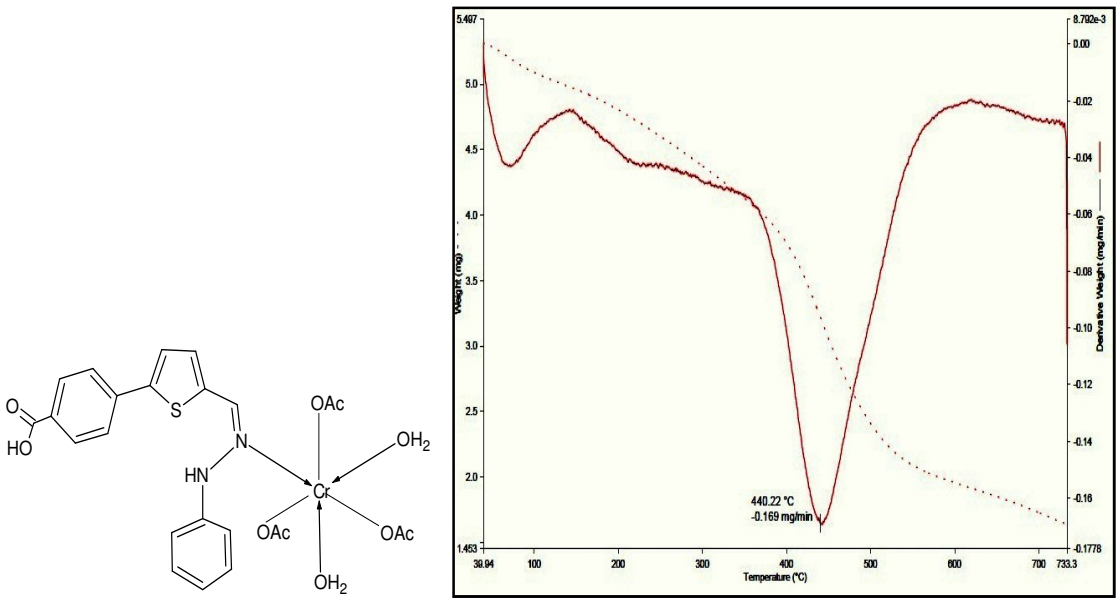

Fig. 2.2 Structure, TGA and DTA curves of $[CrL^2Ac_3(H_2O)_2]$

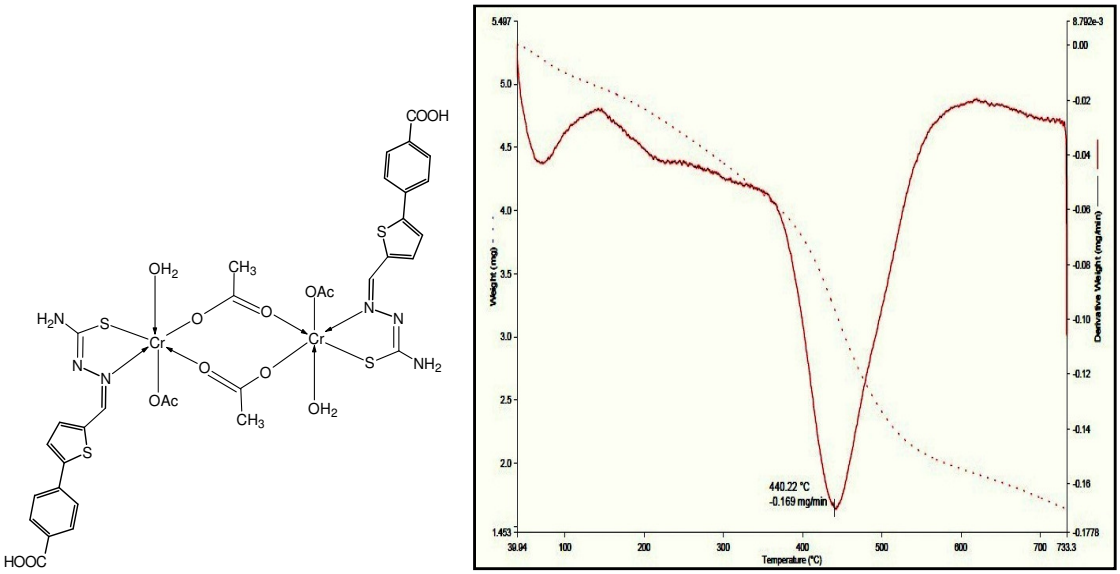

Fig. 2.3 Structure, TGA and DTA curves of $[CrL^3Ac_2(H_2O)]_2$

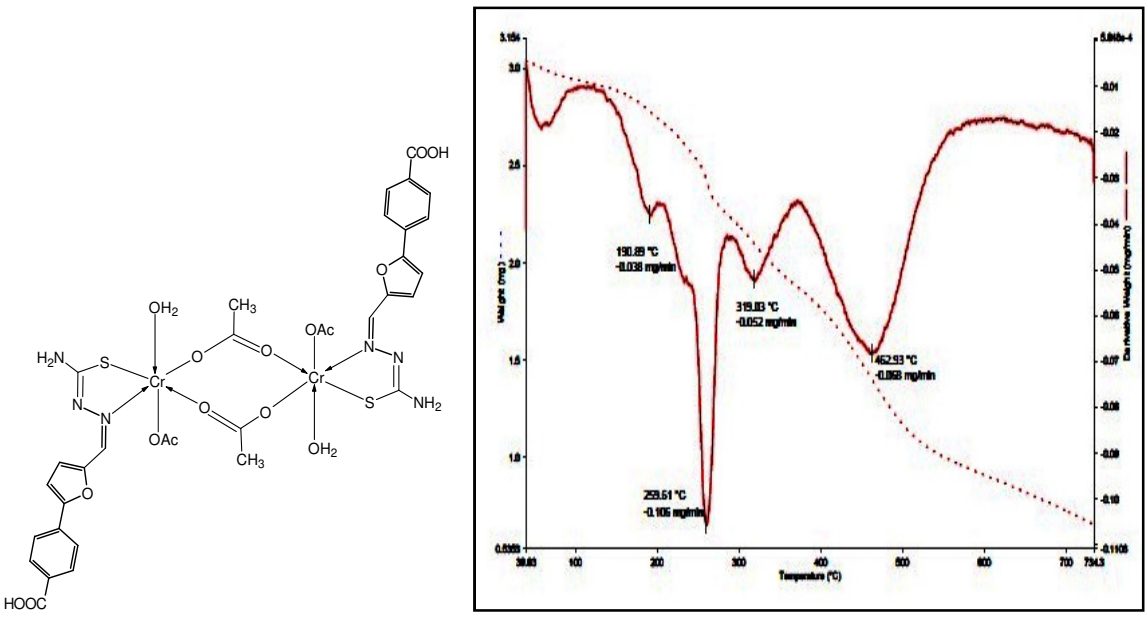

Fig. 2.4 Structure, TGA and DTA curves of $[CrL^4Ac_2(H_2O)]_2$

Table 2.2 Thermal decomposition data of Cr(III) complexes of (E)-3-[thiophen-2-ylmethyleneamino]benzoic acid (T2YMABA) and (E)-4-(5-[(2-phenylhydrazono)methyl]thiophen-2-yl)benzoic acid (PHMT2YBA)

Complex	Stage	Temp range in TG (^{0}C)	Peak temp in TG (^{0}C)	Peak temp in DTA (^{0}C)	Loss of mass %			Probable assignment
					From TG	Cald.	From Pyrolysis	
$[CrL^1Ac_2(H_2O)]_2$	I	60-140	80	84	4.87	4.31	-	Loss of $2H_2O$
	IIa	140-305	255	258	13.98	14.11	-	Loss of two acetate groups
	IIb	305-375	341	344	10.22	10.53	-	Loss of two CO_2 molecules from ligands
	III	375-600	454	456	38.92	38.76	-	Loss of rest of both ligands
	IV	600-748	712	715	13.54	14.11	-	Loss of two bridged acetate groups
					81.53	81.82	81.10	
$[CrL^2Ac_3(H_2O)_2]$	I	60-145	82	85	5.98	6.13	-	Loss of $2H_2O$
	II	145-298	222	224	10.28	10.05	-	Loss of one acetate
	III	298-742	438	441	71.11	70.87	-	Loss of ligand and two acetate groups
					87.37	87.05	86.54	

L^1= T2YMABA, L^2 = PHMT2YBA

Table 2.3 Thermal decomposition data of Cr(III) complexes of (E)-4-(5-[(2-carbamothioylhydrazono)methyl]thiophen-2-yl)benzoic acid (CTHMT2YBA) and (E)-4-(5-[(2-carbamothioylhydrazono)methyl]furan-2-yl)benzoic acid(CTHMF2YBA)

Complex	Stage	Temp range in TG (^{0}C)	Peak temp in TG (^{0}C)	Peak temp in DTA (^{0}C)	Loss of mass %			Probable assignment
					From TG	Cald.	From Pyrolysis	
$[CrL^3Ac_2(H_2O)]_2$	I	60-152	65	66	4.02	3.66	-	Loss of $2H_2O$
	II	152-346	236	239	21.52	21.14	-	Loss of two acetate groups and two CO_2 molecules
	III	346-741	451	452	59.28	59.56	-	Loss of rest of both ligands and two bridged acetate groups
					84.82	84.35	83.94	
$[CrL^4Ac_2(H_2O)]_2$	I	62-137	78	82	3.89	3.78	-	Loss of $2H_2O$
	IIa	137-199	188	191	3.52	3.36	-	Loss of 2 NH_2 groups
	IIb	199-242	232	234	9.08	9.24	-	Loss of two CO_2 molecules
	IIc	242-288	257	260	12.14	12.39	-	Loss of two acetate groups
	III	288-373	318	319	13.06	12.39	-	Loss of two bridged acetate groups
	IV	373-734	461	463	42.01	42.87	-	Loss of rest of both ligands
					83.70	84.03	82.95	

L^3 = CTHMT2YBA, L^4 = CTHMF2YBA

Table 2.4 Kinetic parameters of the decomposition of Cr(III) complex of (E)-3-[thiophen-2-ylmethyleneamino]benzoic acid (T2YMABA) from TG using mechanistic equations

Complex	Mechanistic equations									
	Parameter*	1	2	3	4	5	6	7	8	9
$[CrL^1Ac_2(H_2O)]_2$	E	85.95	96.46	111.21	101.23	61.008	27.489	16.319	48.956	52.594
	A	6.22×10^9	1.5×10^{11}	7.16×10^{12}	1.89×10^{11}	4.1×10^6	32.424	0.4997	23×10^4	6.06×10^3
Stage I	ΔS	-58.82	-32.38	-0.226	-30.425	-119.69	-217.38	-252.08	-162.71	-154.76
	r	0.8400	0.8701	0.904	0.8824	0.9230	0.9071	0.8863	0.8770	0.8942
	E	165.48	181.25	202.5	188.16	109.47	51.06	31.59	92.3425	97.58
Stage IIa	A	7.93×10^{16}	4.02×10^{18}	4.31×10^{20}	6.67×10^{18}	5.28×10^{10}	4.18×10^3	14.33	1.69×10^8	5.31×10^8
	ΔS	73.85	106.49	145.36	110.70	-44.38	-180.33	-227.53	-92.16	-82.63
	r	0.8693	0.8921	0.9174	0.9012	0.9331	0.9240	0.9130	0.8993	0.9117
	E	295.77	324.91	364.40	337.73	199.31	94.60	59.69	167.41	177.15
Stage IIb	A	5.13×10^{22}	1.13×10^{25}	9.16×10^2	3.6×10^{25}	7.56×10^{14}	4.99×10^5	351.59	4.64×10^{11}	2.41×10^{12}
	ΔS	183.84	228.67	284.38	238.33	33.92	-141.83	-202.17	-27.58	-73.89
	r	0.8927	0.9135	0.9359	0.9217	0.9499	0.9448	0.9389	0.9219	0.9325
	E	237.75	257.73	284.72	266.48	151.64	69.93	42.69	129.81	136.47
Stage III	A	2.55×10^{14}	5.07×10^{15}	1.58×10^{17}	5.61×10^{15}	3.76×10^8	255.58	1.776	3.21×10^6	7.45×10^6
	ΔS	23.48	48.33	76.90143	49.17	-88.17	-206.23	-247.54	-127.74	-120.76
	r	0.9144	0.9315	0.9500	0.9382	0.9607	0.9539	0.9454	0.9366	0.9458

*E in $kJmol^{-1}$; A in s^{-1}, ΔS in $JK^{-1}mol^{-1}$

Table 2.5 Kinetic parameters of the decomposition of Cr(III) complexes of (E)-3-[thiophen-2-ylmethyleneamino]benzoic acid (T2YMABA) and (E)-4-(5-[(2-phenylhydrazono)methyl]thiophen-2-yl)benzoic acid (PHMT2YBA) from TG using mechanistic equations

Complex	Mechanistic equations									
	Parameter*	1	2	3	4	5	6	7	8	9
$[CrL^1Ac_2(H_2O)]_2$ Stage IV	E	369.34	401.84	284.72	266.49	238.83	111.66	69.27	204.12	214.78
	A	$3. x10^{17}$	$1.7 x10^{19}$	$1.5 x10^{17}$	$5.61 x10^{15}$	$5.79 x10^{10}$	3066.01	9.2039	$2.31 x10^{8}$	$6.83 x10^{8}$
	ΔS	81.98	113.48	76.90	49.17	-48.81	-188.09	-236.39	-94.72	-85.72
	r	0.8930	0.9123	0.9329	0.9198	0.9449	0.9375	0.9287	0.9184	0.9283
$[CrL^2Ac_3(H_2O)_2]$ Stage I	E	83.157	94.397	110.79	99.65	61.910	27.944	16.621	48.336	52.38
	A	$2.76 x10^{9}$	$8.8 x10^{10}$	$7.72 x10^{12}$	$1.34 x10^{11}$	$6.46 x10^{6}$	41.009	0.5887	20660.05	62811.57
	ΔS	-65.59	-36.79	0.4056	-33.305	-115.93	-215.44	-250.72	-163.71	-154.46
	r	0.8349	0.8674	0.9059	0.8814	0.9289	0.9143	0.8949	0.8769	0.8961
Stage II	E	110.31	118.58	128.12	121.74	65.05	28.55	16.38	57.73	60.08
	A	$9.04x10^{8}$	$4.52x10^{9}$	$1.41x10^{10}$	$2.41x10^{9}$	$2.67x10^{4}$	$1.99x10^{3}$	$6.3x10^{3}$	$1.66x10^{3}$	$2.2x10^{3}$
	ΔS	-78.8	-65.50	-56.05	-70.71	-165.58	-244.61	-273.29	-188.70	-186.47
	r	0.9797	0.9848	0.9894	0.9865	0.9916	0.9888	0.9845	0.9854	0.9878
Stage III	E	121.49	129.79	140.74	133.36	72.50	32.29	18.88	63.70	66.41
	A	$8.8 x10^{9}$	$4.5 x10^{10}$	$2.1 x10^{11}$	$2.7 x10^{10}$	$1.5 x10^{5}$	5.082	0.1255	6138.59	8882.89
	ΔS	-58.75	-45.14	-32.28	-49.38	-149.95	-235.61	-266.38	-176.61	-173.53
	r	0.9449	0.9558	0.9665	0.9599	0.9700	0.9623	0.9513	0.9569	0.9624

*E in $kJmol^{-1}$; A in s^{-1}, ΔS in $JK^{-1}mol^{-1}$

Table 2.6 Kinetic parameters of the decomposition of Cr(III) complex of (E)-4-(5-[(2-carbamothioylhydrazono)methyl]thiophen-2-yl)benzoic acid (CTHMT2YBA) from TG using mechanistic equations

Complex	Mechanistic equations									
	Parameter*	1	2	3	4	5	6	7	8	9
$[CrL^3Ac_2(H_2O)]_2$	E	83.16	94.39	110.79	99.66	61.91	27.94	16.62	48.34	52.38
	A	2.76×10^9	8.8×10^{10}	7.72×10^{12}	1.34×10^{11}	6.46×10^6	41.01	0.5887	20660.1	62811.6
Stage I	ΔS	-65.22	-36.44	0.7667	-32.94	-115.57	-215.08	-250.35	-163.71	-154.1
	r	0.8349	0.8675	0.9059	0.8814	0.9289	0.9143	0.8949	0.8769	0.8961
	E	124.37	133.33	145.23	137.19	75.24	33.59	19.71	65.65	68.59
	A	1.28×10^{10}	7.64×10^{10}	4.46×10^{11}	4.92×10^{10}	2.49×10^5	6.5667	0.1499	8435.495	12892.4
Stage II	ΔS	-58.81	-43.975	-29.307	-47.64	-148.99	-236.67	-268.1	-177.16	-173.63
	r	0.9374	0.9499	0.9627	0.9547	0.9681	0.9601	0.9488	0.9517	0.9582
	E	221.49	237.67	258.81	244.56	135.46	62.08	37.62	118.54	123.76
	A	5.81×10^{13}	6.53×10^{14}	8.22×10^{15}	5.41×10^{14}	4.92×10^7	90.7×10^{10}	0.8730	914489.5	1688475
Stage III	ΔS	11.19	31.29	52.35	29.73	-105.05	-214.85	-253.45	-138.20	-133.10
	r	0.9316	0.9446	0.9574	0.9493	0.9629	0.9561	0.9473	0.9472	0.9535

*E in $kJmol^{-1}$; A in s^{-1}, ΔS in $JK^{-1}mol^{-1}$

Table 2.7 Kinetic parameters of the decomposition of Cr(III) complex of (E)-4-(5-[(2-carbamothioylhydrazono)methyl]furan-2-yl)benzoic acid (CTHMF2YBA) from TG using mechanistic equations

Complex	Mechanistic equations									
	Parameter*	1	2	3	4	5	6	7	8	9
$[CrL^4Ac_2(H_2O)]_2$	E	38.72	54.99	88.58	64.98	65.12	29.39	17.49	24.62	41.13
	A	628.43	1.17×10^5	3.13×10^9	8.73×10^5	1.41×10^7	59.43	0.7432	73.62	1058.32
Stage I	ΔS	-192.69	-149.23	-64.49	-132.52	-109.35	-212.30	-248.73	-210.53	-188.36
	r	0.9954	0.9978	0.9743	0.9935	0.9221	0.9072	0.8877	0.9941	0.9705
	E	197.58	211.98	230.497	217.97	121.84	57.27	35.75	107.01	111.59
	A	4.33×10^{10}	1.41×10^{22}	6.89×10^{23}	1.82×10^{22}	1.393×10^{12}	2.29×10^4	46.98	8.89×10^9	2.29×10^{10}
Stage IIa	ΔS	146.52	175.48	207.82	177.62	-16.05	-165.04	-216.53	-58.07	-50.20
	r	0.9260	0.9396	0.9534	0.9446	0.9609	0.9561	0.9502	0.9438	0.9504
	E	317.09	341.77	373.59	352.17	200.13	95.99	61.24	174.85	182.69
	A	7.9×10^{30}	2.12×10^{33}	1.51×10^{36}	6.61×10^{33}	1.009×10^{19}	7.19×10^7	1.12×10^4	7.78×10^{15}	3.88×10^{16}
Stage IIb	ΔS	342.21	388.68	443.33	398.15	114.51	-98.88	-171.7	54.92	68.29
	r	0.9171	0.9319	0.9473	0.9376	0.9569	0.9534	0.9494	0.9378	0.9451

*E in $kJmol^{-1}$; A in s^{-1}, ΔS in $JK^{-1}mol^{-1}$

Table 2.8 Kinetic parameters of the decomposition of Cr(III) complex of (E)-4-(5-[(2-carbamothioylhydrazono)methyl]furan-2-yl)benzoic acid (CTHMF2YBA) from TG using mechanistic equations

Complex	Mechanistic equations									
	Parameter*	1	2	3	4	5	6	7	8	9
$[CrL^4Ac_2(H_2O)]_2$	E	317.26	360.19	419.59	379.51	238.57	114.82	73.574	190.721	205.33
Stage IIc	A	2.82×10^{28}	3.2×10^{32}	7.15×10^{37}	6.37×10^{33}	1.89×10^{21}	9.93×10^{8}	6.54×10^{4}	1.26×10^{16}	2.6×10^{17}
	ΔS	294.95	372.57	474.98	397.45	157.65	-77.461	-157.49	58.50	83.69
	r	0.8887	0.9097	0.9351	0.9187	0.9544	0.9515	0.9483	0.9210	0.9329
Stage III	E	294.48	323.44	363.28	336.34	199.29	94.733	59.88	166.89	176.73
	A	2.31×10^{23}	5.9×10^{25}	6.55×10^{28}	2.06×10^{26}	2.5×10^{15}	9.51×10^{5}	552.29	1.18×10^{12}	6.61×10^{12}
	ΔS	196.68	242.71	301.05	253.15	44.47	-136.15	-198.10	-19.52	-5.17
	r	0.8828	0.9049	0.9297	0.9139	0.9462	0.9409	0.9347	0.9143	0.9261
Stage IV	E	223.27	242.91	269.53	251.53	143.89	66.075	40.14	122.32	128.899
	A	2.59×10^{13}	4.95×10^{14}	1.47×10^{16}	5.39×10^{14}	1.1×10^{18}	134.68	1.134	$9. \times 10^{5}$	2.21×10^{6}
	ΔS	4.385	28.90	57.12	29.61	-98.44	-211.64	-251.36	-137.81	-130.91
	r	0.9114	0.9293	0.9485	0.9363	0.9591	0.9518	0.9424	0.9345	0.9439

*E in $kJmol^{-1}$; A in s^{-1}, ΔS in $JK^{-1}mol^{-1}$

Table 2.9 Kinetic parameters of the decomposition of Cr(III) complex of (E)-3-[thiophen-2-ylmethyleneamino]benzoic acid (T2YMABA) from TG using non mechanistic equation (Coats-Redfern) and its correlation with mechanistic equation

Complex (stage)	Non-mechanistic/ mechanistic equation	Kinetic parameters*				Order of reaction (n)	Mechanism of decomposition
		E	A	ΔS	r		
$[CrL^1Ac_2(H_2O)]_2$	Coats-Redfern	61.01	$4.1x10^6$	-119.69	0.9230	1	F_1 mechanism. Mampel equation. Random nucleation. One nucleus at each particle
Stage I	Equation V	61.01	$4.1x10^6$	-119.69	0.9230		
Stage IIa	Coats-Redfern	109.47	$5.3x10^{10}$	-44.38	0.9331	1	F_1 mechanism. Mampel equation. Random nucleation. One nucleus at each particle
	Equation V	109.47	$5.3x10^{10}$	-44.38	0.9331		
Stage IIb	Coats-Redfern	177.1	$7.162x10^{12}$	-4.83	0.9325	2/3	R_3 mechanism. Phase boundary reaction. Spherical symmetry
	Equation IX	177.15	$2.41x10^{12}$	-13.89	0.9325		
Stage III	Coats-Redfern	151.6	$3.76x10^8$	-88.17	0.9607	1	F_1 mechanism. Mampel equation. Random nucleation. One nucleus at each particle
	Equation V	221.165	$3.76x10^8$	-88.17	0.9607		
Stage IV	Coats-Redfern	214.7	$2.04x10^9$	-76.64	0.9283	2/3	R_3 mechanism. Phase boundary reaction. Spherical symmetry
	Equation IX	214.78	$6.83x10^8$	-85.72	0.9283		

*E in $kJmol^{-1}$; A in s^{-1}, ΔS in $JK^{-1}mol^{-1}$

Table 2.10 Kinetic parameters of the decomposition of Cr(III) complexes of (E)-4-(5-[(2-phenylhydrazono)methyl]thiophen-2-yl)benzoic acid (PHMT2YBA) and (E)-4-(5-[(2-carbamothioylhydrazono)methyl]thiophen-2-yl)benzoic acid (CTHMT2YBA) from TG using non mechanistic equation (Coats-Redfern) and its correlation with mechanistic equation

Complex (stage)	Non-mechanistic/ mechanistic equation	Kinetic parameters*				Order of reaction (n)	Mechanism of decomposition
		E	A	ΔS	r		
$[CrL^2Ac_3(H_2O)_2]$	Coats-Redfern	61.91	$6.46x10^6$	-115.9	0.9289	1	F_1 mechanism. Mampel equation. Random nucleation. One nucleus at each particle
Stage I	Equation V	61.91	$6.46x10^6$	-115.9	0.9289		
Stage II	Coats-Redfern	65.05	$2.67x10^4$	-165.58	0.9916	1	F_1 mechanism. Mampel equation. Random nucleation. One nucleus at each particle
	Equation V	65.05	$2.67x10^4$	-165.58	0.9916		
Stage III	Coats-Redfern	72.50	$1.5x10^5$	-37.18	0.9953	1	F_1 mechanism. Mampel equation. Random nucleation. One nucleus at each particle
	Equation V	72.50	$1.5x10^5$	-37.18	0.9953		
$[CrL^3Ac_2(H_2O)]_2$ Stage I	Coats-Redfern	61.910	$6.46x10^6$	-115.57	0.9289	1	F_1 mechanism. Mampel equation. Random nucleation. One nucleus at each particle
	Equation V	61.910	$6.46x10^6$	-115.57	0.9289		
Stage II	Coats-Redfern	75.24	$2.49x10^5$	-148.99	0.9681	1	F_1 mechanism. Mampel equation. Random nucleation. One nucleus at each particle
	Equation V	75.24	$2.49x10^5$	-148.99	0.9681		
Stage III	Coats-Redfern	135.46	$4.92x10^7$	-105.05	0.9629	1	F_1 mechanism. Mampel equation. Random nucleation. One nucleus at each particle
	Equation V	135.46	$4.92x10^7$	-105.05	0.9629		

*E in $kJmol^{-1}$; A in s^{-1}, ΔS in $JK^{-1}mol^{-1}$

Table 2.11 Kinetic parameters of the decomposition of Cr(III) complex of (E)-4-(5-[(2-carbamothioylhydrazono)methyl]furan-2-yl)benzoic acid (CTHMF2YBA) from TG using non mechanistic equation (Coats-Redfern) and its correlation with mechanistic equation

Complex (stage)	Non-mechanistic/ mechanistic equation	Kinetic parameters*				Order of reaction (n)	Mechanism of decomposition
		E	A	ΔS	r		
$[CrL^4Ac_2(H_2O)]_2$ Stage I	Coats-Redfern	25.88	12.13	-225.51	0.9949	1/3	R_2 mechanism. Phase boundary reaction. Cylindrical symmetry
	Equation VIII	24.62	73.62	-10.52	0.9941		
Stage IIa	Coats-Redfern	121.84	$1.39x10^{10}$	-16.05	0.9609	1	F_1 mechanism. Mampel equation. Random nucleation. One nucleus at each particle
	Equation V	121.84	$1.39x10^{10}$	-16.05	0.9609		
Stage IIb	Coats-Redfern	200.13	$1.01x10^{10}$	-16.06	0.9569	1	F_1 mechanism. Mampel equation. Random nucleation. One nucleus at each particle
	Equation V	200.13	$1.01x10^{10}$	-16.06	0.9609		
Stage IIc	Coats-Redfern	238.57	$1.89x10^{21}$	-157.65	0.9544	1	F_1 mechanism. Mampel equation. Random nucleation. One nucleus at each particle
	Equation V	238.57	$1.89x10^{21}$	-157.65	0.9544		
Stage III	Coats-Redfern	199.29	$2.59x10^{15}$	-44.47	0.9462	1	F_1 mechanism. Mampel equation. Random nucleation. One nucleus at each particle
	Equation V	199.29	$2.59x10^{15}$	-44.47	0.9462		
Stage IV	Coats-Redfern	143.89	$1.1x10^{8}$	-98.44	0.9591	1	F_1 mechanism. Mampel equation. Random nucleation. One nucleus at each particle
	Equation V	143.89	$1.1x10^{8}$	-98.44	0.9591		

*E in $kJmol^{-1}$; A in s^{-1}, ΔS in $JK^{-1}mol^{-1}$

Part II
Thermoanalytical studies

Chapter 4

Nimmy Kuriakose “Physicochemical, thermoanalytical, electrochemical and antitumour studies of transition metal complexes of schiff bases derived from heterocyclic carbonyl compounds” Thesis. Department of Chemistry, St. Thomas College, University of Calicut, 2015

CHAPTER 4

THERMAL DECOMPOSITION KINETICS OF Ni(II) COMPLEXES OF T2YMABA, PHMT2YBA, CTHMT2YBA, CTHMF2YBA AND I3YT2YMAPA

Thermogravimetry and differential thermal analysis methods were carried out to study the thermal behavior of Ni(II) complexes of (E)-3-[thiophen-2-ylmethyleneamino] benzoic acid (T2YMABA), (E)-4-(5-[(2-phenylhydrazono)methyl) thiophen-2-yl]benzoic acid (PHMT2YBA), (E)-4-(5-[(2-carbamothioylhydrazono)methyl]thiophen-2-yl)benzoic acid (CTHMT2YBA), (E)-4-(5-[(2-carbamothioyl hydrazono)methyl]furan-2-yl)benzoic acid (CTHMF2YBA) and 3-(1H-indol-3-yl)-2-[(E)-(thiophen-2-ylmethylidene)amino] propanoic acid (I3YT2YMAPA). These complexes were synthesized by refluxing the ligands with the metal acetate in ethanolic medium and were characterized by different techniques. The detailed procedures are given in Part I. The thermal behaviors of all these chelates are described in detail here using Coats-Redfern method and nine mechanistic equations. The thermodynamic and kinetic parameters like activation energy, change in entropy and Arrhenius frequency factor were calculated and the non-isothermal methods were employed for the evaluation of reaction mechanism as suggested by Satava.

Figures 2.5 to 2.9 represent the structures and instrumental TGA/DTA curves of Ni(II) complexes with five different ligands. The thermal decomposition data of these compounds are given in Tables 2.12 and 2.13.

The decomposition pattern of $[NiL^1Ac(H_2O)_3]$ (L^1= T2YMABA) comprises of two stages. The first stage represents the loss of all the three coordinated water molecules from the complex in the temperature range 117-243^{0}C The loss of ligand and acetate group is assigned in the second stage at 429^{0}C. The overall mass loss according to the TG

curve and the theoretical mass loss for the conversion of the complex into corresponding oxide are 81.15% and 81.34% respectively. The mass loss from pyrolysis is also found to be 81.41% which is in good agreement with the theoretical value.

The complex $[NiL^2{}_2Ac_2(H_2O)_2]$ (where L^2=PHMT2YBA) has two stages of decomposition reaction. The first one is due to the loss of two coordinated water molecules and two carboxyphenyl moieties of ligand from the complex. The second stage corresponds to the loss of two acetate groups and the rest of both ligands at around 401^0C. Overall mass loss from TG curve (91.62%) and the same from theoretical calculations (91.28%) are found to be in good agreement with the mass loss of 91.48% in pyrolytic studies.

The decomposition of Ni(II) complex of CTHMT2YBA, $[NiL^3{}_2(H_2O)_2]$ also resulted with a definite three stage pattern. The first stage ($65\text{-}130^0$C) is assigned to the loss of two water molecules. The second stage is further divided into three substages. In the first substage two COOH groups are lost. Then two NH_2 groups and two phenyl groups are removed in the second and third substages respectively. The third stage corresponds to the loss of rest of both the ligands at 364^0C. The percentage mass loss according to the TG curve is 88.89% which is in good agreement with the theoretical value (89.37%). The mass loss from the pyrolysis is found to be 88.19%.

Ni(II) complex of the ligand CTHMF2YBA, $[NiL^4{}_2(H_2O)_2]$ also underwent a three stage decomposition pattern. Loss of two water molecules are observed at $65\text{-}130^0$C in the initial stage. Here also as in the case of previous chelate, the second stage consists of three substages. Two COOH groups, two NH_2 molecules and two phenyl rings are lost at around 235^0C, 259^0C and 319^0C respectively in each of these substages. In the third

stage of decomposition the rest of both the ligands are lost. 88.12% mass loss is observed from the thermogravimetric curves. The theoretical and pyrolytic mass loss percentages are 88.85% and 87.67% respectively.

Thermogravimetric curves of $[NiL^5Ac(H_2O)_3]$ (where L^5= I3YT2YMAPA) gave a three stage decomposition pattern. The first stage comprises of two substages in the temperature range 60-120^{0}C and 120-305^{0}C. The first substage of the curve represents the loss of a water molecule from the chelate molecule, which confirmed the presence of coordinated water molecules in the complex. The remaining two water molecules and the acetate group are lost in the next substage. The second stage represents the loss of tryptophan moiety from the ligand. The removal of rest of the ligand is assigned in the third stage. The overall mass loss according to the TG curve is 84.20%. The theoretical mass loss for the conversion of the complex into metal oxide is 84.08%. The mass loss according to the pyrolytic data is also found to be 83.16%.

Kinetics of decomposition

The kinetic parameters such as energy of activation E, pre-exponential factor A and entropy of activation ΔS calculated for the various stages of decomposition of the complexes using mechanistic and non mechanistic kinetic equations are summarized in Tables 2.14 to 2.17. The mechanisms of decomposition of various stages as well as the order of reactions of all the various decomposition stages of the complexes are given in Tables 2.18 to 2.21.

In the decomposition of $[NiL^1Ac(H_2O)_3]$ and $[NiL^2{}_2Ac_2(H_2O)_2]$ complexes (where L^1= T2YMABA and L^2= PHMT2YBA), first order kinetics was found to be followed by all the decomposition stages. Since the parameters E, A and ΔS values obtained from the

Coats-Redfern method with n=1 are in close agreement with those obtained from the Mampel equation, it can be concluded that the rate controlling process of the reaction is random nucleation with the formation of one nucleus in each particle.

For the complex $[NiL^3{}_2(H_2O)_2]$ (L^3=CTHMT2YBA), first stage and the three substages of second stage decomposition process are assigned first order. For the last stage, R_3 mechanism and hence order of the reaction 2/3 can be assigned. In the case of $[NiL^4{}_2(H_2O)_2]$ complex, order 1/3 is suggested for the stage IIc in which two phenyl rings are lost and for all other stages first order kinetics is assigned.

In the case of thermal decomposition of the Ni(II) complex of 3-(1H-indol-3-yl)-2-[(E)-(thiophen-2-ylmethylidene)amino]propanoic acid (I3YT2YMAPA), i.e. $[NiL^5Ac(H_2O)_3]$ for the stages Ia, Ib and III, the kinetic parameters derived using the non mechanistic equation with n=1 are in good agreement with those values obtained from the equation V (Mampel equation) of mechanistic equations. Whereas for stage II, in which the tryptophan moiety is lost from the molecule, R_3 mechanism based on phase boundary reaction with spherical symmetry is assigned since the kinetic parameters of integral method matched with those obtained from equation IX. Hence the order would be 2/3 for this stage.

Initial decomposition temperatures, inflection temperatures, peak temperatures and the activation energy of decomposition reactions can be used to determine the thermal stability of the metal complexes. In the case of Ni(II) complexes, the relative thermal stabilities can be given as $[NiL^4{}_2(H_2O)_2] < [NiL^5Ac(H_2O)_3] < [NiL^3{}_2(H_2O)_2] < [NiL^1Ac(H_2O)_3] < [NiL^2{}_2Ac_2(H_2O)_2]$.

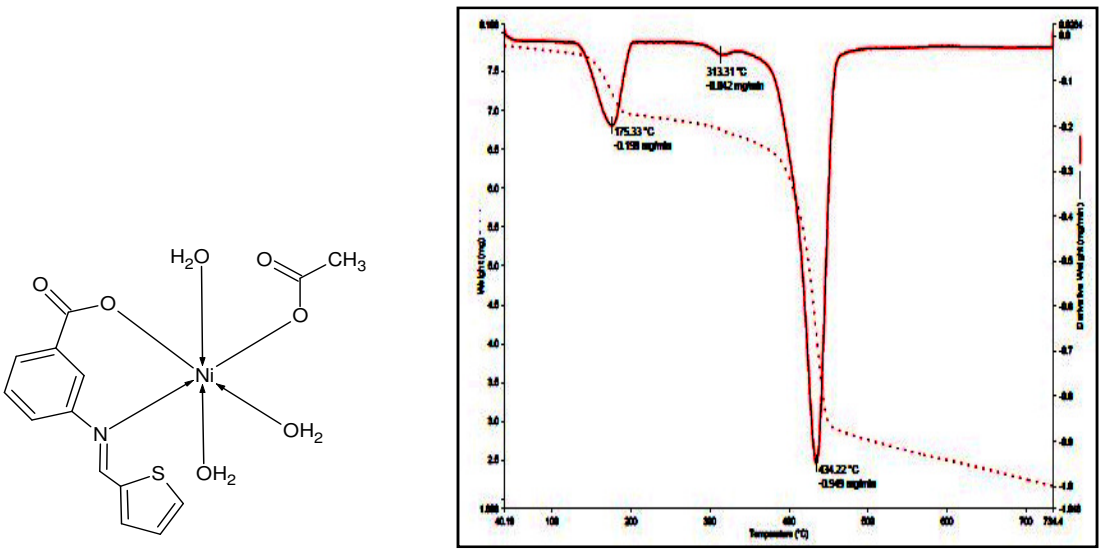

Fig. 2.5 Structure, TGA and DTA curves of $[NiL^{1}Ac(H_2O)_3]$

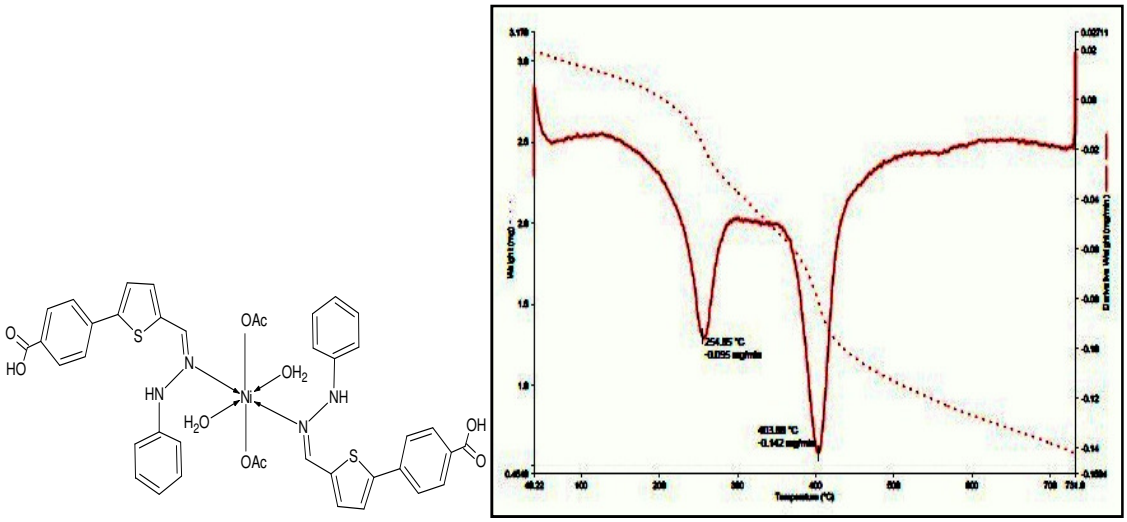

Fig. 2.6 Structure, TGA and DTA curves of $[NiL^{2}{}_2Ac_2(H_2O)_2]$

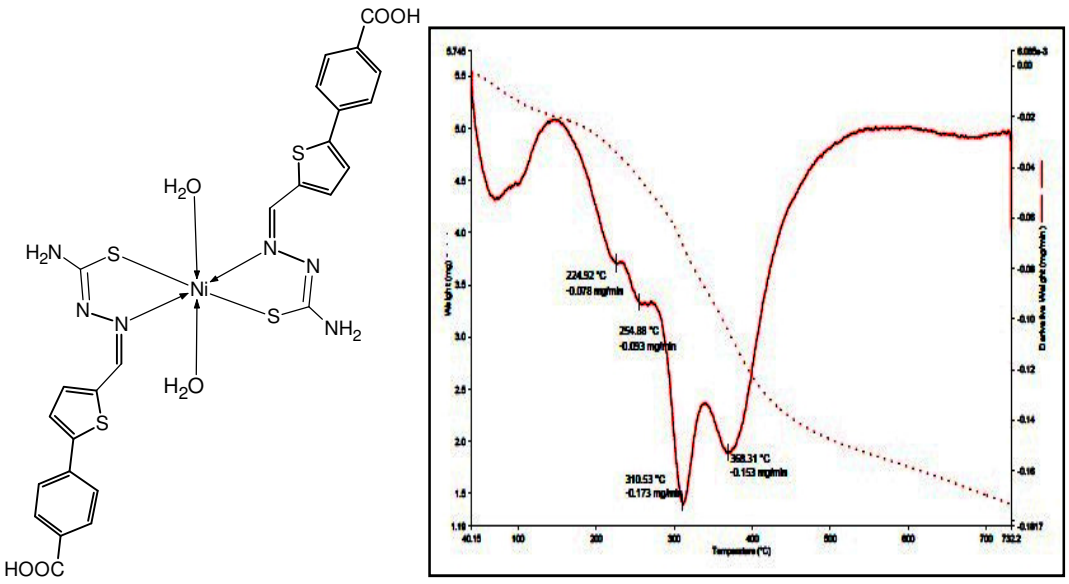

Fig. 2.7 Structure, TGA and DTA curves of $[NiL^{3}{}_{2}(H_2O)_2]$

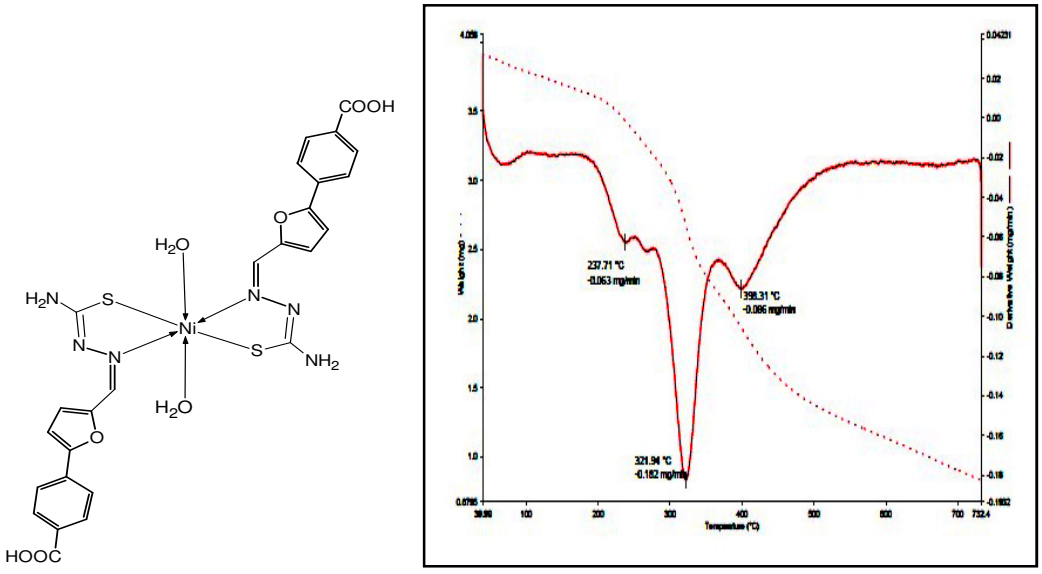

Fig. 2.8 Structure, TGA and DTA curves of $[NiL^{4}{}_{2}(H_2O)_2]$

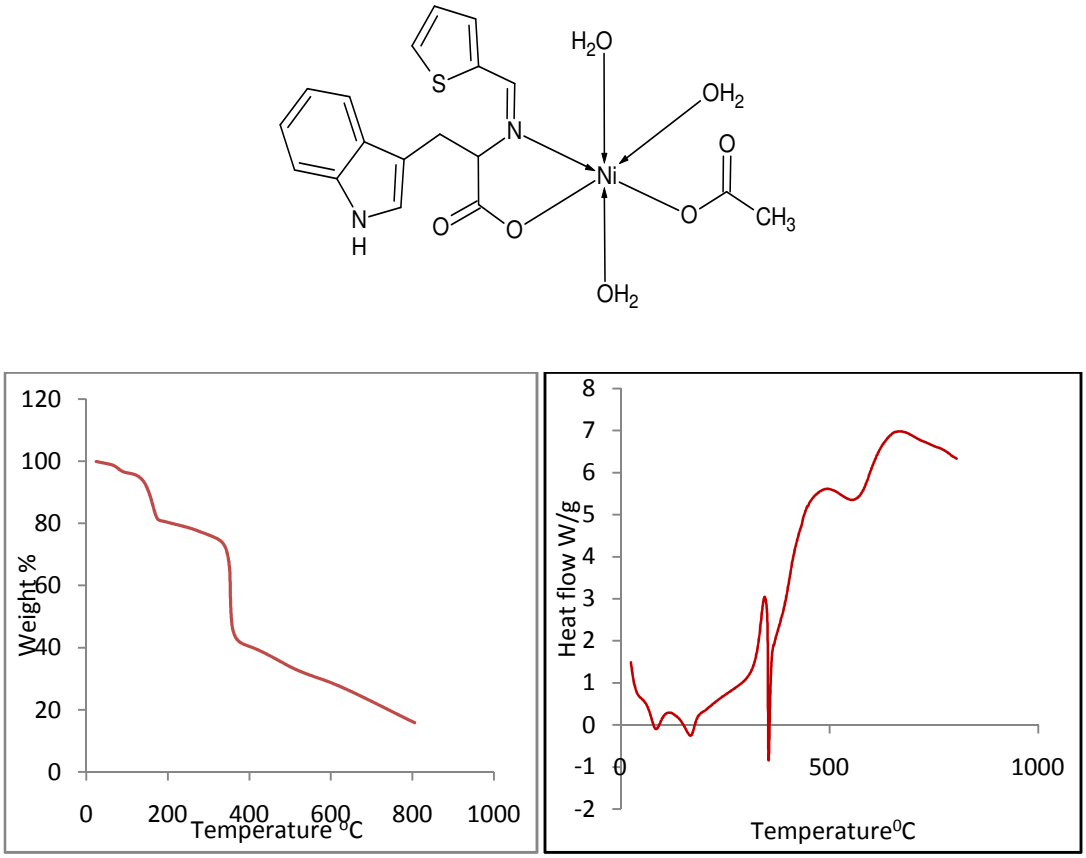

Fig. 2.9 Structure, TGA and DTA curves of $[NiL^5Ac(H_2O)_3]$

Table 2.12 Thermal decomposition data of Ni(II) complexes of (E)-3-[thiophen-2-ylmethyleneamino]benzoic acid (T2YMABA), (E)-4-(5-[(2-phenylhydrazono)methyl]thiophen-2-yl)benzoic acid (PHMT2YBA) and (E)-4-(5-[(2-carbamothioylhydrazono)methyl] thiophen-2-yl)benzoic acid (CTHMT2YBA)

Complex	Stage	Temp range in TG (^{0}C)	Peak temp in TG (^{0}C)	Peak temp in DTA (^{0}C)	Loss of mass %			Probable assignment
					From TG	Cald.	From Pyrolysis	
$[NiL^1Ac(H_2O)_3]$	I	117-243	172	175	13.28	13.43	-	Loss of 3 H_2O
	II	243-734	429	434	67.87	67.91	-	Loss of ligand and acetate group
					81.15	81.34	81.41	
$[NiL^2{}_2Ac_2(H_2O)_2]$	I	70-342	253	255	33.10	32.44	-	Loss of two H_2O and two carboxyphenyl moieties of ligand
	II	373-734	401	404	58.52	58.84	-	Loss of 2 acetate groups and rest of both ligands
					91.62	91.28	91.48	
$[NiL^3{}_2(H_2O)_2]$	I	60-156	89	91	5.48	5.12	-	Loss of 2 H_2O
	IIa	156-237	221	225	12.92	12.80	-	Loss of 2 COOH groups
	IIb	237-276	252	255	4.04	4.55		Loss of 2 NH_2 groups
	IIc	276-338	309	311	20.91	20.05	-	Loss of 2 phenyl groups
	III	338-732	364	369	45.54	45.85	-	Loss of rest of both ligands
					88.89	89.37	88.19	

L^1 = T2YMABA, L^2= PHMT2YBA, L^3= CTHMT2YBA

Table 2.13 Thermal decomposition data of Ni(II) complexes of (E)-4-(5-[(2-carbamothioylhydrazono)methyl]furan-2-yl)benzoic acid (CTHMF2YBA) and 3-(1H-indol-3-yl)-2-[(E)-(thiophen-2-ylmethylidene)amino]propanoic acid (I3YT2YMAPA)

Complex	Stage	Temp range in TG (^{0}C)	Peak temp in TG (^{0}C)	Peak temp in DTA (^{0}C)	Loss of mass %			Probable assignment
					From TG	Cald.	From Pyrolysis	
$[NiL^4_2 (H_2O)_2]$	I	65-130	78	84	5.68	5.36	-	Loss of 2 H_2O
	IIa	130-245	235	238	13.11	13.41	-	Loss of 2 COOH groups
	IIb	245-278	259	262	4.82	4.76	-	Loss of two NH_2 molecules
	IIc	278-366	319	322	22.50	22.65	-	Loss of two phenyl rings
	III	366-732	396	399	42.01	42.67	-	Loss of rest of both ligands
					88.12	88.85	87.67	
$[NiL^5Ac (H_2O)_3]$	Ia	60-120	85	89	3.80	3.84	-	Loss of one H_2O
	Ib	120-305	165	168	20.08	20.26	-	Loss of one acetate group and two H_2O molecules
	II	305-412	355	359	36.92	37.10	-	Loss of tryptophan moiety
	III	412-800	559	564	23.40	23.45	-	Loss of rest of the ligand
					84.20	84.08	83.16	

L^4 = CTHMF2YBA, L^5= I3YT2YMAPA

Table 2.14 Kinetic parameters of the decomposition of Ni(II) complexes of (E)-3-[thiophen-2-ylmethyleneamino]benzoic acid (T2YMABA) and (E)-4-(5-[(2-phenylhydrazono)methyl]thiophen-2-yl)benzoic acid (PHMT2YBA) from TG using mechanistic equations

Complex	Parameter*	Mechanistic equations								
		1	2	3	4	5	6	7	8	9
$[NiL^1Ac(H_2O)_3]$	E	129.62	141.08	158.70	146.67	86.21	39.38	23.77	71.25	75.62
	A	1.1×10^{12}	1.78×10^{13}	7.7×10^{14}	2.1×10^{13}	4.58×10^{7}	105.09	1.08	2.4×10^{5}	$6. \times 10^{5}$
Stage I	ΔS	-17.63	5.44	36.77	6.86	-101.58	-209.54	-247.55	-145.23	-137.47
	r	0.9007	0.9169	0.9398	0.9249	0.9565	0.9476	0.9360	0.9221	0.9338
Stage II	E	162.08	162.65	163.22	162.84	77.10	33.76	19.31	76.68	76.82
	A	1.49×10^{9}	8.5×10^{8}	2.16×10^{8}	1.97×10^{8}	808.60	0.3117	0.017	364.99	251.76
	ΔS	-76.42	-81.09	-92.49	-93.23	-196.36	-261.72	-285.86	-202.98	-206.07
	r	0.9287	0.9292	0.9298	0.9294	0.9221	0.9008	0.8706	0.9211	0.9214
$[NiL^2{}_2Ac_2(H_2O)_2]$	E	103.82	114.94	130.19	119.88	70.61	32.20	19.39	58.23	61.99
	A	7.26×10^{11}	1.84×10^{13}	8.5×10^{14}	2.31×10^{13}	4.5×10^{7}	113.28	1.20	2.72×10^{5}	6.9×10^{5}
Stage I	ΔS	-22.57	4.29	36.18	6.20	-103.12	-210.31	-248.07	-145.59	-137.75
	r	0.8811	0.9046	0.9303	0.9140	0.9445	0.9339	0.9205	0.9109	0.9237
Stage II	E	419.75	450.46	490.53	463.524	261.99	125.56	80.09	229.94	239.83
	A	4.4×10^{30}	8.02×10^{30}	3.82×10^{35}	2.2×10^{33}	3.6×10^{18}	3.7×10^{7}	6614.3	3.7×10^{15}	1.6×10^{16}
	ΔS	334.93	378.22	429.48	386.51	103.68	-106.72	-178.55	46.41	58.96
	r	0.9275	0.9406	0.9536	0.9454	0.9608	0.95749	0.9538	0.9455	0.9516

*E in $kJmol^{-1}$; A in s^{-1}, ΔS in $JK^{-1}mol^{-1}$

Table 2.15 Kinetic parameters of the decomposition of Ni(II) complex of (E)-4-(5-[(2-carbamothioylhydrazono)methyl]thiophen-2-yl)benzoic acid (CTHMT2YBA) from TG using mechanistic equations

Complex	Mechanistic equations									
	Parameter*	1	2	3	4	5	6	7	8	9
$[NiL^3{}_2(H_2O)_2]$ Stage I	E	60.84	68.89	80.49	72.62	43.79	18.75	10.40	34.24	37.10
	A	4.1×10^5	4.0×10^6	6.11×10^7	3.5×10^7	5097.26	0.8785	0.03599	71.465	140.4
	ΔS	-138.90	-119.95	-97.46	-121.16	-175.55	-247.59	-274.16	-211.03	-205.41
	r	0.8458	0.8778	0.9145	0.8912	0.9335	0.9112	0.8772	0.8814	0.9009
Stage IIa	E	170.50	182.54	198.23	187.66	103.911	48.07	29.45	91.36	95.23
	A	9.7×10^{15}	1.3×10^{17}	2.32×10^{18}	1.25×10^{17}	1.24×10^9	584.4*	3.60	1.8×10^7	3.6×10^7
	ΔS	56.94	78.97	102.49	78.22	-75.015	-196.14	-238.45	-110.09	-104.39
	r	0.8458	0.8778	0.9145	0.8912	0.9335	-0.9112	0.8772	0.8814	0.9009
Stage IIb	E	337.95	373.77	423.09	389.74	235.01	113.10	72.47	194.98	207.15
	A	8.03×10^{30}	1.9×10^{34}	4.8×10^{38}	1.8×10^{35}	1.56×10^{21}	9.05×10^8	61806.7	5.7×10^{16}	6.9×10^{17}
	ΔS	342.02	406.81	491.03	425.66	156.08	-78.15	-157.89	71.18	91.91
	r	0.8854	0.9078	0.9328	0.9169	0.9497	0.9459	0.9418	0.9186	0.9302
Stage IIc	E	247.91	276.44	317.05	289.52	177.05	83.71	52.59	143.69	153.7
	A	5.5×10^{19}	1.5×10^{22}	2.46×10^{25}	5.9×10^{22}	6.4×10^{13}	1.4×10^5	150.8	1.96×10^{10}	1.2×10^{11}
	ΔS	127.52	174.11	235.59	185.47	13.83	-151.78	-208.77	-53.44	-38.27
	r	0.8727	0.8985	0.9279	0.9092	0.9471	0.9413	0.9344	0.9098	0.9238
Stage III	E	254.16	281.93	321.12	294.57	177.59	83.39	51.99	145.48	155.15
	A	4.5×10^{17}	5.52×10^{19}	2.7×10^{22}	1.47×10^{20}	9.34×10^{11}	1.5×10^4	31.18	7.82×10^8	3.6×10^9
	ΔS	86.79	126.71	178.19	134.87	-22.06	-171.10	-222.62	-80.97	-68.28
	r	0.9726	0.9859	0.9961	0.9909	0.9944	0.9935	0.9923	0.9921	0.9957

*E in $kJmol^{-1}$; A in s^{-1}, ΔS in $JK^{-1}mol^{-1}$

Table 2.16 Kinetic parameters of the decomposition of Ni(II) complex of (E)-4-(5-[(2-carbamothioylhydrazono)methyl]furan-2-yl)benzoic acid (CTHMF2YBA) from TG using mechanistic equations

		Mechanistic equations								
complex	Parameter*	1	2	3	4	5	6	7	8	9
$[NiL^4_2 (H_2O)_2]$ Stage I	E	91.51	101.62	115.56	106.14	62.59	28.23	16.78	51.28	54.71
	A	1.87×10^{10}	3.6×10^{11}	1.16×10^{13}	4.02×10^{11}	4.07×10^{6}	32.11	0.49489	32821.9	77198.2
	ΔS	-49.62	-25.04	3.83	-24.12	-119.72	-217.42	-252.11	-159.81	-152.699
	r	0.9007	0.9169	0.9398	0.9249	0.9565	0.9476	0.9361	0.9221	0.9338
Stage IIa	E	144.36	158.73	178.12	165.04	96.29	44.55	27.29	80.68	85.46
	A	5.20×10^{14}	1.95×10^{16}	1.41×10^{18}	2.85×10^{16}	2.3×10^{9}	827.27	4.66	1.0×10^{7}	2.8×10^{7}
	ΔS	32.39	62.539	98.09	65.67	-70.12	-193.49	-236.54	-115.24	-106.52
	r	0.90066	0.9169	0.9398	0.9249	0.9565	0.9476	0.9360	0.9221	0.9338
Stage IIb	E	425.48	467.89	525.78	486.65	141.03	141.03	91.05	244.15	258.42
	A	1.4×10^{39}	1.4×10^{43}	2.1×10^{48}	2.5×10^{44}	4.44×10^{11}	4.4×10^{11}	4.1×10^{6}	2.7×10^{21}	5.1×10^{22}
	ΔS	500.61	576.93	675.97	600.63	-26.37	-26.37	-122.66	161.1	185.38
	r	0.8957	0.9163	0.9387	0.9245	0.9538	0.9510	0.9479	0.9264	0.9367
Stage IIc	E	345.47	372.83	409.65	384.77	220.67	105.51	67.12	190.91	199.99
	A	1.64×10^{39}	3.1×10^{30}	1.98×10^{33}	9.15×10^{30}	3.4×10^{17}	1.1×10^{7}	3111.3	2.56×10^{14}	1.2×10^{15}
	ΔS	289.51	333.12	386.82	342.10	85.02	-115.27	-183.74	25.21	38.38
	r	0.9279	0.9425	0.9580	0.9482	0.9677	0.9647	0.9614	0.9488	0.9561
Stage III	E	81.19	91.21	105.66	95.86	57.16	24.55	13.69	45.23	81.19
	A	$6. \times 10^{5}$	6.1×10^{6}	8.1×10^{7}	5.1×10^{6}	4942.95	0.7744	0.0308	76.36	6.85×10^{5}
	ΔS	-139.9	-121.67	-100.17	-123.21	-180.91	-253.75	-280.55	-215.58	-139.9
	r	0.8496	0.8801	0.9154	0.8929	0.9339	0.9122	0.8793	0.8834	0.8496

*E in $kJmol^{-1}$; A in s^{-1}, ΔS in $JK^{-1}mol^{-1}$

Table 2.17 Kinetic parameters of the decomposition of Ni(II) complex of 3-(1H-indol-3-yl)-2-[(E)-(thiophen-2-ylmethylidene)amino]propanoic acid (I3YT2YMAPA) from TG using mechanistic equations

Complex	Parameter*	Mechanistic equations								
		1	2	3	4	5	6	7	8	9
$[NiL^5Ac(H_2O)_3]$	E	106.46	118.19	134.37	123.44	73.26	33.624	20.41	60.19	64.18
	A	$6.66x10^{12}$	$2.43 x10^{14}$	$1.9 x10^{16}$	$3.6 x10^{14}$	$2.95 x10^{8}$	307.16	2.45	$1.19 x10^{6}$	$3.4 x10^{6}$
Stage Ia	ΔS	-0.9406	28.97	65.224	32.33	-84.27	-198.81	-238.98	-130.12	-121.21
	r	0.85222	0.8780	0.9093	0.8885	0.9254	0.9126	0.8967	0.8844	0.8988
Stage Ib	E	52.95	59.46	69.09	62.55	36.19	14.13	6.78	28.20	30.58
	A	682.04	2805.43	12894.03	1654.87	26.88	0.0418	0.0031	0.9750	1.434
	ΔS	-193.91	-182.16	-169.42	-186.49	-220.74	-274.49	-295.92	-248.32	-245.11
	r	0.7262	0.7588	0.8031	0.7741	0.8147	0.7351	0.6106	0.7387	0.7644
Stage II	E	346.49	375.08	419.86	389.21	231.91	110.72	70.33	193.58	204.69
	A	$4.9 x10^{25}$	$8.72 x10^{27}$	$1.78 x10^{31}$	$3.5 x10^{28}$	$8.9 x10^{16}$	$5.66 x10^{6}$	1840.3	$1.7 x10^{123}$	$1.1 x10^{14}$
	ΔS	240.84	283.78	347.15	295.25	73.36	-121.82	-188.6	2.020	17.72
	r	0.9194	0.9289	0.9443	0.9342	0.9572	0.9531	0.9485	0.9340	0.9416
Stage III	E	82.60	91.52	103.55	95.43	51.37	18.55	7.61	41.67	44.64
	A	29.06	70.25	124.68	30.74	0.9560	0.0048	0.0005	0.0806	0.0933
	ΔS	-225.43	-218.09	-213.32	-224.96	-253.82	-297.79	-317.04	-274.37	-273.16
	r	0.8741	0.8997	0.9255	0.9093	0.9263	0.8675	0.7253	0.8853	0.9015

*E in $kJmol^{-1}$; A in s^{-1}, ΔS in $JK^{-1}mol^{-1}$

Table 2.18 Kinetic parameters of the decomposition of Ni(II) complexes of (E)-3-[thiophen-2-ylmethyleneamino]benzoic acid (T2YMABA) and (E)-4-(5-[(2-phenylhydrazono)methyl]thiophen-2-yl)benzoic acid (PHMT2YBA) from TG using non mechanistic equation (Coats-Redfern) and its correlation with mechanistic equation

Complex (stage)	Non-mechanistic/ mechanistic equation	Kinetic parameters*				Order of reaction (n)	Mechanism of decomposition
		E	A	ΔS	r		
$[NiL^1Ac(H_2O)_3]$ Stage I	Coats-Redfern	86.21	$4.58x10^7$	-101.58	0.9565	1	F_1 mechanism. Mampel equation. Random nucleation. One nucleus at each particle
	Equation V	86.21	$4.58x10^7$	-101.58	0.9565		
Stage II	Coats-Redfern	77.10	808.60	-196.36	0.9221	1	F_1 mechanism. Mampel equation. Random nucleation. One nucleus at each particle
	Equation V	77.10	808.60	-196.36	0.9221		
$[NiL^2{}_2Ac_2(H_2O)_2]$ Stage I	Coats-Redfern	70.61	$4.5x10^7$	-103.12	0.9445	1	F_1 mechanism. Mampel equation. Random nucleation. One nucleus at each particle
	Equation V	70.61	$4.5x10^7$	-103.12	0.9445		
Stage II	Coats-Redfern	261.99	$3.6x10^{18}$	-103.68	0.9608	1	F_1 mechanism. Mampel equation. Random nucleation. One nucleus at each particle
	Equation V	261.99	$3.6x10^{18}$	-103.68	0.9608		

*E in $kJmol^{-1}$; A in s^{-1}, ΔS in $JK^{-1}mol^{-1}$

Table 2.19 Kinetic parameters of the decomposition of Ni(II) complex of (E)-4-(5-[(2-carbamothioylhydrazono)methyl]thiophen-2-yl)benzoic acid (CTHMT2YBA) and its correlation with mechanistic equation

Complex (stage)	Non-mechanistic/ mechanistic equation	Kinetic parameters*				Order of reaction (n)	Mechanism of decomposition
		E	A	ΔS	r		
$[NiL^3_2(H_2O)_2]$ Stage I	Coats-Redfern	43.79	5097.26	-175.55	0.9335	1	F_1 mechanism. Mampel equation. Random nucleation. One nucleus at each particle
	Equation V	43.79	5097.26	-175.55	0.9335		
Stage IIa	Coats-Redfern	103.91	$1.24x10^9$	-75.02	0.9335	1	F_1 mechanism. Mampel equation. Random nucleation. One nucleus at each particle
	Equation V	103.91	$1.24x10^9$	-75.02	0.9335		
Stage IIb	Coats-Redfern	235.01	$1.56x10^{21}$	-156.08	0.9497	1	F_1 mechanism. Mampel equation. Random nucleation. One nucleus at each particle
	Equation V	235.01	$1.56x10^{21}$	-156.08	0.9497		
Stage IIc	Coats-Redfern	177.05	$6.4x10^{13}$	13.83	0.9471	1	F_1 mechanism. Mampel equation. Random nucleation. One nucleus at each particle
	Equation V	177.05	$6.4x10^{13}$	13.83	0.9471		
Stage III	Coats-Redfern	153.39	$1.9x10^6$	-68.74	0.9957	2/3	R_3 mechanism. Phase boundary reaction. Spherical symmetry
	Equation IX	155.15	$3.6x10^9$	-68.28	0.9957		

*E in $kJmol^{-1}$; A in s^{-1}, ΔS in $JK^{-1}mol^{-1}$

Table 2.20 Kinetic parameters of the decomposition of Ni(II) complex of (E)-4-(5-[(2-carbamothioylhydrazono)methyl]furan-2-yl)benzoic acid (CTHMF2YBA) from TG using non mechanistic equation (Coats-Redfern) and its correlation with mechanistic equation

Complex (stage)	Non-mechanistic/ mechanistic equation	Kinetic parameters*				Order of reaction (n)	Mechanism of decomposition
		E	A	ΔS	r		
$[NiL^4_2 (H_2O)_2]$ Stage I	Coats-Redfern	62.59	4.07×10^6	-119.72	0.9565	1	F_1 mechanism. Mampel equation. Random nucleation. One nucleus at each particle
	Equation V	62.59	4.07×10^6	-119.72	0.9565		
Stage IIa	Coats-Redfern	96.29	2.3×10^9	-70.12	0.9565	1	F_1 mechanism. Mampel equation. Random nucleation. One nucleus at each particle
	Equation V	96.29	2.3×10^9	-70.12	0.9565		
Stage IIb	Coats-Redfern	141.03	4.44×10^{11}	-26.37	0.9538	1	F_1 mechanism. Mampel equation. Random nucleation. One nucleus at each particle
	Equation V	141.03	4.44×10^{11}	-26.37	0.9538		
Stage IIc	Coats-Redfern	182.57	8.23×10^{13}	-15.78	0.9409	1/3	R_2 mechanism. Phase boundary reaction. Cylindrical symmetry
	Equation VIII	190.90	2.56×10^{14}	25.21	0.9487		
Stage III	Coats-Redfern	48.80	145.42	-210.23	0.9022	1	F_1 mechanism. Mampel equation. Random nucleation. One nucleus at each particle
	Equation V	57.16	4942.9	-180.91	0.9339		

*E in $kJmol^{-1}$; A in s^{-1}, ΔS in $JK^{-1}mol^{-1}$

Table 2.21 Kinetic parameters of the decomposition of Ni(II) complex of 3-(1H-indol-3-yl)-2-[(E)-(thiophen-2-ylmethylidene)amino] propanoic acid (I3YT2YMAPA) from TG using non mechanistic equation (Coats-Redfern) and its correlation with mechanistic equation

Complex (stage)	Non-mechanistic/ mechanistic equation	Kinetic parameters*				Order of reaction (n)	Mechanism of decomposition
		E	A	ΔS	r		
$[NiL^5Ac(H_2O)_3]$ Stage Ia	Coats-Redfern	73.26	$2.95x10^8$	-84.27	0.9254	1	F_1 mechanism. Mampel equation. Random nucleation. One nucleus at each particle
	Equation V	73.26	$2.95x10^8$	-84.27	0.9254		
Stage Ib	Coats-Redfern	36.19	26.88	-220.49.	0.7351	1	F_1 mechanism. Mampel equation. Random nucleation. One nucleus at each particle
	Equation V	36.19	26.88	-220.49	0.7351		
Stage II	Coats-Redfern	204.65	$3.28x10^{14}$	26.77	0.9415	2/3	R_3 mechanism. Phase boundary reaction. Spherical symmetry
	Equation IX	204.69	$1.1x10^{14}$	17.72	0.9416		
Stage III	Coats-Redfern	51.37	0.9560	-253.82	0.9263	1	F_1 mechanism. Mampel equation. Random nucleation. One nucleus at each particle
	Equation V	51.37	09560	-253.82	0.9263		

*E in $kJmol^{-1}$; A in s^{-1}, ΔS in $JK^{-1}mol^{-1}$

SUMMARY

Thermogravimetric studies of Cr(III) and Ni(II) complexes of novel Schiff base ligands such as I3YT2YMAPA, T2YMABA, CTHMT2YBA, PHMT2YBA and CTHMF2YBA were conducted. The regions of thermal stability and the temperature of decomposition were noted from the data. Also the temperatures of maximum rate of decomposition of each complex were assigned from the thermograms. The thermogravimetric data of all the complexes were subjected to kinetic studies. Mechanistic and non mechanistic equations were employed for the analysis of different stages of thermograms. Kinetic parameters like Arrhenius frequency factor, energy of activation and entropy of activation of all the stages were calculated. The mechanism of decomposition reaction in each stage and hence the order of decomposition reactions also were determined. The thermal stabilities of the chelates were compared with the aid of energy of activation, initial/final decomposition temperature, inflection temperature and peak temperature from the TG and DTA data.

In order to ascertain the order of the decomposition reactions, nine mechanistic equations and an integral equation formulated by Coats and Redfern, which is a non mechanistic equation, were employed and the kinetic parameters were calculated. Comparing the correlation between the kinetic parameters obtained from these mechanistic equations and the Coats-Redfern method, reaction mechanisms and orders of different decomposition stages were ascertained.

Thermal decomposition studies on Cr(III) complexes with four different heterocyclic Schiff bases, 3-[thiophen-2-ylmethyleneamino]benzoic acid (T2YMABA), 4-(5-[(2-carbamothioylhydrazono)methyl]thiophen-2-yl)benzoic acid (CTHMT2YBA),

4-(5-[(2-phenylhydrazono)methyl]thiophen-2-yl)benzoic acid (PHMT2YBA) and 4-(5-[(2-carbamothioylhydrazono)methyl]furan-2-yl)benzoic acid (CTHMF2YBA) are discussed in Chapter 3. The complexes of Cr(III) with T2YMABA and CTHMF2YBA exhibited four stage decomposition pattern in which the coordinated water molecules were lost during the first stage decomposition and acetate groups, CO_2 molecules and bridged acetate groups were lost in subsequent stages. Whereas the other two complexes with PHMT2YBA and CTHMT2YBA ligands, exhibited three stages of decomposition in the TGA/DTA curves. The kinetic parameters also were calculated. The thermal stabilities of these complexes were found to be increasing in the order $[CrL^3Ac_2(H_2O)]_2$<$[CrL^4Ac_2(H_2O)]_2$<$[CrL^1Ac_2(H_2O)]_2$< $[CrL^2Ac_3(H_2O)_2]$.

Chapter 4 explains the thermal decomposition studies of the complexes of Ni(II) with the novel Schiff bases synthesized. The Ni(II) complexes 3-[thiophen-2-ylmethyleneamino)benzoic acid (T2YMABA) and 4-(5-[(2-carbamothioylhydrazono) methyl]hiophen-2-yl)benzoic acid (CTHMT2YBA) showed two stage decomposition process. Well defined three stage decomposition pattern, with certain definite substages was exhibited by the nickel chelates of PHMT2YBA, CTHMF2YBA and I3YT2YMAPA. Kinetic parameters such as E, A, ΔS along with the correlation coefficient of each stages of decomposition were calculated. Attempts were made to derive the order of reaction of thermal decomposition processes of these complexes. Generally it is noticed that the orders of various disintegration steps involved during the thermal studies of the present compounds follows the order 1, 1/3 and 2/3. The relative thermal stabilities was found to be in the order $[NiL^4{}_2(H_2O)_2]$<$[NiL^5Ac(H_2O)_3]$< $[NiL^3{}_2(H_2O)_2]$< $[NiL^1Ac(H_2O)_3]$ < $[NiL^2{}_2Ac_2(H_2O)_2]$.

REFERENCES

1. C. Daval, *Inorganic Thermogravimetric Analysis*, Elsevier, New York, 2nd Ed. (1963).
2. A. K. Srivastava, P.C. Jain, *Instrumental Approach to Chemical Analysis*, (2009).
3. W. J. Smoothers, M. S. Yaochiang, *Handbook of Differential Thermal Analysis,* Chemical Publising Co., New York (1966).
4. D. Schulze, *Differential Thermoanalyser*, VEB Verlangder Wissanchften, Berlin (1966).
5. K. D. W. van , H. C. van , F. Huntjens, *J. Fuel*, 30 (1951) 253.
6. C. D. Doyle, *J. App. Polymer Sci.*, 5 (1961) 285.
7. H. H. Horowitz, G. Metzger, *Anal. Chem.*, 35 (1963) 1464.
8. W. W. Wendlandt, *Thermal Methods of Analysis*, John Wiley, New York, 2nd Ed. (1974).
9. E. S. Freeman, B. Carroll, *J. Phys. Chem.*, 62 (1958) 394.
10. J. Sestak, V. Satava, W. W. Wendlandt, *Thermochim. Acta,* 7 (1973) 333.
11. J. Sestak, *Talanta,* 13 (1966) 567.
12. Varhegy, *J. Anal. Appl. Pyrol*, 79 (2007) 278.
13. A. W. Coats, J. P. Redfern, *Analyst*, 88 (1963) 2938.
14. J. Sestak, *Silikaty*, 11 (1967) 153.
15. B. Carroll, E. P. Manche, *Thermochim. Acta,* 2 (1972) 449.
16. J. G. Santos, M. M. Conceicao, M.M. Trinade, *J. Therm. Anal. Calorim.,* 75 (2004) 591.

17. A. G. Souza, M. M. Oliveira, I. M. G Santos, M. M. Conceicao, *J. Therm. Anal. Calorim.,* 67 (2002) 359.

18. G. M. Luckaszewski, J. P. Redfern, *Lab. Pr.,* 10 (1961) 721.

19. D. Rainville, *Special Functions*, Mac Millan, New York, 44 (1960).

20. J. Sestak, G. Berggren, *Thermochim. Acta*, 3 (1971)1.

21. V. Satava, *Thermochim. Acta*, 2 (1971) 243.

22. V. M. Gorbachev, *J. Therm. Anal.,* 8 (1975) 349.

23. M. D. Jaddo, M. T. Pope, *J. Therm. Anal.,* 4 (1972) 37.

24. V. P. Ivanov, *Zap. Uses. Miner. Obschch.,* 90 (1961) 50.

25. C. G. Scency, J. F. Smith, J. O. Hill, R. J. Magee, *J. Therm. Anal.,* 9 (1976) 415.

26. M. Lehtinen, K. Maire, *Acta Pharma. Farn.,* 90 (1981) 187.

27. N. Kavitha, P.V. A. Lakshmi, *J. Saudi Chem. Soc.*, doi:10.1016/j.jscs.2015.01.003 (2015).

28. A. Azza, Abu-Hussen, *J. Coord. Chem*., 59 (2) (2006) 157.

29. K. Singh, M. S. Barwa, P. Tyagi, *European J. Med. Chem*., 42 (3) (2007) 394.

30. M. Sharaby, *Spectrochim. Acta*, 66(4) (2007) 1271.

31. S. A. Abdel Latif, H. B. Hassib, Y.M. Issa, *Spectrochim. Acta*, 67 (3) (2007) 950.

32. M. Sonmez, M. Sekerci, *Polish J. Chem*., 76 (2002) 907.

33. E. Canpolat, M. Kaya, *J. Coord. Chem*.**,** 57(14) (2004) 1217.

34. G. G. Mohamed, M. M. Omar, A. M. Hindy, *Turk J. Chem*., 30 (2006) 361.

35. A. M. Khedr, H. M. Marwani, *Int. J. Electrochem. Sci*., 7 (2012) 10074.

36. L. Pardeshi, R. A. Bhobe, *Acta Cienc. Indica,* 9 (1983) 18.

37. A. K. Galwey, M. E. Brown, *Hand Book in Thermal Analysis*, (1998) 147.

38. Brown M.E., Maciejewski M., Vyazovkin S., Nomen R., Sempere J., *Thermochim. Acta*, 355 (2000) 125.

39. L. Pardeshi, R. A. Bhobe, *Acta Cienc. Indica,* 8 (1982) 178.

40. K. N. Johri, B. S. Arora, *Thermochim. Acta,* 54 (1982) 237.

41. C. Reverte, J. L. Dirion, M. Cabassud, *J. Anal. Appl. Pyrol.*, 79 (2007) 297.

42. B. Sleema, G. Parameswaran, *Asian J. Chem.,* 13-2 (2001) 709.

43. P.V. Marykutty, G. Parameswaran, *Asian J. Chem.,* 13-3 (2001) 905.

44. R. Seshadri Naidu, Raghava Naidu, *Indian J. Chem.,* 15A (1977) 652.

45. A. P. Mishra, M. Khare, *J. Indian Chem. Soc.,* 77 (2000) 367.

46. K. J. Thomas, G. Parmeswaran, *J. Therm. Anal.,* 45-6 (1996) 1491.

47. Joby Thomas, Geetha Parameswaran, *Asian J. Chem.,* 14-3 (2002) 1370.

48. S. Volker, T. Rieckmann, *J. Appl. Polym. Sci*., 62 (2002) 165.

49. J. H. Tassel van , W. W. Wendlandt, *J. Amer. Chem. Soc.*, 81 (1959) 813.

50. G. M. Lukaszewski, J. P. Redfern, *J. Chem. Soc.*, (1962) 4802.

51. M. S. Masoud, S. A. Abon, H. M. Kamel, *Indian J. Chem.,* 41A (2002) 297.

Part III
Corrosion inhibition studies

Chapter 1

Nimmy Kuriakose “Physicochemical, thermoanalytical, electrochemical and antitumour studies of transition metal complexes of schiff bases derived from heterocyclic carbonyl compounds” Thesis. Department of Chemistry, St. Thomas College, University of Calicut, 2015

CHAPTER 1

INTRODUCTION AND REVIEW

Corrosion is the gradual destruction or disintegration of metal by chemical or electrochemical reaction with their environment. It involves the electrochemical oxidation of metals in the presence of an oxidant such as oxygen. A well known example of electrochemical corrosion is rusting, which involves the formation of iron oxides. Corrosion of metals typically produces oxide or salt of the original metal[1]. Not only metals, materials such as ceramics or polymers are also vulnerable to corrosion. Corrosion can cause degradation in the useful properties of materials such as strength, appearance and permeability to liquids and gases.

Many metals corrode merely from exposure to moisture in air, but the process can be accelerated by the presence of certain substances. It is observed that corrosion is concentrated locally in the form a pit or crack, and in some cases it is extended across a wide area more or less uniformly. The thermodynamic or chemical energy stored in a metal or that is freed by its corrosion varies from metal to metal. For example, the most common iron ore hematite is an oxide of iron. The most common product of the corrosion of iron, rust, has a similar chemical composition and colour. The energy required to convert iron ore to metallic iron is returned when the iron corrodes to form the original compound, only the rate of energy change is different[1]. Metals such as iron, magnesium and

aluminum have higher and metals such as copper, silver and gold have relatively lower energy.

Economic impact of corrosion

The direct cost associated with metallic corrosion in the US industry was reported as around $280 billion in 2002, by the US Federal Highway Administration[2]. It is reported that rust is one of the most common causes of bridge accidents. The collapse of the Mianus river bridge in 1983 was due to the corrosion of the bearings which resulted in the death of three drivers on the roadway at the time. In West Virginia, the Silver bridge which was a steel suspension bridge collapsed within a minute, killing 46 people on the bridge at the time. Here also the rust was the reason. The corrosion of concrete covered steel and iron causes severe structural problems. As rust has a much higher volume than the originating mass of iron, its build-up can also cause failure by forcing apart adjacent parts. The corrosion spots must be detected before the total destruction of the concrete structure by measuring half-cell potential.

Protection from corrosion

Some metals are more intrinsically resistant to corrosion than others. Application of water and oil based corrosion inhibitors can prevent the oxidation and the formation of rust on metal surfaces. There are various ways of protection of metals from corrosion.

Surface coatings: Anticorrosion methods like plating, painting and the application of enamel provide a barrier between the metal surface and the damaging environment. Plating with more noble materials than the substrate is very effective. For example, chromium or zinc can be plated on steel. Painting either by roller or brush is more desirable for tight spaces; spray would be better for larger coating areas such as steel

decks and waterfront applications[2]. A slip resistant coating with polyurethane, like Durabak-M26, can act as an anti-corrosive membrane. Although coatings are relatively easy to apply, temperature and humidity can affect dryness and durability of the coatings.

Reactive coatings: The electrochemical reactions on surfaces can be prevented by coating corrosion inhibitor chemicals which form an electrically insulating or chemically impermeable coating on the exposed areas. Chemicals like chromates, phosphates, salts in hard water, polyaniline, other conducting polymers and a wide range of long chain organic molecules with ionic end groups which resemble surfactants can be used. The advantage of this method is that it makes the system less sensitive to scratches or defects in the coating and there is possibility of adding extra inhibitors whenever the surface gets exposed.

Anodization: Anodizing is very resilient to weathering and corrosion, so it is commonly used for buildings and other areas where the surface will come into regular contact with the corroding environments. But failure in frequent cleaning will end with panel edge staining.

Bio-film coatings: The application of certain species of bacterial films on the surface of metals in highly corrosive environments is a new method of corrosion inhibition. The corrosion resistance is increased outstandingly in this process. Interestingly, it is reported that mild steel corrosion from sulfate-reducing bacteria can be inhibited by an antimicrobial biofilms[3].

Controlled permeability formwork (CPF): It is a method of preventing the corrosion of reinforcement by naturally enhancing the durability of the cover during concrete

placement. The effects of carbonation, chlorides, frost and abrasion can be reduced with this method[3].

Cathodic protection: Here the corrosion of a metal surface is prevented by making the surface as cathode of an electrochemical cell. Steel, fuel pipelines, tanks, ships, steel pier piles and offshore oil platforms are often protected in this way.

Anodic protection: An anodic current is impressed on the metal structure to be protected.. This method is employed in aggressive environments, like sulfuric acid. Materials like stainless steel that exhibit passivity are protected in this way.

Impressed current cathodic protection: This system use anodes connected to a DC power source. Anodes for ICCP systems are tubular and solid rod shapes of various specialized materials. These include high silicon cast iron, graphite, mixed metal oxide or platinum coated titanium or niobium coated rod and wires[4].

Corrosion inhibitors: This is an important method of prevention of corrosion especially in hydrochloric acid and sulphuric acid solutions which are used for the pickling of aluminium and electrochemical etching. The corrosion inhibitors decrease the rate of metal dissolution in acid solutions. They usually include organic compounds of nitrogen. The effect of such organic compounds on the corrosion behaviour of iron and steel in acidic solutions are studied and these compounds are characterised by their rapid action[4].

The inhibitory action of organic corrosion inhibitors is due to the adsorption of molecules on the metal-solution interface. Four distinct mechanisms are believed to occur[5], (1) electrostatic attraction between the metal and charged molecules (2) interaction between uncharged electron pairs in the inhibitor and the metal (3) interaction between the metal and the p-electrons of the inhibitor and (4) a combination of

mechanism (1) and (3). If the inhibitor molecule has greater tendency to form stronger coordination bonds with the metal, the inhibition efficiency is increased. Usually phosphorus containing molecule is found to have the strongest tendency to prevent corrosion followed by sulphur, nitrogen and oxygen[6]. The presence of lone pairs of electrons on N, O and S atoms contribute to their structural features that results in the adsorption of these molecules on the metal surface[7,8]. Generally the efficiency of the organic inhibitor compounds incorporating hetero atoms like O, N, S and in some cases Se and P are reported as very efficient corrosion inhibitors[9-11]. The efficiency of these compounds depends upon electron density present around the hetero atoms and the number of adsorption sites on the surfaces[12]. Moreover, the charge density and molecular size of the compounds also play important roles[13-18]. The mode of adsorption and formation of metallic complexes determines the activity and efficiency of the inhibitor molecules[19]. The capacity of hetero atoms to form coordinate-covalent bond with metal is highlighted in their activity. Compounds having π-bonds also can exhibit good inhibitive properties due to interaction of π-orbital with metal surface[20]. When both the above features combine, enhanced inhibition can be observed[21-23].

Literature search established that benzotriazoles and their derivatives, quinoline and benzaldehyde derivatives, alkaloids, quaternary imidazoline derivative, quaternary salts of benzenethiol, pyridine bases, triazoles, thiourea, imidazole azo derivatives, derivatives of toluidenes and chloroanilines etc possess marked inhibitory action[24-29].

Schiff bases as corrosion inhibitors

The Schiff bases are compounds containing azomethine (C=N) linkage. These compounds are cheap and are characterized by high effectiveness and easy applications.

Ashish Kumar Singh et. al. reported that the corrosion inhibition effect of three Schiff base compounds namely, ethylenediamine bis-isatin (EDBI), hexane 1,4-diamine bis-isatin (HDBI) and thiocarbohydrazide bis-isatin (TCBI) were studied by gravimetric, potentiodynamic polarization, electrochemical impedance spectroscopy, atomic force microscopy and scanning electron microscopy[30]. Adsorption of these inhibitors was according to the Frumkin isotherm. It was found that efficiency order followed by these inhibitors is TCBI>EDBI>HDBI. They reached into the conclusion that an efficient corrosion inhibitor molecule must have large size, planarity, unoccupied d-orbital and also an extensive number of π-electrons.

The corrosion inhibition effect of some Schiff bases N,N′-bis(2-hydroxy benzylidene)-1,3-diaminobenzene, N,N′-bis(4-bromobenzylidene)-1,3-diamino benzene and N,N′-bis(2-hydroxy-5-bromobenzylidene)-1,3-diaminobenzene was investigated on aluminium alloy in 0.5M HCl acid by M. T. Muniandy et. al.[31]. Weight loss measurements, potentiodynamic polarization studies and scanning electron microscopic (SEM) analysis showed that the inhibition ability of these Schiff bases are almost similar in acid medium. The potentiodynamic polarization studies revealed that, all the Schiff bases are mixed type inhibitors with a predominantly cathodic action. The inhibition efficiencies were found to increase linearly with inhibitor concentration. The inhibitor molecules obeyed Langmuir adsorption isotherm on aluminium surface. The formation of a protective layer on the metal surface was revealed by SEM studies. The inhibition

performance depends strongly on the type of functional groups substituted on the benzene ring.

M.D. Shah et. al. investigated the inhibition activity of trisalicylidene and tribenzylidene derivatives of triethylenetetramine on zinc metal in HCl medium[32]. 96-100% of inhibition efficiency was observed by the inhibitors at 1% concentrations in 0.5M and 1.0M HCl solutions. The efficiency of the former Schiff base was decreased after 120 minutes when temperature was increased from 35 to 65 ºC while that of the other inhibitor remains almost constant 99.7%. The activation energies of corrosion were higher in the presence of inhibitors than in the blank. The spontaneity of adsorption of the inhibitor on the metal surface was evident from the negative values of heat of adsorption and free energy of adsorption. Cathodic polarization was found to be predominant in electrochemical studies. It was also suggested that Langmuir isotherm was obeyed on both anodic and cathodic sites.

The corrosion inhibition efficiencies of N, N'-bis (salicylidene)-1, 4-diamino phenelyne (SDP) and N, N'-bis (3-methoxy salicylidene)-1, 4 diaminophenelyne (MSDP) on an alloy (AA6061) in 1M hydrochloric acid were evaluated by weight loss method and scanning electron microscopic technique by S.P. Fakrudeen et. al.[33]. The gravimetric study showed that the inhibition efficiency of these Schiff bases increases with increase in concentration and vary with solution temperature and immersion time. The mechanism of corrosion inhibition was postulated based on the thermodynamic parameters. The adsorption of molecules on the alloy surfaces obeyed Freundlich isotherm.

S. Thirugnanaselv et. al.[34] have reported that the corrosion inhibition efficiency of the Schiff base (4Z)-4-(3-phenylallylideneamino)-3-hydroxy naphthalene-1-sulfonic acid

(AC) on AZ31 magnesium alloy corrosion in 0.05mol/L HCl was studied by using weight loss method, electrochemical impedance spectroscopy and potentiodynamic polarization techniques. It is found that the Schiff base AC inhibited both anodic and cathodic reactions at all concentrations, and thus acting as a mixed type inhibitor, which is evident from the potentiodynamic polarization curves. The EIS measurements indicate that the polarization resistance increases as the additive concentration is increased, which may be attributed to the decrease in double layer capacitance. Langmuir adsorption isotherm was obeyed by the adsorption of AC molecules on the AZ31 magnesium alloy surface in 0.05mol/L HCl.

Vidhi Panchal et. al. investigated the effect of some newly synthesized Schiff bases namely o-chloroaniline-N-(p-methoxybenzylidene) and p-chloroaniline-N-(p-methoxybenzylidene) on Al-Mg alloy in 2 M HCl. Methods of study involved weight loss, galvanostatic polarization and EIS measurements[35]. It is concluded that the percentage of inhibition efficiency was enhanced with inhibitor concentration and diminished with hike in temperature. The inhibition mechanism of the Schiff bases was postulated based on thermodynamic parameters and activation energy values. The inhibitors were found to adsorb on the metal surface according to the Langmuir isotherm. The results of polarization studies showed that these Schiff bases act as mixed type, but the cathode was more preferentially polarized.

Schiff bases as corrosion inhibitors on mild steel

Mild steel is an important metal regarding to its wide applications in industry in various mechanical and structural purposes. Being widely used in engineering fabrications it is much prone to corrosion by different corrosion agents of which

dangerous acids like HCl and H_2SO_4 are most common. HCl and H_2SO_4 have been used for drilling operations, pickling baths and in descaling processes.

Corrosion of mild steel and its alloys in different acid media has been extensively studied. The pH of solution, dissolved oxygen and temperature affect the rate of corrosion. It is adversely affected in the pH range 4 to 10 but fairly resistant to attack by alkali. Organic compounds bearing hetero atoms are found to be very effective as corrosion inhibitors for mild steel. Many investigators have explored the effect of some nitrogen containing compounds on corrosion of mild steel in different acid media.

Fatemeh baghaei[36] studied the inhibition effect of a newly synthesized Schiff base, namely 4-nitro-2-methoxy phenyl-N-salicylidine on mild steel in 0.5M HCl acid using electrochemical impedance spectroscopy (EIS), Tafel polarization and weight loss measurements. The inhibition efficiencies were found to increase with increase in the Schiff base concentration. Tafel polarization studies proved that the Schiff base have a mixed type inhibitory nature. The adsorption studies of this compound on a mild steel surface revealed that Langmuir adsorption isotherm was obeyed by the molecule and thermodynamic parameters proved that adsorption of inhibitor was of physical in nature.

Ashassi and co-workers[37] employed electrochemical and weight loss measurements to study the anticorrosive property of (4-chloro-benzylidene)-pyridine-2-yl-amine, benzylidene-pyridine-2-yl-amine and (4-benzylidene)-pyridine-2-yl- amine at 25^0C in hydrochloric acid medium. The inhibition performance was found to be changed with the concentration and presence of substituent on the benzene ring. Langmuir adsorption isotherm was followed during the process. Polarization curves revealed that the Schiff bases were acting as mixed type inhibitors. The inhibition efficiency increased

as the inhibitor concentration increased.. Temperature studies were conducted in 25–43^{0}C range. The energy of activation and thermodynamic parameters were also calculated. The high degree of correlation between the inhibition efficiency and parameters from QSAR models suggested that these compounds are good corrosion inhibitors.

T. Sethi et. al. conducted weight loss and thermometric methods to study the corrosion inhibition of mild steel in hydrochloric acid and sulphuric acid solutions by Schiff bases N-(4-N,N-dimethylaminobenzal)-p-anisidine, N-(4-N,N-dimethylamino benzal)-p-toluidine and N-(4-N,N-dimethylaminobenzal)-2,4-dinitroaniline[38]. The inhibition efficiencies were found to be dependent on both the concentrations of inhibitors and the acids. The Schiff bases exhibited better inhibition efficiency in HCl rather than in sulphuric acid. Maximum inhibition efficiency observed was 95.55% for mild steel in HCl solution. The inhibition efficiencies of the Schiff bases when compared with that of their parent amines proved that the presence of azomethine linkage substantially increases the inhibition property. Also it was found that inhibition efficiency of all amines increases with concentration and decreases with increasing concentration of the acids.

Mass loss and thermometric methods were used to study the corrosion inhibitory effect of synthesised Schiff's bases, N-(furfurilidine)–4-methoxyaniline (SB1), N-(furfurilidine)–4-methylaniline (SB2), N-(salicylidine)–4-methoxyaniline (SB3), N-(cinnamalidine)–4–methoxyaniline (SB4) and N-(cinnamalidine)-2-methylaniline (SB5) on mild steel in sulphuric acid solutions by Upadhyay et. al.[39]. Results of both methods were in appreciable agreement with each other and inhibition efficiency was found to depend upon the concentration of inhibitor as well as that of acid. Maximum inhibition

efficiency was shown at highest concentration of Schiff's bases at the highest strength of acid.

Weight loss, potentiodynamic polarisation and electrochemical impedance spectroscopy techniques were adopted for the study of inhibitory action of the synthesized thiosemicarbazones, 4[N-(4′-chlorobenzalidene)amino]antipyrinethiosemi carbazone, 4[N-(benzalidene)amino]antipyrinethiosemicarbazone and 4[N-(4′-methoxy benzalidene) amino]antipyrinethiosemicarbazone towards mild steel corrosion in 4M HCl solution by M. Yadav et. al.[40]. Scanning electron microscopy was used to characterize the surface morphology of the mild steel specimens in the presence and absence of inhibitor. The experimental results showed that the inhibition efficiency increases as the concentration of the inhibitors were increased. The mixed type inhibitory action was indicated by the polarization measurements. The adsorption of studied Schiff bases on mild steel surface obeyed Langmuir adsorption isotherm. Quantum chemical calculations were carried out by semi-empirical AM1 method. A good correlation between the theoretical data and the experimental results was found.

Corrosion inhibitory effects of a novel inhibitor namely 5,5'-[(1Z,1'Z)-(1,4-phenylenebis(methanylylidene)]bis(azanylylidene))bis(1,3,4-thiadiazole-2-thiol) on mild steel in 1.0M HCl was explored by Ahmed A. Al-Amiery et. al.[41] at different temperatures. Results of various electrochemical studies showed that the inhibitory power of the ligand on mild steel increased with concentration and decreased at elevated temperatures. The impedance parameters indicated the adsorption of the inhibitor on the metal surface forming a protective layer is responsible for the inhibitory property.

Scope of the present investigation

The invention of new and improved corrosion inhibitors has now become a challenging task since corrosion is one among the major problems faced by many industrial and research fields. Most of the well known corrosion inhibitors are organic molecule, containing hetero atoms like nitrogen, oxygen, sulphur etc. These inhibitors have electron transfer centres which are capable of forming strong coordinate bond with the metal surface. Several Schiff bases were investigated as corrosion inhibitors for different metals and alloys in acidic media as revealed by the literature survey. The presence of C=N linkage, the electron cloud on aromatic ring, electronegative hetero atoms like nitrogen, oxygen and sulphur in the Schiff base molecule make them excellent corrosion inhibitors. Eventhough the corrosion behaviour of various heterocyclic Schiff bases were studied earlier, only a few of the articles were reported on the corrosion inhibition behaviour of thiophene 2-carbaldehyde Schiff bases.

In the present course of investigation it was proposed to perform the corrosion inhibition study of five novel heterocyclic Schiff bases derived from thiophene-2-carbaldehyde and various amino compounds on mild steel in 1.0M HCl and 0.5M H_2SO_4 solutions, since no works were reported on the anticorrosion behavior of these Schiff bases. The corrosion behavior was analyzed by weight loss measurements, Tafel polarization analysis and electrochemical impedance spectroscopic techniques. The study of corrosion inhibition of these compounds on mild steel is a subject of pronounced technological significance. Also the mechanism of corrosion inhibition is studied by plotting various adsorption isotherms. Thermodynamic parameters such as adsorption equilibrium constant and free energy of adsorptions are also calculated from suitable

adsorption isotherms. The corrosion inhibition efficiencies of the Schiff bases were also compared with that of parent amines.

The effect of temperature on corrosion behaviour of Schiff bases was evaluated to determine the thermodynamic parameters such as activation energy, entropy and enthalpy. In the present study, an attempt was also made to correlate the corrosion inhibition capacity of these molecules with their structural interactions on mild steel surface.

Part III
Corrosion inhibition studies

Chapter 2

Nimmy Kuriakose “Physicochemical, thermoanalytical, electrochemical and antitumour studies of transition metal complexes of schiff bases derived from heterocyclic carbonyl compounds” Thesis. Department of Chemistry, St. Thomas College, University of Calicut, 2015

CHAPTER 2

MATERIALS AND METHODS

This chapter deals with the study of the corrosion inhibition behaviour of the newly synthesized Schiff bases on mild steel. Conventional methods like weight loss measurements and electrochemical measurements such as Tafel polarization studies and electrochemical impedance spectroscopy (EIS) are employed for the analysis of corrosion inhibition nature of the Schiff bases. The preparation of metal specimens, aggressive solutions and different methods adopted for the evaluation of corrosion inhibition properties are described in detail here.

Metal specimens

For weight loss studies, mild steel specimens of composition: C, 0.56 %; Mn, 0.025%; S, 0.09 %; P, 0.01 %; Si, 0.02 % and the remaining Fe, were cut in the dimension 1.0x 1.0x 0.0.098cm and abraded with various grades of silicon carbide papers (120, 400, 600, 800, 1000 and 1200) to obtain well polished surfaces as per ASTM standards. The exact surface area of the metal specimens was accurately determined using vernier calipers and screw gage. Then the metal pieces were degreased with acetone, washed with detergent and distilled water, dried and finally weighed. Specimens were immersed in aggressive solutions in the absence and presence of the inhibitor in different concentrations.

Aggressive solutions

0.1M HCl and 0.5M H_2SO_4 solutions were prepared using distilled water. Stock solutions of each Schiff base inhibitor were prepared with respective acids and diluted to

different concentrations in the range 0.2mM –1.0mM. For weight loss studies, 50ml acid solutions were used, but 100ml was appropriate for the electrochemical investigations.

Weight loss measurements

In weight loss studies, the metal surfaces were directly subjected to acidic environments for a particular period of time in the absence and presence of inhibitors and then weight loss was measured from which the inhibition efficiencies were calculated.

Aggressive solutions which contain different concentrations of the inhibitor were prepared and well polished mild steel (MS) specimens were immersed in these solutions for 24 hour. A blank experiment was also conducted without adding the inhibitor. The weight loss of metal specimens was measured after 24 h. The reproducibility of the experiments was ensured by carrying out duplicate and the average values were reported. The corrosion rates and percentage of inhibition efficiencies of each inhibitor were calculated by the following equations. The corrosion rates were expressed in mm/y and the inhibition efficiencies were obtained from corrosion rates.

$$\text{Rate of corrosion } W = \frac{K \times \text{wt.loss in grams}}{\text{Area in sq.cm} \times \text{time in Hrs} \times \text{Density}} \quad (1)$$

where 'K' =87600 (This factor is used for the conversion of cm/hour into mm/year)

Density of MS specimen= 7.88g/cc

Percentage of inhibition or the inhibition efficiency (η) of the inhibitor was calculated by

$$\eta = \frac{W - W'}{W} \times 100 \quad (2)$$

where W & W' are the corrosion rates of the MS specimens in the absence and presence of the inhibitor respectively[42].

The corrosion inhibition efficiency of Schiff bases was compared with their parent amine, in aggressive solutions for a period of 24 h. This evaluation explores the role of azomethine linkage in Schiff base in the corrosion inhibition activity.

Adsorption isotherms

The inhibitory action of Schiff bases is due to the adsorption of these molecules on the surface of the metal. The adsorption on the metal surface may be physical, chemical or both. The extend of corrosion inhibition can be explained by considering the adsorption isotherms. These isotherms can represent the molecular interactions of the inhibitor molecules with the active sites on the metal surfaces. The most commonly used adsorption isotherms are Langmiur, Freundlich, Temkin and Frumkin. All the isotherms are represented as equations below and the best fit isotherm is accepted with the aid of correlation coefficient.

Langmiur adsorption isotherm $\frac{C}{\theta} = \frac{1}{K_{ads}} + C$ (3)

Freundlich adsorption isotherm $\theta = K_{ads}C$ (4)

Temkin adsorption isotherm $e^{f\theta} = K_{ads}\,C$ (5)

Frumkin adsorption isotherm $\frac{\theta}{1-\theta}\exp(f\theta) = K_{ads}\,C$ (6)

where C is the concentration of the inhibitor, θ is the fractional surface coverage, f is the molecular interaction parameter and K_{ads} is the adsorption equilibrium constant. Among the different isotherms considered, the one which has the highest the correlation co-efficient (R^2) value was accepted for interpreting the mechanism of adsorption[43-46].

The following is the relation between fractional surface coverage and percentage inhibition efficiency, $\theta = \frac{\text{Percentage inhibition efficiency}}{100}$ (7)

The adsorption equilibrium constant K_{ads} is related to the standard free energy of adsorption ΔG^0_{ads}, by

$$\Delta G^0_{ads} = -RT\ln (55.5\ K_{ads}) \quad (8)$$

where 55.5 is the molar concentration of water, R is the universal gas constant and T is the temperature in Kelvin[47].

Effect of temperature

The variation of corrosion inhibition with temperature was studied in the range 30-60^{0}C. The specimens for weight loss measurements were kept at different temperatures ie, 30^{0}C, 40^{0}C, 50^{0}C and 60^{0}C on a thermostat for 24 hours in the presence and absence of Schiff bases in acidic solution and the data obtained was utilized to calculate the thermodynamic parameters of corrosion such as activation energy (E_a), Arrhenius parameter (A), enthalpy of corrosion (ΔH^*) and entropy of corrosion (ΔS^*). The energy of activation can be calculated using Arrhenius equation,

$$K = A \exp\left(-\frac{E_a}{RT}\right) \quad (9)$$

where K is the rate constant, A is the pre exponential or Arrhenius factor, E_a is the activation energy, R is the universal gas constant and T is the temperature in Kelvin scale. A plot of logK Vs 1000/T will be a straight line with a slope $-E_a/2.303R$ and intercept log A.

From the transition state theory[48] the enthalpy and entropy of activation (ΔH^*, ΔS^*) can be calculated as,

$$K = \left(\frac{RT}{Nh}\right) \exp\left(\frac{\Delta S^*}{R}\right) \exp\left(\frac{-\Delta H^*}{RT}\right) \quad (10)$$

where, N is the Avogadro number and h is the Plancks constant. The plot of logarithmic form of this equation gives a straight line with a slope $-\Delta H/2.303R$ and intercept

$log\frac{R}{Nh} + \frac{\Delta S}{2.303\,R}$, from which enthalpy of activation and entropy of activation can be calculated.

Electrochemical measurements

Electrochemical techniques are extensively used in the study of corrosion of metals. These advanced techniques are helpful in determining the corrosion rate and exploring the mechanism of corrosion. One of the prominent advantage of electrochemical method is that it requires short measurement time and provides a fast and accurate mechanistic information about the corrosion.

The electrochemical behaviour of the metal in the presence and absence of the inhibitor can be determined by electrochemical systems and thus provide a mechanistic way to predict the inhibitive efficiency of the various organic compounds in acidic media[49-54]. Most popular electrochemical corrosion measurement techniques are electrochemical impedance spectroscopy (EIS) and polarization studies. Polarization techniques are further classified into Tafel polarization analysis and linear polarization resistance analysis.

Metallic corrosion involves the anodic oxidation of the metal and the cathodic reaction which may be either the reduction of dissolved oxygen or the evolution of hydrogen. Analysis of charge transfer processes during electrode reactions give parameters such as corrosion potential, corrosion current density, charge transfer resistance, cathodic and anodic slope values etc which will lead to the determination of rate of corrosion, the mechanism of corrosion and inhibition efficiency of molecules.

Electrochemical impedance spectroscopy (EIS)

Electrochemical impedance spectroscopy (EIS) or AC impedance methods are widely utilized in recent years as an advanced and accurate method in corrosion experiments[55-61]. Kinetic and mechanistic information on corrosion inhibition can be obtained by impedance measurements. The system response provides information about the reactions taking place at the interface. The identification of dielectric and electric properties of components under investigation is made possible by the system. Electrochemical analysis can be performed with the help of suitable equivalent electrical circuits[62].

The electrochemical system employed for the corrosion evaluation is an Ivium compactstat-e system which is associated with an advanced version of 'IviumSoft' software which makes it possible that analytical procedures like selection of proper equivalent circuit, simulation of curves, calculation of resistance and current densities easier. Three electrode assembly was used as the electrochemical cell in which a saturated calomel electrode (SCE) is the reference electrode, platinum electrode of 1cm^2 area is the counter or auxiliary electrode and well polished metal surface of 1cm^2 exposed area towards the corroding medium is the working electrode.

The measurement of capacitance (C_{dl}) around the electrical double layer formed between the charged metal surface and the oppositely charged ions of acid solution can be considered as equivalent to an electrical capacitor. The presence of a corrosion inhibitor in the solution will result in decreasing of electrical capacity which is due to the formation of an adsorption layer of the inhibitor molecules on the electrode surface. As the concentration of the inhibitor increases the capacitance also decreases.

While impedance measurement, a small and steady sinusoidal current is applied and the resulting current is measured along with the phase angle, from which the real and imaginary parts of impedances are derived. The real component of impedance Z′(ω) corresponds to the resistance and the imaginary part Z″(ω) corresponds to capacitance and they are related as

$Z(\omega) = Z'(\omega) + jZ''(\omega)$

where Z(ω) is the impedance, Z'(ω) is given by $Z_0\cos\Phi$ and Z''(ω) is given by $Z_0\sin\Phi$, Z_0 is the magnitude of the impedance and j is the imaginary number $\sqrt{-1}$.

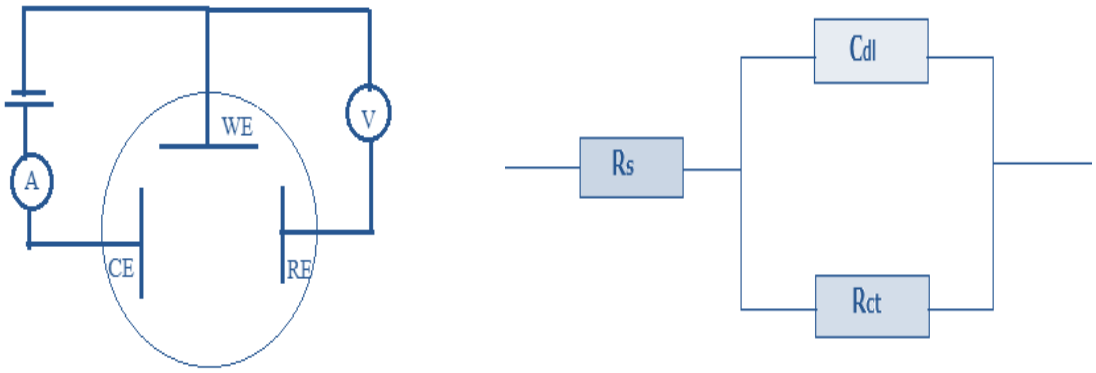

Fig. 3.1 Equivalent circuit model

Impedance measurement plots

Impedance measurements can be plotted using the Nyquist (Cole-Cole) plot, Bode plot and impedance plot. In Nyquist plots, which are commonly used, the square of the real part of impedance is plotted against the square of imaginary part. The solution resistance R_s (ohmic resistance), which is the resistance between the working electrode and reference electrode, is given by the impedance at high frequencies in the semicircular Nyquist plot. The frequency reaches its high limit at the leftmost end of the semicircle, where the semicircle touches the x- axis. The frequency reaches its low limit at the

rightmost end of the semicircle where the impedance of the system will be the sum of R_s and R_{ct} (Figure 3.2). R_{ct} is the charge transfer resistance at the electrode-solution interface. From the values of the charge transfer resistances, the inhibition efficiency of the compounds can be calculated using the following equation

$$\eta_{EIS}\,\% = \frac{R_{ct} - R'_{ct}}{R_{ct}} X100 \qquad (11)$$

where R_{ct} and R'_{ct} are the charge transfer resistances of working electrode with and without the inhibitor respectively[63].

.

.

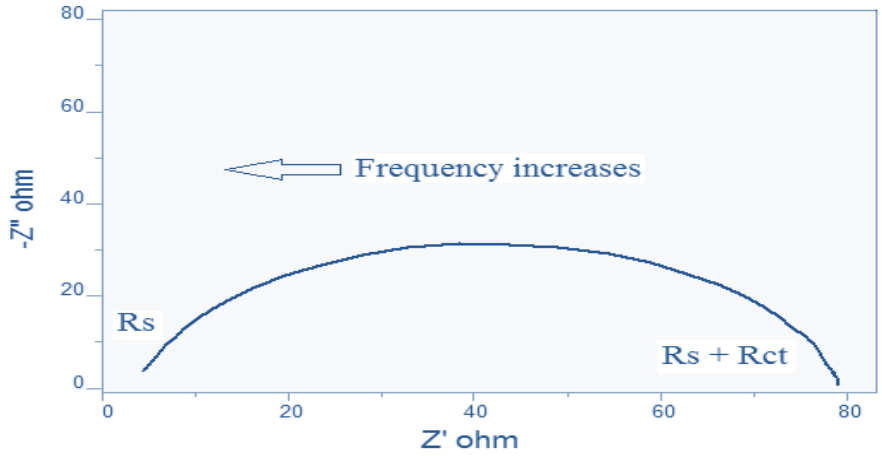

Fig. 3.2 A Nyquist plot

In Bode plots, the impedance magnitude |Z| and phase angle θ, are plotted against frequency. |Z| is obtained from the equation $|Z| = \sqrt{Z'^2 + Z''^2}$. The curve representing log|Z| versus log frequency will give the value of R_s and R_{ct}. This curve is called the impedance plot. The break point of this curve should lie on a straight line with a slope -1. On extrapolation to y-axis, at f=1 or logf = 0, the value of C_{dl} is obtained.

$$|Z| = \frac{1}{C_{dl}} \qquad (12)$$

In the plot of θ against log f, appearance of a peak which corresponds to f (θ^{max}) shows the maximum phase shift and from which C_{dl} can be evaluated. Frequency break points associated with each step are the characteristic of Bode and impedence plots. The Bode plot is an alternative to the Nyquist plot since the problem of longer measurement period associated with low frequency can be avoided.

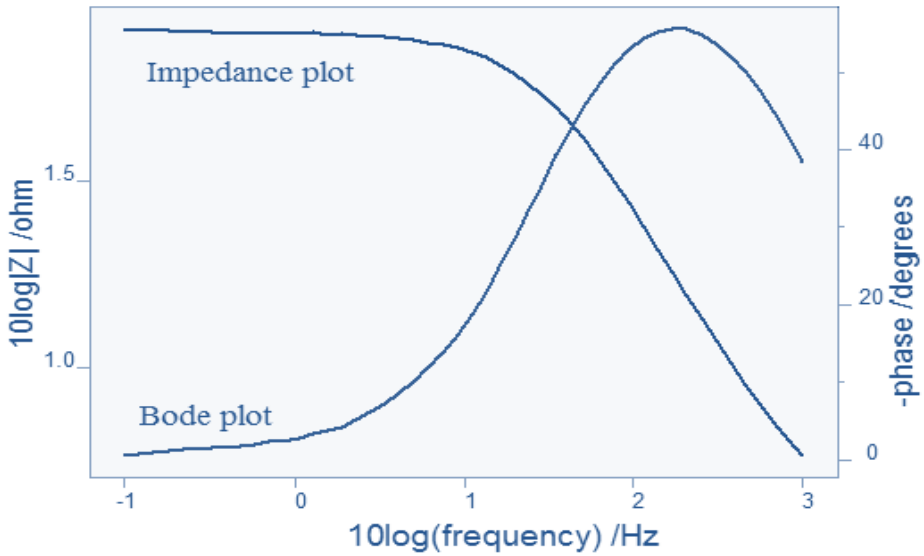

Fig. 3.3 Bode and impedance plots

Potentiodynamic polarization studies

Polarization method is evolved when the potential of the working electrode is changed ie, polarized and measuring the current produced as a function of time or potential. Polarization may be activation polarization and concentration polarization, the former generated by the resistance developed when electrical charges transfer through double layer and the latter from the concentration gradient between the interface of bulk solution and the electrode. When the polarization potential comes in the range of activation polarization, there are two types of polarization measurements i) Tafel extrapolation and ii) linear polarization measurements.

Tafel extrapolation method

Polarization can be either anodic or cathodic; the anodic reaction being oxidation of the metal and cathodic being the reduction of H^+ ions to H_2. When the rates of anodic and cathodic processes become equal, there is no charge accumulation. The mixed potential at this moment is called the open circuit potential (OCP) and designated as corrosion potential or E_{corr}. To get the applied current density, i_{app} as a function of the applied potential E, the potential between the reference electrode and the working electrode is controlled and scanned at constant rate.

The famous Butler-Volmer equation[64] describes the polarization of reversible electrodes which are controlled by activation process

$$i_{app} = i_{corr} \left\{ exp\left[\frac{\alpha_a}{RT} zF(E - E_{corr}) \right] - exp\left[-\frac{\alpha_c}{RT} zF(E - E_{corr}) \right] \right\} \quad (13)$$

where i_{app} is applied or measured current density; i_{corr} is corrosion current density; α_a and α_c are the charge transfer coefficients for anodic and cathodic reactions respectively. E-E_{corr} is the polarization ie, the difference between applied and corrosion potential; z is metal valence; F is Faraday constant; R, the gas constant and T is the absolute temperature. A plot of electrode potential versus the logarithm of current density was found to be in a straight line. For anodic and cathodic polarizations, the corresponding equations can be deduced and from which the Tafel slope for the anodic and cathodic processes can be represented as

$$b_a = \frac{2.303\ RT}{\alpha_a\ zF} \text{ and} \quad (14)$$

$$b_c = \frac{2.303\ RT}{\alpha_c\ zF} \quad (15)$$

The slope of a Tafel plot provides information about the mechanism of the electrode process and the extrapolations of the linear segment of cathodic and anodic curves gives E_{corr}. The log i_{corr} values at the point of intersection of coordinates will give corrosion current density from which the percentage of inhibition can be calculated by the following equation

$$\eta_{pol}\,\% = \frac{I_{corr} - I'_{corr}}{I_{corr}} X100 \qquad (16)$$

where i_{corr} and i'_{corr} are uninhibited and inhibited corrosion current densities respectively[65].

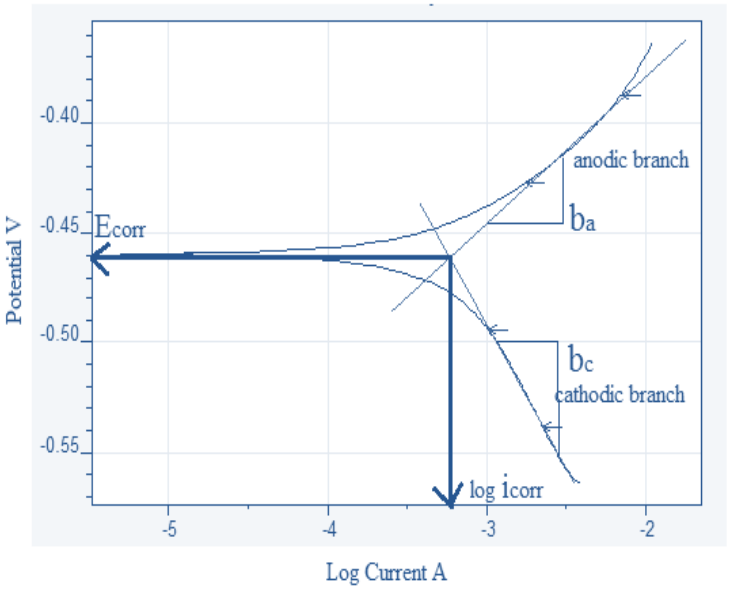

Fig. 3.4 Tafel extrapolation method

Linear polarization method

The rate of corrosion is mainly controlled by the charge transfer process at the metal-solution interface. So when the inhibitor molecules are adsorbed on the metal surfaces the rate of charge transfer process is decreased. As a result, the rate of corrosion is decreased and thereby the polarization resistance is increased. Linear polarization

technique is based on the fact that for a potential displacement in the range of +/- 10mV, the applied current density is a linear function of the electrode potential.

Stern and Geary equation[66] which relates i_{corr} to the inverse of polarisation resistance is

$$i_{corr} = \left(\frac{1}{2.303\ R_p}\right)\left(\frac{b_a b_c}{b_a + b_c}\right) = \frac{B}{R_p} \qquad (17)$$

where R_p is $\frac{\Delta E}{\Delta i}$, which is the polarization resistance and B is a constant. The variation of i_{app} is linear with the potential. The slope of the linear polarisation curve dE/di gives the polarisation resistance, which can be obtained by drawing a tangential line to the curve at E_{corr} and at zero current. The corrosion inhibition efficiency can be calculated using the equation

$$\eta_{R_p}\ \% = \frac{R'_p - R_p}{R'_p} \text{ X100} \qquad (18)$$

where R'_p and R_p are the polarization resistance in the presence and absence of inhibitor respectively.

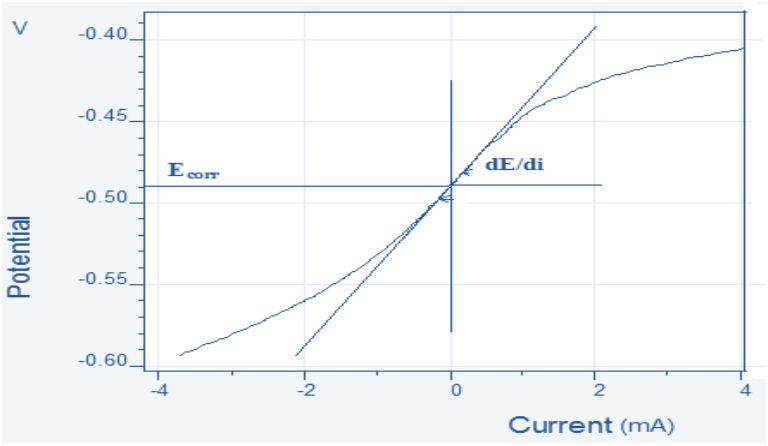

Fig. 3.5 Linear polarization method

Part III
Corrosion inhibition studies

Chapter 3

Nimmy Kuriakose “Physicochemical, thermoanalytical, electrochemical and antitumour studies of transition metal complexes of schiff bases derived from heterocyclic carbonyl compounds” Thesis. Department of Chemistry, St. Thomas College, University of Calicut, 2015

CHAPTER 3

CORROSION INHIBITION INVESTIGATIONS ON SCHIFF BASE INHIBITORS I3YT2YMAPA, T2YMABA, PHMT2YBA, CTHMT2YBA AND CTHMF2YBA ON MILD STEEL IN ACIDIC MEDIA

Five different heterocyclic Schiff base inhibitors, 3-(1H-indol-3-yl)-2-[(E)-(thiophen-2-ylmethylidene)amino]propanoic acid (I3YT2YMAPA), (E)-3-[thiophen-2-ylmethylene amino]benzoic acid (T2YMABA), (E)-4-(5-[(2-phenylhydrazono)methyl] thiophen-2-yl)benzoic acid (PHMT2YBA), (E)-4-(5-[(2-carbamothioylhydrazono) methyl]thiophen-2-yl)benzoic acid (CTHMT2YBA) and (E)-4-(5-[(2-carbamothioyl hydrazono)methyl]furan-2-yl)benzoic acid (CTHMF2YBA) were synthesized and characterised as described in part I. The corrosion inhibition efficiencies of these compounds on mild steel (MS) in hydrochloric acid and sulphuric acid medium were investigated using the conventional gravimetric studies and electrochemical studies like potentiodynamic polarization and electrochemical impedance spectroscopic studies. Adsorption studies were conducted to analyse the mechanism by which these Schiff bases exhibit corrosion inhibition. To determine thermodynamic parameters of corrosion, corrosion rates of mild steel in aggressive medium at different temperatures were also estimated. Surface morphological analysis was also conducted using scanning electron microscopy.

This chapter is divided into two sections; Section I describes the corrosion inhibition behaviour of the Schiff base inhibitors in 1.0M hydrochloric acid medium and Section II deals with their corrosion inhibition behaviour in 0.5M sulphuric acid medium. In each section the weight loss measurements, electrochemical impedance spectroscopic analyses and potentiodynamic polarization studies are described.

SECTION I

CORROSION INHIBITION STUDIES OF SCHIFF BASE INHIBITORS I3YT2YMAPA, T2YMABA, PHMT2YBA, CTHMT2YBA AND CTHMF2YBA ON MILD STEEL IN 1.0M HCl

The corrosion inhibition studies of the Schiff base inhibitors I3YT2YMAPA, T2YMABA, PHMT2YBA, CTHMT2YBA and CTHMF2YBA were conducted in 1.0M HCl by preparing inhibitor solutions in the range 0.2mM-1.0mM. The MS specimens used for the study were prepared in accordance with ASTM standards. Weight loss studies and electrochemical studies were performed to evaluate the inhibition capacities of these inhibitors.

Weight loss studies

The well polished MS specimens were immersed in hydrochloric acid medium in the presence and absence of the Schiff base inhibitors. The weight loss occurred for the specimens after 24 h were noted and corrosion rates were calculated. Each Schiff base inhibitor gave different corrosion inhibition values characteristic of each one.

Table 3.1 exhibits the corrosion rates of mild steel in 1.0M HCl in the presence of various concentrations of Schiff bases. The corrosion rates of steel specimens appreciably decreased in all cases with the inhibitor concentration. The metal specimen immersed in the acid solution in the absence of Schiff base showed a corrosion rate of 5.94 mm/y. On close comparison of the corrosion rates it is understandable that the mild steel specimen in HCl solution in the presence of Schiff base I3YT2YMAPA displayed appreciable lower corrosion rate. The decrease in the corrosion rate with the inhibitor concentration suggests that the metal dissolution process is considerably hindered by the azomethine

molecules. Figure 3.6 compares the corrosion rates of mild steel specimens in the presence of varying concentrations of imines.

Table 3.1 Corrosion rates of MS in mmy^{-1} in the presence and absence of Schiff base inhibitors I3YT2YMAPA, T2YMABA, PHMT2YBA, CTHMT2YBA and CTHMF2YBA in 1.0M HCl

C (mM)	Inhibitors				
	I3YT2YMAPA	T2YMABA	PHMT2YBA	CTHMT2YBA	CTHMF2YBA
0	5.94	5.94	5.94	5.94	5.94
0.2	3.96	4.43	4.03	4.64	4.53
0.4	2.98	3.19	3.48	3.98	4.19
0.6	2.15	2.79	1.93	2.66	2.99
0.8	1.72	1.95	1.85	2.36	1.88
1.0	0.96	1.60	1.17	1.56	1.66

Corrosion inhibition efficiencies of Schiff bases on mild steel in HCl medium were investigated and reported in Table3.2. Figure 3.7 compares the inhibition efficiencies of Schiff bases at various concentrations on MS. It is unambiguous from the data that all azomethines showed fair corrosion inhibition efficiencies against the metallic corrosion especially the MS corrosion. The inhibition efficiencies were increased with the inhibitor concentrations. At a maximum concentration of 1.0mM, Schiff bases displayed 70-83% inhibition efficiencies. It was difficult to increase the concentration of imines in acid medium due to their poor solubility and therefore the corrosion investigations were limited in the concentration range 0.2 - 1.0mM. On examination of the data it is evident that the Schiff base I3YT2YMAPA showed pronounced corrosion inhibition efficiency than all other Schiff bases at all concentrations. The enhanced efficiency of this molecule

can be correlated with its molecular structure. Presence of two aromatic ring system; one from the aldehyde part and other from amino part together with azomethine linkage and nitrogen atom of the indole moiety make the molecule so electron rich which help to bind on the surface metal atoms of mild steel. In addition to this, the molecules possess almost planar structure which was confirmed by the optimized geometry determination and this scenario is beneficial to the strong binding of the molecule on the metal surface.

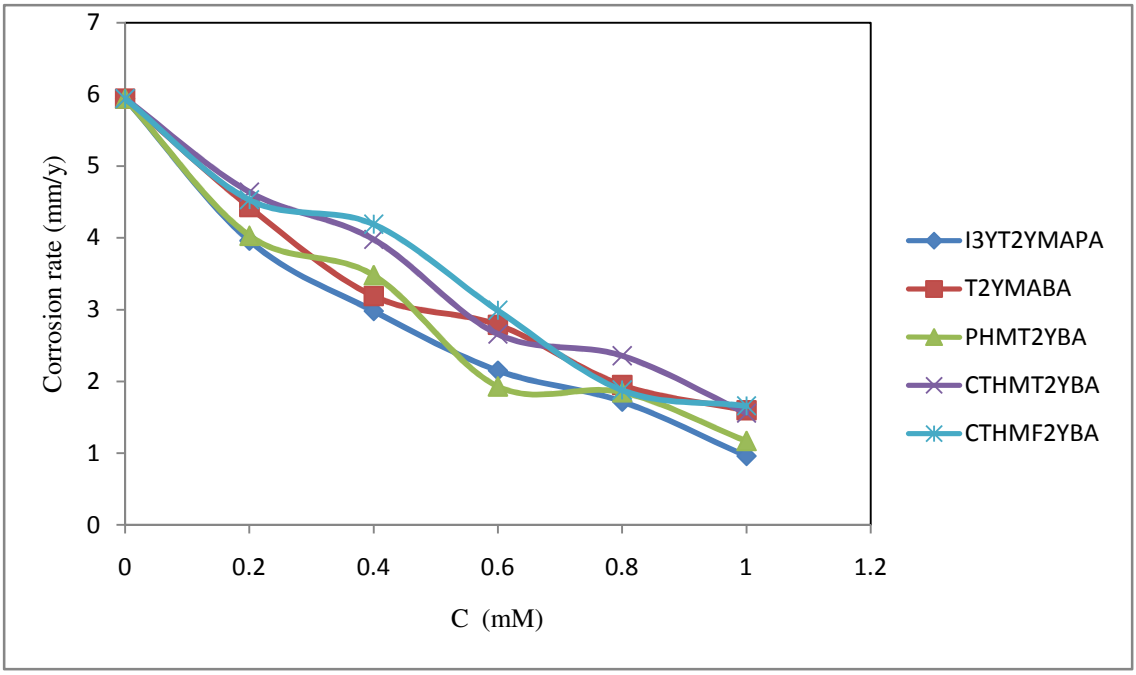

Fig. 3.6 Variation of corrosion rates of MS with the concentration of Schiff base inhibitors I3YT2YMAPA, T2YMABA, PHMT2YBA, CTHMT2YBA and CTHMF2YBA in 1.0M HCl

The Schiff base PHMT2YBA also showed appreciable inhibition efficiency against mild steel corrosion. A maximum of 80% inhibition efficiency was achieved by this molecule at a concentration of 1.0mM. This molecule possess three aromatic ring systems; two from the aldehyde side and one from amino part. The electron density of the aromatic ring systems, azomethine linkage and highly polarisable sulphur atom are the root causes in which the molecule showed better inhibition efficiency. Even though the

molecule is not planar completely as per the optimized geometry, the two benzene rings and the sulphur atom remain in the same plane, which is a fair condition to adsorb the molecule on the metal surface.

Table 3.2 Inhibition efficiencies of Schiff base inhibitors I3YT2YMAPA, T2YMABA, PHMT2YBA, CTHMT2YBA and CTHMF2YBA on MS in 1.0M HCl

C (mM)	Inhibitors				
	I3YT2YMAPA	T2YMABA	PHMT2YBA	CTHMT2YBA	CTHMF2YBA
0.2	33.26	25.32	32.06	20.54	23.64
0.4	49.82	46.08	41.33	32.71	29.46
0.6	63.75	52.90	67.46	55.17	49.69
0.8	71.08	67.17	68.81	60.19	69.28
1.0	83.86	72.99	80.32	73.75	71.99

The low corrosion inhibition of the molecule T2YMABA, compared to the previously described molecules, may be attributed to deviation from co-planarity in its molecular geometry. Even though the molecule is equipped with active corrosion inhibition probes, the puckered shape of the molecule prevents the appreciable interaction with the metal atoms. The molecules CTHMT2YBA and CTHMF2YBA showed comparatively low corrosion inhibition efficiency. A maximum of approx. 70% efficiency was noticed by these molecules at 1.0mM concentration. On comparing the structures of two molecules, one can understand that the only difference between the two molecules is presence of sulphur in former which is replaced by oxygen atom in the second one. Even though the first molecule is equipped with more electron rich sulphur atom, the molecule is somewhat more puckered than the other one. The second one contains more electron negative oxygen as the hetero atom, but achieved more planar

structures. These two molecules displayed almost same corrosion inhibition efficiencies on mild steel surface. Figure 3.8 shows the optimized geometries of the Schiff base inhibitors.

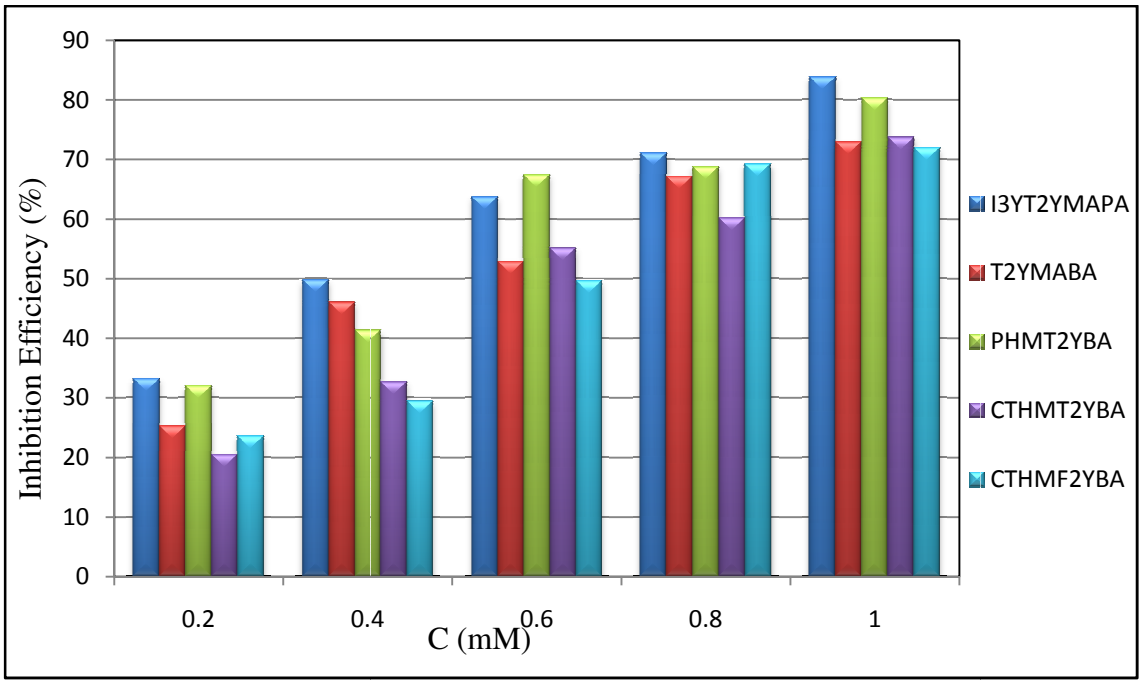

Fig. 3.7 Comparison of corrosion inhibition efficiencies (η_w%) of Schiff base inhibitors I3YT2YMAPA, T2YMABA, PHMT2YBA, CTHMT2YBA and CTHMF2YBA on MS in 1.0M HCl

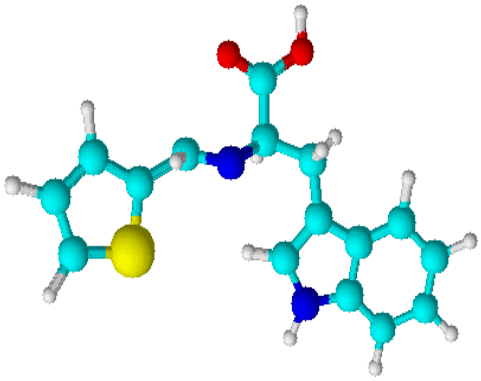

3-(1H-indol-3-yl)-2-[(E)-(thiophen-2-ylmethylidene)amino]propanoic acid (I3YT2YMAPA)

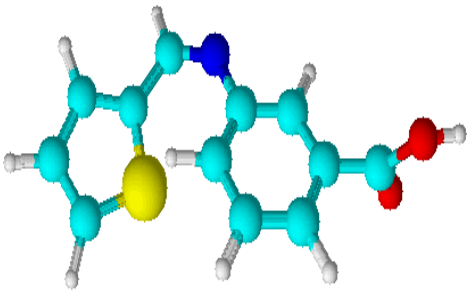

(E)-3-[thiophen-2-ylmethyleneamino] benzoic acid (T2YMABA)

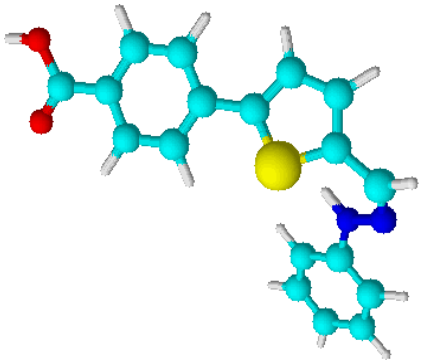

(E)-4-(5-[(2-phenylhydrazono)methy] thiophen-2-yl) benzoic acid (PHMT2YBA)

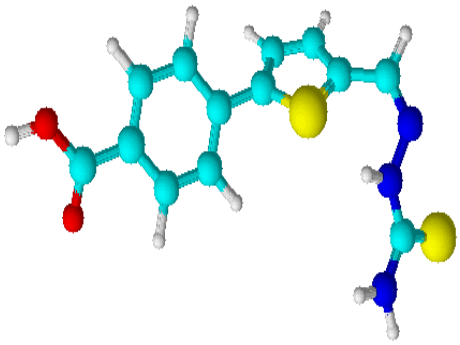

(E)-4-(5-[(2-carbamothioylhydrazono)methyl] thiophen-2-yl)benzoic acid (CTHMT2YBA)

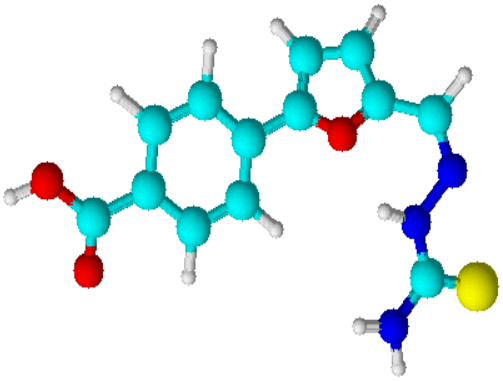

(E)-4-(5-[(2-carbamothioylhydrazono)methyl]furan-2-yl)benzoic acid (CTHMF2YBA)

Fig. 3.8 Optimized geometries of Schiff base molecules

Comparison of corrosion inhibition efficiencies of Schiff base inhibitors with their parent amines

The corrosion inhibition behaviour of Schiff base inhibitors were compared with their parent amines at three different concentrations. The results are given in Table 3.3. The parent amines such as 2-amino-3-(3-indolyl)propionic acid (AIPA), 3-aminobenzoic acid (3ABA), thiocarbamoyl hydrazide (TCH) and phenyl hydrazine (PH) exhibited much lower corrosion inhibition on MS when compared to that of the Schiff bases. The superior inhibitory power of the Schiff base inhibitors was clearly established, which can be attributed to the presence of azomethine linkage. The results are pictured in Figure 3.9.

Table 3.3 Corrosion inhibition efficiencies (η_w%) of Schiff base inhibitors I3YT2YMAPA, T2YMABA, PHMT2YBA, CTHMT2YBA, CTHMF2YBA and their parent amines in 1.0M HCl

Compounds	Concentration (mM)		
	0.2	0.6	1.0
AIPA	10.27	31.18	48.42
3ABA	4.29	29.13	38.42
PH	11.91	31.85	44.33
TCH	2.49	29.54	49.86
I3YT2YMAPA	33.26	63.75	83.86
T2YMABA	25.32	52.90	72.99
PHMT2YBA	32.06	67.46	80.32
CTHMT2YBA	20.54	55.17	73.75
CTHMF2YBA	23.64	49.69	71.99

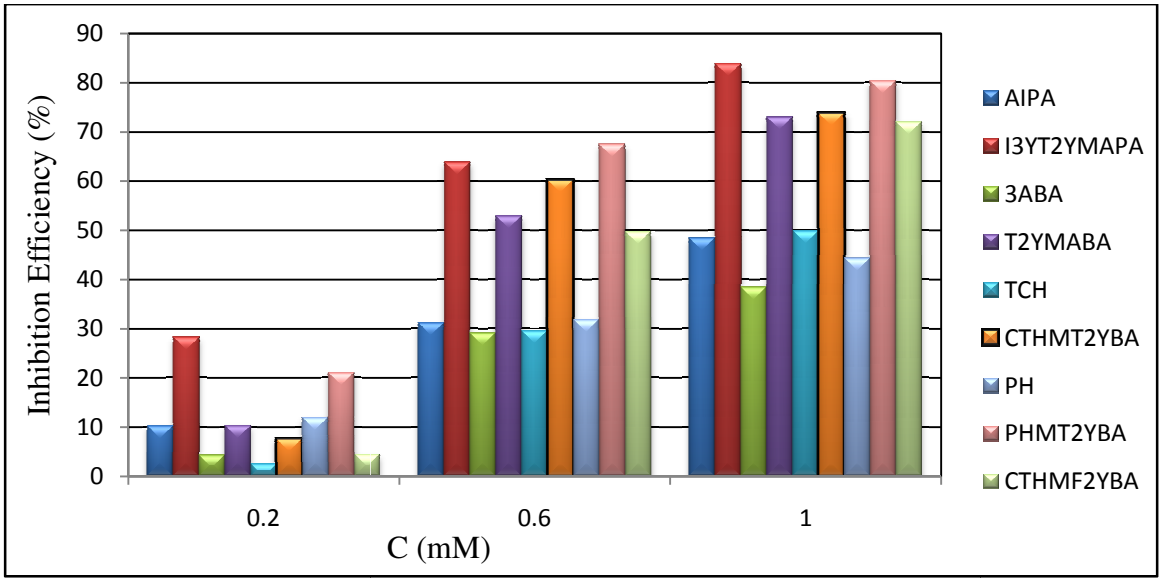

Fig. 3.9 Comparison of corrosion inhibition efficiencies (η_w%) of Schiff base inhibitors I3YT2YMAPA, T2YMABA, PHMT2YBA, CTHMT2YBA, CTHMF2YBA and their parent amines in 1.0M HCl

Adsorption isotherms

The corrosion inhibition property of inhibitor molecules is due to the adsorption on the surface of metal specimens. The mechanism of adsorption and the surface behaviour of organic molecules can be studied by adsorption isotherms. Different models of adsorption isotherms considered are Langmiur, Temkin, Frumkin and Freundlich isotherms. For verifying the mechanism of inhibition, various adsorption isotherms were plotted and the most appropriate one with the highest correlation coefficient (R^2) was selected. Parameters like adsorption equilibrium constant K_{ads} and free energy of adsorption ΔG_{ads} were calculated from the adsorption isotherms. From the adsorption studies it was found that Schiff bases I3YT2YMAPA, PHMT2YBA, CTHMT2YBA and CTHMF2YBA followed Freundlich adsorption isotherm during the inhibition process on the MS surface. Langmuir isotherm was obeyed by T2YMABA

molecules. The adsorption isotherms are represented in the Figures 3.10 to 3.14 and the parameters obtained by the analysis of isotherms are listed in Table 3.4.

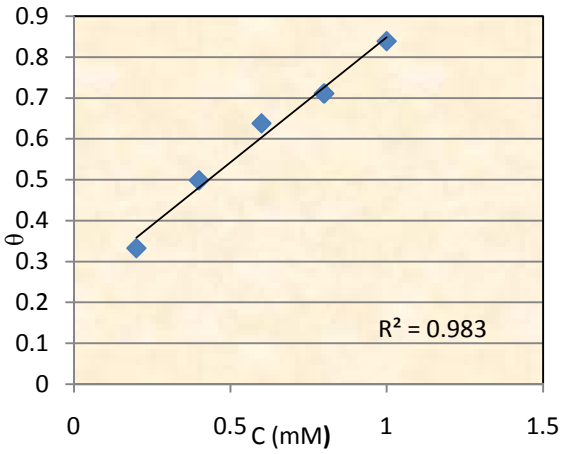

Fig. 3.10 Freundlich adsorption isotherm for I3YT2YMAPA on MS in 1.0M HCl

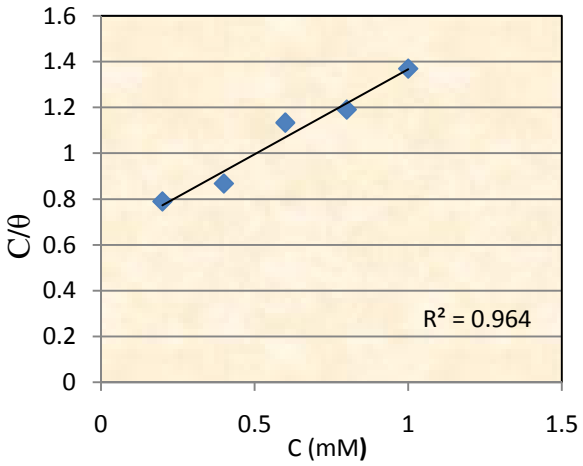

Fig. 3.11 Langmuir adsorption isotherm for T2YMABA on MS in 1.0M HCl

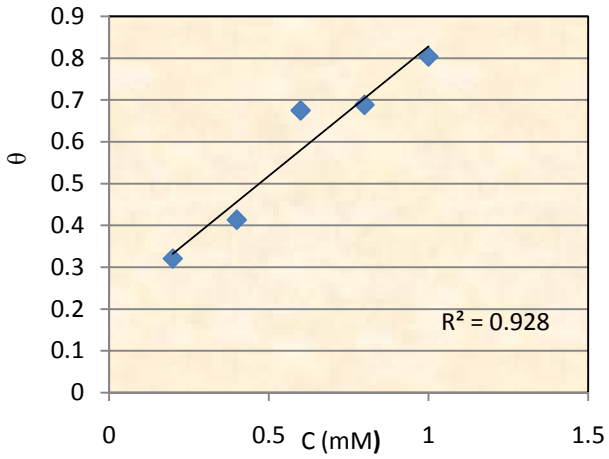

Fig. 3.12 Freundlich adsorption isotherm for PHMT2YBA on MS in 1.0M HCl

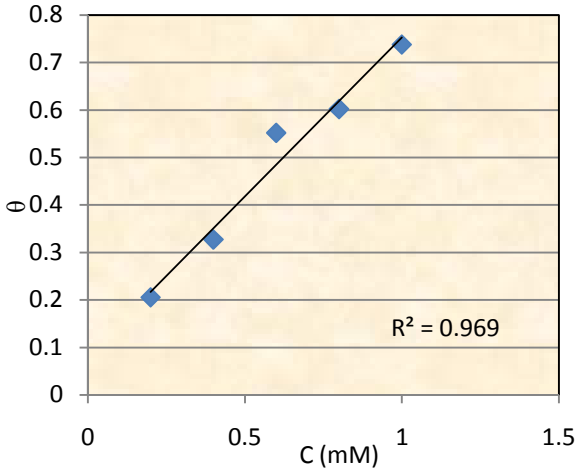

Fig. 3.13 Freundlich adsorption isotherm for CTHMT2YBA on MS in 1.0M HCl

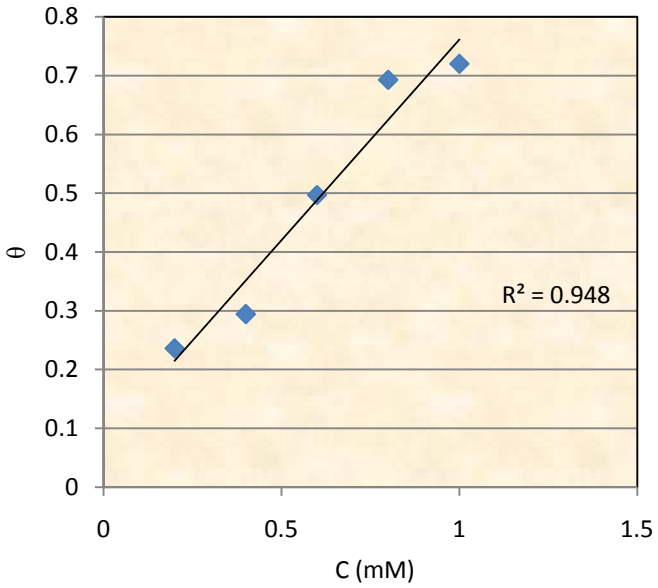

Fig. 3.14 Freundlich adsorption isotherm for CTHMF2YBA on MS in 1.0M HCl

Table 3.4 Thermodynamic parameters for the adsorption of I3YT2YMAPA, T2YMABA, PHMT2YBA, CTHMT2YBA and CTHMF2YBA on MS in 1.0M HCl

Parameter	Inhibitor				
	I3YT2YMAPA	T2YMABA	PHMT2YBA	CTHMT2YBA	CTHMF2YBA
K_{ads}	4237.29	1600	4807.69	12048.19	12820.51
ΔG_{ads} ($kJmol^{-1}$)	-31.18	-28.724	-31.49	-33.81	-33.96

Negative values ΔG^0_{ads} for all Schiff base inhibitors indicate the spontaneity of the adsorption process on the metal surface. ΔG^0_{ads} values up to -20kJ mol^{-1} indicate electrostatic interaction between the charged molecule and the charged surface of the metal through physisorption while ΔG^0_{ads} more negative than -40kJ indicates strong adsorption of the inhibitor molecules on the metal surface through co-ordinate type bond, which is called chemisorption[67]. In the case of inhibitors considered here ΔG^0_{ads} ranges

between -28 $kJmol^{-1}$ and -34 $kJmol^{-1}$ for MS specimens suggesting that the adsorption of all these molecules involves both electrostatic adsorption and chemisorption. For the Schiff base inhibitors CTHMT2YBA and CTHMF2YBA, the free energy of adsorptions were comparatively higher than that of the other imines suggesting that these inhibitors are more strongly adsorbed forming a monolayer on the surface of the MS specimens through chemical interaction.

Effect of temperature

To evaluate the effect of temperature on corrosion rate of the MS specimens, weight loss studies of the Schiff base inhibitors were conducted in the temperature range 30-60^0C. The activation energy of corrosion with and without the inhibitor was calculated by Arrhenius equation

$$K = A \exp\left(-\frac{E_a}{RT}\right) \quad (8)$$

where K is the rate of corrosion, E_a the activation energy, A the frequency factor, T the temperature in Kelvin scale and R is the gas constant. The linear plots between log K and 1000/T having regression coefficients close to unity indicate that the corrosion of MS in HCl can be explained by the simple kinetic model for all the Schiff bases. Plots of log K Vs 1000/T and log (K/T) Vs 1000/T in the presence and absence of the inhibitor are represented in Figures 3.15-3.24. Enthalpy and entropy of activation (ΔH*, ΔS*) were calculated from the transition state theory using the equation

$$K = \left(\frac{RT}{Nh}\right) \exp\left(\frac{\Delta S^*}{R}\right) \exp\left(\frac{-\Delta H^*}{RT}\right) \quad (9)$$

where N is the Avogadro number and h is the Plancks constant. Table 3.5 shows the activation energy and thermodynamic parameters of corrosion. The increase of activation energy of dissolution of the metal with increase in the inhibitor concentration implies the increase in the reluctance of dissolution of metal. Positive signs of enthalpies with a regular rise reflect the endothermic nature of dissolution and the increasing difficulty of corrosion with the inhibitor. The entropy of activation also increases with the inhibitor concentration. For the lower concentrations of the inhibitor, the entropy of activation is negative indicating that the activated molecules are in highly ordered state than that at the initial state. But as the concentration of inhibitor rises, the disordering of activated complex becomes more significant and the entropy of activation becomes positive.

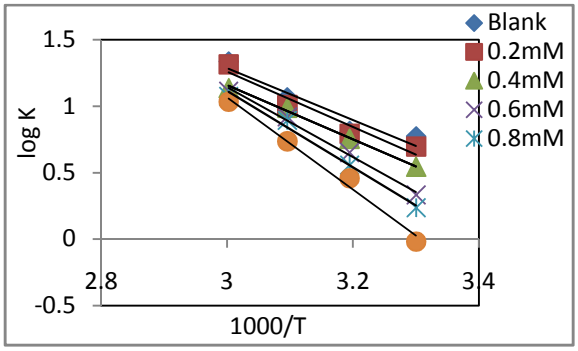

Fig. 3.15 Arrhenius plots for the corrosion of MS in the absence and presence of I3YT2YMAPA in1.0M HCl

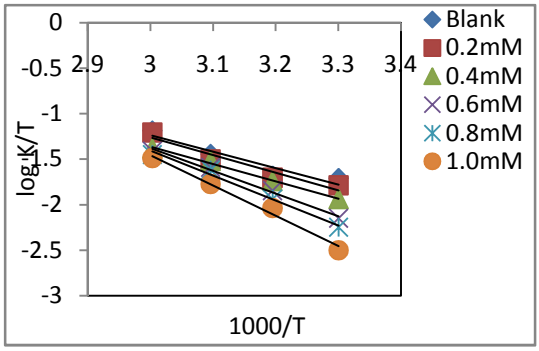

Fig. 3.16 Plots of log(K/T) vs 1000/T for the corrosion of MS in the absence and presence of I3YT2YMAPA in1.0M HCl

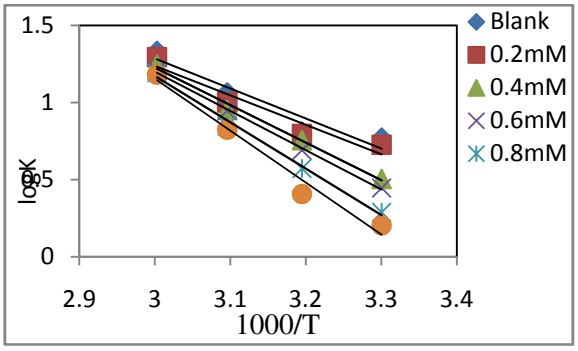

Fig. 3.17 Arrhenius plots for the corrosion of MS in the absence and presence of T2YMABA in1.0M HCl

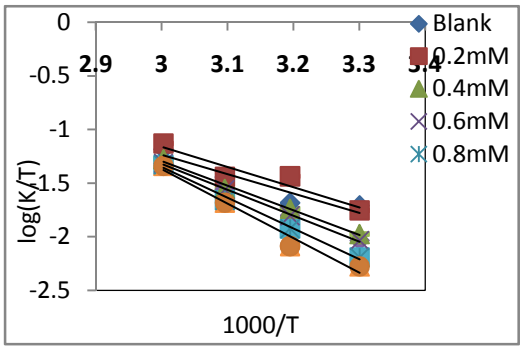

Fig. 3.18 Plots of log(K/T) vs 1000/T for the corrosion of MS in the absence and presence of T2YMABA in1.0M HCl

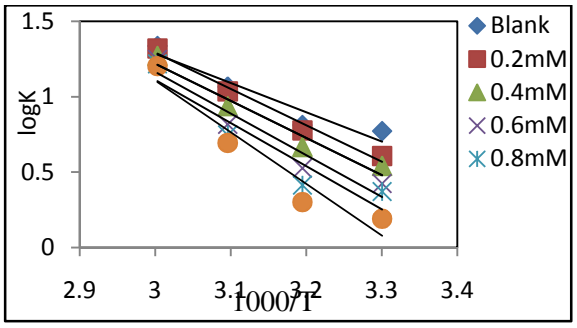

Fig. 3.19 Arrhenius plots for the corrosion of MS in the absence and presence of PHMT2YBA in1.0M HCl

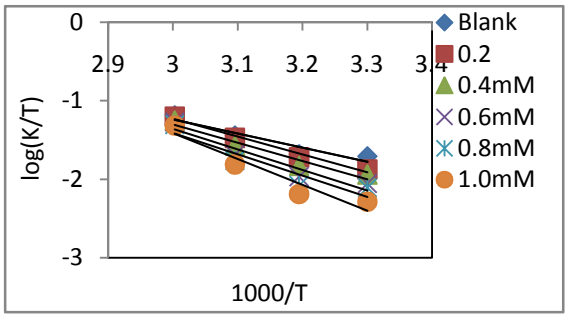

Fig. 3.20 Plots of log(K/T) vs 1000/T for the corrosion of MS in the absence and presence of PHMT2YBA in1.0M HCl

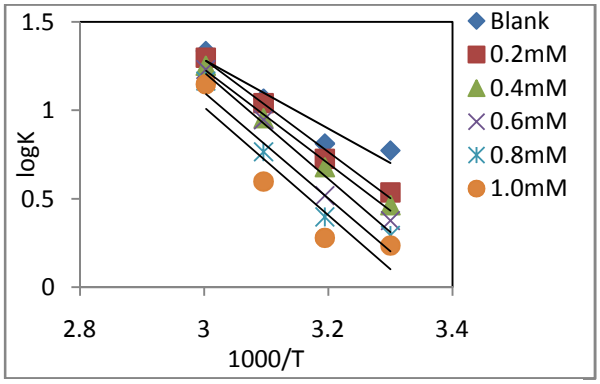

Fig. 3.21 Arrhenius plots for the corrosion of MS in the absence and presence of CTHMT2YBA in1.0M HCl

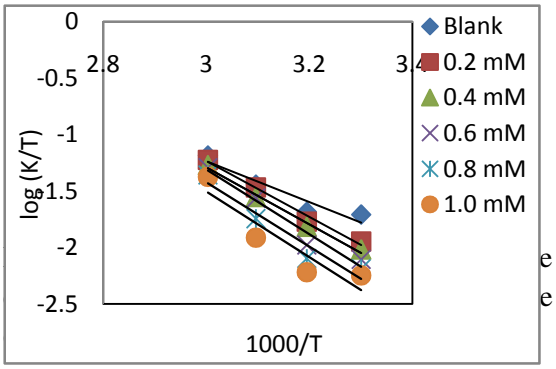

Fig. 3.22 Plots of log(K/T) vs 1000/T for the corrosion of MS in the absence and presence of CTHMT2YBA in1.0M HCl

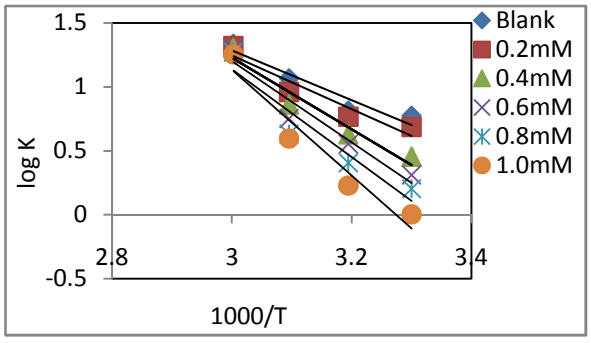

Fig. 3.23 Arrhenius plots for the corrosion of MS in the absence and presence of CTHMF2YBA in1.0M HCl

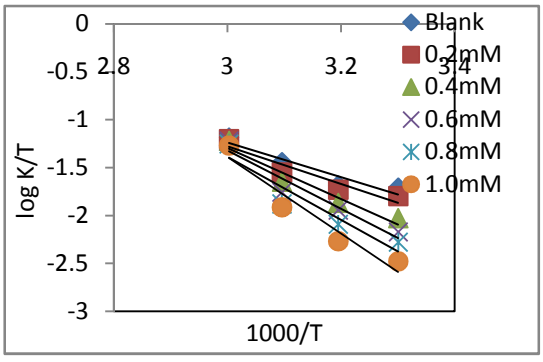

Fig. 3.24 Plots of log(K/T) vs 1000/T for the corrosion of MS in the absence and presence of CTHMF2YBA in1.0M HCl

Table 3.5 Thermodynamic parameters of corrosion of MS in the presence and absence of Schiff base inhibitors I3YT2YMAPA, T2YMABA, PHMT2YBA, CTHMT2YBA, and CTHMF2YBA in 1.0M HCl

Inhibitor	C (mM)	E_a (kJ mol^{-1})	A	ΔH* (kJ mol^{-1})	ΔS* (J mol^{-1} K^{-1})
	Blank	37.2	$1.3x10^7$	37.2	-61.33
	0.2	39.83	$3.1X10^7$	39.82	-53.92
	0.4	38.96	$1.8X10^7$	38.96	-58.51
I3YT2YMAPA	0.6	50.47	$1.13X10^9$	50.5	-24.24
	0.8	55.13	$5.68X10^9$	55.12	-10.82
	1.0	66.37	$2.88X10^{11}$	66.36	21.85
	0.2	36.56	$9.2X10^7$	36.6	-64.22
	0.4	46.64	$3.4X10^8$	46.6	-34.16
T2YMABA	0.6	48.83	$7.1X10^8$	48.8	-28.09
	0.8	57.57	$1.5X10^{10}$	57.6	-2.47
	1.0	64.39	$1.72x10^{11}$	64.4	17.64
	0.2	46.07	$3.231X10^8$	47.1	-34.65
	0.4	47.11	$3.98X10^8$	52.86	-32.91
PHMT2YBA	0.6	52.87	$2.81X10^9$	54.76	-16.67
	0.8	54.76	$4.92X10^9$	65.57	-12.003
	1.0	65.59	$2.4X10^{11}$	68.54	20.32
	0.2	50.04	$1.34X10^9$	50.03	-22.80
	0.4	50.91	$1.61X10^9$	50.89	-21.27
CTHMT2YBA	0.6	57.49	$1.66X10^{10}$	57.47	-1.89
	0.8	57.22	$1.15X10^{10}$	57.21	-4.96
	1.0	58.34	$1.41X10^{10}$	58.32	-3.23
	0.2	40.1	$3.36X10^7$	40.09	-53.46
	0.4	53.41	$3.93X10^9$	53.4	-13.88
CTHMF2YBA	0.6	60.75	$5.25X10^{10}$	60.75	7.68
	0.8	65.65	$2.63X10^{11}$	65.64	21.08
	1.0	79.07	$3.31X10^{13}$	79.06	61.29

Surface morphological studies

SEM images of mild steel specimens were taken to ascertain the mechanism of action of Schiff base inhibitors on the metal surface. Figures 3.25 to 3.27 respectively show the SEM images of bare MS surface, MS specimen in 1.0M HCl and MS specimen in 1.0M HCl containing I3YT2YMAPA with 1.0mM concentration. The irregularities on the bare metal surface are due to the effect of surface polishing. In the acidic solution the metal specimens undergo severe corrosion which is evident from Figure 3.26. Comparing the textures of images 3.26 and 3.27, it can be well understood that the metal surface is less damaged in the presence of inhibitor I3YT2YMAPA, which is due to the formation of a protective film through adsorption on metal surface and thereby suppressing the rate of corrosion.

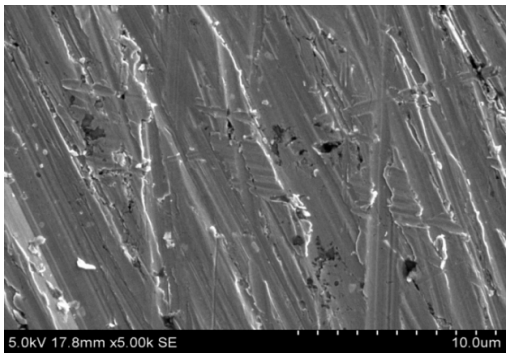

Fig. 3.25 SEM image of bare MS surface

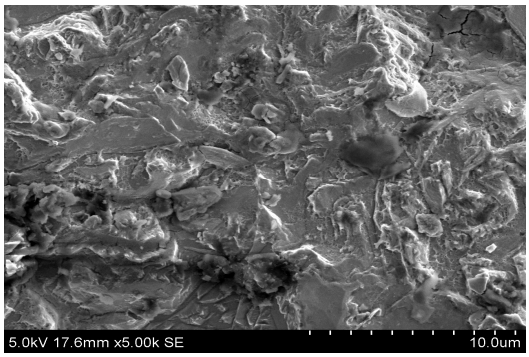

Fig. 3.26 SEM image of MS surface in 1.0M HCl (blank)

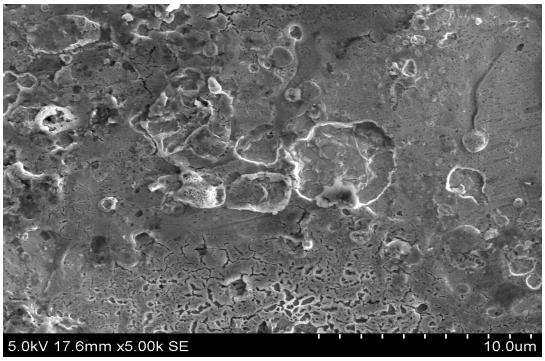

Fig. 3.27 SEM image of MS surface in 1.0M HCl and I3YT2YMAPA(1.0mM)

Electrochemical studies on corrosion

Electrochemical corrosion techniques involve EIS measurements and potentiodynamic polarization studies. These analytical methods give fast and reproducible results. The experiments were performed on three electrode assembly, in which a platinum electrode acted as the inert electrode and SCE as the reference electrode. The working electrode was $1cm^2$ exposed area of the metal specimen. Tafel polarization measurements give data from which the prediction of the site of adsorption, whether cathodic, anodic or both. The metal specimens were immersed in the acid solution for 30 minutes prior to the analysis with and without inhibitor and the results can provide a mechanistic way to explain the inhibitive action of the various organic compounds in acidic media.

Electrochemical impedance spectroscopic studies

The impedance parameters like charge transfer resistance (R_{ct}), solution resistance (Rs), double layer capacitance (C_{dl}) and percentage inhibition efficiency ($\eta_{EIS}\%$) calculated from the Rct values are given in the Table 3.6. Nyquist plots and the combined Bode-impedance plots of the five Schiff base inhibitors I3YT2YMAPA, T2YMABA, PHMT2YBA, CTHMT2YBA and CTHMF2YBA are given in Figures 3.28-3.32. The value of R_{ct} is a measure of electron transfer across the exposed area of the metal surface and it is inversely proportional to rate of corrosion. The charge transfer resistance was found to increase with the inhibitor concentration in the case of all the inhibitors. The rate of charge transfer between the metal and the solution determined the rate of metal dissolution process. The adsorbed molecules hinder the charge transfer on the metal surface. The decrease in capacitance values C_{dl} with inhibitor concentration is due to the

decrease in local dielectric constant and/or increase in the thickness of the electrical double layer[68-70].

.

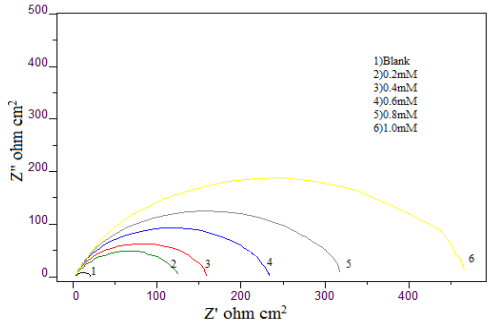

Fig3.28a Nyquist plots of MS in the presence and absence of I3YT2YMAPA in 1.0M HCl

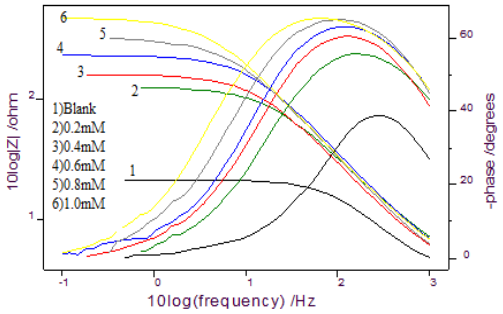

Fig. 3.28b Bode plots of MS in the presence and absence of I3YT2YMAPA in 1.0M HCl

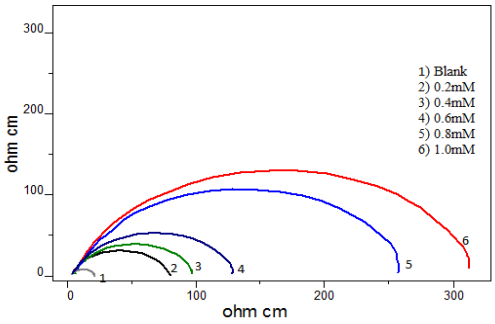

Fig. 3.29a Nyquist plots of MS in the presence and absence of T2C3ABA in 1.0M HCl

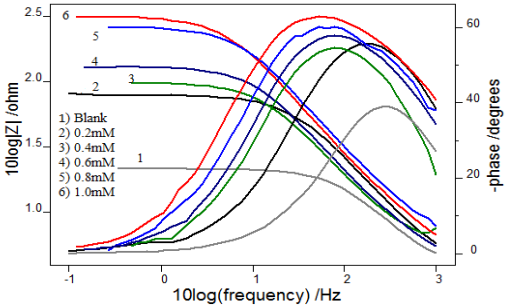

Fig. 3.29b Bode plots of MS in the presence and absence of T2C3ABA in 1.0M HCl

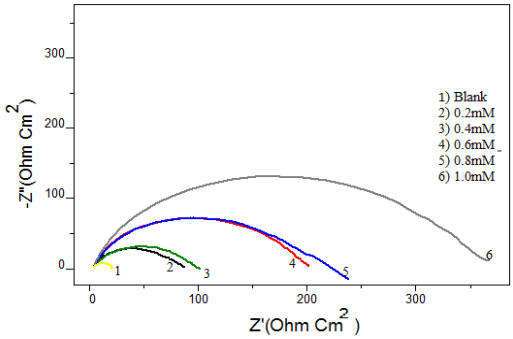

Fig. 3.30a Nyquist plots of MS in the presence and absence of PHMT2YBA in 1.0M HCl

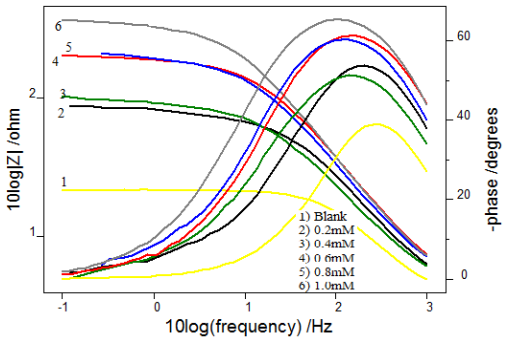

Fig. 3.30b Bode plots of MS in the presence and absence of PHMT2YBA in 1.0M HCl

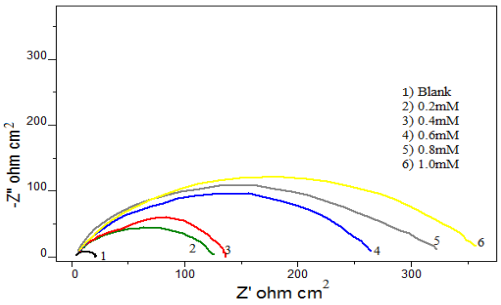

Fig. 3.31a Nyquist plots of MS in the presence and absence of CTHMT2YBA in 1.0M HCl

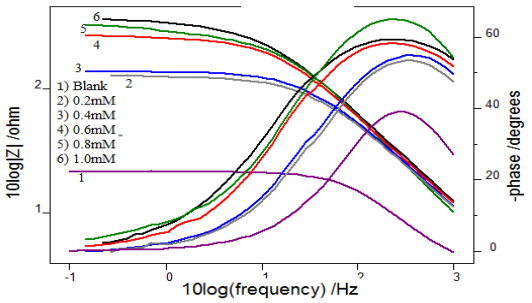

Fig. 3.31b Bode plots of MS in the presence and absence of CTHMT2YBA in 1.0M HCl

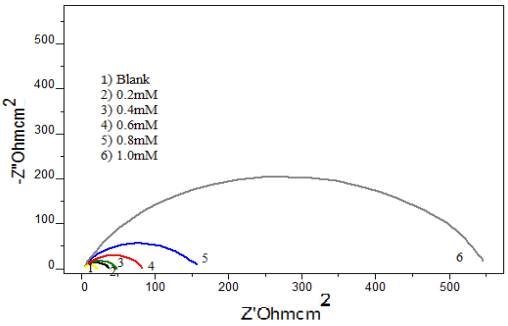

Fig. 3.32a Nyquist plots of MS in the presence and absence of CTHMF2YBA in 1.0M HCl

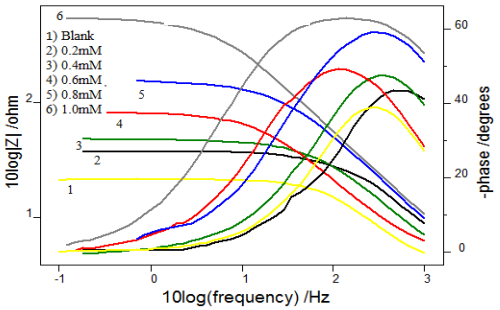

Fig. 3.32b Bode plots of MS in the presence and absence of CTHMF2YBA in 1.0M HCl

Table 3.6 Electrochemical impedance parameters of MS in the presence and absence of Schiff base inhibitors I3YT2YMAPA, T2YMABA, PHMT2YBA, CTHMT2YBA and CTHMF2YBA in 1.0M HCl

Inhibitors	C (mM)	C_{dl} ($\mu F\ cm^{-2}$)	R_{ct} ($\Omega\ cm^{-2}$)	η_{EIS}%
	0	95.8	16.4	-
I3YT2YMAPA	0.2	68.3	109	84.95
	0.4	77.0	142	88.45
	0.6	64.6	211	92.23
	0.8	75.5	286	94.27
	1.0	82.3	427	96.16
T2YMABA	0.2	73.4	70.3	76.67
	0.4	120	86.7	81.08
	0.6	111	117	85.99
	0.8	77.5	238	93.11
	1.0	91.7	290	94.34
PHMT2YBA	0.2	79	68.9	76.19
	0.4	113	79.6	79.39
	0.6	63.7	174	90.57
	0.8	75.6	176	90.68
	1.0	69.6	317	94.83
CTHMT2YBA	0.2	46.8	36.7	55.31
	0.4	37.0	117	85.98
	0.6	40.7	229	92.84
	0.8	41.8	269	93.90
	1.0	44.8	309	94.69
CTHMF2YBA	0.2	38.1	29	43.45
	0.4	55.5	38.8	57.73
	0.6	11.5	68.6	76.09
	0.8	38.9	131	87.48
	1.0	5.1	208	92.12

It is quite evident from the impedance data that the Schiff base inhibitor I3YT2YMAPA exhibited marked inhibition efficiency compared to others. A maximum of 96.16% was obtained with 1.0mM concentration of the inhibitor. Even at the lowest concentration, this molecule exhibited 84.95% inhibition efficiency. The presence of aromatic rings in the thiophene-2-carbaldehyde part and in the tryptophan part which involves an indole moiety made this ligand an excellent inhibitor. Besides aromatic rings, azomethine linkage also helps the molecule to bind strongly on the metal surface and to exhibit very high inhibition efficiency. The results were in good agreement with that obtained from weight loss measurements for I3YT2YMAPA.

Other inhibitors T2YMABA, PHMT2YBA, CTHMT2YBA and CTHMF2YBA also were able to produce good inhibition efficiencies even though slightly less than that of I3YT2YMAPA. The first three ligands were having almost comparable inhibition efficiency at their highest concentration, ie; around 94%. The presence of highly polarizing sulphur atom in the thiophene ring system and the azomethine linkage are responsible for their higher activities. The corrosion inhibition efficiencies of various Schiff base inhibitors are compared in Figure3.33.

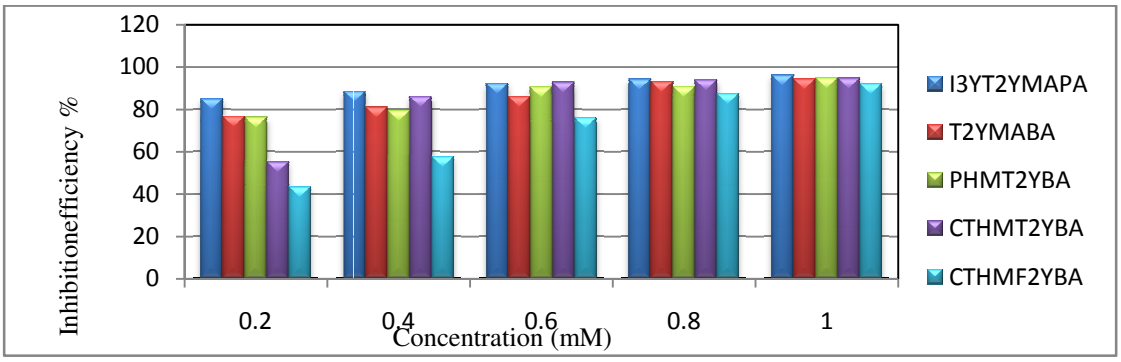

Fig. 3.33 Comparison of corrosion inhibition efficiencies (η_{EIS}%) of Schiff bases, I3YT2YMAPA, T2YMABA, PHMT2YBA, CTHMT2YBA and CTHMF2YBA on MS in 1.0M HCl

Potentiodynamic polarization studies

The corrosion inhibition efficiencies of Schiff bases were determined by polarization studies which involve Tafel extrapolation analysis and linear polarization studies. From these techniques, corrosion parameters such as corrosion potential (E_{corr}), corrosion current density (i_{corr}), polarization resistance (R_p) were measured. Using these parameters inhibition efficiencies were determined. Figures 3.34 to 3.38 represent the Tafel plots and polarization curves of MS in the presence and absence of five Schiff base inhibitors.

Table 3.7 provides the Tafel data and linear polarization data obtained by the potentiodynamic polarization studies of all these inhibitors. In this measurement also the inhibitor I3YT2YMAPA exhibited highest inhibition efficiency in the lowest concentration compared to that of other inhibitors. The percentage of inhibition efficiencies calculated from polarisation measurements are higher than that obtained from the gravimetric studies since the analyses were carried out electrochemically and the contact time between the working electrode and the acid solution is only about half an hour whereas in the latter the contact time is 24 hours.

On analysing the data it is obvious that the corrosion current densities decreased significantly as the concentration of the Schiff bases increased. The adsorption of these organic molecules on metal surface could hinder the metal dissolution appreciably by inhibiting the anodic or cathodic process of corrosion or both. On evaluation of the Tafel and polarization curves, one can see that slope of the Tafel lines in presence of inhibitor varied considerably compared to the Tafel lines of uninhibited solution. The inhibitor can be regarded as mixed type inhibitors since the slopes of both Tafel lines are affected

considerably. If the anodic or cathodic slopes vary from the slope of the uninhibited solution, the inhibitor can be treated as an anodic or cathodic type inhibitor[71].

Table 3.7 Potentiodynamic polarization parameters of MS in the presence and absence of Schiff base inhibitors, I3YT2YMAPA, T2YMABA, PHMT2YBA, CTHMT2YBA and CTHMF2YBA in 1.0M HCl

Inhibitor	Tafel Data						Linear polarization data	
	C (mM)	$-E_{corr}$ (mV/SCE)	I_{corr} ($\mu A/cm^2$)	$-b_c$ (mV/dec)	b_a (mV/dec)	η_{pol}%	R_p(ohm)	η_{Rp}%
I3YT2YMAPA	0	465	726	106	72	-	38.14	-
	0.2	465	141	97	79	80.58	188.9	80.79
	0.4	479	94.6	83	87	86.97	377.0	88.76
	0.6	476	53.6	85	78	92.62	463.8	92.16
	0.8	485	42.4	83	72	94.16	567.1	93.04
	1.0	476	34.1	87	89	95.33	651.2	95.25
T2YMABA	0.2	476	183	89	79	74.79	82.3	73.51
	0.4	483	174	93	89	76.03	114	80.88
	0.6	475	111	90	68	84.71	152	85.66
	0.8	479	49.2	89	79	93.22	313	93.04
	1.0	487	40.4	86	76	94.44	367.3	94.07
PHMT2YBA	0.2	501	173	83	74	76.17	86.5	74.79
	0.4	500	131	81	91	81.96	125.4	82.62
	0.6	517	76	84	100	89.53	214	89.81
	0.8	515	68	76	94	90.63	221	90.14
	1.0	516	39	85	95	94.63	405	94.62
CTHMT2YBA	0.2	510	316	103	63	56.47	47.59	54.19
	0.4	512	204	105	72	71.90	68.78	68.30
	0.6	502	132.6	99	58	81.74	173	87.39
	0.8	513	89.1	90	70	87.73	294	92.58
	1.0	499	42.2	94	51	94.19	369	94.09
CTHMF2YBA	0.2	499	222	101	63	69.43	64.33	66.11
	0.4	488	199	104	63	72.59	76.03	71.33
	0.6	497	202	109	74	72.18	78.07	72.08
	0.8	508	64	89	94	91.18	238.4	90.85
	1.0	505	56.7	83	85	92.19	305.4	92.86

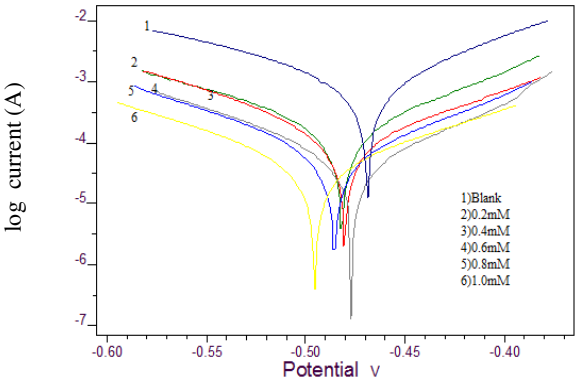

Fig. 3.34a Tafel plots of MS in the presence and absence of I3YT2YMAPA in 1.0M HCl

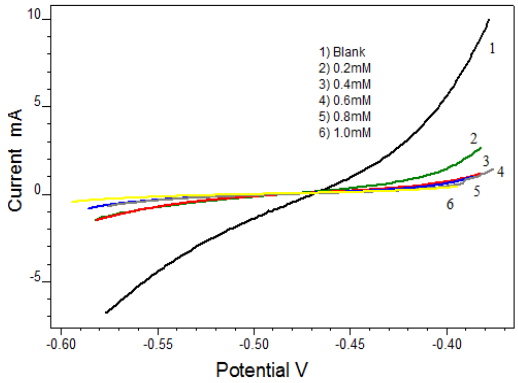

Fig. 3.34b Linear polarization curves of MS in the presence and absence of I3YT2YMAPA in 1.0M HCl

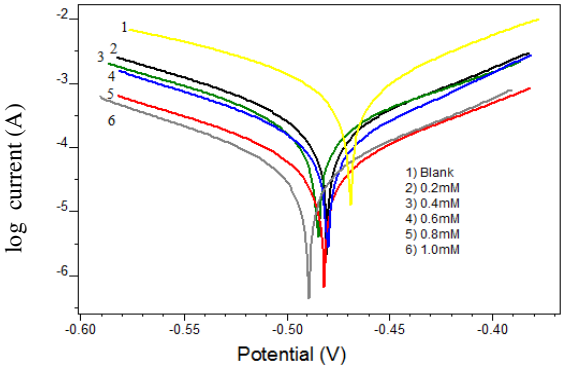

Fig. 3.35a Tafel plots of MS in the presence and absence of T2YMABA in 1.0M HCl

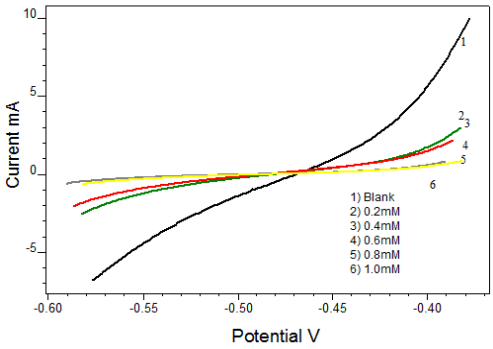

Fig. 3.35b Linear polarization curves of MS in the presence and absence of T2YMABA in 1.0M HCl

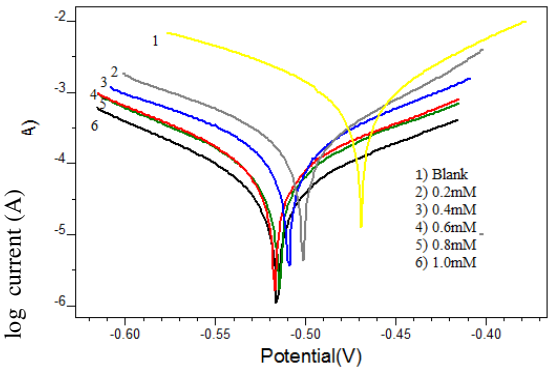

Fig. 3.36a Tafel plots of MS in the presence and absence of PHMT2YBA in 1.0M HCl

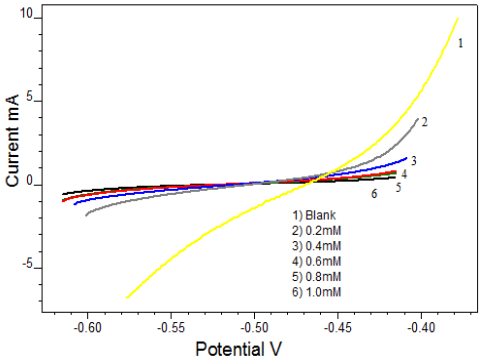

Fig. 3.36b Linear polarization curves of MS in the presence and absence of PHMT2YBA in 1.0M HCl

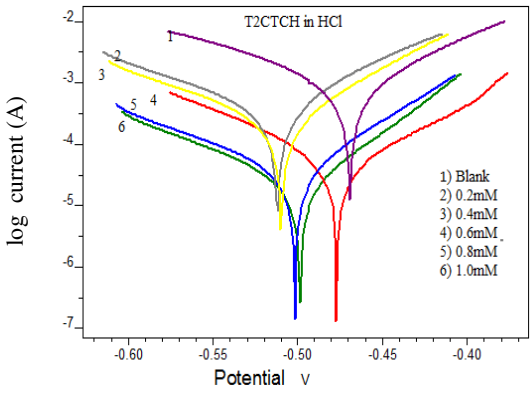

Fig. 3.37a Tafel plots of MS in the presence and absence of CTHMT2YBA in 1.0M HCl

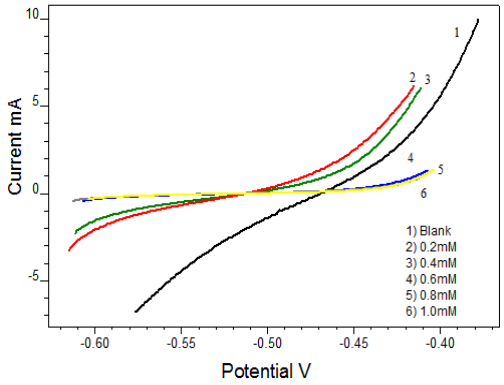

Fig. 3.37b Linear polarization curves of MS in the presence and absence of CTHMT2YBA in 1.0M HCl

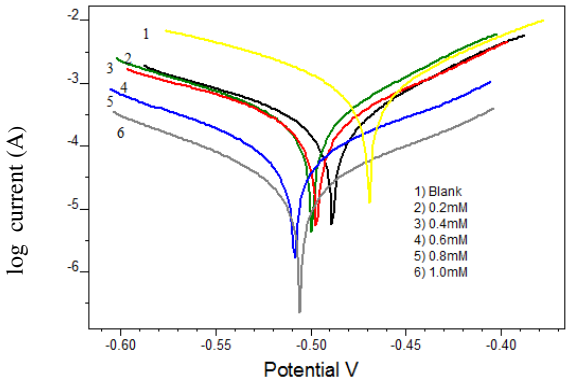

Fig. 3.38a Tafel plots of MS in the presence and absence of CTHMF2YBA in 1.0M HCl

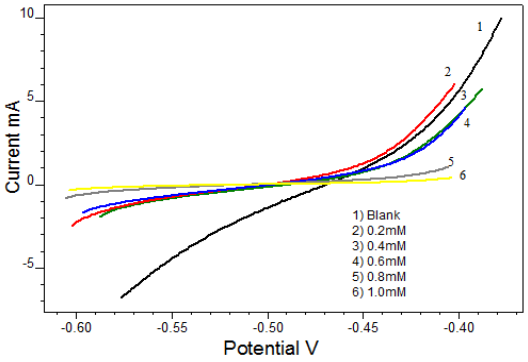

Fig. 3.38b Linear polarization curves of MS in the presence and absence of CTHMF2YBA in 1.0M HCl

On analyzing the data presented in Table 3.7, it can be found that the anodic and cathodic slope variations are different for each inhibitor. I3YT2YMAPA was found to be predominantly cathodic type. For the inhibitors T2YMABA, CTHMT2YBA and CTHMF2YBA the cathodic slope is slightly varied suggesting that these molecules are acting on both the cathode and anode and thus can be regarded as a mixed type inhibitor. Whereas PHMT2YBA molecules acted as anodic inhibitor. Generally if the shift of E_{corr} is greater than 85 with respect to E_{corr} of uninhibited solution along with the considerable change of anodic or cathodic slopes, the inhibitor can be viewed as cathodic or anodic

type. Figure 3.39 represents a comparison of corrosion inhibition efficiencies of all Schiff base inhibitors. According to polarization studies, the general trend of inhibition efficiency follows the order I3YT2YMAPA > PHMT2YBA > CTHMT2YBA > T2YMABA > CTHMF2YBA. This order is same as that obtained from weight loss method.

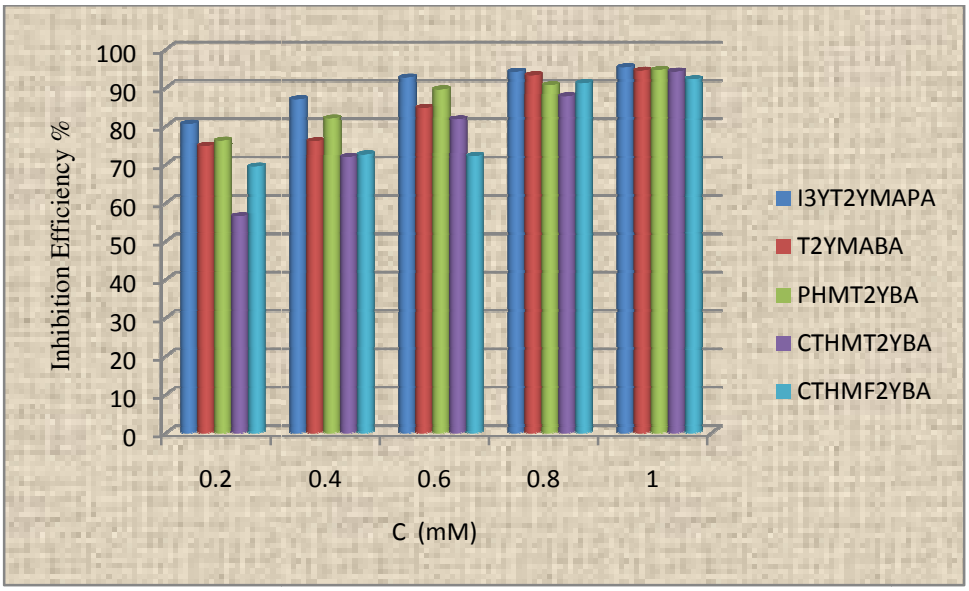

Fig. 3.39 Comparison of corrosion inhibition efficiencies (η_{pol}%) of Schiff bases I3YT2YMAPA, T2YMABA, PHMT2YBA, CTHMT2YBA and CTHMF2YBA on MS in 1.0M HCl

Mechanism of inhibition

It is well known that the surface of the metal is positively charged in acidic media. It is believed that the Cl^- ions can be specifically adsorbed on the metal surface and creates an excess of negative charge on the surface[72]. This will favour the adsorption of protonated inhibitor on the surface and hence reduce the dissolution of Fe to Fe^{2+}. Besides this electrostatic interaction between the protonated inhibitor and the metal surface, other possible interactions are i) interaction of unshared electron pairs in the molecule with the metal ii) interaction of π-electrons with the metal and iii) a

combination of types (i–ii). If one examines the structures of Schiff bases, many potential sources of inhibitor–metal interaction can be recognized. The unshared pair of electrons present on N atoms in each inhibitor is of key importance in making coordinate bond with the metal. The π-electron cloud of the aromatic rings and the azomethine linkage also participate in the inhibition mechanism. Furthermore, the double bonds in the inhibitor molecule permit the back donation of metal d electrons to the π* orbital and this type of interaction cannot occur with amines[73]. This can be justified by the lower inhibition efficiency of the parent amines than that of Schiff base inhibitors. Figure 3.40 illustrate the mechanism of action of inhibitor molecules on the metal surfaces.

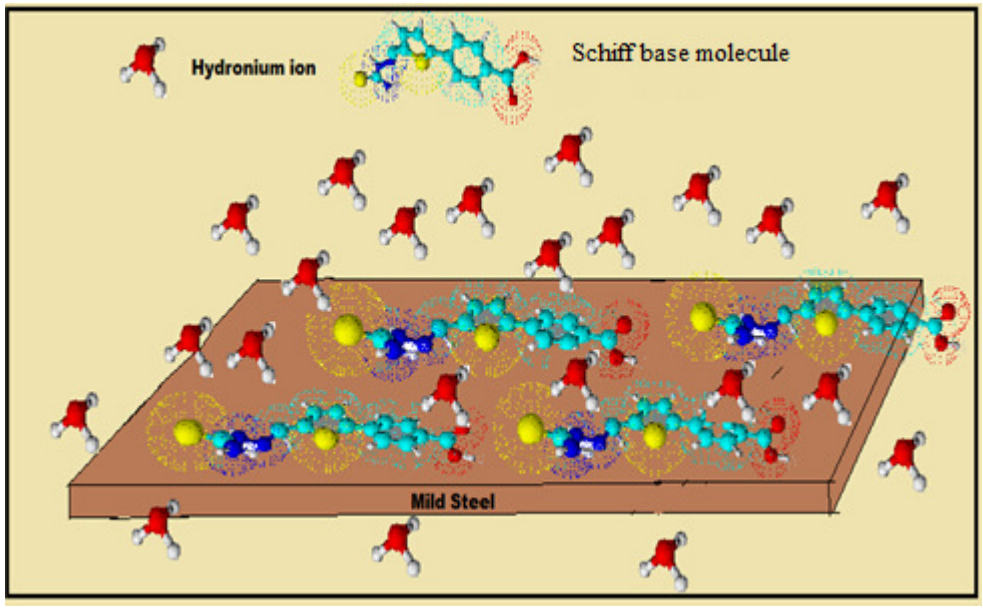

Fig. 3.40 Mechanism of corrosion inhibition by Schiff base inhibitor molecules on MS surface

SECTION II

CORROSION INHIBITION STUDIES OF SCHIFF BASE INHIBITORS I3YT2YMAPA, T2YMABA, PHMT2YBA, CTHMT2YBA AND CTHMF2YBA ON MILD STEEL IN 0.5M H_2SO_4

The corrosion inhibiton of the mild steel specimens are studied in 0.5M sulphuric acid solution. Different methods like weight loss measurements, electrochemical impedance studies and potentiodynamic polarisation studies were performed and are detailed in this section. Generally it was found that the inhibition efficiencies of the Schiff base inhibitors in 0.5M H_2SO_4 medium were not that much pronounced as in the hydrochloric acid medium. Sulphuric acid being more aggressive than hydrochloric acid will cause a higher rate of corrosion of mild steel specimens.

Weight loss studies

The mild steel specimens were immersed in 0.5M sulphuric acid medium for 24 hours in the presence and absence of inhibitors. Corrosion rates and inhibition efficiency values characteristic of each compound are given in Tables 3.8 and 3.9.

The Schiff base inhibitor I3YT2YMAPA exhibited least corrosion rates compared to other compounds. The inhibition performance of this compound was the highest ie, 92% at a concentration of 1.0mM. Generally as the inhibitor concentration is increased the inhibition efficiency also increased for all the inhibitors. The aromatic rings in addition to the azomethane linkage and highly polarizable S atom make the molecule to attract the surface metal atoms strongly which results in the greater inhibition performance.

Table 3.8 Corrosion rates (mmy^{-1}) of MS in the presence of Schiff base inhibitors I3YT2YMAPA, T2YMABA, PHMT2YBA, CTHMT2YBA and CTHMF2YBA in 0.5M H_2SO_4

C(mM)	I3YT2YMAPA	T2YMABA	PHMT2YBA	CTHMT2YBA	CTHMF2YBA
0	26.11	26.11	26.11	26.11	26.11
0.2	16.76	24.97	24.83	24.68	15.99
0.4	12.21	22.09	22.98	21.38	15.88
0.6	10.01	20.67	18.67	19.14	10.78
0.8	7.36	16.05	17.09	14.93	10.35
1.0	5.98	14.13	12.33	12.65	9.05

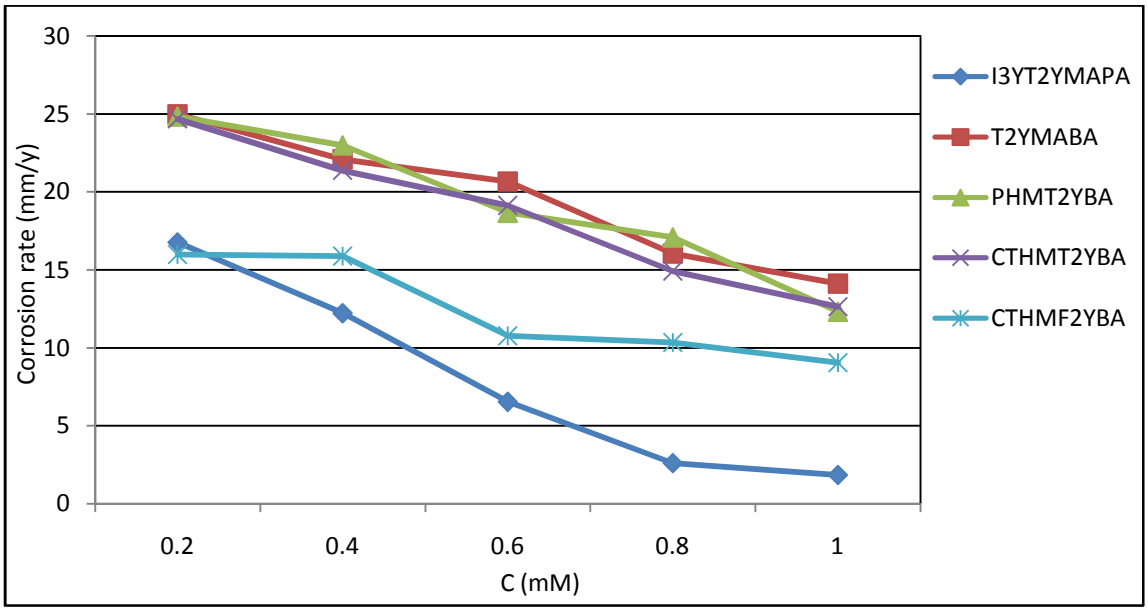

Fig. 3.41 Variation of corrosion rates of MS with the concentration of Schiff base inhibitors I3YT2YMAPA, T2YMABA, PHMT2YBA, CTHMT2YBA and CTHMF2YBA in 0.5M H_2SO_4

Schiff base inhibitors T2YMABA, PHMT2YBA and CTHMT2YBA showed comparatively poor corrosion inhibition efficiency on MS surface in 0.5M H_2SO_4 medium. Eventhough these molecules possesses active corrosion inhibition probes, they displayed lower corrosion inhibition power, which may be attributed to a) high corrosive nature of

sulphuric acid medium and b) intensive hydrolysis of these inhibitors in sulphuric acid medium. The furfural derived Schiff base inhibitor CTHMF2YBA showed fair corrosion inhibition efficiency on MS surface. Comparison of corrosion rates and inhibition efficiencies are demonstrated in Figures 3.41 and 3.42 respectively.

Table 3.9 Inhibition efficiencies of Schiff base inhibitors I3YT2YMAPA, T2YMABA, PHMT2YBA, CTHMT2YBA and CTHMF2YBA on MS in 0.5M H_2SO_4

C (mM)	Inhibitors				
	I3YT2YMAPA	T2YMABA	PHMT2YBA	CTHMT2YBA	CTHMF2YBA
0.2	35.81	4.35	4.88	1.18	38.75
0.4	53.21	15.39	11.96	5.46	39.15
0.6	61.69	20.84	28.50	18.09	58.72
0.8	71.81	38.53	34.55	26.67	60.36
1.0	77.09	45.89	52.79	51.56	65.32

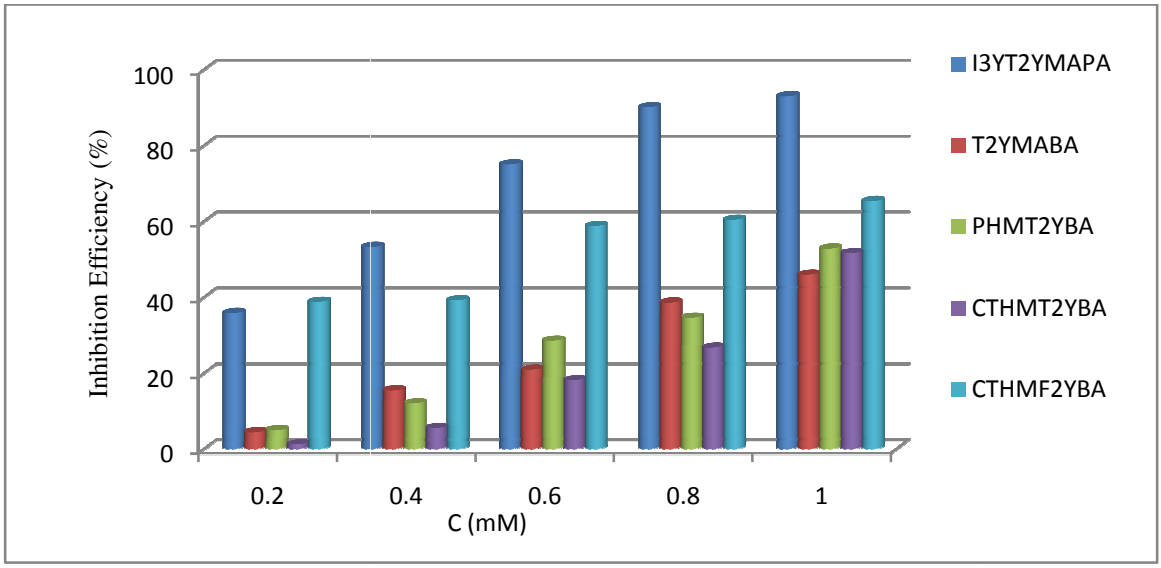

Fig. 3.42 Comparison of corrosion inhibition efficiencies (η_w%) of Schiff base inhibitors I3YT2YMAPA, T2YMABA, PHMT2YBA, CTHMT2YBA and CTHMF2YBA on MS in 0.5M H_2SO_4

Adsorption isotherms

The adsorption isotherms help to verify the mechanism of interaction of the inhibitor on the surface of MS specimens. Different adsorption isotherms were considered and the best fit model of isotherm was selected with the aid of correlation coefficient. The adsorption isotherms are represented in Figures 3.43-3.47.

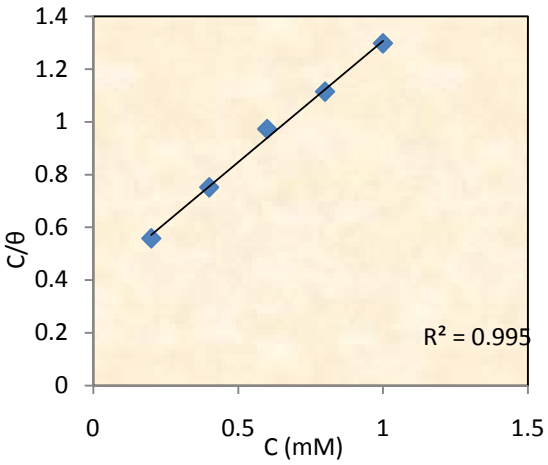

Fig. 3.43 Langmuir adsorption isotherm for I3YT2YMAPA on MS in 0.5M H_2SO_4

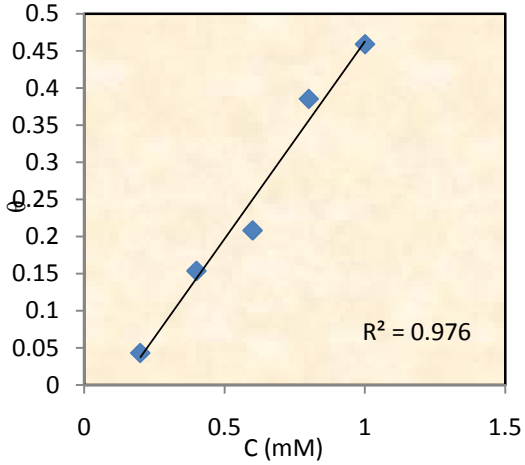

Fig.3.44 Freundlich adsorption isotherm for T2YMABA on MS in 0.5 M H_2SO_4

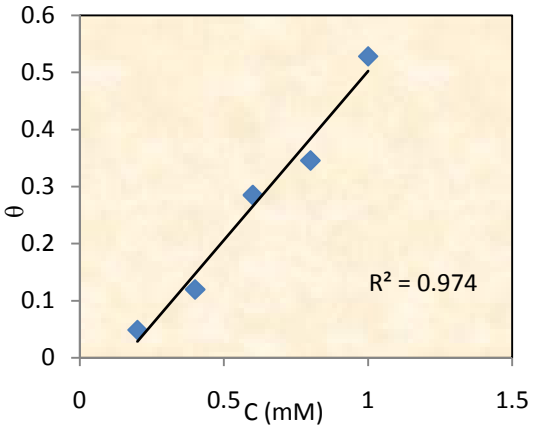

Fig. 3.45 Freundlich adsorption isotherm for PHMT2YBA on MS in 0.5M H_2SO_4

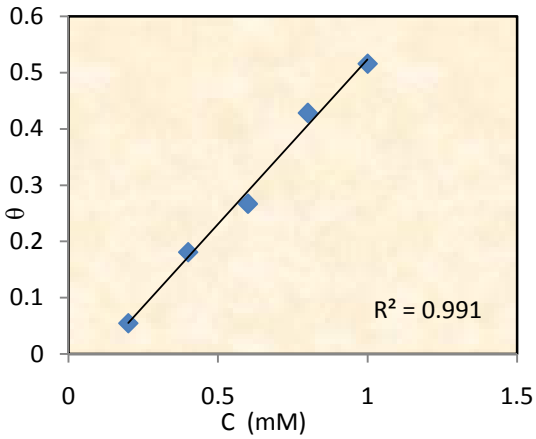

Fig. 3.46 Freundlich adsorption isotherm for CTHMT2YBA on MS in 0.5 M H_2SO_4

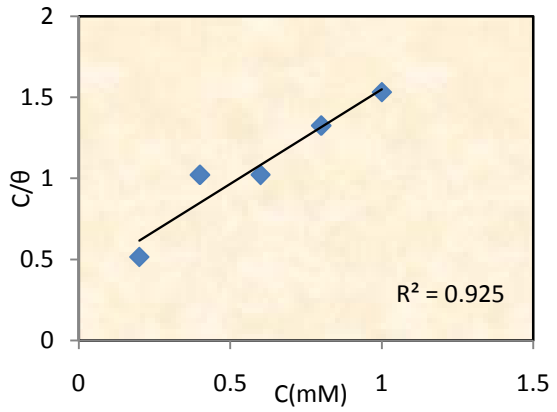

Fig. 3.47 Langmuir adsorption isotherm for CTHMF2YBA on MS in 0.5M H_2SO_4

The best fit adsorption isotherm for T2YMABA, PHMT2YBA and CTHMT2YBA was Freundlich isotherm, which can be represented as

$\theta = K_{ads}$ C

where C is the concentration of the inhibitor, θ is the fractional surface coverage and K_{ads} is the adsorption equilibrium constant. At the same time for I3YT2YMAPA and CTHMF2YBA inhibitors, Langmuir isotherm was the suitable one. Langmiur adsorption isotherm can be represented as

$$\frac{C}{\theta} = \frac{1}{K_{ads}} + C$$

K_{ads} and $\Delta G^0_{ads,}$ are calculated for each inhibitor and are reported in Table 3.10. The negative value of free energy of adsorption indicates the spontaneity of the process. In the present investigation ΔG^0_{ads} values for all the molecules suggested that the adsorption involved both physisorption and chemisorption. The low values of the adsorption equilibrium constant for T2YMABA, PHMT2YBA and CTHMT2YBA were an indication of possibility of multilayer adsorption of these molecules on the metal surface. Inhibitors I3YT2YMAPA and CTHMF2YBA exhibited high values of K_{ads} and ΔG_{ads} suggesting that there was a monolayer of protective molecules formed on the surface

through chemical interaction. Even though the rates of corrosion of metal specimens were high in sulphuric acid, it can be concluded that these molecules were able to make an effective protection barrier preventing the dissolution of Fe atoms.

Table 3.10 Thermodynamic parameters for the adsorption of Schiff base inhibitors I3YT2YMAPA, T2YMABA, PHMT2YBA, CTHMT2YBA and CTHMF2YBA on MS in 0.5M H_2SO_4

Parameter	I3YT2YMAPA	T2YMABA	PHMT2YBA	CTHMT2YBA	CTHMF2YBA
Isotherm	Langmuir	Freundlich	Freundlich	Freundlich	Langmuir
K_{ads}	2590	531	592	609	2611
ΔG_{ads}(kJ/mol)	-30	-25.75	-26.03	-26.1	-30

Surface morphological studies

The effect of I3YT2YMAPA molecules on MS surface was studied with SEM analyses. SEM images of MS surfaces in the absence of medium, in the presence of corroding medium (0.5M H_2SO_4) and in the presence of corroding medium and inhibitor are given in Figures 3.48-3.50 respectively. On comparing Figures 3.48 and 3.49, it can be established that the surface of MS was seriously damaged in the acidic solution. Figure 3.50 represents the surface image of the metal in the presence of the I3YT2YMAPA molecules (0.1mM, 24 h). Morphology of this image clearly proved that the damage occurred for the surface was fairly reduced in presence of the inhibitor.

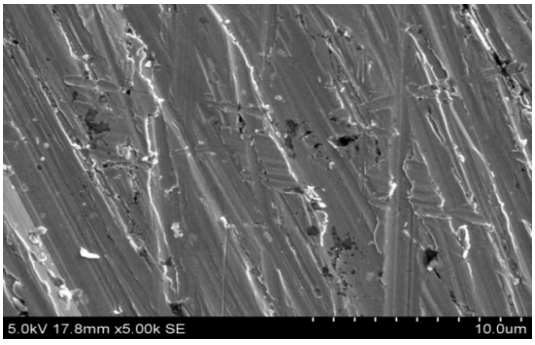

Fig. 3.48 SEM image of the bare MS

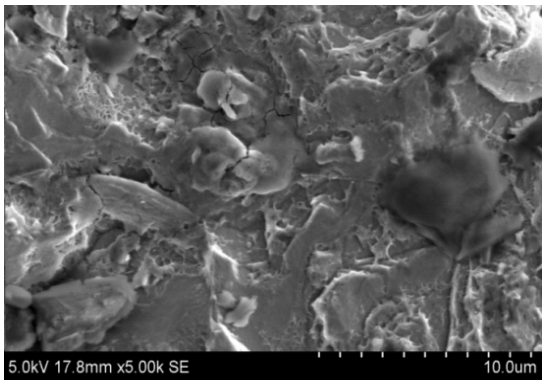

Fig. 3.49 SEM image of MS surface in 0.5M H_2SO_4 after 24 h

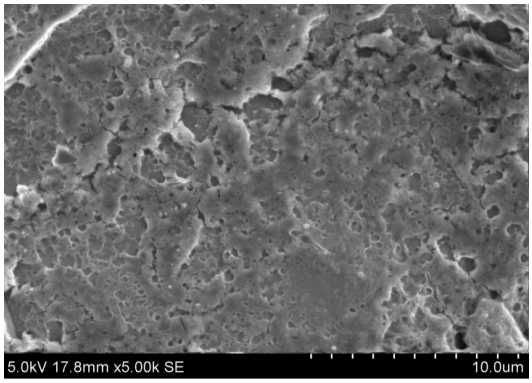

Fig. 3.50 SEM image of MS surface in 0.5M H_2SO_4 and I3YT2YMAPA after 24 h

Corrosion inhibition studies on parent compounds

Corrosion inhibition characteristics of the parent compounds of each Schiff base inhibitor were studied and compared. The results are given in table 3.11.

The parent compounds consists of 2-amino-3-(3-indolyl)propanoic acid (AIPA), 3-amino benzoic acid (ABA), thiocarbamoylhydrazide (TCH), phenyl hydrazine (PH), 4-(5-formylthiophen-2-yl)benzoic acid (FT2YBA) and 4-(5-formylfuran-2-yl)benzoic acid (FF2YBA). These compounds were taken in 0.2, 0.6 and 1.0mM concentrations in 0.5M H_2SO_4 and their inhibition efficiencies against MS corrosion for a period of 24 hours were studied using gravimetric method.

Table 3.11 Corrosion inhibition efficiencies (η_w%) of parent compounds AIPA, 3ABA, FT2YBA, FF2YBA, TCH and PH on MS surface in 0.5M H_2SO_4

C (mM)	AIPA	3ABA	FT2YBA	FF2YBA	TCH	PH
0.2	4.27	4.14	30.75	49.21	1.89	20.85
0.6	28.31	10.83	41.34	57.65	8.14	32.64
1.0	52.24	21.35	53.64	62.32	18.5	40.01

On comparison, it can be inferred that the higher inhibition performance of the Schiff base inhibitor were due to the presence of azomethine linkage in them. The amino acid, 2-amino-3-(3-indolyl)propanoic acid (AIPA) gave a highest 52% inhibition at 1.0mM concentration whereas the Schiff base inhibitor produced a much better result at the corresponding concentration i.e.; 77%. The parent amine ABA and TCH showed very little activity in sulphuric acid medium. The arylated compounds of thiophene-2-carboxaldehyde and furan-2-carboxaldehyde gave somewhat better efficiencies. The presence of aromatic rings in them might have improved their inhibition character.

Electrochemical studies on corrosion

Electrochemical methods involve impedance and potentiodynamic measurements in sulphuric acid medium. Electrochemical impedance measurements are quick when compared to the weight loss measurements.

The five novel Schiff base inhibitors were subjected to electrochemical corrosion inhibition studies on MS in 0.5M H_2SO_4 medium. EIS and Tafel polarization studies were performed to get a quick and reliable result on the inhibition capacities of the inhibitors on mild steel.

Electrochemical impedance spectroscopic (EIS) studies

The EIS experiments were carried out on an Ivium compact stat-e electrochemical system. 1M HCl was taken as the electrolyte and the working area of the metal specimens were exposed to the electrolyte for 1 h prior to the measurement. EIS measurements were performed at constant potential (OCP) in the frequency range from 1 KHz to 100 mHz with amplitude of 10 mV as excitation signal.The mild steel specimens were subjected to EIS measurements in sulphuric acid medium in the absence and presence of the inhibitors. Different concentrations of the Schiff base inhibitors were prepared and the

working electrode of the EIS system was made into contact with these solutions. Impedance plots, Nyquist plots (or Cole-Cole plot) and Bode plots were obtained in acid medium. The plots are given in Figures 3.51-3.55. The impedance parameters like charge transfer resistance (R_{ct}), solution resistance (R_s), double layer capacitance (C_{dl}) and percentage inhibition efficiency ($\eta_{EIS}\%$) calculated from the R_{ct} values are given in the Table 3.12. The percentage of inhibitions of each Schiff base were calculated using charge transfer resistance values by the following expression

$$\eta_{EIS}\ \% = \frac{R_{ct} - R'_{ct}}{R_{ct}} X100$$

where R_{ct} and R'_{ct} are the charge transfer resistances of working electrode with and without inhibitor respectively.

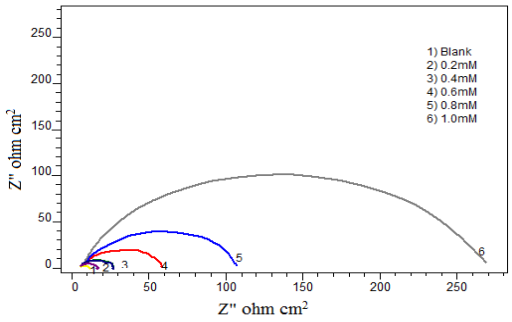

Fig. 3.51a Nyquist plots of MS in the presence and absence of I3YT2YMAPA in 0.5M H_2SO_4

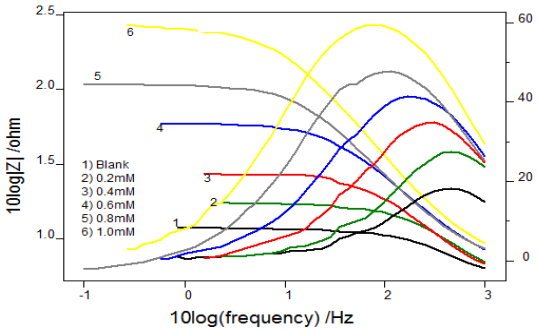

Fig. 3.51b Bode plots of MS in the presence and absence of I3YT2YMAPA in 0.5M H_2SO_4

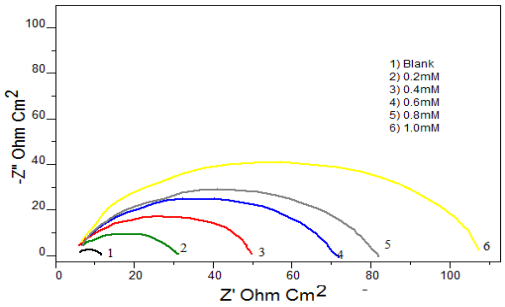

Fig. 3.52a Nyquist plots of MS in the presence and absence of T2YMABA in 0.5M H_2SO_4

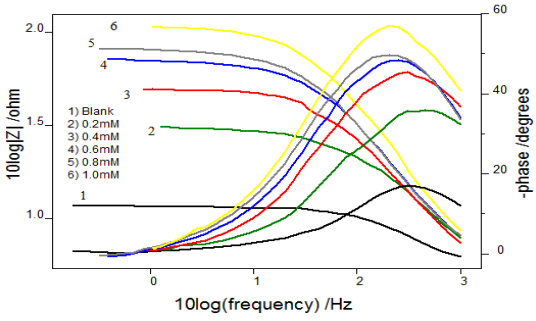

Fig. 3.52b Bode plots of MS in the presence and absence of T2YMABA in 0.5M H_2SO_4

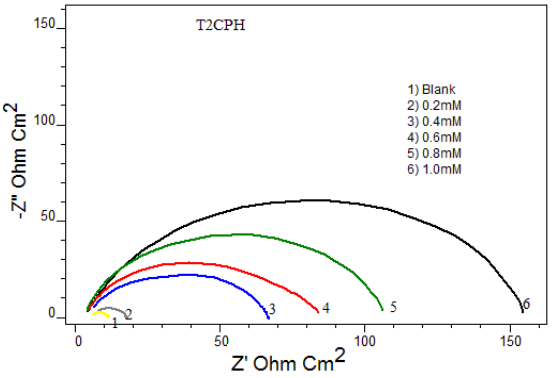

Fig. 3.53a Nyquist plots of MS in the presence and absence of PHMT2YBA in 0.5M H_2SO_4

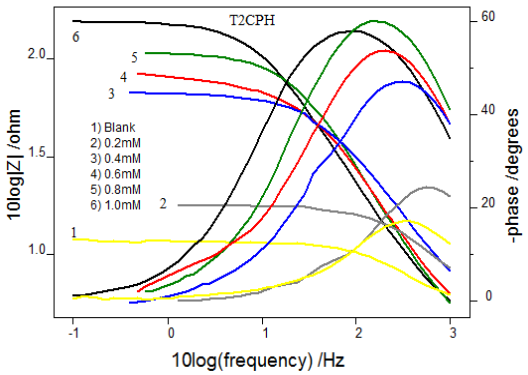

Fig. 3.53b Bode plots of MS in the presence and absence of PHMT2YBA in 0.5M H_2SO_4

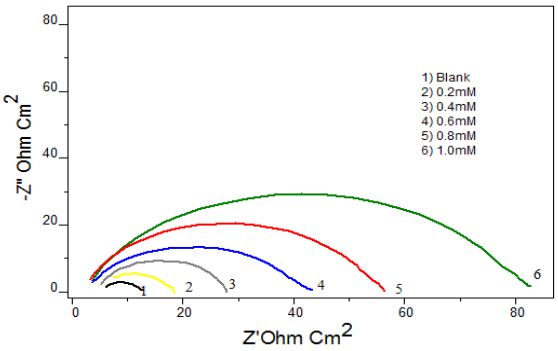

Fig. 3.54a Nyquist plots of MS in the presence and absence of CTHMT2YBA in 0.5M H_2SO_4

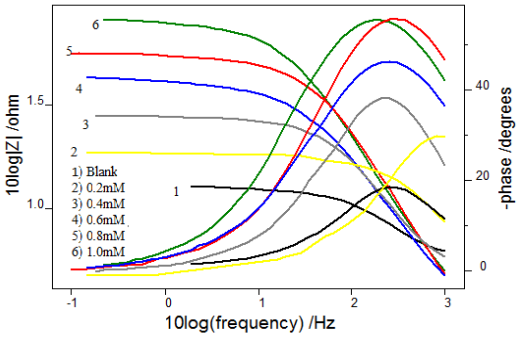

Fig. 3.54b Bode plots of MS in the presence and absence of CTHMT2YBA in 0.5M H_2SO_4

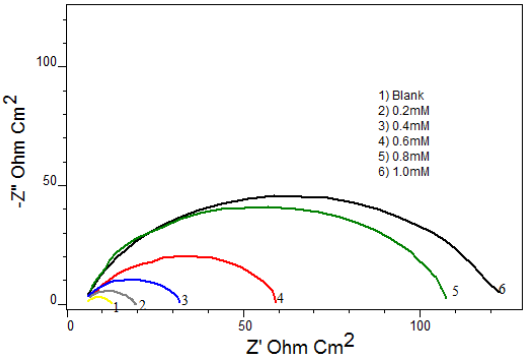

Fig. 3.55a Nyquist plots of MS in the presence and absence of CTHMF2YBA in 0.5M H_2SO_4

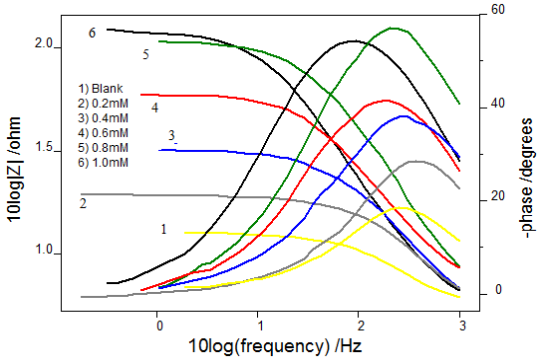

Fig. 3.55b Bode plots of MS in the presence and absence of CTHMF2YBA in 0.5M H_2SO_4

It is evident from the plots that the impedance response of metal specimens showed a marked difference in the presence and absence of the inhibitors. The Schiff base I3YT2YMAPA showed the highest R_{ct} value 232. R_{ct} is a measure of electron transfer across the exposed area of the metal surface and it is inversely proportional to rate of corrosion. This compound showed the highest inhibition efficiency of 97% at 1.0mM concentration. Inhibitors T2YMABA, PHMT2YBA, CTHMT2YBA and CTHMF2YBA also exhibited appreciable inhibition capacities against corrosion. PHMT2YBA showed significant inhibition efficiency (80%) even at the lowest concentration taken of 0.2mM. Generally the R_{ct} values were found to increase with increasing inhibitor concentration. Decrease in capacitance values CPE with inhibitor concentration can be attributed to the decrease in local dielectric constant and /or increase in the thickness of the electrical double layer. This emphasizes the action of inhibitor molecules by adsorption at the metal–solution interface. The percentage of inhibition (η_{EIS} %) showed a regular increase with increase in inhibitor concentration for all the Schiff base inhibitors and this trend is represented in Figure 3.56.

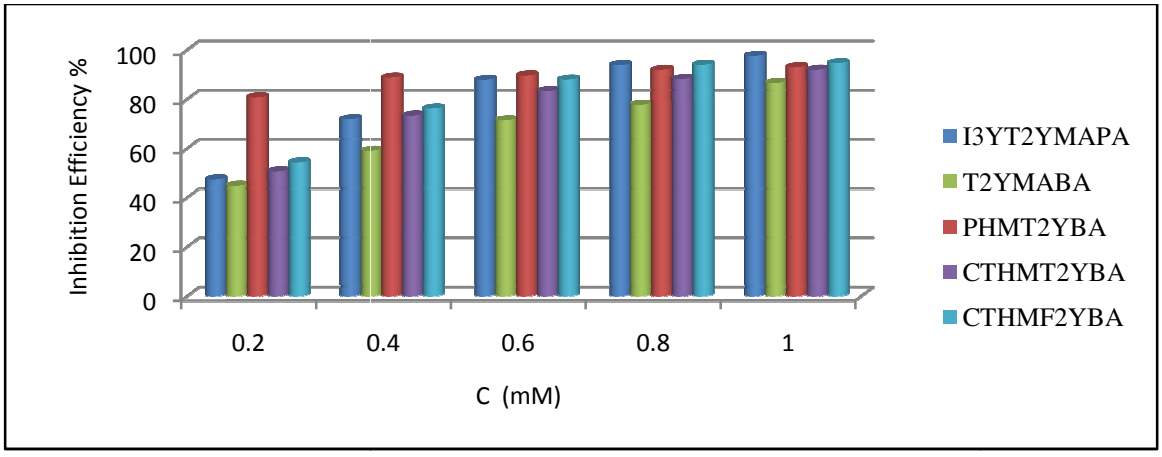

Fig.3.56 Comparison of corrosion inhibition efficiencies (η_{EIS}%) of Schiff base inhibitors I3YT2YMAPA, T2YMABA, PHMT2YBA, CTHMT2YBA and CTHMF2YBA on MS in 0.5M H_2SO_4

Table 3.12 Electrochemical impedance parameters of MS in the presence and absence of Schiff base inhibitors I3YT2YMAPA, T2YMABA, PHMT2YBA, CTHMT2YBA and CTHMF2YBA in 0.5 M H_2SO_4

Inhibitor	C (mM)	C_{dl}	R_{ct}	η_{EIS}%
	0	116	5.57	-
I3YT2YMAPA	0.2	89.8	10.6	47.45
	0.4	84.5	19.8	71.86
	0.6	77.2	46	87.89
	0.8	69.1	90	93.81
	1.0	70.1	232	97.59
T2YMABA	0.2	129	10.1	44.85
	0.4	107	13.6	59.04
	0.6	167	19.5	71.43
	0.8	123	25	77.72
	1.0	95	41.5	86.57
PHMT2YBA	0.2	79	28.9	80.73
	0.4	113	49.6	88.77
	0.6	63.7	53.8	89.64
	0.8	75.6	68.9	91.91
	1.0	69.6	79.6	93.00
CTHMT2YBA	0.2	42.9	11.3	50.71
	0.4	10.2	20.9	73.34
	0.6	12.3	33.3	83.27
	0.8	9.8	47.1	88.17
	1.0	7.7	69.2	91.95
CTHMF2YBA	0.2	82.7	12.2	54.34
	0.4	80.5	23.4	76.19
	0.6	76.6	46.3	87.96
	0.8	46.3	92.5	93.97
	1.0	10.2	104	94.64

The inhibition efficiencies resulted from EIS analysis are higher than that obtained from gravimetric studies and these results are not comparable. Since electrochemical analysis is a rapid corrosion monitoring technique it will only exhibit the corrosion inhibition capacities of molecules on MS at the early stage of treatment. The molecules will gradually hydrolyze into their parent compounds and thus show poor inhibition efficiency in H_2SO_4 medium for a long span of 24 hours. That's why gravimetric corrosion inhibition results are lower than the electrochemical results. Comparatively least efficiency was reported in the case of inhibitor T2YMABA. Even at the highest concentration (1mM) it has showed 86.57% inhibition efficiency. The order of performances of the studied Schiff base inhibitors on MS can be given as I3YT2YMAPA > CTHMF2YBA > PHMT2YBA > CTHMT2YBA > T2YMABA.

Potentiodynamic polarization studies

The behaviors of the present inhibitors towards polarization of metal specimens were studied by Tafel extrapolation analysis and linear polarization studies. Polarization studies were performed by recording anodic and cathodic polarization curves. Polarization plots were obtained in the electrode potential range from -100 to +100 mV Vs corrosion potential (E_{corr}) at a scan rate of 1mV/sec. Tafel polarization analysis were done by extrapolating anodic and cathodic curves to the potential axis to obtain corrosion current densities(I_{corr}). The percentage of inhibition efficiency (η_{pol}%) was evaluated from the measured I_{corr} values using the following relation

$$\eta_{pol}\,\% = \frac{I_{corr} - I'_{corr}}{I_{corr}} X100$$

where I_{corr} and I'_{corr} are the corrosion current densities of the exposed area of the working electrode in the absence and presence of inhibitor respectively. From the polarization

analyses, polarization parameters like corrosion current densities (I_{corr}), corrosion potential (E_{corr}), cathodic Tafel slope (b_c) and anodic Tafel slope (b_a) were determined and are listed in Table 3.13. Using these parameters percentage of inhibition efficiency ($\eta_{pol\%}$) for MS specimens was determined. From the slope analysis of the linear polarization curves at the vicinity of corrosion potential of blank as well as at different concentrations of the inhibitor, the values of polarization resistance (R_p) in acid solution were obtained. From the evaluated polarization resistance, the inhibition efficiency was calculated using the relationship

$$\eta_{R_p}\,\% = \frac{R'_p - R_p}{R'_p}\,X100$$

where R'_p and R_p are the polarization resistance in the presence and absence of the inhibitor respectively.

It is evident, from the Tafel parameters for the inhibition of various Schiff base inhibitors on metal surface, that the corrosion current density (I_{corr}) was decreased with increasing the inhibitor concentration. From linear polarization analysis it can be seen that the polarization resistance was considerably increased with the inhibitor concentration for all the studied inhibitors. This behavior can be attributed to the increase of adsorption of the molecules with concentration. The I3YT2YMAPA molecules showed a highest of 97.59% inhibition efficiency at 1.0mM concentration in the Tafel analysis. This was followed by compound CTHMF2YBA, which has got 94.85% efficiency at the highest concentration. Other Schiff bases also gave good inhibition performances; all of them showing >30 % inhibition capacity even at the lowest concentration (0.2mM). The Tafel curves and linear polarization curves are given in Figures 3.57-3.61.

Table 3.13 Potentiodynamic polarization parameters in the presence and absence of Schiff base inhibitors I3YT2YMAPA, T2YMABA, PHMT2YBA, CTHMT2YBA and CTHMF2YBA in 0.5M H_2SO_4

Inhibitor	Tafel data						Linear polarization data	
	C (mM)	$-E_{corr}$ (mV/SCE)	I_{corr} ($\mu A/cm^2$)	$-b_c$ (mV/dec)	b_a (mv/dec)	$\eta_{pol\%}$	R_p (ohm)	$\eta_{Rp\%}$
	0	472	1443	131	91	-	12.5	-
I3YT2YMAPA	0.2	471	733	112	66	49.20	21.08	40.70
	0.4	472	656	115	75	54.54	25.7	51.36
	0.6	418	359	117	69	75.12	46.48	73.11
	0.8	496	110	122	102	92.38	156.5	92.01
	1.0	463	34.7	86	36	97.59	274.3	95.44
T2YMABA	0.2	483	899	86	164	37.69	19	34.21
	0.4	460	571	62	108	60.43	30.18	58.58
	0.6	481	401	66	141	72.21	38.1	67.19
	0.8	482	367	72	123	74.57	42.56	70.63
	1.0	478	232	58	130	83.92	60.46	79.34
PHMT2YBA	0.2	520	850	112	90	41.09	48	73.96
	0.4	478	199	104	63	86.21	60	79.17
	0.6	501	359	117	69	75.12	86.5	85.55
	0.8	481	80.1	92	45	84.45	113.5	88.98
	1.0	498	122	90	84	91.55	115	89.13
CTHMT2YBA	0.2	527	484	100	80	66.46	32	60.94
	0.4	458	451	103	63	68.75	34	63.24
	0.6	473	320	107	69	77.82	48	73.95
	0.8	493	205	98	68	85.79	69	81.88
	1.0	478	158	103	71	89.05	94	86.70
CTHMF2YBA	0.2	-520	951	125	106	34.09	26.2	52.29
	0.4	478	231	130	58	83.99	75.2	83.38
	0.6	501	172	100	74	88.08	106.9	88.31
	0.8	481	141	97	79	90.23	133.5	90.64
	1.0	498	132	96	84	94.85	147	91.49

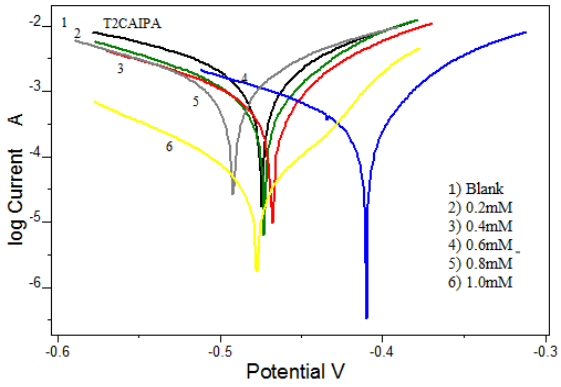

Fig. 3.57a Tafel plots of MS in the presence and absence of I3YT2YMAPA in 0.5M H_2SO_4

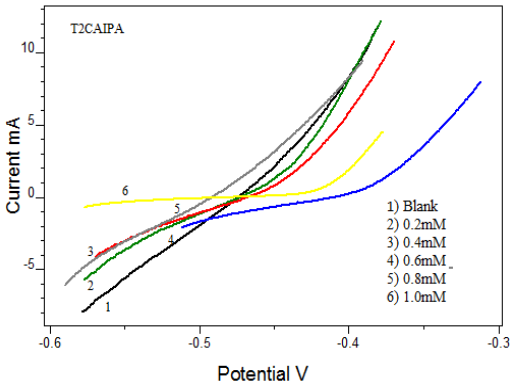

Fig. 3.57b Linear polarization curves of MS in the presence and absence of I3YT2YMAPA in 0.5M H_2SO_4

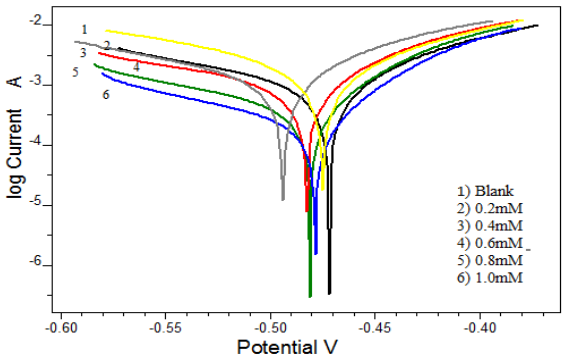

Fig. 3.58a Tafel plots of MS in the presence and absence of T2YMABA in 0.5M H_2SO_4

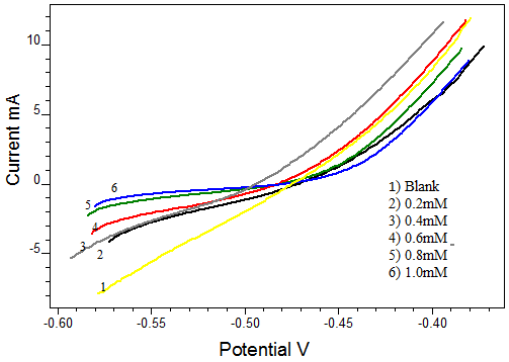

Fig. 3.58b Linear polarization curves of MS in the presence and absence of T2YMABA in 0.5M H_2SO_4

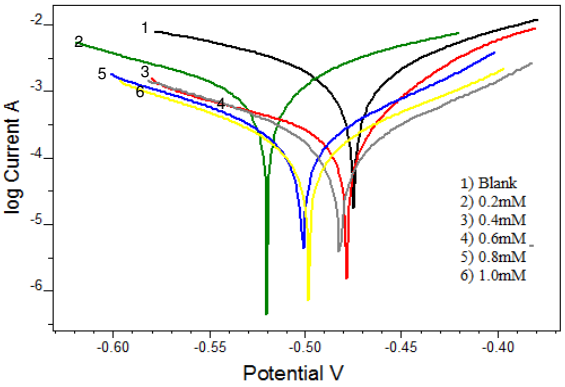

Fig. 3.59a Tafel plots of MS in the presence and absence of PHMT2YBA in 0.5M H_2SO_4

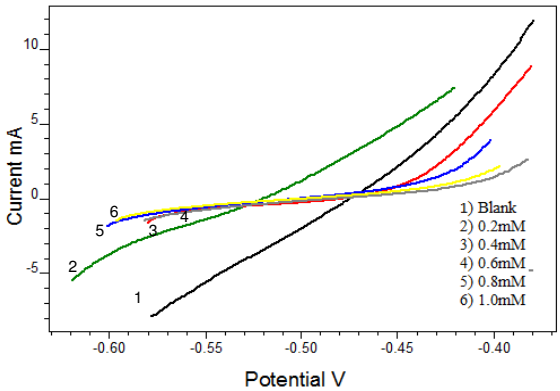

Fig. 3.59b Linear polarization curves of MS in the presence and absence of PHMT2YBA in 0.5M H_2SO_4

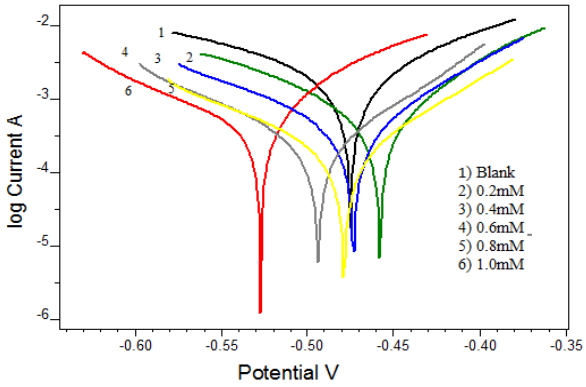

Fig. 3.60a Tafel plots of MS in the presence and absence of CTHMT2YBA in 0.5M H_2SO_4

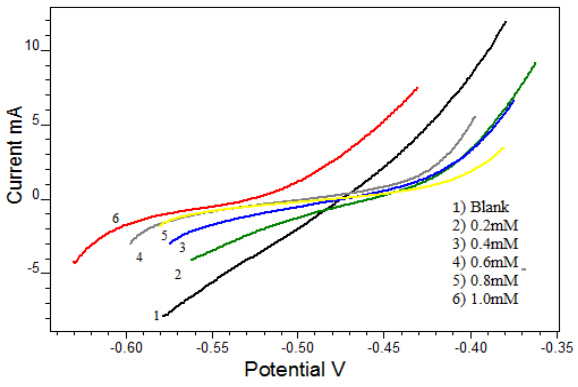

Fig. 3.60b Linear polarization curves of MS in the presence and absence of CTHMT2YBA in 0.5M H_2SO_4

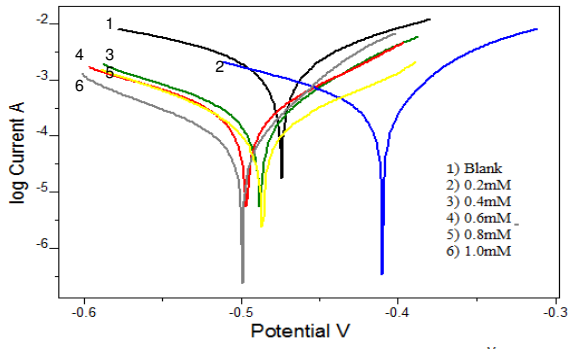

Fig. 3.61a Tafel plots of MS in the presence and absence of CTHMF2YBA in 0.5M H_2SO_4

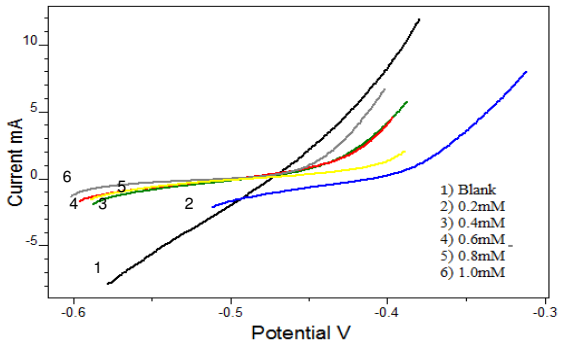

Fig. 3.61b Linear polarization curves of MS in the presence and absence of CTHMF2YBA in 0.5M H_2SO_4

Even though the inhibitors T2YMABA, PHMT2YBA and CTHMT2YBA showed very poor inhibitive capacity at 24h as per weight loss studies, their corrosion inhibition power according to the polarization studies were much higher than that expected. The presence of hetero atoms, aromatic rings and azomethine linkage present in the molecule would result in the enhanced the corrosion inhibition of these inhibitors. On close examination of the Tafel slopes, it is evident that these compounds namely I3YT2YMAPA, T2YMABA and PHMT2YBA showed much variations in cathodic and anodic slopes which suggest that they could affect the anodic and cathodic sites of corrosion and hence be called as mixed corrosion inhibitors. In the case of

CTHMT2YBA, the cathodic slope variation was not that much pronounced, compared with others and therefore this molecule can be regarded as a anodic inhibitor. Corrosion potential (E_{corr}) of MS specimens did not change appreciably during all the measurements. The corrosion inhibition efficiencies of Schiff base inhibitors are in the order I3YT2YMAPA > CTHMF2YBA > PHMT2YBA > CTHMT2YBA > T2YMABA which is same as the result of EIS measurements. A comparison of inhibition efficiencies are given in Figure 3.62.

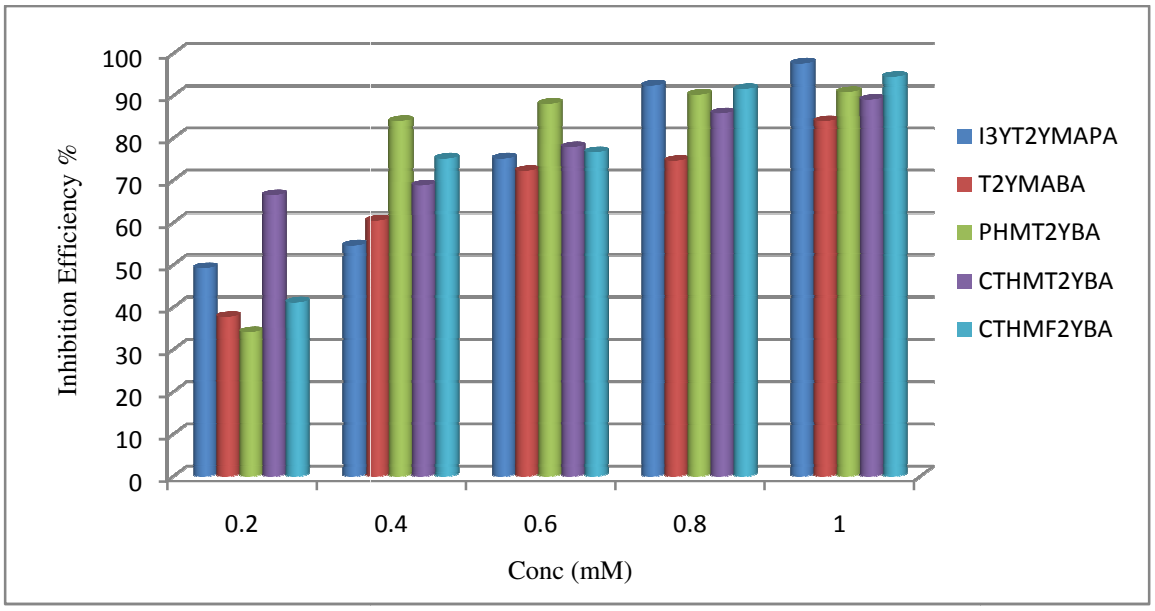

Fig. 3.62 Comparison of corrosion inhibition efficiencies (η_{pol}%) of Schiff base inhibitors I3YT2YMAPA, T2YMABA, PHMT2YBA, CTHMT2YBA and CTHMF2YBA on MS in 0.5M H_2SO_4

SUMMARY

The corrosion inhibition efficiencies of newly synthesized heterocyclic Schiff base inhibitors namely 3-(1H-indol-3-yl)-2-[(E)-(thiophen-2-ylmethylidene)amino] propanoic acid (I3YT2YMAPA), (E)-3-(thiophen-2-ylmethylene amino)benzoic acid (T2YMABA), (E)-4-(5-((2-carbamothioylhydrazono)methyl) thiophen-2-yl)benzoic acid (CTHMT2YBA), (E)-4-(5-((2-phenylhydrazono)methyl)thiophen-2-yl)benzoic acid (PHMT2YBA) and (E)-4-(5-((2-carbamothioylhydrazono)methyl)furan-2-yl)benzoic acid (CTHMF2YBA) against MS specimens in 1.0M HCl and 0.5M H_2SO_4 solutions were analysed using weight loss studies and electrochemical methods such as electrochemical impedance spectroscopy (EIS) and potentiodynamic polarization studies. It was found that all the inhibitors exhibited very good corrosion inhibition property on mild steel in HCl medium. Generally the corrosion inhibition efficiency was poor in H_2SO_4 medium than in HCl medium. Adsorption studies and surface morphological analysis were conducted to establish the mechanism of corrosion inhibition of these inhibitors.

According to the weight loss studies in HCl medium, the inhibition efficiencies were increased with the inhibitor concentrations for all the compounds. At a maximum concentration of 1.0mM, all the studied inhibitors displayed 70-83% inhibition efficiencies by the weight loss studies. At the electrochemical studies, they performed very potential anticorrosive activity (92-96%) towards MS at 1.0mM concentration. The compound I3YT2YMAPA exhibited the highest inhibition performance against mild steel (96.16%). The electron density of the aromatic ring systems, azomethine linkage and highly polarisable sulphur atom are the root causes by which the molecule showed better inhibition efficiency. Adsorption studies revealed that Freundlich isotherm was the

best fit isotherm for I3YT2YMAPA, PHMT2YBA, CTHMT2YBA and CTHMF2YBA molecules whereas Langmuir isotherm was followed by T2YMABA in 1.0M HCl medium. The values of themodynamic parameters suggested that adsorption process was spontaneous and the interaction between the metal and inhibitor molecules involves both electrostatic-adsorption and chemisorptions. The role of azomethine group in the inhibitory action was proved when the parent compounds of the Schiff base inhibitors were taken for corrosion studies. The activities were higher for the Schiff bases than the parent compounds. The corrosion inhibition performances of the compounds at elevated temperatures were also studied in HClmedium. Data obviously established that the rate of corrosion is increased at elevated temperatures.

The electrochemical studies on corrosion in HCl medium were performed and the order of inhibition capacity of bases was the same as that obtained from gravimetric studies, I3YT2YMAPA > PHMT2YBA > CTHMT2YBA > T2YMABA > CTHMF2YBA. Potentiodynamic polarization studies suggested that all inhibitors acted as a mixed type inhibitors for MS specimens in 1.0M HCl. Generally it is noticed that the inhibition efficiencies of these Schiff base inhibitors are quite higher by electrochemical studies than weight loss studies.

In 0.5M sulphuric acid medium, the gravimetric studies gave a different order of corrosion inhibition efficiency for the Schiff base inhibitors, i.e. I3YT2YMAPA > CTHMF2YBA > PHMT2YBA > CTHMT2YBA > T2YMABA. A maximum of 77.1% was obtained by I3YT2YMAPA at 1mM concentration. The inhibition efficiencies were lesser than that in HCl medium, which can be explained with the aggressive nature of the sulphuric acid. Weight loss measurements on both Schiff base inhibitors and their

corresponding parent compounds were performed and compared. Langmuir isotherm was the best fit one for I3YT2YMAPA and CTHMF2YBA and Freundlich isotherm for others. The ΔG^0_{ads}values for all the molecules suggested that the adsorption involved both physisorption and chemisorption.

Electrochemical impedance and potentiodynamic investigations in 0.5M H_2SO_4 gave higher corrosion inhibition efficiencies compared to gravimetric studies. Inhibition efficiency greater than 95% was expressed by I3YT2YMAPA in both experiments. I3YT2YMAPA, T2YMABA and PHMT2YBA showed much variations in cathodic and anodic slopes which suggest that these molecules could affect the anodic and cathodic sites of corrosion and can be called as mixed corrosion inhibitors. In the case of CTHMT2YBA, the cathodic slope variation was not that much pronounced when compared with others, and hence this molecule was regarded as an anodic inhibitor.

REFERENCES

1) S. R. Rao, "*Resource Recovery And Recycling From Metallurgical Wastes"*, Elsevier, (2006) 179.

2) L. David, Liptak, G. Bela, "*Environmental Engineers' Handbook"*, CRC Press, (1997) 973.

3) C.G. Munger, *"Corrosion Prevention By Protective Coatings"*, NACE (1999).

4) M. Behpour, S. M. Ghoreish, A. Gandomi, N. Niasar, N. Soltani, M. Niasari M, *J. Mater. Sci.*, 44 (2009) 2444.

5) H. Shorky, M. Yuasa, I Sekine , R.M. Issa, H.Y. El-Baradie, G.K. Gomma, *Corros. Sci*., 40 (1998) 2173.

6) S. Sankarap, F. Apavinasam, M. Pushpanaden, F. Ahmed, *Corros. Sci.*, 32 (1991) 193.

7) K. Yesim, G. Seda, E. Asli, *Prot. Met. Phys. Chem. Surf*., 48 (2012) 710.

8) A. Asan, S. Soylu, T. Kıyak, F. Yıldırım, S. G. Oztas, N. Ancın, M. Kabasakaloglu, *Corros. Sci*., 48 (2006) 3933.

9) E. Sputnik, Z. Ademovic, *Proceedings of the 8th European Symposium on Corrosion Inhibitors,* (1995) 257.

10) B.G. Clubby, *Chemical Inhibitors for Corrosion Control*, Royal Soc. Chem., Cambridge, (1990) 141.

11) M. Gojic, L. Kosec, *ISIJ Int.*, 37 (7) (1997) 685.

12) M. Metikos Hukovic, R. Babic, Z. Grubac, S. Brinic, *J. Appl. Electrochem.,* 24 (1994) 325.

13) L. Kobotiatis, N. Pebere, P.G. Koutsookos, *Corros. Sci,*. 41 (1999) 41.

14) V. Guillamuin, G. Mankowski, *Corros. Sci.,* 41 (1999) 421.

15) W. Quafsaoui, C.H. Blanc, N. Beberé, A. Srhiri, G. Mankowski, *J. Appl. Electrochem.,* 30 (2000) 959.

16) C. Blanc, S. Gastaud, G. Mankowski, *J. Electrochem. Soc.,* 150 (2003) 396.

17) A. Mozalev, A. Poznyok, I. Mazaleva, A.W. Hassel, *Electrochem. Com.,* 3 (2001) 299.

18) E. E. Ebenso, P. C. Okafor, U. J. Eppe, *Anticorr. Meth. Mat.,* 50 (6) (2003) 414.

19) I. N. Putilova, S. A. Balizin, V. P. Baranmik, *Metallic Corrosion Inhibitors*, Pergaman Press, London, (1960).

20) A. Raman, P. Labine, *Reviews on Corrosion Inhibitor Science and Technology*, NACE, Houston, TX, 1 (1986) 20.

21) M. Hosseini, S.F.L. Mertens, M. Ghorbani, M.R. Arshadi, *Mater. Chem. Phys*., 78 (2003) 800.

22) A. K. Singh, M. A. Quraishi, *Corros. Sci*., 52 (2010) 152.

23) A. K. Singh, M. A. Quraishi, E. E. Ebenso, *Int. J. Electrochem. Sci*., 6 (2011) 5673.

24) B. Joseph, S. John, A. Joseph, B. Narayana, *Indian J. Chem. Technol*., 17 (2010) 366.

25) P.C. Okafor, Y. Zheng*, Corros. Sci.,* 51 (2009) 850.

26) A.M. Shams El Din, A.A. El Hosary, R.M. Saleh, J.M. Abd El-Kader, Werkst. *Corrosion*, 28 (1977).

27) M.S. Abdel Aal, A.A. Abdel Wahab, A. El. Saied, *Corrosion (*NACE), 37 (1981) 557.

28) M.N. Desai, P.O. Chauhan, N.K. Shah, *7th Symposium on Corrosion Inhibitors, Ferrara, Italy (1990); 8th Symposium on Corrosion Inhibitors*, Ferrara, Italy (1995).

29) L. Wang, J.X. Pu, H.C. Luo*, Corros. Sci., 45* (2003) 677.

30) A. K. Singh, M. A. Quraishi, *Int. J. Electrochem. Sci*., 7 (2012) 3222.

31) M. T. Muniandy et. al., *Surf. Rev. Lett.,* 18 (2011)127.

32) M.D. Shah, A.S. Patel, G.V. Mudaliar, N.K. Shah, *Portugaliae Electrochim. Acta*, 29(2) (2011) 101.

33) S. P. Fakrudeen, H.C. Ananda Murthy, B. Raju, *J. Chilian Chem. Soc.,* 57, 4 (2012) 1364.

34) S. Thirugnanaselvi, S. Kuttirani, A. Roseline Emelda, *Science Direct*, 24 (6) (2014) 1969.

35) V. Panchal , A. Patel, N. Shah, *Scientific paper*, UDC :620.197.3 :669.715,

36) F. B. Ravar, A. Dadgarinezhad, *Gazi University J. Sci.*, 25(4) (2012) 835.

37) A. Sorkhabia, B. Shaabanib, D. Seifzadeha, *Appl. Surf. Sci*., 239 (2005) 154.

38) T. Sethi, A. Chaturvedi, R.K. Upadhyay, S. P. Mathur, *J. Chilean Chem. Soc.,* 52, 3 (2007) 1206.

39) R. K. Upadhyay, S. P. Mathur, *E-Journal of Chemistry*.net. 4(3) (2007) 408.

40) M. Yadav, D. Behera, S. Kumar, *Canadian Metallurgical Quarterly*, 53(2) (2014) 220.

41) A. A. Al-Amiery, A. A. H. Kadhum, A. Hameed M. A., Abu Bakar Mohamad,H. Pua Soh, Materials, 7 (2014) 662.

42) Jeyaprabha, S. Muralidharan, D. Jayaperumal, G. Venkatachari, N.S. Rengaswamy *Antcorr. Meth. Mat.,* 45(3) (1998) 148.

43) X. Li, S. Deng, H. Fu, T. Li, *Electrochim. Acta*, 54 (2009) 4089.

44) E. Kamis, *Corrosion,* 46 (1990) 478.

45) S. S. Abd El-Rehim, A. Magdy, M. Ibrahim, F. Khaled, *J. Appl. Electrochem.*, 29 (1999) 599.

46) E. McCafferty, H. Leidheiser Jr., "*Corrosion Control By Coating"*, Science Press, Princeton, (1979).

47) E. Cano, J.L. Polo, A. La Iglesia, J.M. Bastidas, *Adsorption*, 3 (2004) 219.

48) M. Bouklah, N. Benchat, B. Hammouti, A. Aouniti, S. Kertit, *Mater. Lett.*, 60 (2006) 1901.

49) J. O'M. Bockris, A. K. N. Reddy, "*Modern Electrochemistry-2*", Plenum Press, New York, (1970).

50) E. Gileadi, *"Electrode Kinetics For Chemists, Chemical Engineers And Material Scientists*", VCH publishers, New York (1993).

51) D. A. Jones, "*Principles and Prevention of Corrosion*", Macmillam publishing, New York, (1992).

52) R. Baboian, "*Electrochemical Techniques for Corrosion*", National association of corrosion engineers, Houston, TX (1977).

53) U. Bertocci, F. Mansfeld, "*Electrochemical Corrosion Testing*", ASTM STP 727, ASTM international, West Conshohocken, PA (1979).

54) H. H. Uhlig, R. W. Revie, "*Corrosion And Corrosion Control*", John Wiely & Sons, New York, (1985).

55) E. Barsoukov, J. R. Macdonald, *"Impedance Spectroscopy, Theory, Experiment and Applications",* Wiley Interscience publications, New York, 2nd Ed., (2005).

56) F. Mansfield, *Electrochim. Acta,* 35 (1990) 1533.

57) M. Kendig, J. Scully, *J. Electrochem. Soc.,* 141 (1994) 1823

58) F. Mansfeld, M. Kendig, *"Evaluvation of Protective Coatings with Impedance measurements",* International Congress on Metallic corrosion, 3 (1984) 74.

59) G. Reinhard, U. Rammelt. *Corrosion,* 15 (1984) 175.

60) T. Strivens, C.Taylor, *Mater. Chem.,* 7 (1982) 199.

61) F. Mansfeld, M.W. Kendig, *Corrosion,* 37(9) (1981) 545.

62) D. D. MacDonald, *"Transient Techniques in Electrochemistry"*, Plenum press. New York, (1977).

63) A. Raman, P. Labine "*Reviews on Corrosion Inhibitor Science and Technology",* NACE, Houston, TX , 1 (1986).

64) T. Badea, M. Nicola, I. D. Vaireanu, I. Maior, A. Cojocaru, *"Electrochimie si Coroziune, Matrixrom, Bucuresti"*, (2005) 150.

65) M. G. Fontana, N. D. Greene, *"Corrosion Engineering"*, McGraw-Hill, New York, (1978).

66) M. Stern, A. L. Geary, *J. Electrochem. Soc.*, 105 (1958) 638.

67) E. Cano, J. L. Polo, A. La Iglesia, J. M. Bastidas, *Adsorption,* 10(3) (2004) 219.

68) P. Bommersbach, C. Alemany-Dumont, J. P. Millet, B. Normand, *Electrochem. Acta*, 51(6) (2005) 1076.

69) I. L. Rosenfield, "*Corrosion Inhibitors",* McGraw-Hill, New York, (1981) 66.

70) M. El Azhar, B. Mernari, M. Traisnel, F. Bentiss, M. Lagrenee, *Corros. Sci.*, 43(12) (2001) 2229.

71) D. P. Schweinsberg, G.A. George, A. K. Nanayakkara, D. A. Steinert, *Corros. Sci.,* 28(1) (1988) 33.

72) H. Shokry, M. Yuasa, I. Sekine, R. M Issa, H. Y. El-baradie, G. K Gomma, *Corros. Sci.*, 40(12) (1998) 2173.

73) A. K. Singh, M. A. Quraishi, *J. Appl. Electrochem.*, 40(7) (2010) 1293.

Part IV
Antitumour studies

Chapter 1

Nimmy Kuriakose “Physicochemical, thermoanalytical, electrochemical and antitumour studies of transition metal complexes of schiff bases derived from heterocyclic carbonyl compounds” Thesis. Department of Chemistry, St. Thomas College, University of Calicut, 2015

CHAPTER 1

INTRODUCTION AND REVIEW

Tumour has a reputation as a deadly disease. A tumour, also known as a neoplasm, is an abnormal mass of tissue which may be solid or fluid-filled. It is a subject of widespread fear since millions of new cases of tumour were reported globally for the last few years. It is reported that about 8.2 million deaths or 14.6% of all human deaths are due to tumour[1,2]. Depending on the shape and the kind of tissue that tumours affect, there are over 100 different types of tumours and a variety of names for them. A tumour is a kind of lump or swelling, it does not necessarily pose a health threat. Nearly fifty percentage of cancer patients die due to the disease or because of the treatment strategies[3]. It is a great matter of concern that the most common types of tumour at present are not easy to treat except which arise from the modern lifestyle. The prognosis of the cancer is quite difficult once it is malignant in the body.

A tumour does not mean cancer ; tumours can be benign (not cancerous), pre-malignant (pre-cancerous) or malignant (cancerous). Tumour sizes may vary enormously. In January 2012, Nguyen Duy Hai, a 32-year-old Vietnamese man underwent a 12-hour operation to remove a 200-pound tumour from his leg. The success of the operation was rated only 50% by lead surgeon Dr. McKay McKinnon. Cancers of lung, prostate, stomach and colorectal are the common types in males whereas in females, the common types of cancers are the cervical, breast and lung[4]. Skin cancer is not included in these statistics and if it were it would account for at least 40% of cases[5,6]. Generally seen cancers in children are brain tumour and leukaemia[7]. Statistics indicate that the risk of cancer is increasing significantly. The increase in life span and changes in lifestyle have

major role in increasing the number of people affected with tumour. The fact that the probability of a secondary cancer is high in people who recovered from cancer primarily[8,9].

History of cancer

Lung cancer

Cancer is known since the early stages of human history. The report of a breast cancer from circa in 1600 BC is considered as the first record of cancer[10-14]. Different types of cancers were described by Hippocrates who gave the Greek name *karkinos* (crab)[15,16]. It was Celsus who changed the *karkinos* into *cancer* (Latin word) meaning crab. He also proposed the treatment style of surgery for cancer[17]. In the second century Galen suggested purgatives as an alternative to surgery[18].

By 17th century, the doctors were able to discover the cause of death by analyzing the body[19]. Wilhelm Fabry reported that milk clot in the mammary duct caused breast cancer. Francois de la Boe Sylvius postulated that acidic lymph fluid was responsible for cancer development. In 1761, the physician John Hill found that the cause of nose cancer is tobacco snuff. Later it is published that cancer of the scrotum, commonly seen in chimney cleaners are due to the smoke dust in the chimney. In1874, the English surgeon Campbell De Morgan formulated that cancer spreads through the lymph nodes to other sites by metastasis[20].

Classifications of cancer

Cancer is broadly classified into five classes:

1. Sarcomas: affects bone, cartilage, fat, connective tissues, muscles and other supportive tissues.
2. Lymphomas: affects lymph nodes and immune system tissues.
3. Carcinomas: affects internal and external parts of the body such as lung, breast and colon.
4. Leukemias: begin in the bone marrow and accumulate in the blood stream.
5. Adenomas: affects thyroid, the pituitary gland, the adrenal gland and other glandular tissues.

Carcinogens

Carcinogens are substances, exposure to which causes specific types of cancer. Some of the main carcinogens are described below:

Chemicals

Tobacco smoke: One third of the cancer death is due to tobacco smoking. Cancers of lung, larynx, stomach and pancreas are caused due to tobacco smoking. Literature shows that more than fifty types of carcinogens are present in tobacco smoke.

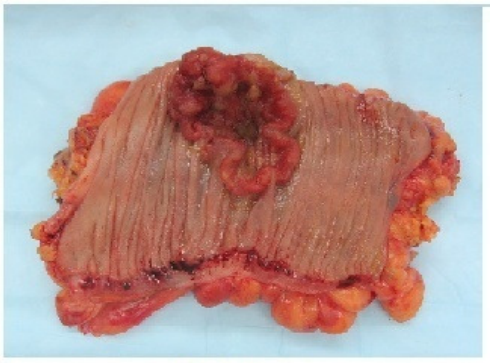

Colon cancer

Alcohol: In Europe both males and females suffer from cancer because of alcohol consumption. Tumours of the liver and digestive tract are reported in people with alcohol addiction.

Chemicals at work site: It is reported that around two lakh people are affected with cancer from their worksite. Exposure to asbestos fibers and tobacco smoke causes mesothelioma and lung cancer. Frequent contact with benzene can result in leukemia[21].

Radiations

Radiations can cause tumour in any part of the body irrespective of the age. Ionizing radiations and non-ionizing ultraviolet radiations cause almost 10% of invasive cancers. Medical imaging and radon gas is one of the main sources of ionizing radiations. UV radiations from the sun are responsible for non-melanoma cancer. Long time exposure to radon can result in increased risk of cancer. Ionizing radiations are not a strong mutagen, but together with tobacco or radon they become a more potent source of cancer. Radiation exposure before birth has ten times the effect. Leukemia may be developed in children and adolescents as in adults on radiation exposure.

Prolonged exposure to radiations from the sun, especially the non-ionizing medium wave UVB, can lead to melanoma skin cancer which is one of the most common type of cancer. Radiations from mobile phones and similar sources are also regarded as cancer causing agents by World Health Organization.

Diet and exercise

Lack of proper diet and exercise are considered as the major cause of more than thirty percentage of cancer deaths. Obesity and excess body weight can cause different types of tumours, resulting about 20% deaths due to cancer. Physical inactivity may have negative effects on immune system and endocrine system and can contribute to cancer development.

Some specific foods are linked to specific cancers. Aflatoxin B1, a frequent food contaminate, can result in liver cancer and Betel nut chewing causes oral cancer. A high-salt diet is linked to gastric cancer.

Heredity

Genetic defects are responsible for the hereditary tumours. Majority of ovarian cancer and breast cancer are due to genetic disorder. More than 75% risk of breast cancer and ovarian cancer can be resulted from them. It is found that in about 3% of people suffering from colorectal cancer, hereditary nonpolyposis colorectal cancer (HNPCC or Lynch syndrome) is also associated.

Infection

Approximately 18% of cancer deaths are related to infectious diseases. Cancer causing viruses are known as *oncovirus*. Examples are Epstein–Barr virus, human papilloma virus, hepatitis B and C viruses, Human T-cell leukemia virus-1 and Kaposi's sarcoma herpes virus. Cancers like gastric carcinoma are caused by bacteria. Infections by parasites are also responsible for cancer.

Physical agents

These are substances that can cause cancer on prolonged exposure. For example, asbestos can cause mesothelomia in serous-membrane. Particulate matter which are non fibrous in nature, like crystalline silica, cobalt and nickel powders are also carcinogenic. Attapulgite, rock wool, wollastonite and glass wool are also responsible for cancer.

Hormones

Some hormones can promote proliferation of cell. Differentiation, proliferation and apoptosis of cancer cells can be due to Insulin like hormones and the attached

protein. Some hormones can produce tumour in endometrium, breast and prostate. Obese people have higher levels of some hormones and are associated with cancer. Growth hormones can also promote osteosarcoma. Up to a certain extent the excessive hormone levels can be reduced by regular and systematic exercises by which the risk of cancer can be minimized. These hormone levels can be reduced artificially by some specific treatments.

Pathophysiology

Repeated mutations in DNA can result in development of tumour. Each mutation can alter the nature of the cell. Cancer is due to the uncontrolled cell growth which is the result of changes in genes. Mutations will result in two types of genes, oncogenes and tumour suppressor genes. The first one promotes tissue growth and and the second one suppresses cell division. Tumours are the result of inappropriate performance of oncogenes or tumour suppressor genes. Errors during mitosis can result in complete destruction of chromosomes. Genetic deformations are possible by a number of mechanisms.

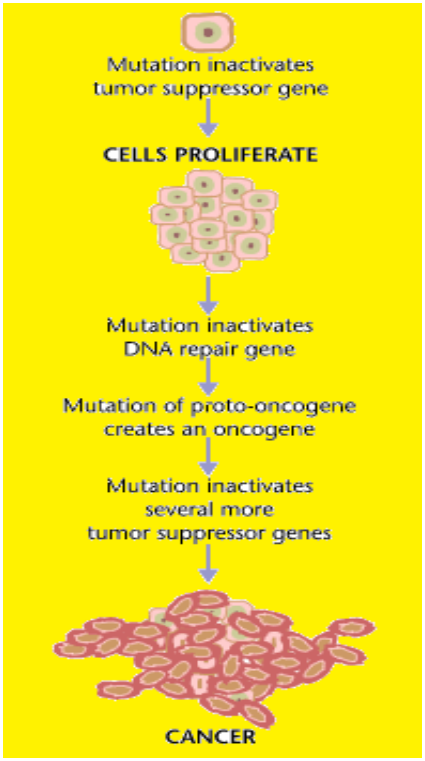

Moreover the presence of certain environments like ionising radiations, carcinogens or hypoxia can case genetic deformations. The defects are self multiplying, resulting in excess reproduction of the cells compared to normal cells.

The conversion of normal cell into a cancer cell is similar to an uncontrolled chain reaction. These

chain processes may result in more invasive stages and thereby develop the cancer in a faster rate[22].

Epigenetics

Epigenetic changes also can cause cancer[23]. Modifications in the genome without alteration in nucleotides are termed epigenetic alterations. Even though there are many types of epigenetic changes related to cancer, those changes in DNA repair genes are mainly responsible for cancer.

Epigenetic alterations occur frequently in cancers and will result in alteration in hyper or hypomethylation of DNA or chromosomal changes[24,25]. The poor performance of DNA repairing genes will allow permanent changes in DNA. When DNA repair is deficient DNA damages remain in cells at a higher level than usual level and these excess damages cause increased mutation or epimutation[26-29]. It is found that many heavy metals also are carcinogenic and they can reduce the activity of DNA repair genes.

Metastasis

Metastasis is the spread of cancer to other parts of the body. It was found that all types of cancers has the ability to metastasize. It is the most devastating aspect of cancer and it is often resistant to conventional treatment methods. The newly formed tumour cells are known as metastatic tumours, which will ultimately result in death of the organism[30]. In the late stages of cancer metastasis becomes prominent either through blood or lymphatic system[31-33]. Metastasis is very common in liver, bones and brain. The various steps in metastasis include invasion, intravasation, extravasation, proliferation and angiogenesis[34].

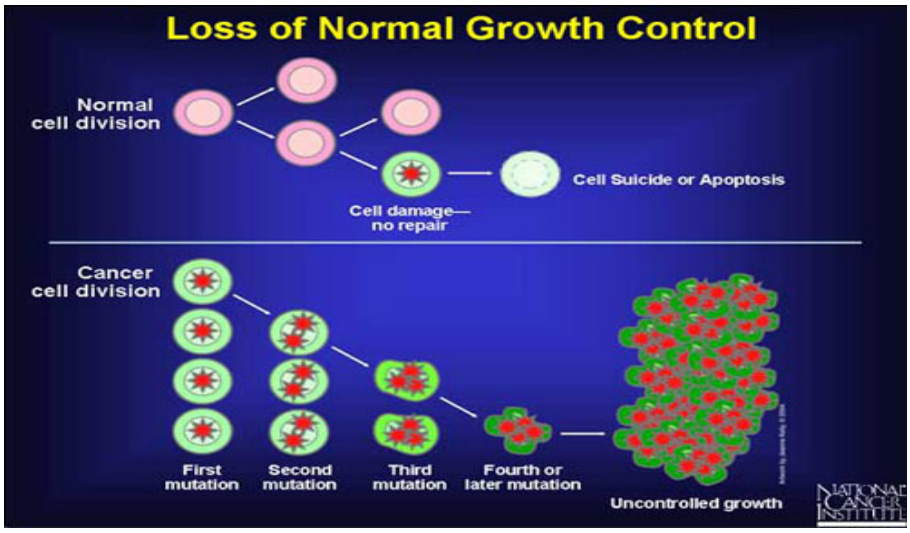

Anticancer drugs

The anticancer drugs either kill cancer cells or modify their growth. They are used along with treatments like radiotherapy, immunotherapy and surgery, against solid metastatic tumours. The mechanism of action of each anticancer drug is different on normal and tumour cells. The efficiency of anticancer drugs is based on their toxicity on normal cells, since there is biochemical similarity between cancer cells and normal cells. The fact that cancer cells can develop resistance against a specific drug, suggested the possibility of using combinations of various drugs during the treatment.

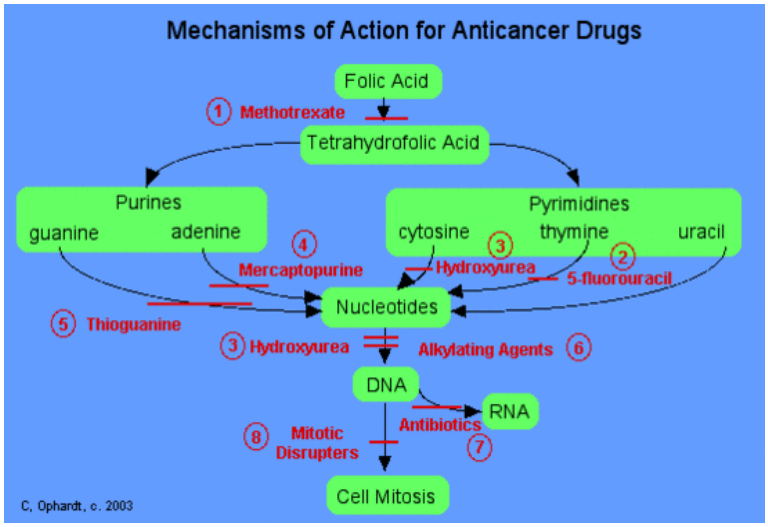

Classification of anticancer drugs

1. Alkylating agents
    - Platinum coordination complexes: Cisplatin, Carboplatin, Oxaliplatin
    - Nitrogen mustards: Melphalan, Ifosfamide, Cyclophosphamide,
    - Nitrosoureas
    - Triazene
    - Alkylsulfonates
    - Ethyleneimines
    - Methyl hydrazines
2. Antimetabolites
    - Folate antagonists: Methotrexate
    - Pyrimidine antagonists: 5-Fluorouracil, Cytarabibe
    - Purine antagonists
3. Natural products
    a. Plant products
        - Taxanes: Paclitaxel, Docetaxel
        - Vinca alkaloids: Vincristine, Vinblastine
        - Epipodophyllotoxins: Etoposide
        - Camptothecins: Irinotecan

    b. Microorganism products
        - Enzymes: L-Asparaginase

          Antibiotics: Bleomycin, Doxorubicin,

4. Miscellaneous
    - Imatinib mesylate
    - Epirubicin
    - Hydroxy urea
    - Bortezomib
    - Gemcitabine
    - Leucovorin
    - Zoledronic acid
    - Geftinib

- Rituximab
- Pamidronate

5. Hormones and Antagonists

- Estrogens: Ethinyloestradiol
- Androgen: Testosterone propionate
- Corticosteroids: Dexamethasone, Prednisone
- Aromatase inhibitor: Anastrazole, Letrozole
- Antiestrogens: Tamoxifen
- Progesteron derivative: Megestrol Acetate
- Antiandrogen: Bicalutamide, Flutamide

Coordination complexes as antitumour drugs – a review

The therapeutic use of transition metal complexes in cancer and leukemia treatment date from the sixteenth century. In 1960 the anti-tumour activity of an inorganic complex cis-diamminedichloroplatinum(II) (cisplatin) was discovered. It has developed into one of the most frequently used and most effective cytostatic drug for treatment of solid carcinomas. Other metals like gallium, germanium, tin, bismuth, titanium, ruthenium, rhodium, iridium, molybdenum, copper and gold were shown effective against tumors in man and animals[35]. Research on other metals mainly transition metals as anticancer drugs have proved the dominance of these metals by low cost, increased coordination sites, changes in oxidation states, changes in ligand affinity and the substitute kinetics, as well as the excited light-emiting properties that can be used for treatment and so on. Those related coordination compounds vary in composition and

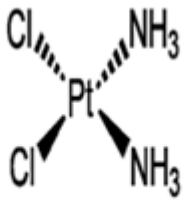

Fig. 4.1 Structure of cisplatin

structure, including amino acid complexes, heterocyclic complexes, Schiff base complexes, dicyclopentadienyl coordination compounds, binuclear complexes and so on.

Cisplatin or *cis*-diamminedichloroplatinum(II) (Figure 4.1) is the first member of a class of platinum containing anti-cancer drugs, which also includes carboplatin and oxaliplatin. These platinum complexes react *in vivo*, binding to and causing cross-linking of DNA, which ultimately triggers apoptosis[36]. Cisplatin moves into the cell through diffusion and active transport. The compound *cis*-$[Pt(NH_3)_2(Cl)_2]$ was first described by Michele Peyrone in 1845 and known for a long time as Peyrone's salt. Inside the cell it causes platination of DNA, which involves cross-linking as well as formation of adducts, usually through guanine. Formation of cisplatin DNA adducts causes distortion and results in inhibition of DNA replication.

Gold complexes also show anti-cancer activity. These complexes act through a different mechanism as compared to cisplatin[37]. The target site of Au complexes is mitochondria not DNA. Certain gold complexes with aromatic bipyridyl ligands have shown cytotoxicity against cancer cells. The 2-[(dimethylamino)methyl]phenyl gold(III) complex has also proven to be antitumor agent against human cancers. Gold nano particles when used in combination with radiotherapy or chemotherapy enhance DNA damage and make the treatment target more specific[38].

Ansari et. al.[39] in 2009 studied some complexes of Mn(III) induce tumor selective apoptosis of human cells. Some oxindole-Schiff base copper(II) complexes were analysed by Ramadoss Gomathi et. al.[40] to explore the potential antitumor activity towards different cells. Cytotoxicity experiments carried out towards human liver HepG2

cells confirmed its proapoptosis property and the copper complexes were found to have excellent anticancer activity against HepG2 liver cells.

Several Schiff bases and their complexes were reported to possess potential anticancer properties. Shahriar Ghammamy et. al.[41] synthesized complexes such as [Fe(pythsal Br)]Cl_2 with the NSNO-donor tetradentate Schiff base ligands. The ligand pythsal HX [(5-X-N-(2-Pyridylethyl sufanylethyl)salicylidenemine] (X=I, Br) was obtained from the inserted condensation of (1,2-pyridyl)-3-thia-5-aminopentane with the respective derivative of salicyladehyde in a 1:1 molar ratio and their iron (III) complexes were studied for their antitumor properties.

Kuzmin et. al. [42] reported that a series of macrocyclic Schiff bases of 2,6-bis (formyl aryloxymethyl)pyridines were synthesized and studied their anticancer activity relationship by the topological approach. The anticancer activity and structural parameters of the molecules were correlated and on the basis of *in vitro* screening data their structures were characterized. The influence of structure of the studied compounds, as reflected by the parameters studied on the anticancer activity, was established.

Gupta et. al.[43] in 2011 synthesized new ligands, N-benzyl-2-(diethylamino) acetamide, (HL_1) and 2-(diethylamino)-N-phenylethylacetamide(HL_2) and these ligands have been used to synthesize copper(II) complexes $[Cu(HL_1)_2(ClO_4)_2]$ and $[Cu(HL_2)_2(ClO_4)_2]$ respectively. Antitumour screening of these complexes against the U87 and HeLa cancerous cells revealed excellent activity. The complexes were effective for growth inhibition and cell death in a concentration and time dependent manner for both U87 and HeLa cell lines. The anticancer activity might be due to the formation of DNA adducts with cancer cell and thereby inhibiting the DNA replication.

1,2-pyrazole derivatives were found to possess various biological activities by Mathew V. et. al.[44]. It was also observed that incorporation of aryl substituent and halogen atoms into the heterocyclic ring systems enhanced the biological activities considerably. Non-steroidal aromatase inhibitors obtained from triazole derivatives are used in the treatment of breast cancer[45].

Studies have shown that amino acid Schiff bases and their metal complexes have anticancer as well as antiviral activities and could also inhibit superoxide anion radicals [46]. In 1971, Hodnet et. al.[47] synthesized a series of Schiff base metal complexes and carried out antitumor experiments, which indicated that aldehyde substituent was superior to amine substituent in anticancer effect and salicylaldehyde Schiff bases were superior to other aldehyde Schiff bases. To overcome the toxicity and poor water-solubility of amino acid Schif bases, either Schiff bases can be sulphonated or hydrophilic groups might be introduced in the parent compound, or a second ligand might be introduced hoping to improve its activity.

A number of Schiff base copper(II) complexes are regarded as the most promising alternatives to cisplatin as anticancer drugs. In particular, the involvement of copper in human diseases has been described from medicinal, chemical and biochemical view, focusing on the molecular physiology of Cu transport.

Hernández W. et. al.[48] studied the antitumor activity of the copper(II) complexes with acylthiourea ligands. The *in vitro* activity studies against the mouse mammary adenocarcinoma TA3 cell line showed that these complexes have much higher cytotoxic activity (IC(50) values in the range of 3.9-6.9muM) than their corresponding ligands (40-240muM). This clearly indicates that the antitumor activity is increased on coordination

of the chelate ligands around the Cu(II) metal. Furthermore, this result confirmed that the involvement of the nitro and chloro substituent groups in the complex activities is slightly relevant. The high accumulation of the copper complexes in TA3 tumour cells and the much faster binding to cellular DNA were consistent with the *in vitro* cytotoxic activities found for these copper complexes.

Three new copper complexes were synthesized with pyridoxal semicarbazone as ligand by Violeta Jevtovic[49] and were subjected to anticancer tests. Specifically, an activity was demonstrated in breast cancer cells. Birjesh Singh[50] synthesized a Cu(II) complex with 6-thioguanine and C-57BL/6 mice has been used for anticancer screening of metal complex for *in vitro* and *in vivo* study. The results revealed that the complex is more potent as compared to the pure drug as regards to its anticancer activity.

Investigations of D. Palanimuthu et. al.[51] says that copper complexes of thiosemicarbazides especially those derived from glyoxal-bis(4-methyl-4-phenyl-3-thiosemicarbazone) have great cytotoxic activity against various human cancer cells, almost same as that adriamycin drug. The corresponding zinc complex showed much less activity than the copper complex. It was found that the Cu complexes were able to inhibit the DNA synthesis and can produce apoptosis. DNA cleavage was found to occur because of these complexes. It is found that *in vivo* administration of copper complex significantly inhibited the tumour growth in HCT116 xenografts in nude mice.

Unfortunately, the majority of drugs currently on the market are not specific, which leads to many common side effects associated with cancer chemotherapy. Because the common approach of all chemotherapy is to decrease the growth rate of the cancer

cells, the side effects are seen in bodily systems that naturally have a rapid turnover of cells including skin, hair, gastrointestinal and bone marrow.

Scope of present investigation

Copper(II) complexes are regarded as the most promising alternatives to cisplatin and other anticancer drugs. A number of Cu(II) chelate complexes that exhibit cytotoxic activity through cell apoptosis or enzyme inhibition have been reviewed. Such complexes can significantly increase the survival of the hosts. Current interest in copper complexes is stemming from their potential use as antitumor agents. The special structure and ligand diversity determine the chemical and biological significance of these Schiff base complexes.

In the present work, some new copper(II) complexes were prepared with different Schiff base ligands like 3-(1H-indol-3-yl)-2-[(thiophen-2-ylmethylidene)amino] propanoic acid (I3YT2YMAPA), 3-[thiophen-2-ylmethyleneamino]benzoic acid (T2YMABA), 4-(5-[(2-carbamothioylhydrazono)methyl]thiophen-2-yl)benzoic acid (CTHMT2YBA), 4-(5-[(2-phenylhydrazono)methyl]thiophen-2-yl)benzoic acid (PHMT2YBA), 4-(5-[(2-carbamothioylhydrazono)methyl]furan-2-yl)benzoic acid (CTHMF2YBA), 2-(1-[pyridin-3-yl]ethylidene)hydrazinecarbothioamide (P3YEHCTA), 3-(1-(2-phenylhydrazono)ethyl)pyridine (PHEP), 3-[anthracen-9(10H)-ylideneamino] propanoic acid (A9Y3APA), 2-[anthracen-9(10H)-ylideneamino]-3-(1H–imidazole–4-yl)propanoic acid (A9Y3IMPA) and 2-[anthracen-9(10H)-ylideneamino]-3-phenyl propanoic acid (A9Y3PPA).

These complexes were screened for their *in vitro* cytotoxic activity against Dalton's lymphoma ascites cells. The toxicity of the copper complexes were checked by *in vivo* studies. Then the highly active copper(II) complexes were selected for conducting

in vivo ascites tumour studies on Swiss albino mice, in which the mortality rate of the tumour bearing mice were noted. The percentage increase in life span was determined for different concentrations of each drug and compared with standard drug cyclophosphamide.

Part IV
Antitumour studies

Chapter 2

Nimmy Kuriakose “Physicochemical, thermoanalytical, electrochemical and antitumour studies of transition metal complexes of schiff bases derived from heterocyclic carbonyl compounds” Thesis. Department of Chemistry, St. Thomas College, University of Calicut, 2015

CHAPTER 2

MATERIALS AND METHODS

Some of the newly synthesized copper complexes were taken for antitumour studies since a variety of Schiff bases and their copper complexes were reported to have marked antitumour activity. The activities of the complexes were studied at Amala Cancer Research Centre, Thrissur, Kerala. Firstly the copper complexes of different ligands were subjected to *in vitro* cytotoxic activity studies and then highly active complexes were selected for conducting *in vivo* antitumour studies.

Drug

Cu(II) complexes of different Schiff base ligands, 3-(1H-indol-3-yl)-2-[(thiophen -2-ylmethylidene)amino]propanoic acid (I3YT2YMAPA), 3-[thiophen-2-ylmethylene amino]benzoic acid (T2YMABA), 4-(5-[(2-carbamothioylhydrazono)methyl]thiophen-2-yl)benzoic acid (CTHMT2YBA), 4-(5-[(2-phenylhydrazono)methyl]thiophen-2-yl) benzoic acid (PHMT2YBA), 4-(5-[(2-carbamothioylhydrazono)methyl]furan-2-yl) benzoic acid (CTHMF2YBA), 2-(1-[pyridin-3-yl]ethylidene)hydrazinecarbothioamide (P3YEHCTA), 3-(1-(2-phenyl hydrazono)ethyl)pyridine (PHEP), 3-[anthracen-9(10H)-ylideneamino]propanoic acid (A9Y3APA), 2-[anthracen-9(10H)-ylideneamino]-3-(1H–imidazole–4-yl)propanoic acid (A9Y3IMPA) and 2-[anthracen-9(10H)-ylideneamino]-3-phenyl propanoic acid (A9Y3PPA) are screened for their antitumour activity.

The first five Cu(II) complexes were synthesized and characterised as described in Part I. The remaining complexes were prepared according to the procedure given in published works[52,53]. The structures of these complexes and the standard drug cyclophosphamide are given in Figure 4.2. All the chemicals were of analar quality and

purchased from E. Merck. Commercial solvents used for the synthesis were purified by standard methods.

Animals

Swiss albino male mice (20-25g) were obtained from the Small Animal Breeding Station (SABS), College of Veterinary and Animal Sciences, Mannuthy, Thrissur, Kerala. They were kept under standard conditions of temperature and humidity in well ventilated cages in the animal house of Amala Cancer Research Centre, Thrissur. The animals were provided with standard mouse chow (Sai Durga). Studies were carried out with the prior approval of the Institutional Animal Ethics Committee (IAEC) and strictly according to the guidelines of Committee for the Purpose of Control and Supervision of Experiments on Animals (CPCSEA) constituted by the Animal Welfare Division, Government of India.

Cell lines

Dalton's lymphoma ascites cells (DLA), maintained in the intraperitoneal cavity of mouse, were used for the study**.** The ascites fluid was removed by aspiration and the cells were sedimented by centrifugation for 10 minutes. The cells were further washed with Phosphate Buffered Saline (PBS) twice and were suspended uniformly. The numbers of cells were assessed by haemocytometer. One million cells in 0.1ml of PBS (pH = 7.2) were used for each experiment**.**

Short term *in vitro* cytotoxic analysis

Materials required

1. Dalton's lymphoma ascites cells
2. Phosphate Buffered Saline (PBS) : 500ml solution contains

- NaCl - 4g

- Na_2HPO_4 - 0.72g
- KH_2PO_4 - 0.1g
- KCl - 0.1g

3. Trypan blue solution
4. Haemocytometer.
5. Pipette (1ml, 500µl, 100µl capacity)
6. Test tubes (10ml)
7. Microscope
8. Dimethyl sulphoxide (DMSO)

Preparation of the drug

The drug was prepared by dissolving ten milligrams of each copper(II) complexes in 1ml dimethyl sulphoxide (DMSO), which is a non-toxic solvent compared to other organic solvents. From this stock solution, using a micropipette, five different concentrations i.e., 200µg/ml, 100µg/ml, 50µg/ml, 20µg/ml and 10µg/ml were prepared with Phosphate Buffered Saline solution.

Trypan blue exclusion method

Cu(II) complexes of Schiff bases were studied for short term *in vitro* cytotoxicity using Dalton's lymphoma ascites (DLA) cells. The tumour cells were aspirated from the peritoneal cavity of tumour bearing mice. The cells were washed thrice with Phosphate Buffered Saline or normal saline. Trypan blue exclusion method was followed to determine the cell viability**.**

Ten copper complexes of different ligands were taken for cytotoxic study. Five different concentrations (200µg/ml, 100µg/ml, 50µg/ml, 20µg/ml and 10µg/ml) of each

complex were prepared with Phosphate Buffered Saline (PBS) solution in test tubes. Viable cell suspension ($1x10^6$ cells in 0.1ml) was added to tubes containing various concentrations of the test compounds and the volume was made upto 1ml using Phosphate Buffered Saline(PBS). Two control tubes containing only the cell suspension were also kept. These assay mixture were incubated for 3 hours at 37^oC. Further cell suspension was mixed with 0.1 ml of 1% trypan blue, kept for 2-3 minutes and loaded on a microscope connected with haemocytometer. Dead cells take up the blue colour of trypan blue while live cells do not take up the dye and they have the typical shiny appearance. The numbers of stained and unstained cells were counted separately through the microscope using haemocytometer. Then the effect of various concentrations of the samples to produce cytotoxicity was calculated as,

$$\% \text{ cytotoxicity} = \frac{\text{Number of dead cells}}{\text{Number of dead cells + number of live cells}} \times 100$$

The Schiff base ligands were also subjected to *in vitro* cytotoxicity studies to ascertain their activity in comparison with their copper complexes.

Toxicity studies of Schiff base complexes

Materials required

1. Swiss albino mice (male) -12 numbers
2. Dimethyl sulphoxide (DMSO)
3. Drug solution
4. Injection syringe (1ml)
5. Test tubes (10ml)

Preparation of the drug

Three different concentrations of the drug were prepared as follows.

1. 20mg/kg b.wt. : 4mg of the Cu(II) complex was dissolved in 100µl DMSO and made upto 2ml with distilled water.
2. 10mg/kg b.wt. : 4mg of the Cu(II) complex was dissolved in 100µl DMSO and made upto 4ml with distilled water.
3. 2mg/kg b.wt. : 4mg of the Cu(II) complex was dissolved in 100µl DMSO and made upto 20ml with distilled water.

Toxicity studies

Swiss albino mice, weighing 20-25g were taken for conducting the toxicity studies of the complexes. In order to find out the nontoxic concentration, the mice were divided into 4 groups (4 animals/group). The drug was administrated to each group as follows:

Group 1: control (untreated)

Group 2: 20mg/kg b.wt, treated,

Group 3: 10mg/kg b.wt, treated,

Group 4: 2mg/kg b.wt, treated.

The drug (200µl) was given as injection to intraperitoneal cavity of each animal once on alternate days and continued for five days. They were kept under standard conditions of temperature and humidity in well ventilated cages at animal house of Amala Cancer Research Centre, Thrissur. The animals were provided with standard mouse chow and water. The animals were observed for their mortality each day. From the death rate of the mice, the nontoxic concentration was determined.

***In vivo* ascites tumour reduction studies**

Materials required

1. Swiss albino mice (male) weighing about 25g - 48 numbers
2. Dimethyl sulphoxide (DMSO)
3. Drug [Cu(II) complexes]
4. Cyclophosphamide solution
5. Injection syringe (1ml)
6. Distilled water

Preparation of the drug

2mg/kg b.wt concentration solutions of the drugs were prepared first, as described earlier. Then it was properly diluted using distilled water in order to get solutions of the concentrations 0.5mg/kg b.wt and 0.25mg/kg b.wt. These two concentrations were employed for the *in vivo* tumour reduction studies.

Preparation of the standard drug **(**Cyclophosphamide)

The standard drug solution was prepared by dissolving 20mg cyclophosphamide in 3.2ml distilled water to form 25mg/kg b.wt solution.

Ascites tumour reduction studies

The effect of copper complexes on the survival rate of ascites tumour bearing cells was noted as follows.

Animals weighing 20-25g were divided into four groups (6 animals/group) as follows:

Group 1: Control group (untreated)

Group 2: Reference group (treated with standard drug cyclophosphamide)

Group 3: Treated group (0.5mg/kg b.wt)

Group 4: Treated group (0.25mg/kg b.wt)

The animals were kept in well ventilated cages and provided with food and water regularly. All animals were injected with ($1x10^6$) viable Dalton's lymphoma ascites (DLA) cells in phosphate buffered saline (PBS). The tumour cells were aspirated from 15 day old DLA tumour mice. The concentration of the cells was adjusted with the help of the haemocytometer. Group 1 that received only the DLA cell line served as control. Group 2 was taken as the reference group. After 24 hours of tumour inoculation the drug was given as an injection into the intraperitoneal cavity of each animal of group 3 and group 4. Group 3 animals were injected with 100µl drug solution of 0.5mg/kg b.wt concentration and group 4 animals were injected with 0.25mg/kg b.wt drug solution. The reference group was treated with the standard drug cyclophosphamide (25mg/kg b.wt). The injections were continued for five alternate days. Then the mice were observed every day. Mean survival rate in each group was calculated by determining the standard deviations. The percentage of increase of life span (ILS) of animals treated with the standard and new drugs was calculated using the formula

$$\% \text{ ILS} = \frac{[T-C]}{C} \text{ X } 100$$

where T and C are mean survival rate of treated and control mice respectively.

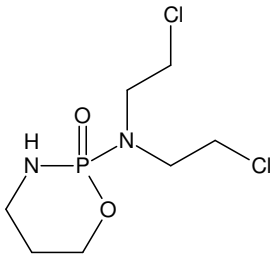

Cyclophosphamide

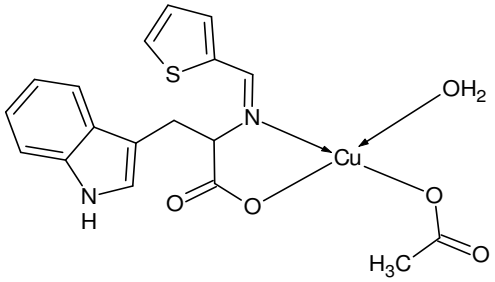

Cu(II) complex of I3YT2YMAPA

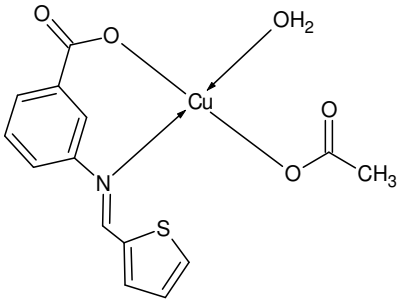

Cu(II) complex of T2YMABA

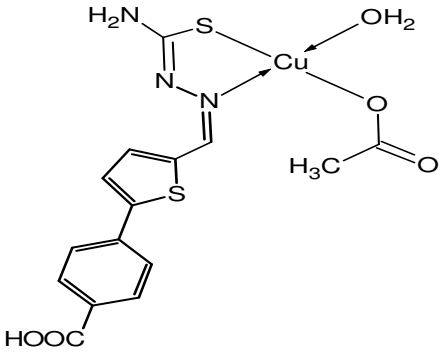

Cu(II) complex of CTHMT2YBA

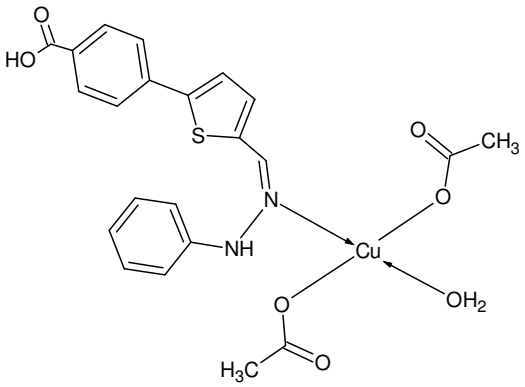

Cu(II) complex of PHMT2YBA

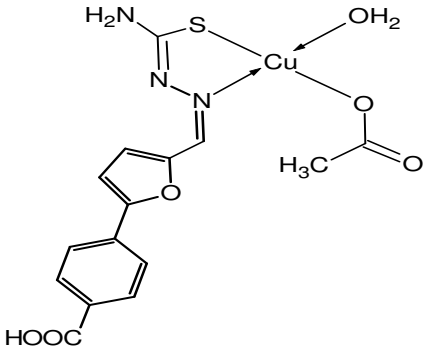

Cu(II) complex of CTHMF2YBA

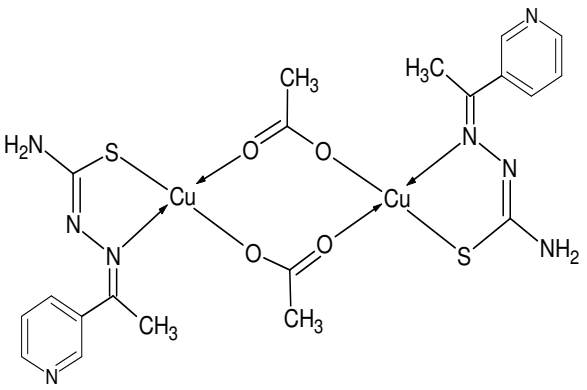

Cu(II) complex of P3YEHCTA

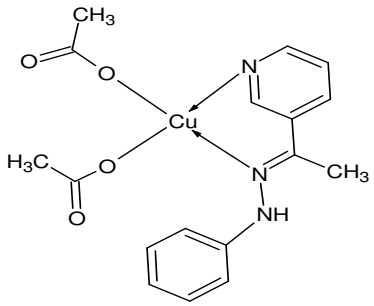

Cu(II) complex of PHEP

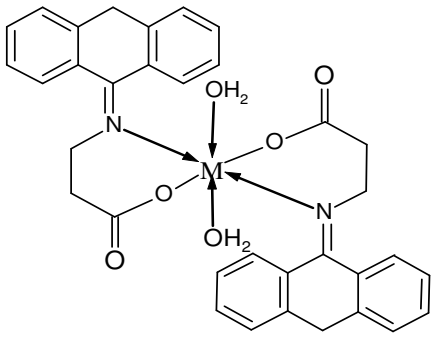

Cu(II) complex of A9Y3APA

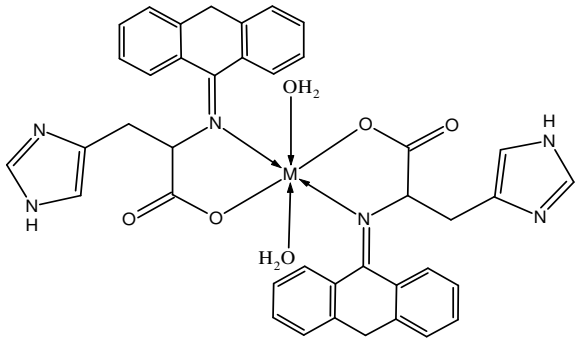

Cu(II) complex of A9Y3IMPA

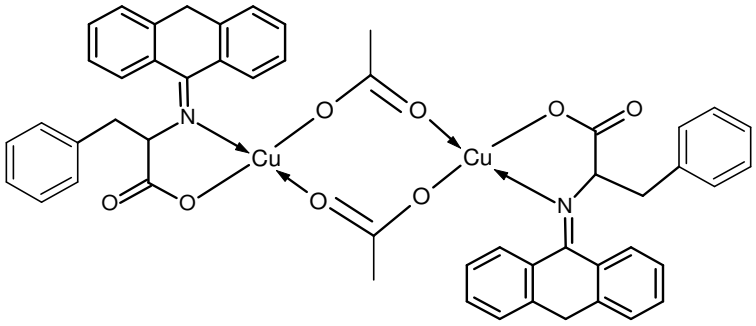

Cu(II) complex of A9Y3PPA

Fig. 4.2 Structures of antitumour drugs, cyclophosphamide and Cu(II) complexes of Schiff bases

Part IV
Antitumour studies

Chapter 3

Nimmy Kuriakose “Physicochemical, thermoanalytical, electrochemical and antitumour studies of transition metal complexes of schiff bases derived from heterocyclic carbonyl compounds” Thesis. Department of Chemistry, St. Thomas College, University of Calicut, 2015

CHAPTER 3

ANTITUMOUR STUDIES ON COPPER(II) COMPLEXES OF SCHIFF BASES, I3YT2YMAPA, T2YMABA, CTHMT2YBA, PHMT2YBA, CTHMF2YBA, P3YEHCTA, PHEP, A9Y3APA, A9Y3IMPA AND A9Y3PPA

The antitumour activity of Cu(II) complexes of ten different Schiff bases namely 3-(1H-indol-3-yl)-2-[(thiophen-2-ylmethylidene)amino]propanoic acid (I3YT2YMAPA), 3-[thiophen-2-ylmethyleneamino]benzoic acid (T2YMABA), 4-(5-[(2-carbamothioyl hydrazono)methyl]thiophen-2-yl)benzoic acid (CTHMT2YBA), 4-(5-[(2-phenyl hydrazono)methyl]thiophen-2-yl)benzoic acid (PHMT2YBA), 4-(5-[(2-carbamothioyl hydrazono)methyl]furan-2-yl)benzoic acid (CTHMF2YBA), 2-(1-[pyridin-3-yl] ethylidene)hydrazinecarbothioamide (P3YEHCTA), 3-(1-[2-phenylhydrazono]ethyl) pyridine (PHEP), 3-[anthracen-9(10H)-ylideneamino]propanoic acid (A9Y3APA), 2-[anthracen-9(10H)-ylideneamino]-3-(1H–imidazole–4-yl)propanoic acid (A9Y3IMPA) and 2-[anthracen-9(10H)-ylideneamino]-3-phenyl propanoic acid (A9Y3PPA) are described in this chapter. According to the literature survey, large number of Schiff base complexes of transition metals especially that of copper possess marked antitumour activity. It is reported that the copper complex can block the DNA replication thereby preventing the tumour growth. Here the Cu(II) complexes of the Schiff bases are prepared and screened for their antitumour activity.

All the copper complexes were first subjected to short term *in vitro* cytotoxicity studies using Dalton's lymphoma ascites cells (DLA). Different concentrations of the complexes were prepared and analysed for their cytotoxicity by Trypan blue exclusion method. Also all the Schiff bases, namely I3YT2YMAPA, T2YMABA, CTHMT2YBA,

PHMT2YBA, CTHMF2YBA, P3YEHCTA, PHEP, A9Y3APA, A9Y3IMPA and A9Y3PPA were subjected to cytotoxicity studies in order to ascertain their activities towards DLA tumour cells and compared the activities with that of their Cu(II) complexes. Then three of the highly active compounds i.e., Cu(II) complexes of I3YT2YMAPA, T2YMABA and CTHMT2YBA were selected for conducting *in viv*o ascites tumour reduction analysis.

Preparation and characterisation of drugs

The detailed procedure for the synthesis and characterisation of copper(II) complexes of I3YT2YMAPA, T2YMABA, CTHMT2YBA, PHMT2YBA and CTHMF2YBA are well documented in Part I. The drugs, copper(II) chelates of P3YEHCTA, PHEP, A9Y3APA, A9Y3IMPA and A9Y3PPA were prepared and their physicochemical properties were evaluated as per the references[52,53]. The Cu(II) complexes of I3YT2YMAPA, T2YMABA, CTHMT2YBA, PHMT2YBA, CTHMF2YBA, P3YEHCTA, PHEP and A9Y3PPA were found to have 1:1 stoichiometry between the metal and ligand and possess square planar geometry. P3YEHC and A9Y3PPA complexes existed in dimeric form. Copper complexes of A9Y3APA and A9Y3IMPA were having 1:2 metal-ligand stoichiometry and octahedral geometry.

Antitumour activity analysis

Antitumour activity of the Schiff bases and their Cu(II) chelates were performed by three methods which were already explained in the previous chapter. They are (i) Short term *in vitro* cytotoxic studies (ii) Toxicity studies and (iii) *In vivo* tumour reduction studies. Reagents and methods employed for these investigations were

previously narrated in chapter 2 of this part. For the *in vivo* cytotoxic studies and screening the effect of copper chelates on the tumour reduction, Dalton's lymphoma ascites tumour cell lines were used.

***In vitro* cytotoxicity studies**

The short term *in vitro* cytotoxicity of the complexes was screened by Trypan blue exclusion method as described in the previous chapter. Different concentrations of the complexes prepared in DMSO are 200µg/ml, 100µg/ml, 50µg/ml, 20µg/ml and 10µg/ml. After the incubation period of 3 hours the samples were analysed using a haemocytometer. The dead cells which have taken the blue colour were counted in a haemocytometer and the percentage of cytotoxicity was calculated. The *in vitro* cytotoxicity data of these drugs at different concentrations are listed in Table 4.1. The principle behind this method is that the drug at toxic concentration damages the cell and makes pores on the membrane through which trypan blue enters. The damaged cells are stained blue by the dye, trypan blue and can be distinguished from viable cells. Live cells were not taking the dye and hence found clear. The Cu(II) complex of 3-(1H-indol-3-yl)-2-[(thiophen-2-ylmethylidene)amino]propanoic acid (I3YT2YMAPA) exhibited the highest cytotoxic activity of 100% at a concentration of 200µg/ml. It is obvious from the table that the cytotoxic activity decreases with the decrease in the drug concentration. The drug concentration of 200µg/ml produced 83% of cell death in DLA cell suspension in the case of Cu(II) complex of T2YMABA and 82% in the case of Cu(II) complex of CTHMT2YBA.

In order to ascertain the effect of chelation of Schiff bases towards antitumour activity, the cytotoxicity of the free Schiff bases also were performed using DLA cell

lines. Microscopic view of the DLA cells (untreated and treated) are given in Figure 4.3. The dead and live cells are easily distinguishable from the picture since the dead cells uptake the blue colour of the dye. *In vitro* cytotoxic studies on Dalton's lymphoma ascites cells revealed that all the Schiff bases have much less cytotoxic activity against the tumour cells, compared to their complexes. Only the higher concentrations of various Schiff bases showed slight cytotoxicity against the DLA cells. The lower concentrations of all the ligands showed little cytotoxic activity. Figures 4.4-4.8 show graphical comparison of cytotoxic activities of the copper (II) complexes with their corresponding Schiff bases.

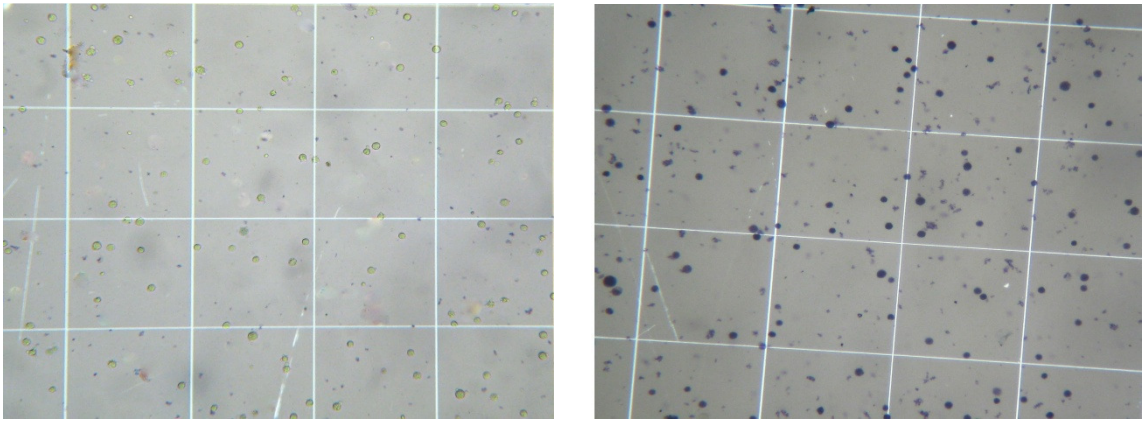

(a) (b)

Fig. 4.3 Microscopic view of a) live DLA tumour cells (control) b) dead tumour cells subjected to *in vitro* cytotoxic studies with 200µg/ml concentration of Cu-I3YT2YMAPA complex

Table 4.1 *In vitro* cytotoxicity data of Schiff base ligands and their Cu(II) complexes at different concentrations on Dalton's lymphoma ascites cells

Drug	% of dead cells				
	10µg/ml	20µg/ml	50µg/ml	100µg/ml	200µg/ml
I3YT2YMAPA	0	0	2	7	16
Cu(II) complex of I3YT2YMAPA	35	55	70	80	100
T2YMABA	0	0	0	5	10
Cu(II) complex of T2YMABA	10	40	75	80	83
CTHMT2YBA	0	0	5	10	14
Cu(II) complex of CTHMT2YBA	18	30	48	64	82
PHMT2YBA	0	0	0	3	8
Cu(II) complex of PHMT2YBA	38	44	54	60	77
CTHMF2YBA	0	0	0	2	9
Cu(II) complex of CTHMF2YBA	30	36	47	59	74
P3YEHCTA	0	0	0	3	6
Cu(II) complex of P3YEHCTA	8	16	28	45	80
PHEP	0	0	0	0	3
Cu(II) complex of PHEP	4	10	22	40	70
A9Y3APA	0	0	0	3	8
Cu(II) complex of A9Y3APA	0	10	20	35	65
A9Y3IMPA	0	0	0	2	5
Cu(II) complex of A9Y3IMPA	4	10	20	36	60
A9Y3PPA	0	0	0	0	2
Cu(II) complex of A9Y3PPA	20	30	60	70	75

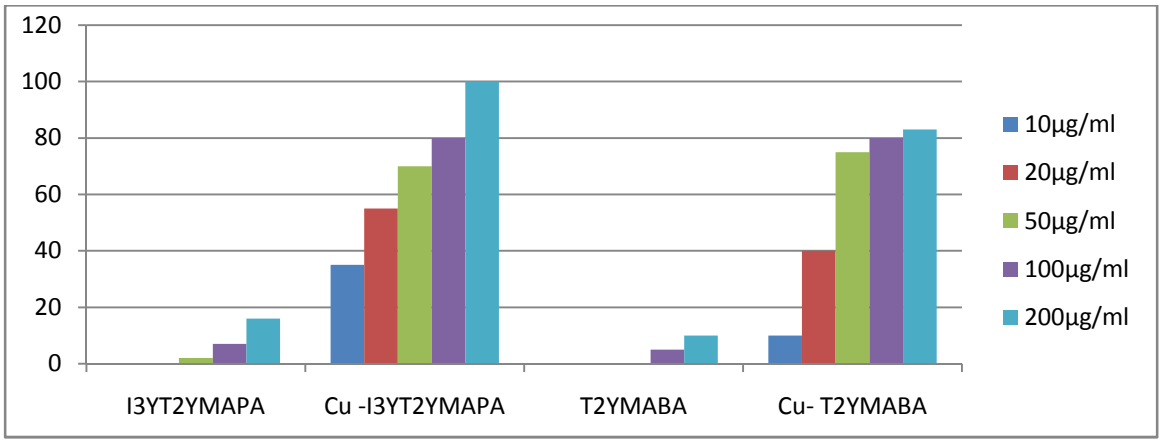

Fig. 4.4 *In vitro* cytotoxicity data of I3YT2YMAPA and T2YMAPA and their Cu(II) complexes on DLA cell lines

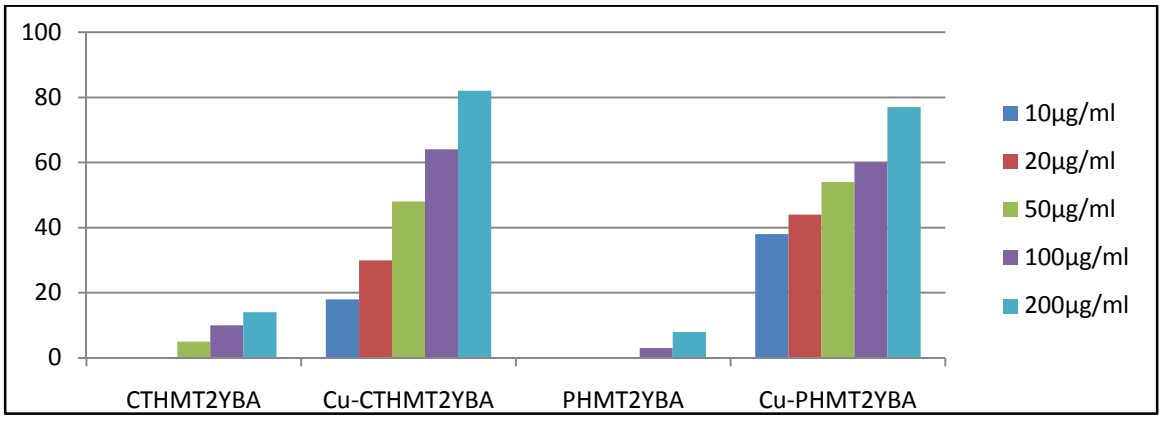

Fig. 4.5 *In vitro* cytotoxicity data of CTHMT2YBA and PHMT2YBA and their Cu(II) complexes on DLA cell lines

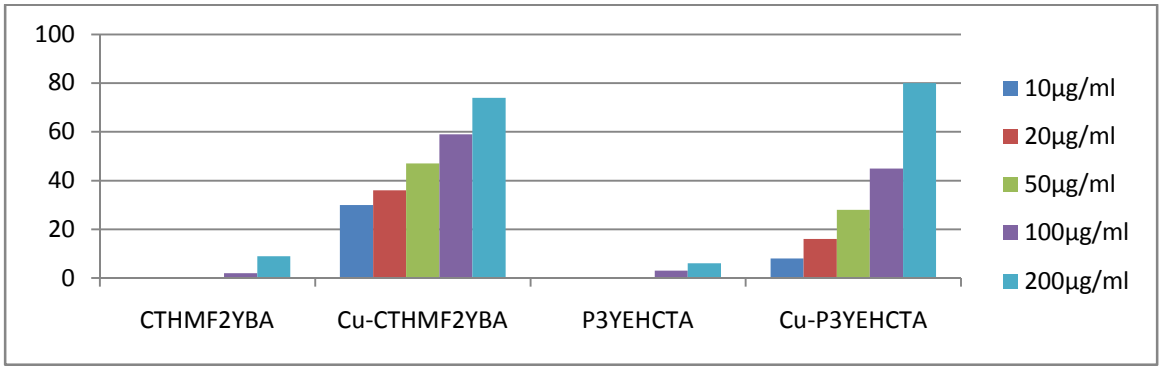

Fig. 4.6 *In vitro* cytotoxicity data of CTHMF2YBA and P3YEHCTA and their Cu(II) complexes on DLA cell lines

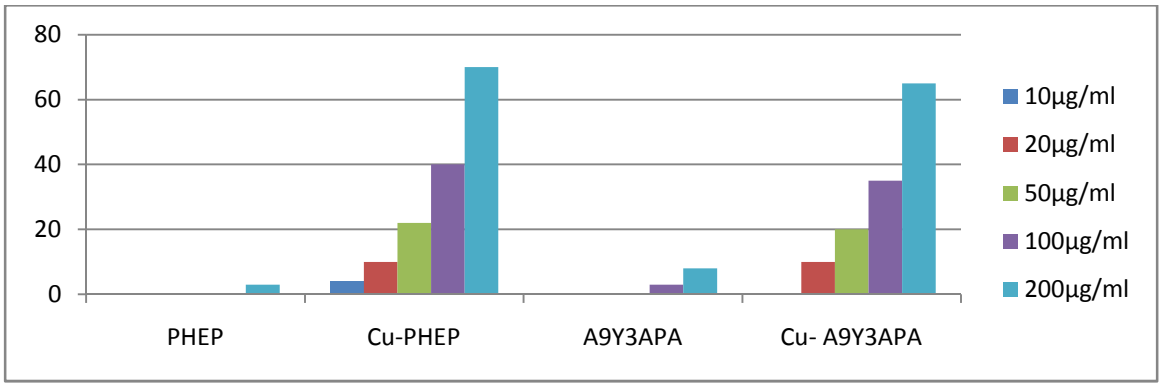

Fig. 4.7 *In vitro* cytotoxicity data of PHEP and A9Y3APA and their Cu(II) complexes on DLA cell lines

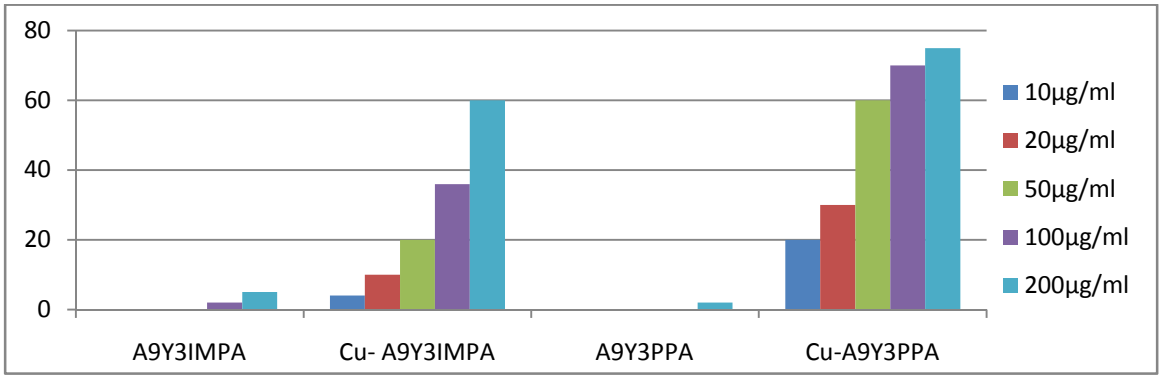

Fig. 4.8 *In vitro* cytotoxicity data of A9Y3IMPA and A9Y3PPA and their Cu(II) complexes on DLA cell lines

Investigations on the cytotoxic activity of T2YMABA and its copper chelate showed very promising results as given in the table. Even a drug concentration of 50µg/ml was quite enough to exhibit 75% activity while the free ligand was absolutely non active towards the DLA cells. A9Y3PPA showed little or practically no cytotoxic action whereas its copper complex exhibited remarkably high *in vitro* cytotoxic property on DLA tumour cell lines. A drug concentration of 100µg/ml was found to be sufficient for 70% cytotoxicity. Figure 4.9 shows the comparison of cytotoxic activities of the three

highly active copper complexes with their corresponding Schiff bases, I3YT2YMAPA, T2YMABA and CTHMT2YBA.

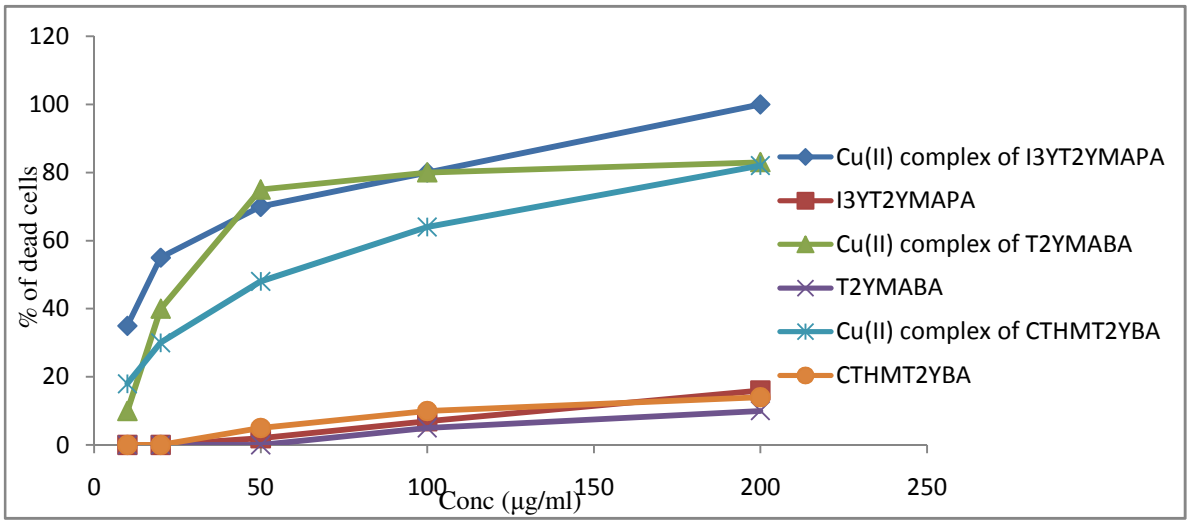

Fig. 4.9 Cytotoxic action of I3YT2YMAPA, T2YMABA, CTHMT2YBA and their copper(II) complexes

Toxicity studies of the copper(II) complexes on Swiss albino mice

In vivo toxicity studies on Swiss albino mice were conducted to ascertain the optimum nontoxic concentration of the drug. 20mg/kg b.wt, 10mg/kg b.wt and 2mg/kg b.wt concentrations of Cu(II) complex of I3YT2YMAPA were prepared and administered to three different groups of mice. After the intraperitoneal injection of the drug, the mice were observed for their mortality rate. The observations of the death of the mices are given in Table 4.2. Group 1 animals were taken as the control, they were not injected with any drug. In group 2, where 20mg/kg b.wt drug was inoculated, one mouse was found dead on the second day after the injection. The remaining animals were also dead within 4 days. So it was concluded that this concentration was highly toxic for mice. Group 3 animals were treated with 10mg/kg b.wt drug concentration. In this group, two mice were found dead on the third day. And the remaining mice were dead on the fifth

and the seventh day. Whereas in group 4(drug concentration 2mg/kg b.wt), the death of the first animal was on the fifth day, followed by one death on seventh day and two on eighth day. Analysing the observations it is inferred that the 20mg/kg b.wt and 10mg/kg b.wt concentrations of the drug are highly toxic to Swiss albino mice. So these concentrations were avoided. In group 4, since the death of mice started on fifth day, it was concluded that a lower concentration of Cu(II) complexes (<2mg/kg b.wt) is safe for the animals. Hence drug concentrations of 0.5mg/kg b.wt and 0.25mg/kg b.wt were selected for the further *in vivo* studies.

Table 4.2 Toxicity studies data of copper(II) complex of I3YT2YMAPA on Swiss albino mice

Drug concentration	Number of dead mice								
	Day 1	Day 2	Day 3	Day 4	Day 5	Day 6	Day 7	Day 8	Day 15
Group 1: Control	0	0	0	0	0	0	0	0	0
Group 2: 20mg/kg b.wt	0	1	2	1	-	-	-	-	-
Group 3: 10mg/kg b.wt	0	0	2	0	1	0	1	-	-
Group 4: 2 mg/kg b.wt	0	0	0	0	1	0	1	2	-

Tumour reduction studies

The *in vivo* toxicity studies revealed that 0.5mg/kg b.wt and 0.25mg/kg b.wt concentrations of the drug are nontoxic to the animals. Since the higher concentrations of the drug were found to be toxic to the mice, concentrations greater than 0.5mg/kg b.wt were avoided. The copper complexes of I3YT2YMAPA, T2YMABA and CTHMT2YBA which exhibited significant cytotoxic action in the *in vitro* analysis, were selected for

tumour reduction experiments *in vivo*. This analysis unambiguously illustrates the inhibitory power of the complexes on the growth of Dalton's lymphoma ascites tumour in Swiss albino mice. Two different concentrations of the complexes, such as 0.5mg/kg b.wt and 0.25mg/kg b.wt were adopted for these studies since these very low concentrations of the copper complexes were found to be nontoxic to Swiss albino mice. The increase in life span was calculated using the formula $\frac{[T-C]}{C}$ X100 where T and C are the mean survival rate of the treated and control animals respectively. In order to study the comparison of the antitumour activity of the novel copper complexes synthesized with that of standard antibiotics generally employed in cancer treatment, the tumour reduction properties of the standard drug cyclophosphamide at a concentration of 25mg/kg b.wt was also investigated.

In these experiments using the liposome encapsulated drug, i. e., the copper complexes, significant inhibitory effect on the growth of DLA cell line tumour on Swiss albino mice was observed. The tumour development was very quick, visible and prominent in the control as it was clear from the increased enlargement of abdominal cavity. On the other hand, the animals treated with the drug, especially treated with 0.5mg/kg b.wt concentration showed the symptoms of ascites tumour only after the drug doses were over. Moreover the treated mice died at slower rate than the control.

Tumour reduction effect of Cu(II) complex of 3-(1H-indol-3-yl)-2-[(thiophen-2-ylmethylidene)amino]propanoic acid (I3YT2YMAPA)

The antitumour activity of the complex [Cu(I3YT2YMAPA)Ac(H_2O)] was investigated by observing the mortality rate of the tumour induced animals. The *in vivo* cytotoxic studies on Swiss albino mice, developed with DLA cancer cell lines, showed

that the administration of the drug considerably increases the life span of the tumour bearing mice. Table 4.3 gives the mean survival rate and % increase in life span exhibited by this drug at different concentrations. The mean survival rate was found out by calculating the standard deviation of the days, on which each animal was found dead.

The control group animals survived only for 13.17 ± 4.4 days. The animals which were injected with the standard drug cyclophosphamide had a life span of 16.7 ± 3.0 days ie; the increase in life span is 26.8% compared to that of the control group. The Cu(II) complex with a drug concentration of 0.5mg/kg b. wt, increased the survival rate of the animals by 23.0 ± 1.8 days. So the increase in the average life span of the mice was found to be 74.64% which was very high, compared to that of the standard drug. The drug with a lower concentration of 0.25mg/kg body weight resulted in increase of life span of animals by 36.67%. Here both the concentrations were found to have very good antitumour activity against the Dalton's lymphoma ascites tumour than cyclophosphamide.

Table 4.3 Effect of copper(II) complex of I3YT2YMAPA on the mean survival rate of ascites tumour regression induced by Dalton's lymphoma ascites tumour cells

Treatment	Mean survival rate	Increase in life span (%)
Control	13.17 ± 4.4	-
Cyclophosphamide (25mg/kg. b.wt)	16.7 ± 3.0	26.80
I3YT2YMAPA (0.25mg/kg b.wt)	18.0 ± 2.0	36.67
I3YT2YMAPA (0.5mg/kg b.wt)	23.0 ± 1.8	74.64

Tumour reduction effect of Cu(II) complex of 3-[thiophen-2-ylmethyleneamino] benzoic acid (T2YMABA)

The effect of the copper(II) complex of 3-[thiophen-2-ylmethyleneamino] benzoic acid (T2YMABA), along with that of the standard drug cyclophosphamide, on the mean survival rate of the mice is represented in Table 4.4. The group of mice which were administered with the higher concentration drug (0.5mg/kg b.wt) survived for more days. The mean survival rate of this group of mice was 24.4 ± 3.12 with an increase in life span of 72.56%. The lower drug concentration (0.25mg/kg b.wt) also exhibited considerable increase in life span i.e; 34.37% compared to that of the untreated animals. Mean survival rate of this group of mice was 19.2 ± 4.24 days. It is evident that both concentrations of this drug exhibited greater inhibition activity towards the DLA tumour cells than the standard drug cyclophosphamide. Also the the tumour reduction ability of the drug increases with the concentration.

Table 4.4 Effect of copper(II) complex of T2YMABA on the mean survival rate of ascites tumour regression induced by Dalton's lymphoma ascites tumour cells

Treatment	Mean survival rate	Increase in life span (%)
Control	14.14 ± 2.1	-
Cyclophosphamide (25mg/kg. b.wt)	16.7 ± 3.0	26.80
T2YMABA 0.25mg/kg b.wt	19.2 ± 4.24	34.37
T2YMABA 0.5mg/kg b.wt	24.4 ± 3.12	72.56

Tumour reduction effect of Cu(II) complex of 4-(5-[(2-carbamothioylhydrazono) methyl]thiophen-2-yl)benzoic acid (CTHMT2YBA)

Here also the copper(II) complex showed appreciable antitumour activity against the ascites tumour. The results are given in Table 4.5. The 0.5mg/kg b.wt drug concentration produced the survival rate of 20.4 ±3.84 days and 0.25mg/kg b.wt drug produced 16.3 ± 5.5 days. The drug with 0.5mg/kg b.wt concentration showed better result than the standard drug. 57.7% increase in life span was obtained with this concentration. But the lower concentration (0.25mg/kg b.wt) gave comparatively poor performance. Only 22.35% of increase in life span was obtained, which was lower than the activity of the standard drug (26.80%).

Figure 4.10 compares the tumour sizes in Swiss albino mice on eighth day in ascites tumour reduction studies, conducted with copper(II) complex of Schiff base I3YT2YMAPA. Ascites tumour bearing mouse which was induced by intraperitonial inoculation of Dalton's lymphoma ascites tumour cells, is represented as Figure 4.10a. Photographs of ascites tumour bearing Swiss albino mice treated with standard drug cyclophosphamide (25mg/kg. b.wt) and the drug Cu-I3YT2YMAPA complex (0.5mg/kg b.wt) are given as Figures 4.10b and 4.10c respectively. There was a noticeable reduction in tumour size in the mice which was treated with the complex, compared with that of the control mice and the mice treated with the standard drug cyclophosphamide. A comparison of percentage increase in life span of mice when treated with different Cu(II) complexes is given in Figure 4.11, which clearly establishes that all the new copper complexes, which are in square planar geometry, possess marked tumour reduction capacity on ascites tumour bearing Swiss albino mice. They have high growth

inhibition ability than the standard drug cyclophosphamide, even at very low concentration. Out of these three heterocyclic ligand derived Cu(II) complexes the most active one noticed was Cu-I3YT2YMAPA complex which contain an amino acid part in the Schiff base (tryptophan).

Table 4.5 Effect of copper(II) complex of CTHMT2YBA on the mean survival rate of ascites tumour regression induced by Dalton's lymphoma ascites tumour cells (*in vivo*)

Treatment	Mean survival rate	Increase in life span (%)
Control	14.14 ± 2.1	-
Cyclophosphamide (25mg/kg. b.wt)	16.7 ± 3.0	26.80
CTHMT2YBA (0.25mg/kg b.wt)	16.3 ± 5.5	22.35
CTHMT2YBA (0.5mg/kg b.wt)	20.4 ± 3.84	57.71

a) DLA tumour bearing mouse (untreated)

b) DLA tumour bearing mouse, treated with cyclophosphamide (25mg/kg b.wt)

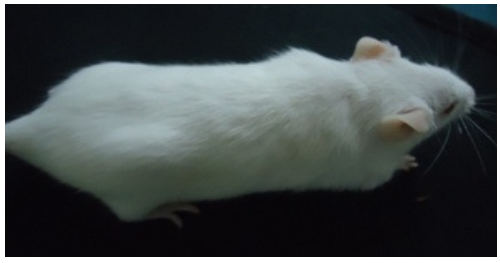

c) DLA tumour bearing mouse, treated with Cu-I3YT2YMAPA complex (0.5mg/kg b.wt)

Fig. 4.10 *In vivo* ascites tumour reduction studies on Swiss albino mice

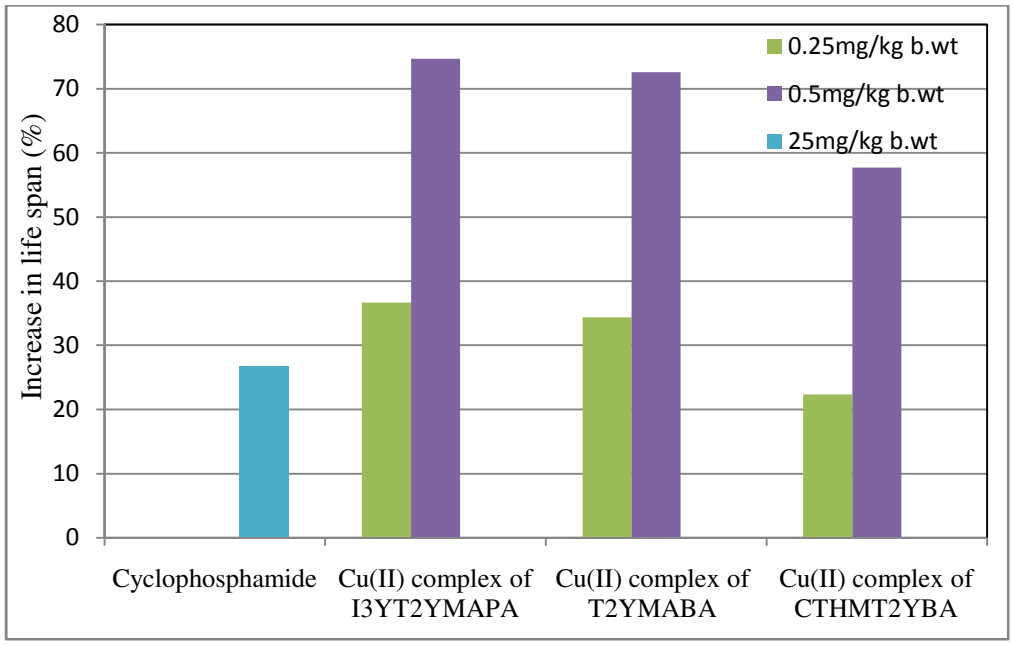

Fig. 4.11 Effect of copper complexes and the standard drug cyclophosphamide, on the growth inhibition of Dalton's lymphoma ascites tumour cells (*in vivo*)

Mechanism of action

The standard drug cyclophosphamide is an alkylating agent. When administered it introduces alkyl radicals into DNA strands of cells and stops cancer cells from growing[54]. Another well known antitumour drug, cisplatin which is a platinum complex, acts by a different mechanism[55]. Following the administration of cisplatin, cis-diaminedichloro platinum(II), one of the chloride ligand is slowly displaced by water (an aqua ligand). This process is termed as aquation. The aqua ligand in the resulting $[PtCl(H_2O)(NH_3)_2]^+$ can be easily displaced, allowing the platinum atom to bind to one of the bases on DNA, most preferably guanine. Subsequent to the formation of $[PtCl(guanine\text{-}DNA)(NH_3)_2]^+$, crosslinks are formed by the displacement of the second chloride ligand, by another guanine. These types of crosslinks in DNA can interfere with

the cell division in tumour cells by mitosis. But in the case of copper complexes a different type of mechanism is believed to occur.

It is considered that the endogenous metals like copper are less toxic. The ability to produce reactive oxygen species (ROS) is the key factor in the anticancer activity of copper complexes[56]. Production of ROS such as hydroxyl radicals driven by the copper ions, is quite regardless of the forms in which they are initially introduced into the body, Cu^{+} or Cu^{2+}. These radicals are believed to be the major cause for the damage of DNA in tumour cells.

It is interesting to note that the free ligands themselves are not good inhibitors. It is the complex formation which makes the transportation of copper ions through the cell membrane possible so that proteasome inhibition occurs[57]. It is found that the lipophilicity of the metal is increased upon ligand coordination and thereby the interaction at the cellular level is enhanced[58].

The presence of copper in the complexes enhances its DNA binding affinity[59]. The binding capacity depends on the size, geometry and electron affinity of the copper complexes. All these copper complexes have square planar geometry, as that of cisplatin. These factors can result in an irreversible modification of the DNA conformation which will finally result in the death of tumour cells. Also the sequestration of copper can prevent the establishment of the tumour blood supply. The chemical framework and ligand donor atom can modulate the hard or soft properties of the metal, thereby influence the performance of the complex. The lipophilic nature of the copper complexes and its solubility in extracellular fluids also can affect their mode of action[60].

The ability of Cu(II) complexes to bind to DNA and exhibit nuclease activity in the presence of reducing agents is established by earlier research works[56]. The character of organic ligands in such copper complexes seems to affect and regulate their activity. These ligands can neutralize the electric charge of the copper ion and can increase the lipophilicity of the complex. Thus the transport across the cell membrane is facilitated. Presence of mimic structures of the organic moieties of the drugs, with that of biomolecules, can enhance the mobility of the drug in the biological systems, especially to cross the cell walls. Also these molecules can intercalate to DNA and interact non-covalently with proteins. The effect of ligand chelation may also be of importance for the biological activity of the complexes, whose exact role has not been elucidated yet.

The copper complex can block the base replication in DNA by binding with the nitrogen base of DNA. The extensive diversity of feasible structure for the Schiff base complexes with the presence of various donor atoms as well as the ability to permeate the bilayer lipidic membrane makes them active antitumour agents[61]. The presence of donor sites like sulphur, oxygen and azomethine group make this type of ligand more flexible and versatile. The extended aromatic π system in these Schiff base complexes enhances the intercalation mode of binding with the DNA and thereby giving marked DNA cleavage activity. Moreover these compounds are stable towards the transchelation reactions with physiological molecules like amino acids or proteins.

The biological activity of the thiosemicarbazones is due to their ability to inhibit the ribonucleotide reductase enzyme in the DNA synthesis process[31]. Moreover, on chelation with copper the inhibitory activity is enhanced, which can be attributed to the structure activity correlation as in the case of cisplatin[62]. The fact that these compounds

are highly selective towards the hormone responsive cancers, makes them an important class of anticancer drug.

It is also suggested that DNA is not the main biological target for this class of metal complexes. Besides DNA binding, super oxide dismutase (SOD) mimetic activities as well as generation of ROS by redox-cycling, which lead to oxidative cell damage, are believed to occur. Generally, these intra-cellular molecular events trigger cancer cell death through an apoptotic mechanism[63,64]. In order to establish the actual mechanism of antitumour action of these Schiff base complexes, cellular level studies are to be conducted.

SUMMARY

The antitumour activity of copper(II) complexes of ten potential Schiff base ligands such as I3YT2YMAPA, T2YMABA, CTHMT2YBA, PHMT2YBA, CTHMF2YBA, P3YEHCTA, PHEP, A9Y3APA, A9Y3IMPA and A9Y3PPA were examined on Dalton's lymphoma ascites tumour cells. Ten new Cu(II) complexes of these Schiff bases were prepared and screened for their *in vitro* cytotoxic activity. The trypan blue exclusion method was adopted and the result revealed that all the complexes have excellent cytotoxic activity against the tumour cell suspension. Three complexes which showed the highest activity during *in vitro* cytotoxic analysis were chosen for the *in vivo* studies on Swiss albino mice. Ascites tumour analysis explored the increased capacity of the copper compound on chelation. Also the activities of these compounds were compared with that of the standard drug cyclophosphamide.

Out of the complexes taken for the cytotoxic studies, the Cu(II) complex of the Schiff base 3-(1H-indol-3-yl)-2-[(thiophen-2-ylmethylidene)amino]propanoic acid (I3YT2YMAPA) showed the maximum cytotoxic activity (100%) against DLA cells in trypan blue exclusion method. An *in vivo* tumour reduction studies of this complex was performed on ascites tumour bearing Swiss albino mice. Nontoxic concentrations of the drug (0.5mg/kg b.wt and 0.25mg/kg b.wt) were found out by toxicity studies for intraperitoneal injection and the result has proven that this compound has greater antitumour activity than the standard drug cyclophosphamide. Both concentrations of the drug used have given promising results. 0.25mg/kg b.wt concentration gave 36.67% and 0.5mg/kg b.wt concentration gave 74.64% increase in life span on Swiss albino mice.

The enhanced activity of the amino acid derivative can be attributed to the presence of hydrophilic parts.

The Cu(II) complex of 3-[thiophen-2-ylmethyleneamino]benzoic acid (T2YMABA) also exhibited excellent antitumour activity. 0.5mg/kg b.wt concentration of the drug produced 72.56% increase in life span, almost same as the previous complex. 0.25mg/kg b.wt concentration also has better performance (ILS: 34.37%) than the standard drug (ILS: 26.80%).

The copper complex of the thiosemicarbazide derivative CTHMT2YBA exhibited pronounced tumour inhibitory power as revealed by the *in vivo* analysis. Eventhough the increase in life span was less than that of the other complexes, 0.5mg/kg b.wt concentration of this drug gave a higher value (57.7%) for increase in life span than that of the standard drug (26.8%). The inhibitory action of the compound may be due to the presence of the donor atoms like oxygen, nitrogen and sulphur and the ability to effectively block the DNA replication in tumour cells.

Current interest in Cu(II) complexes is stemming from their potential use as antitumour agents in smaller animals. The biological properties of these compounds are determined by the ligand present around the metal ion. The results suggest great opportunities for future work in higher animals. In the field of non-platinum compounds showing antitumor potential, copper-based complexes have been given a prominent place. One of the potential approaches in anticancer chemistry is focused on the design of new metal compounds with different substituents and labile sites which may increase their cytotoxicity, specifically to cancer cells. The wide range of coordination numbers, geometries, accessible redox states, kinetic characteristics and the intrinsic properties of

the cationic metal ions and ligands offer much scope for the upcoming research chemists which may help in designing better and efficient metal-based drugs.

REFERENCES

1. *World Cancer Report 2014*. World Health Organization (2014) Chapter 1.3.
2. *"SEER Stat Fact Sheets: All Cancer Sites"*. National Cancer Institute. Retrieved 18, (June 2014).
3. *"The top 10 causes of death Fact sheet"*. World Health Organization, (May 2014).
4. I. Frei, E. Kufe, D. W. Holland, F. James, *Holland-Frei Cancer Medicine*, 6 (2009) 2399.
5. B. O. Cakir, P. Adamson, C. Cingi, *Facial plastic surgery clinics of North America,* 20 (4) (2012) 419.
6. A. Jemal A, F. Bray, M. M. Center, J. Ferlay, E. Ward, D. Forman, *CA: A Cancer J. Clinicians,* 61 (2) (2011) 69.
7. *World Cancer Report 2014*. World Health Organization, (2014) Chapter 6.7.
8. R. Susan, N. Alfred, M. Anna, *Cancer Med*., 6 (2003).
9. G. Pellegriti, F. Frasca, C. Regalbuto, S. Squatrito, R. Vigneri, *J. Can. Epiderm*., 2013 (2013) Article ID: 965212.
10. A. Montazeri, *Health Qual. Life Outcomes,* 7 (2008) 102.
11. "*WHO Disease and Injury Country Estimates"*. World Health Organization, (Nov. 2009).
12. R. Lozano, *Lancet*, 380 (9859) (2012) 2095.
13. "*Cancer*". World Health Organization, (October 2010).
14. Coleman, B. William, Rubinas, C. Tara, *Molecular Pathology: The Molecular Basis of Human Disease*, 4 (2009) 66.

15. G. Pawelec, E. Derhovanessian, A. Larbi, *Critical reviews in oncology/hematology*, 75 (2) (2010) 165.

16. B. Alberts, A. Johnson, J. Lewis, *Molecular biology of the cell*, New York: Garland Science, 4 (2002).

17. V. N. Anisimov, E. Sikora, G. Pawelec, *Biogerontology,* 10 (4) (2009) 323.

18. J. P. de Magalhaes, *Nature Reviews Cancer*, 13 (5) (2013) 357.

19. F. Joseph, S. David, M. James, *Cancer Epidemiology and Prevention*, (2006) 977.

20. Bostwick, G. David, Eble, N. John, *Urological Surgical Pathology*. St. Louis: Mosby, (2007) 468.

21. P. Kaatsch, E. Sikora, G. Pawelec, *Cancer treatment reviews,* 36 (4) (2012) 277.

22. E. M. Ward, M. J. Thun, L. M. Hannan, A. Jemal, *Annals of the New York Academy of Sciences*, 1076 (2006) 29.

23. S. C. Dhara, *Indian J. Chem.,* 8 (1970) 193.

24. R.A. Alderden, H. D. Hall, T, W. Hambley, *J. Chem. Ed.,* 83 (5) (2006) 728.

25. D. Praveen, P. Ranadheer Chowdary, *Indian J. Res. Pharm. Biotech.*, 1(6) (2013) 793.

26. L. H. Einhorn, *J. Clin. Oncol,*. 8 (11) (1990) 1777.

27. M. Peyrone, *Ann. Chemie Pharm.,* 51 (1) (1844) 1.

28. Stephen Trzaska, "Cisplatin". *C & EN News*, 83 (25) (2005).

29. B. Rosenberg, L. Van Camp, T. Krigas, *Nature,* 205 (4972) (1965) 698.

30. B. Rosenberg, L. Van Camp, E. B. Grimley, A. J. Thomson, *J. Biol. Chem.,* 242 (6) (1967) 1347.

31. J. G. Fortner, *J. Surg. Oncol.,* 53(3) (1993) 191.

32. B. Rosenberg, L. Van Camp, J. E. Trosko, V. H. Mansour, *Nature,* 222 (5191) (1969) 385.

33. D. P. Carpenter, *Reputation and power: organizational image and pharmaceutical regulation at the FDA*. Princeton, N.J: Princeton University Press (2010).

34. J. B. Aragon-Ching, J. Zujewski, *Clinical Cancer Res.,* 13(6) (2007)1644.

35. Shazia Rafique, Muhammad Idrees, Anwar Nasim, Haji Akbar, Amin Athar, *Biotech. Mol. Bio. Rev.,* 5(2) (2010) 38.

36. R.A. Alderden, M. D. Hall,T. W. Hambley, *J. Chem. Ed.,* 83 (5) (2006) 728.

37. L. Au, D. Zheng, F. Zhou, Z. Y. Li, X. Li, Y. Xia, *ACS Nano*, 2(8) (2008) 1645.

38. Y. Zheng, L. Sanche, *Radiat. Res*., 172(1) (2009) 114.

39. K.I. Ansari, S. Kasiri, J. D. Grant, S. S. Mandal, *Dalton Transaction*, 40 (2009) 8525.

40. R. Gomathi, A. Ramu, *Int. J. Innov. Res. Sci. Eng. Tech.*, 2(9) (2013) 4853.

41. F. Sabani, L. Ali, S. Foroush, S. Gahammamy, *Bull. Chem. Soc. Ethiop.,* 24(2) (2010) 193.

42. V. E. Kuzmin, V. P. Lozitsky, G. L. Kamalov, R. N. Lozitskaya, A.I. Zheltvay, *Acta Biochim. Polonica*, 47(3) (2000) 867.

43. P. Singh Amit, K. Kaushik Nagendra, K. Verma Akhilesh, Gupta Rajeev, *Indian J. Chem.*, 50 (2011) 474.

44. V. Mathew, J. Keshavaya, V. P. Vaidya, Giles D, *European J. Med. Chem.,* 42 (2007) 823.

45. W. Robert, Brueggemeier, C. H. John, S. D. Edgar, *Endocri. Rev.*, 26 (3) (2004) 331.

46. G. B. Yi, Y. D. Cui, D. Y. Chen, *J. Fine Chemicals*, 18(5) (2001) 252.

47. E. M. Hodnet, W. J. Dunn, *J. Med. Chem.*, 15(3) (1972) 339.

48. W. Hernández, E. Spodine, L. Beyer, U. Schroder, R. Richter, J. Ferreira, M. Pavani, *Bioinorg. Chem. Appl*., doi: 10.1155/BCA.2005.299, (2005) 299.

49. Violete Jevtovic, *Res. in Canc. Tumor,* 3(1) (2014).

50. B. Singh, J. Mishra, K.S. Pitre, A. Pradhan, P. Soni, *Int. J. Biotech.*, 2 (2013) 39.

51. D. Palanimuthu, S. Vijay Shinde , K. Somasundaram, A. G. Samuelson , *J. Med. Chem.*, *56* (3) (2013) 722.

52. Shaju K. Shanughan, *"Evaluation of metal binding capacity of azomethine class of compouds, electrochemical investigations on corrosion and their biological studies"*, Ph. D. Thesis, University of Calicut, (2014).

53. Vinod P. Raphael, *"Physicochemical, corrosion inhibition and biological studies on schiff bases derived from heterocyclic carbonyl compounds and their metal complexes"*, Ph. D. Thesis, University of Calicut, (2014).

54. A. G. Hall, M. J. Tilby, *Blood Rev.*, 6(3) (1992) 163.

55. S. Trzaska*, Chem. Eng. News,* 83 (2005) 25.

56. C. Marzano, M. Pellei, F. Tisato, C. Santini, *Anticancer Agents Med. Chem.,* 9 (2009) 185.

57. R. K. Lin, C. I Chiu, C.H. Hsu, *J. Chinese Chem. Soc.*, 61 (2012) 1333.

58. Joby Thomas, Geetha Parameswaran, *Asian J. Chem.,* 14 (3) (2002) 1354.

59. S. S. Hindo, M. F. Frezza, D. Tomcu, *Euro. J. Med. Chem*., 44 (2009) 4353.

60. Joby Thomas, Geetha Parameswaran, *Asian J. Chem.,* 14 (3) (2002) 1370.

61. G. Filomeni, G. Cerchiaro, A. M. D. Ferreira, A. De Martino, J. Z. Pedersen, G. Rotilio, M. R. Cririolo, *J. Biol. Chem*., 282(16) (2007) 12010.

62. Eichhorn Gunther, L. Shin, Yong Ae, *J. American Chem. Soc.,* 90 (26) (1968) 7323.

63. T. F. Kagawa, B. H. Geierstanger, A. H. J. Wang, P. S. Ho, *J. Biol. Chem.,* 266 (1991) 20175.

64. B. S. Creaven, *Inorg. Chim. Acta,* 363 (2010) 4048.